CRANFIELD UNIVERSITY

MICHAEL ADEDOKUN ADEGBITE

FLOW ACCELERATED PREFERENTIAL WELD CORROSION OF X65 STEEL IN BRINE CONTAINING CARBON DIOXIDE AND OXYGEN

SCHOOL OF APPLIED SCIENCES

PhD
Academic Year: 2011 - 2014

Supervisors: **Dr. Michael J. Robinson**
Dr. Sue A. Impey

April 2014

CRANFIELD UNIVERSITY

SCHOOL OF APPLIED SCIENCES

PhD

Academic Year 2011 - 2014

MICHAEL ADEDOKUN ADEGBITE

FLOW ACCELERATED PREFERENTIAL WELD CORROSION OF X65 STEEL IN BRINE CONTAINING CARBON DIOXIDE AND OXYGEN

Supervisor: **Dr. Michael J. Robinson**
Dr. Sue A. Impey

April 2014

This thesis is submitted in partial fulfilment of the requirements for the degree of PhD

ABSTRACT

Preferential weld corrosion (PWC) remains a major operational challenge that jeopardizes the integrity of oil and gas production facilities. It is the selective dissolution of metal associated with welds, such that the weld metal (WM) and / or the adjacent heat-affected zone (HAZ) corrode rather than the parent metal (PM). Corrosion inhibition is conventionally used to mitigate this problem however several indications suggest that some corrosion inhibitors may increase PWC. Furthermore, it is not possible to detect systems that are susceptible to PWC and or to understand the apparent ineffectiveness of some corrosion inhibitors at high flow rates. Consequently, the aim of this research is to assess the suitability of submerged jet impingement method to study flow accelerated preferential weld corrosion, which is critical to safe and economic operations of offshore oil and gas facilities.

In this research, a submerged jet-impingement flow loop was used to investigate corrosion control of X65 steel weldment in flowing brine, saturated with carbon dioxide at 1 bar, and containing a typical oilfield corrosion inhibitor. A novel jet-impingement target was constructed from samples of parent material, heat affected zone and weld metal, and subjected to flowing brine at velocities up to 10 ms^{-1}, to give a range of hydrodynamic conditions from stagnation to high turbulence. The galvanic currents between the electrodes in each hydrodynamic zone were recorded using zero-resistance ammeters and their self-corrosion rates were measured using the linear polarisation technique. At low flow rates, the galvanic currents were small and in some cases the weld metal and heat affected zone were partially protected by the sacrificial corrosion of the parent material. However, at higher flow rates the galvanic currents increased but some current reversals were observed, leading to accelerated corrosion of the weld region. The most severe corrosion occurred when oxygen was deliberately admitted into the flow loop to simulate typical oilfield conditions. The results are explained in terms of the selective removal of the inhibitor film from different regions of the weldment at high flow rates and the corrosion mechanism in the presence of oxygen is discussed.

Keywords: Carbon steel, carbon dioxide corrosion, submerged jet-impingement, flow-accelerated corrosion, oxygen corrosion, preferential weld corrosion.

ACKNOWLEDGEMENTS

Glory to the Lord, God Almighty.

I am greatly indebted to my wife, Oluyemisi, and the children – Adeoluwa, Ademola and Adeniran. My sincere gratitude to the Nigerian Government, through Petroleum Technology Development Fund and Petroleum Training Institute.

Warm appreciation goes to Dr. Michael J. Robinson and Dr. Sue A. Impey, for their thorough guidance and immeasurable support throughout this study. Many thanks to Dr. Thomas Mayr, Dr. Nigel Simms, Dr. Humberto L. Perotto-Baldivieso, Dr Xianwei Liu, Sharon Mcguire, Jessica Greenwood, Flemming Nielson, Andrew Dyer, Colin Matthews, Rukhsana Ormesher, Keith Richards, and Tony Parker of the School of Applied Sciences, for their assistance and technical support on numerous occasions. The valuable contributions of other academic and non-academic staff are also appreciated.

Special thanks to Rev. ‘Biyi Ajala, Apostle Ladi Lioyd-Kuyinu, Rev. Dr. Dickson O. E. Madoghwe, Pastor John A. Adegbite, Prof. John Ade Ajayi, Dr. B. W. Jimba, Dr. K. I. Idehen, Dr. & Dr, Mrs. Ben Adesola, Dcn. & Dcns. Babarinde and Mr. & Mrs. Kola Olayiwola for their various support to my family and I during this study – your expectations will not be cut off.

I also extend my gratitude to all friends and the members of Cranfield Pentecostal Assembly and Holding Forth the Word Ministry especially Dr. Daniel Kamunge, Dr. Gareth Davies, Dr. Crispin Allison, Dr. Oluyemi Alagbe, Ndubuisi Okereke, Andy Pidcock, ‘Tayo Okonkwo and Ade Ehinmowo - thank you very much for being part of me.

The support of Clariant Oil Services and the immense assistance of others, who though remain anonymous, are also acknowledged with thanks.

TABLE OF CONTENTS

LIST OF FIGURES

LIST OF TABLES

LIST OF EQUATIONS

LIST OF ABBREVIATIONS

CFD	Computational Fluid Dynamics
CU	Cranfield University
DC	Direct Current
EDM	Electrical Discharge Machining
EDX	Energy Dispersive X-Ray
EOR	Enhanced Oil Recovery
FAC	Flow Accelerated Corrosion
FCAW	Flux-Cored Arc Welding
FIB	Focused Ion Beam
GTAW	Gas Tungsten Arc Welding
HAZ	Heat-Affected Zone
HSE	Health Safety and Environment
HSLA	High Strength Low Alloy
LPR	Linear Polarisation Resistance
OCP	Open Circuit Potential
OFN	Oxygen Free Nitrogen
PM	Parent Metal
PWC	Preferential Weld Corrosion
RCE	Rotating Cylinder Electrode
SCE	Standard Calomel Electrode
SEM	Scanning Electron Microscope
SJI	Submerged Jet Impingement
SWIS	Seawater Injection Systems
WM	Weld Metal
XPS	X-Ray Photoelectron Spectroscopy
XRD	X-Ray Diffraction
ZRA	Zero Resistance Ammeter

CHAPTER 1.
INTRODUCTION

This Chapter presents an overview of the importance of preferential weld corrosion (PWC) in the offshore oil and gas industry, as well as attempts made to mitigate the consequences of this challenge. Existing gaps of knowledge in the PWC of high strength low alloy (HSLA) Steel weldment are highlighted. The aim, objectives and scope of this research are also identified.

1.1 Issues and Challenges of Preferential Weld Corrosion

Preferential weld corrosion in carbon steel pipelines has been experienced in many oil and gas production systems. Preferential weld corrosion (PWC) is a selective form of attack, which corrodes either the weld metal and/or heat affected zones rather than adjacent parent material. This is further exacerbated by either high velocity uninterrupted flow in tubing and pipelines or obstructed flow at changes in geometry such as welding seams, valves, sudden expansions, elbows and threaded joints (Meng and Jovancicevic, 2008). PWC of low carbon steels is commonly encountered in seawater injection systems, produced water service, offshore platforms and downhole-production systems, both in oil production and in gas-condensate production. These result in premature failure, with concomitant economic losses and environmental pollution (Dawson et al., 2010; Dawson et al., 1999; Efird, 1991; De Waard and Lotz, 1994).

Corrosion failures of welds occur regardless of the fact that the recommended base metal and filler metal have been selected or made autogenously (without filler metal), industry codes and standards have been followed, and full penetration welds were made with the recommended weld bead profile (Mahajanam and Joosten, 2011; Lee and Woollin, 2005; Lee et al., 2013; Lee and Wu, 2009). The wrought form of a metal or alloy may be resistant to corrosion in a particular environment, however it is quite common to find that the welded part is not (Winning et al., 2004; Turgoose and Palmer,

2005; Tobiassen and Pedersen, 2004). However, there are also many instances where the weld exhibits corrosion resistance superior to that of the unwelded parent metal (Dawson et al., 1999; Lee and Woollin, 2005; Jenkins and MacDougall, 2013). Moreover, service experience has shown that there are times when the weld behaves in an inconsistent manner, such that the galvanic current reverses, with the weld metal becoming anodic and suffering severe localised corrosion, as illustrated in Figure 1-1 (Mahajanam and Joosten, 2011; Alawadhi and Robinson, 2011; Martinez et al., 2011; Davis, 2006; Martin, 2003).

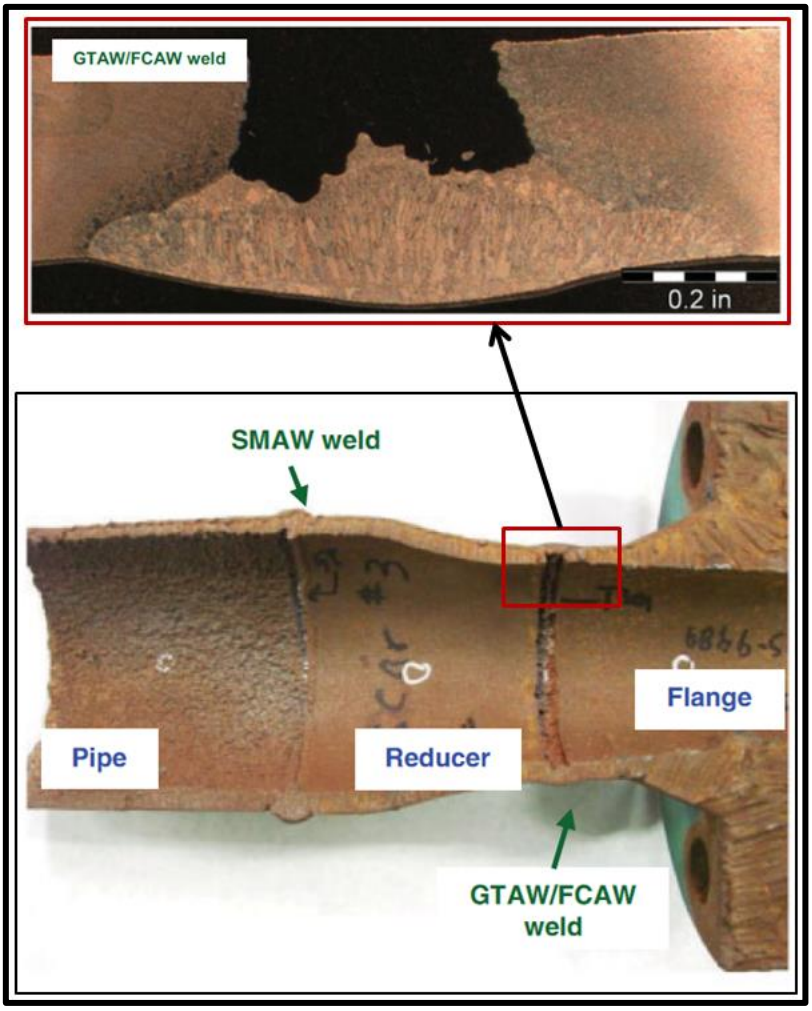

Figure 1-1: Corroded weld in a flowline section. (Mahajanam and Joosten, 2011)

This form of corrosion is controlled by adding a chemical inhibitor, which adsorbs onto the metal surface to form a protective film (Akbar et al., 2011; Zhang and Cheng, 2010; Zhang et al., 2011). The inhibitor should be equally effective on the pipe welds and the parent pipeline steel. Ideally, the weld metal (WM) should be cathodic to the parent metal (PM) so that it does not corrode preferentially. The reversal, which is occasionally experienced in service, is thought to occur at high flow rates, as the inhibitor detaches more easily from the WM, while the PM remains filmed and protected (De Waard and Lotz, 1994; Davis, 2006; Fosbøl et al., 2009). Recent work at Cranfield University has demonstrated that detachment of the inhibitor film is a complex process and sometimes several current reversals can take place as the flow affects the film on each region of the weld in succession (Alawadhi and Robinson, 2011; Martinez et al., 2011).

Several experimental methods have been used to study corrosion in flowing conditions and each one is designed to produce the same hydrodynamic conditions at the metal surface for a full scale pipeline flow (ASTM, 2001; Cayard and Maldonado, 2000; Cai et al., 2012; Efird et al., 1993; Efird, 2006; Alawadhi et al., 2008; Olsen et al., 1997; Nešić, 2007). It is generally agreed that the location and morphology of attack might be influenced by many parameters, including the environment, flow conditions, the weld metal composition relative to the parent metal and the welding procedure, among others. However, from the information available and experience, the mechanisms of this corrosion phenomenon are still unclear. The most accepted explanation of selective corrosion is the difference in composition and microstructure across the weldment. Furthermore, it is still impossible to predict the preferential corrosion rate that may be experienced, the exact location of attack (such as, weld metal and/or heat affected zone), or the effectiveness of corrosion inhibitors. Care is also required in applying remedial measures for different applications because of the complexity of interacting factors that may lead to additional problems. Therefore, corrective measures need to be applied once a problem is identified; hence laboratory testing is essential for applications where preferential attack is anticipated (Mahajanam and Joosten, 2011; Winning et al., 2004; Olsen et al., 1997).

This research seeks to address these asset integrity issues relating to PWC, which are critical to safe and economical operations of industrial systems, in general and offshore pipeline systems in particular.

1.2 Aim and Objectives of Research

The aim of this research is to assess the suitability of submerged jet impingement method to study flow accelerated preferential weld corrosion.

The objectives of this work are to:

1. Develop submerged jet impingement as a novel and convenient method for studying weld corrosion over a wide range of hydrodynamic conditions
2. Study preferential weld corrosion in high strength low alloy steel pipelines by investigating the conditions under which galvanic current reversal takes place
3. Compare effectiveness of a typical oilfield corrosion inhibitor in controlling preferential weld corrosion in characteristic field hydrodynamic conditions
4. Compare the submerged jet impingement and rotating cylinder electrode methods for the study of weld corrosion and chemical inhibitor evaluation.

1.3 Scope of Study

This research is solely focused on "flow accelerated corrosion", defined as "corrosion resulting from the effect of turbulence due to the flow of a fluid that does not contain solid particles in sufficient concentration and/or size to impinge on the metal surface" (Efird et al., 1993). Flow corrosion accelerated by solid particles is termed "erosion-corrosion". Only X65 C-steel pipeline weldment was tested throughout this research.

1.4 Thesis Structure

This thesis is organised into seven chapters. The background and importance of preferential weld corrosion in effectively managing the integrity of aging and new offshore infrastructure, project aim and objectives are highlighted in Chapter 1. A

detailed literature review is presented in Chapter 2; illustrating the importance of HSLA steels as offshore pipeline materials and corrosion as a system characteristic, as well as techniques for evaluation of flow accelerated localized corrosion. Chapter 3 focuses on the design and construction of a novel submerged jet impingement target, used throughout this research. Details of submerged jet impingement (SJI) electrochemical measurements, surface characterisation of corrosion product and potentiodynamic scans to determine corrosion mechanisms are highlighted in Chapter 4. Chapter 5 comprises summaries of evaluations of total corrosion rates in the three major hydrodynamic regions of the jet impingement target. In Chapter 6, effects of hydrodynamic changes, nature of environment and applications of a typical oil field chemical inhibitor are assessed. General discussion and practical implications of results were considered in Chapter 7. Finally, in Chapter 8, conclusions of the results, as well as, recommendations for further work are presented.

1.5 Chapter Summary

A sound knowledge of PWC mechanisms and effective standard testing method(s), as predictive and control tools, are dominant challenges confronting the offshore industry in which high-strength low alloy (HSLA) steels are commonly used. Development of a capable flow accelerated corrosion test technique should therefore enhance effectiveness of PWC management systems, fewer field failures and increased safety, which is the aim of this research.

CHAPTER 2.
LITERATURE REVIEW

The importance of carbon steels as current and future linepipe materials is highlighted. Reviews of the performance of X65 steel weldment in offshore and chemical industries, corrosion as system characteristics, corrosion inhibition and techniques for evaluation of flow accelerated localized corrosion are briefly considered. Current use of laboratory conditions and data to predict field corrosion rate are also appraised.

2.1 High Strength Low Alloy Steels

The X65 pipeline steel used in this work is of the class of steels referred to as high strength low alloy (HSLA) steels. These steels are increasingly being used in offshore structural applications, especially in transportation of hydrocarbons and service fluids. They offer a number of advantages over conventional steels, particularly in service with demanding requirements such as higher strength, improved toughness, ductility, formability and increased weldability. Another impetus for the development of this class of steels is reduced gauge thickness, with associated reduction in material and fabrication costs. Weld assemblies fabricated from these steels are used extensively in the heavy industrial applications including the petroleum and petrochemical industry, land transportation industry, pulp and paper industry, chemical processing industry, electrical power industry, and the building industry, among others.

Over the years, the carbon contents have been gradually reduced to below 0.1 wt% C in order to achieve these strenuous service requirements. The desired strength is mainly achieved through a refinement of the ferrite grain size, produced by the additions of microalloying elements such as aluminium, vanadium, niobium, and titanium in combination with various forms for thermomechanical processing (Cranfield University, 2003). This procedure has resulted in steels with improved resistance to hydrogen-assisted cold cracking, stress corrosion cracking, and brittle fracture initiation in the HAZ region, without compromising the essential and desirable combination of

mechanical and fabrication properties, especially formability and weldability. Controlled rolled HSLA steels (including X52, X60, X65, X70 and X80) are currently produced with minimum yield strength in the range from 350-550 MPa. Above this strength level, quenched and tempered steels are commonly employed.

Relatively small changes in composition and / or variations in processing route can significantly affect the resulting mechanical properties (Arivarasu et al., 2013; Kong et al., 2012). In addition, since fusion welding is the conventional viable process of fabrication of steels, it expected that the joint and the immediate adjoining metals, would exhibit different mechanical properties and / or corrosion resistance (Nešić, 2007).

The presence of a weld often leads to a reduction in corrosion resistance, caused by any / or combination of the following circumstances (Stout, R. D. and Doty, W. D., 1987):

1. Variations of composition and / or microstructure in the parent metal, heat-affected zone and weld metal that result in a condition promoting galvanic corrosion.
2. Presence of welding residual stresses that could result in stress-corrosion cracking (SCC).
3. Presence of weld discontinuities, such as surface flaws, which act as preferential sites for local corrosion attack.
4. Hydrogen cold cracking of the weld. Hydrogen in welding can result from improperly baked or stored electrodes, moisture in the flux, or the presence of moisture and other impurities on the components to be welded.

High strength low-alloy (HSLA) steels used for structural applications are not commonly utilized in severe corrosion environments. However, they are used in moderate corrosive service conditions such as those in oil refinery facilities and sour gas/oil pipelines. Carbon-steels and many other metals and their alloys suffer from severe pitting in environments containing chloride ions (Szklarska-Smialowska, 1991). The corrosion of C-steel in the atmosphere is due to an adsorbed film of water which, while very thin, is sufficient for corrosion to proceed. In oil production applications higher water cuts, increased CO_2 concentrations and, sometimes, higher temperatures have led to severe internal corrosion of C-steel pipes.

2.2 Corrosion

Corrosion is simply "physicochemical interaction between a metal and its environment which results in changes in the properties of the metal and which may often lead to impairment of the function of the metal, the environment, or the technical system, of which these form part" (During, 1997).

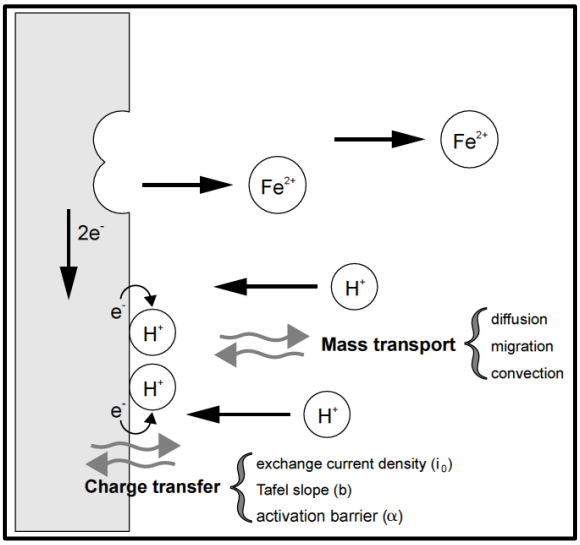

Figure 2-1: Graphical representation of the processes occurring at an electrochemical interface. (Roberge, 2000)

Metals in service often give a superficial impression of permanence, but all except platinum are chemically unstable in air and air-saturated water at ambient temperatures and most are also unstable in air-free water. Hence almost all of the environments in which metals serve are potentially hostile and their successful use in engineering and commercial applications depend on protective mechanisms. Figure 2-1 shows a simplified corrosion processes on a metal / environment interface. In some metal/environment systems the metal is protected by passivity, a naturally formed surface condition inhibiting reaction. In other systems the metal surface remains active and some form of protection must be provided by design (Roberge, 2000; Richardson and Dawson, 2010). This applies particularly to plain carbon and low-alloy steels, which are the most prolific, least expensive and most versatile metallic materials.

Corrosion occurs when protective mechanisms have been overlooked, break down, or have been exhausted, leaving the metal vulnerable to attack.

2.2.1 Mass transport

Corrosion processes in aqueous systems involve consumption of the reactants and formation of products at the metal -electrolyte interface as illustrated in Figure 2-1. For the corrosion process to proceed, reactants must be transported to the metal surface and products away from the surface. Corrosion rates usually depend on the rate at which these transport processes proceed. Generally mass transport in solution takes place according to one or more of the following processes:-

- **Diffusion:** The movement of species from a higher to a lower concentration is known as diffusion. When an electrode is immersed in a solution, if the concentration of reactive species in the solution is higher than that at the electrode surface, diffusion of the species will be towards the electrode. Diffusion in the opposite direction is also possible when reactions produce species at a higher concentration at the electrode surface, and the species diffuse outwards into the solution.

- **Migration:** Migration is the movement of charged species (ions) due to electric field acting on them (potential gradient). The cations (positive ions) will be drawn to the cathode and the anions (negative ions) to the anode.

- **Convection:** This is the movement of species due to mechanical forces. There are two types of convection:

    - Natural: caused by density differences of the solution (usually due to a temperature gradient)

    - Forced: this arises when the solution made to flow (e.g. stirring, pumping, bubbling gas).

2.2.2 Corrosion as a System Characteristic

Some properties of metals can be predicted from their intrinsic characteristics assessed from their compositions, microstructures, thermal history and fabrication methods. These characteristics determine essential properties such as density, thermal and electrical conductivity, ductility and strength under static load in benign environments. These aspects of serviceability are reasonably straightforward and manageable, but there are other aspects of performance which are less obvious and more difficult to control because they depend not only on intrinsic characteristics of the metals but also on the service environment (Mahajanam and Joosten, 2011; Hedges et al., 2006; Kermani, 1995; Kermani and Morshed, 2003). This increases susceptibility to corrosion, metal fatigue, and wear, which can be responsible for complete premature failure with costly and sometimes dangerous consequences.

Degradation by corrosion can best be approached by considering a metal not in isolation but within a wider system with other components such as metal, chemical environment, stress, and time. Thus a metal selected to serve well in one chemical environment or stress system may be totally inadequate for another. Corrosion, fatigue, and wear can interact synergistically, but for the most part, it is usually sufficient to consider corrosion processes as a chemical system comprising the metal itself and its environment as presented in Figure 2-1.

2.2.3 Galvanic Corrosion

Galvanic corrosion occurs when dissimilar metals are brought into contact in the presence of an electrolyte. It can also be caused by any situation that produces changes in electrochemical potential such as differences in temperature and chemicals in the environment. The metal with more noble corrosion potential (cathode) is protected by anodic dissolution (attack) of the less noble metal (anode). The area ratio of the two dissimilar metals is very important. If the anode-to-cathode surface area ratio is small, the galvanic current can be concentrated on a small anodic area; causing significant thickness loss of the anode.

Galvanic corrosion can occur only if the following conditions co-exist (During, 1997):

i. An electrical connection exists between the two (or more) metals
ii. The coupled metals are exposed to a continuous electrolytic environments
iii. A sufficient potential difference exists between the coupled metals
iv. The ability for cathodic reaction(s) to occur on the more noble metal

Remarkably, the electrochemical potential of individual metals that makes the galvanic couple fluctuates slightly depending on the synergism of the couple and environment parameters as summarised in Figure 2-2 (Oldfield, 1988).

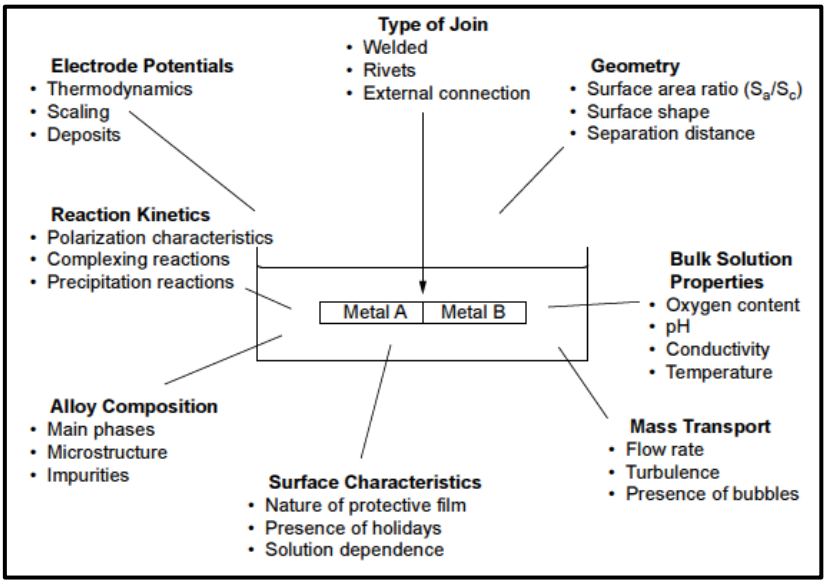

Figure 2-2: Factors affecting galvanic corrosion (Oldfield, 1988)**.**

A weldment (comprising of the parent metal, the heat-affected zone and the weld metal in the vicinity of the welded joint), in an electrolyte, could be considered as 'graded structure' that satisfy the necessary conditions for galvanic corrosion to occur. It is therefore expected that welded joints, including autogenous joints (produced without the filler metal), would be susceptible to galvanic corrosion in offshore pipeline systems due to formation of local anodes and cathodes around the weldment. The surface areas of the weld metal (WM) and the heat-affected zone (HAZ) are significantly small compared with the surface area of the parent metal (PM). Therefore, it would be preferred to have the PM to be anodic to the WM and the HAZ in order to avoid

excessive loss if the thickness of the WM and / or the HAZ were anodic to cathodic PM. Such selective corrosion of the WM and / or the HAZ results in preferential weld corrosion (PWC), which can cause premature failure with concomitant loss of production, facility, lives, aquatic pollution, environmental degradation and economic loss.

2.2.4 Carbon Dioxide Corrosion

The problem of CO_2 corrosion, also known as sweet corrosion has long been recognised and has prompted extensive studies (Shirazi et al., 2006; Schmitt et al., 1999a; Stalker et al., 2004; Nesic and Lee, 2006; Aagotnes et al., 1999). Dry CO_2 gas is not itself corrosive at the temperatures encountered within oil and gas production systems. However, when dissolved in an aqueous phase through which it can promote an electrochemical reaction between steel and the contacting aqueous phase, it becomes corrosive. CO_2 is soluble in water and brines, but has even greater solubility in hydrocarbons. It is well known that hydrocarbon fluids are generally produced in association with an aqueous phase. In many cases the hydrocarbon reservoir will also contain a significant proportion of CO_2. As a result of this, CO_2 will dissolve in the aqueous phase associated with hydrocarbon production. This aqueous phase will corrode carbon steel (Heidersbach, 2011; George et al., 2004; Nesic et al., 1996).

The CO_2 corrosion phenomenon is still not fully understood, though it has been recognized as a challenge in oil and gas production facilities for many years and that much resource has been expended in studying and analysing it. Therefore, most researchers (Nešić, 2007; Altoé et al., 1996; Amin and Ibrahim, 2011; Pereira Farias and Monteiro Quites, 1992; Barker et al., 2012) in sweet corrosion and related fields are of the opinion that a mechanistic understanding of the phenomenon is essential if engineering criteria are to be developed to enable the accurate prediction of the rate and nature of this type of corrosion attack.

2.2.4.1 Mechanism of Carbon Dioxide Corrosion

Various mechanisms have been postulated for the CO_2 (sweet) corrosion process, and all involve either carbonic acid or the bicarbonate ion formed on dissolution of CO_2 in water. This results in rates of corrosion greater than those expected from corrosion in

strong acids at the same pH. CO_2 dissolves in water to give carbonic acid, a weak acid compared to mineral acids as it does not fully dissociate (Zhang and Cheng, 2010; Kermani, 1995; Kermani and Morshed, 2003; Schmitt et al., 1999b; Schmitt and Horstemeier, 2006; Silva et al., 2004; Kermani and Smith, 1997; De Waard and Lotz, 1993).

Corrosion rates depend on the interaction of environmental conditions involved, such as pH, temperature, pressure, solution chemistry, flow and metallurgy of the steel and surface films, among others (De Waard and Lotz, 1994; Kermani and Morshed, 2003; Dayalan et al., 1998; Dugstad, 2006; Dugstad, 1998; Llongueras et al., 2005; M.F.Suhor et al., 2012; Kakooei et al., 2012). CO_2 dissolves in water to form three chemical species (H_2CO_3, HCO_3^- and H^+) that are critical to the rate of subsequent electrochemical reactions:

$$CO_2 + H_2O \leftrightarrow H_2CO_3 \quad \textbf{Equation 2-1}$$

$$H_2CO_3 \rightarrow H^+ + HCO_3^- \quad \textbf{Equation 2-2}$$

$$HCO_3^- \rightarrow H^+ + CO_3^{2-} \quad \textbf{Equation 2-3}$$

The anodic reaction in CO_2 corrosion of the steel is primarily the dissolution of steel:

$$Fe \rightarrow Fe^{2+} + 2e^- \quad \textbf{Equation 2-4}$$

The cathodic reactions during corrosion of carbon steel in seawater saturated with carbon dioxide include reduction (Equation 2-5) and regeneration (Equation 2-6) of carbonic acid:

$$2H_2CO_3 + 2e^- \rightarrow 2HCO_3^- + H_2 \quad \textbf{Equation 2-5}$$

$$2HCO_3^- + 2H^+ \rightarrow 2H_2CO_3 \quad \textbf{Equation 2-6}$$

Such that, the overall cathodic reaction is

$$2H^+ + 2e^- \rightarrow H_2 \quad \textbf{Equation 2-7}$$

In oil and gas field operations it is possible that the water phase will contain not only dissolved carbon dioxide but oxygen may also be present, as a result of ingress into well annuli, inadvertent leaks of pumps / valves or insufficient deaeration. A number of researchers (Martin, 2002; Martin, 2001; Gulbrandsen et al., 2005; Choi and Nešić, 2010) agree that, where such aerated brine containing CO_2 exists, additional cathodic reaction (reduction of oxygen), occurs resulting in accelerated corrosion of carbon steel as shown in Equation 2-8.

$$\mathbf{O_2 + 2H_2O + 4e^- \rightarrow 4OH^-} \qquad \textbf{Equation 2-8}$$

The carbon dioxide enhanced oil recovery (CO_2-EOR) injection operations facilitated by the development of carbon capture, transportation and storage (CCS) technologies also attract significant asset integrity attention due to the presence of dissolved oxygen. Captured CO_2 from anthropogenic sources can potentially contain oxygen that will increase the risk of corrosion. A recent study was conducted by Rosil et al (2014) to investigate the effect of oxygen ingress on the iron carbonate ($FeCO_3$) corrosion product layers generated during CO_2 corrosion of steel. Carbon steel samples were immersed in stagnant CO_2-saturated with 1 wt% brine for 7 days, and the tests were perturbed with 1 ppm O_2 at different experimental times. Iron carbonate film-forming conditions (80°C and pH 6.6 ± 0.1) were maintained throughout experiments. Electrochemical measurements showed a decrease in corrosion rate due to scale formation that conferred some degree of protection to the steel surface. The corrosion rates at the conclusion of all tests were relatively low and localized. Surface analysis showed degradation of iron carbonate crystals and formation of iron oxides. This degradation of initially formed iron carbonate occurred concurrently with the development of localized corrosion features as deep as 100 µm. X-Ray Diffraction (XRD) and Raman Spectroscopy confirm the formation of magnetite (Fe_3O_4), hematite (α-Fe_2O_3), and goethite (α-FeO[OH]) along with siderite ($FeCO_3$) in corrosion products. Similar localized pits and corrosion products are reported in a related study by Dong et al (2014). Therefore it can be concluded that dissolved oxygen in CO_2, even at low concentrations, can have a profound effect on sweet corrosion of mild steel.

In flowing conditions, mass transfer accelerates thereby increasing the corrosion rate. This is consistent with published results (Choi and Nešić, 2010; Dong et al., 2014; John

et al., 2008) suggesting that flow thinned off the surface corrosion film and subsequently exposes the substrate to continuous action of the corrosive environment.

Song, (2010) also showed that for a given O_2 pressure, CO_2 can have a little effect on steel corrosion rate when it is at a low pressure, while this effect becomes progressively more significant as CO_2 pressure increases as shown in Figure 2-3.

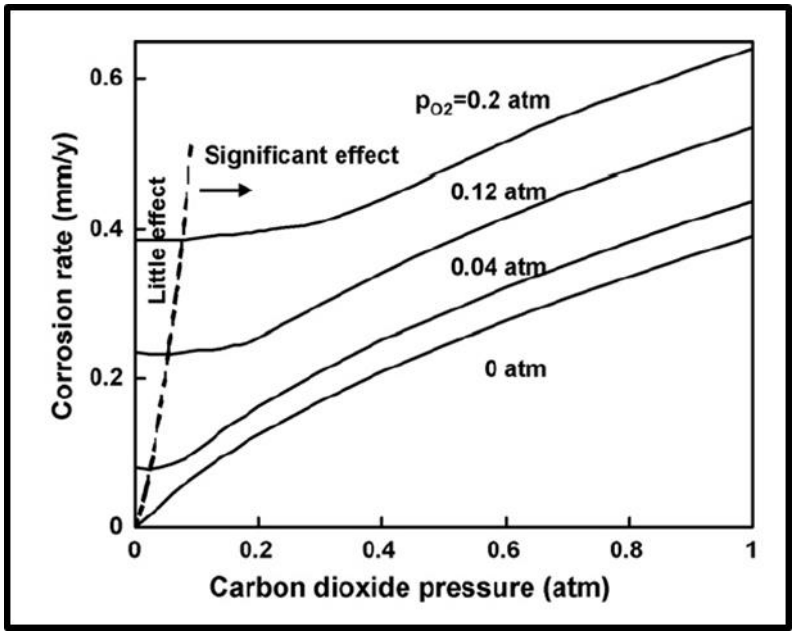

Figure 2-3: Effect of CO_2 pressure on corrosion rate for four O_2 pressures (Song, 2010)

2.2.4.2 Factors Affecting Carbon Dioxide Corrosion

Extensive researches over the past decades show that a variety of factors affect the rate of CO_2 corrosion in the offshore oil and gas industry. These parameters generally categorised into environmental, physical, and metallurgical variables, are interdependent and can interact in many ways to influence CO_2 corrosion, (De Waard and Lotz, 1994; Fosbøl et al., 2009; Kermani, 1995; Kermani and Morshed, 2003; Kermani and Smith, 1997; Dayalan et al., 1998; Dugstad, 2006; Kateřina and Gubner, 2010). The environmental and physical parameters are mainly dependent on the reservoir characteristics and enhanced oil recovery technique(s) used in a particular

oilfield. It is therefore imperative to outline some of these parameters and the extent to which they affect the sweet corrosion process.

a) **Environmental Parameters**: These factors affect the inherent corrosion characteristics of the aqueous phase and consequently, the sweet corrosion. They include:
   - Solution chemistry and supersaturation of CO_2
   - CO_2 partial pressure
   - Operating temperature
   - In situ pH
   - Presence of hydrogen sulphide (H_2S)
   - Presence of acetic acid
   - Presence of oxygen

b) **Physical Parameters**: These parameters influence the hydrodynamics of the system and the interface between the aqueous phase and the steel substrate. Major physical factors include:
   - Wax effect
   - Water wetting
   - Surface (Corrosion product) films
   - Effect of crude oil
   - Fluid dynamics

c) **Metallurgical Parameters**: Metallurgical history and nature (chemical composition, heat treatment and microstructure) of the steel play important roles on the morphology and extent of sweet corrosion.

The effects of dissolved oxygen in solution containing CO_2 have been discussed under Mechanism of Carbon Dioxide Corrosion in section 2.2.4.1. Other critical factors affecting CO_2 corrosion of carbon steels relevant to this research are reviewed below. Effect of flow velocity is highlighted in Flow Accelerated Corrosion sub-heading.

CO_2 Partial Pressure

The partial pressure of CO_2 in a hydrocarbon stream is an important parameter in CO_2 corrosion because the corrosion rate of a CO_2 saturated solution is generally dependent

on the CO_2 partial pressure. This is because the CO_2 partial pressure is directly related to the carbonic acid concentration. Many researchers agree with Song (2010) that, when other conditions are constant and in the absence of oxygen, the corrosion rate of carbon steel increases when the partial pressure of CO_2 increases as shown in Figure 2-3 (Song, 2010). Studies have also shown that there is an increase both in the solubility of CO_2 and the acidity of the produced fluids with increasing CO_2 partial pressure (De Waard and Milliams, 1975).

However, some authors are of the view that there are exceptions to the direct proportionality between the corrosion rate and the CO_2 partial pressure, due essentially to synergy in environmental conditions (Turgoose and Palmer, 2005; Nesic et al., 1996; Videm, 1998).

Corrosion Product / Surface Films

Many authors have shown that the rate and characteristics of carbon dioxide corrosion largely depends on the type of corrosion product in the corrosive solution (environment) and the corrosion (surface) film formed on the metal surface during the corrosion process (Kermani and Morshed, 2003; Llongueras et al., 2005; Gao et al., 2011). De Waard and Lot (1993) demonstrated that the presence of corrosion products in a solution saturated with CO_2 will reduce the corrosion rate and without some of these corrosion products, much higher corrosion rates are possible.

The stability, protectiveness and adherence of these films determine the nature and the rate of corrosion (Kermani and Morshed, 2003). Gao et al (2011) also showed that the protectiveness of the corrosion product films are affected by many factors such as the pressure, temperature, flow rate and pH, with temperature and pressure been the most critical. Most authors agree that when there is no film forming on the metal surface; most of the corrosion attack is general corrosion, and localised corrosion, which is more severe and normally occurs when the corrosion film forms on the metal surface during the corrosion process. Some researchers have suggested that the corrosion product formed on a steel surface are made up of an insoluble part, iron carbonate ($FeCO_3$) and undissolved part from the steel called cementite (Fe_3C) (Nešić, 2007; Dugstad, 1998; Nesic et al., 1996).

Table 2-1 is a summary of CO_2 corrosion films characteristics in the temperature range of 5°C to 150°C (Kermani and Morshed, 2003). Four categories of CO_2 corrosion films were identified:

- Transparent films
- Iron carbide (Fe_3C) films
- Iron carbonate ($FeCO_3$) films
- Iron carbonate and iron carbide (Fe_3C + $FeCO_3$) films

Table 2-1: Characteristics of corrosion films (Kermani and Morshed, 2003)

Corrosion Film Class	Temperature Range of Formation (°C)	Characteristics / nature	Growth Habit and Composition
Transparent	Forms at room temperature and below	< 1 µm thick, transparent – once formed, it is very protective	Forming fast as temperature reduces to < room temperature mainly consisting of Fe and oxygen
Iron carbide	No range	< 100 µm thick, metallic, conductive and non-adherent	Spongy and brittle, consisting of Fe, C and O
Iron carbonate	Min. required in laboratory conditions 50°C to 70°C	Adherent, protective and non-conductive	Cubic morphology, consisting of Fe, C and O
Iron carbonate + iron carbide	Maximum 150°C (higher temperatures not studied)	All depends on how $FeCO_3$ is blended with Fe_3C	Consisting of ferrous carbide and ferrous carbonate

Transparent films

According to Kermani (1995)transparent films are formed at roughly room temperature in aqueous solution containing CO_2, even in a very low ferrous ion (Fe^{2+}) concentration (Kermani, 1995)and these are rarely reported in the literature. Increase in Fe^{2+} has been reported to significantly enhanced the protectiveness of the film (Dugstad, 1998; Crolet et al., 1996), and considerably reduce the corrosion rate of carbon steel in a static (stagnant) condition. However, it has been reported that carbon steels protected by this transparent film may be predisposed to crevice and chloride pitting corrosion (Dugstad, 1998; Crolet et al., 1996); comparable to the mode of corrosion attack on passivated stainless steels.

Cementite Films

It is reported that selective dissolution of carbon steel ferrite phase in flowing aqueous solution containing CO_2 results in formation of ferrous ions with some siderite ($FeCO_3$) and carbonates of alloying metals and a residue of cementite (Fe_3C) (Martinez et al., 2011; Schmitt and Bakalli, 2006). These authors demonstrated that the cementite, which was part of the original steel microstructure, served as the cathodic reaction site. They reasoned that the fragile and porous Fe_3C residue is non-protective and therefore vulnerable to flow conditions and concluded that for $FeCO_3$ films to be formed, Fe^{2+} ions must be in sufficient quantity.

In addition to the galvanic coupling mechanism above, other authors (Dugstad, 1998; Crolet et al., 1996; Crolet et al., 1999) assert that the Fe_3C films play a prominent role in the corrosion process and enhance the rate of corrosion through "localized acidification". They argued that cathodic reactions can occur preferentially at Fe_3C sites such that definite anodic and cathodic sites develop, resulting in difference in the water composition. The aqueous phase at the cathodic sites becomes more alkaline and at the anodic sites more acidic, causing internal localized acidification and promote corrosion on the surface of the metal.

Kermani, (2014) however submits that the accumulation of Fe_3C has a contrasting role on corrosion behaviour depending on its mechanism of formation and its dominance within the film structure and process. On one hand, by preventing the diffusion of ferrous ions from the surface, it promotes the formation of $FeCO_3$ film to offer a degree of protection. By blending uniformly into $FeCO_3$ film, (where cementite matrix provides an anchoring effect to sustain $FeCO_3$ in place) as illustrated in Figure 2-4, it will enhance its properties and protectiveness. Conversely, Fe_3C could provide local acidification and facilitate galvanic corrosion and hence increased rate of attack. Undoubtedly, therefore, metallurgical characteristics of the steel play a crucial role in the nature and stability of corrosion films.

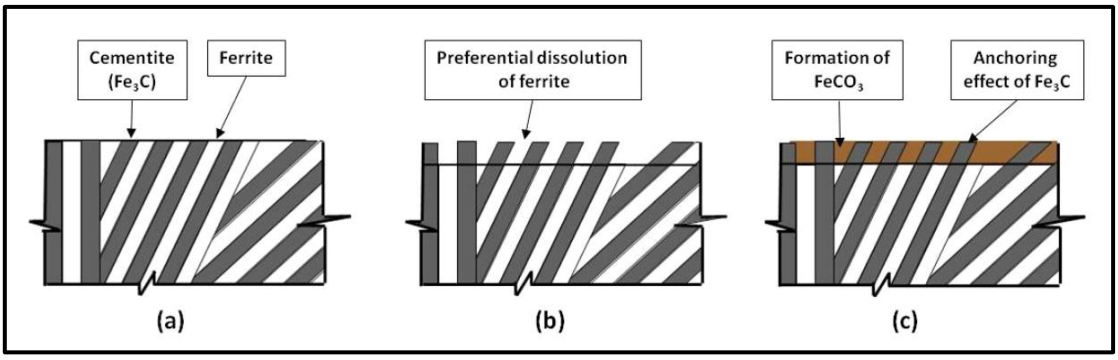

Figure 2-4: Sequence of events in CO_2 corrosion process, (a) the microstructure, (b) anodic corrosion of ferrite phase only and (c) formation of $FeCO_3$ anchored by Fe_3C (Kermani, 2014)**.**

Iron Carbonate - Siderite ($FeCO_3$) Films

The most common type of corrosion product encountered in CO_2 corrosion is iron carbonate (siderite) and is formed when the concentration of Fe^{2+} and CO_3^{2-} exceeds the solubility limit, as shown in Equation 2-9. When the rate at which the corrosion product precipitates on the surface exceeds the rate of corrosion, thick protective scales are formed. However, when the corrosion rate exceeds the rate at which the corrosion product precipitates, a porous and non-protective (Fe_3C) scale is formed (Nešić, 2007). It is important to note that at room temperature, the precipitation process is slow and non-protective scales are formed while at high temperatures precipitation proceeds faster with the formation of protective ($FeCO_3$) scales (Nesic and Lee, 2003).

$$Fe^{2+} + CO_3^{2-} \rightarrow FeCO_3\,(S) \qquad \textbf{Equation 2-9}$$

Schmitt and Horstemeier (2006) are of the opinion that the precipitation rate of $FeCO_3$ is slow but is influenced by temperature and also argued that under supersaturated situations, the corrosion rate could be high until a protective layer was formed. They therefore suggested that the kinetics of $FeCO_3$ precipitate could be the controlling factor for the protectiveness of the corrosion product. They however agreed that at higher pH values (6.5 and above), protective iron carbonate films could be formed at room

temperature. The protectiveness of $FeCO_3$ has also been shown to depend on the extent of surface coverage and the property of the film (Hong et al., 2000). Hong et al (2000). further demonstrated that the tendency to form the $FeCO_3$ film is a function of the saturation factor (F_{sat}) which is given as:

$$\mathbf{F_{sat}} = \frac{[Fe^{2+}]S\,[CO_3{}^{2-}]S}{K_{sp}} \qquad \textbf{Equation 2-10}$$

Where,

- $[Fe^{2+}]$ = surface concentration of Fe^{2+}
- $[CO_3{}^{2-}]$ = surface concentration of $CO_3{}^{2-}$
- K_{sp} = solubility product of $FeCO_3$ in a saturated solution at given temperature

The thickness and adherence of the siderite film has been reported to depend on the steel microstructure (Kermani, 1995; Kermani and Morshed, 2003). The scale formed on normalized steels with pearlite/ferrite microstructure is found to be more adherent with more densely packed large crystals and thicker than those formed on quenched and tempered steels, due to lower residual stresses associated with the former. This further affirms the vital role of the steel metallurgical history on sweet corrosion products/films.

Iron Carbonate and Iron Carbide (Fe_3C + $FeCO_3$) Films

Coexistence of siderite ($FeCO_3$) and cementite (Fe_3C) is the common sweet corrosion film product on carbon steel surfaces in CO_2 containing environments (Kermani, 1995; Dugstad, 1998; Crolet et al., 1996). It has been shown that it is possible for the cementite to embed within the siderite film in the course of carbon steel CO_2 corrosion (Kermani, 2014). The structure of the film depends on where and when siderite precipitation takes place (Dugstad, 1998). One of the possible corrosion processes was illustrated earlier in Figure 2-4 (Kermani, 2014).

The nature and protectiveness of the corrosion product determines the corrosion rate of the metal. Studies have shown that the formation of $FeCO_3$ tends to decrease the corrosion rate (Kermani and Morshed, 2003; Nesic and Lee, 2003) while that of Fe_3C

could result in high corrosion rates especially at the beginning of the CO_2 corrosion process (Gao et al., 2011). Figure 2-5 is a classification of carbon steel corrosion films in CO_2 containing environment based on an analysis of the diffusion/precipitation issues and observed morphologies of protective and non-protective corrosion film layers (Crolet et al., 1996). De Waard and Lotz (1994) demonstrated that generally the presence of corrosion products in a solution saturated with CO_2 will reduce the corrosion rate and that without some of these corrosion products, much higher corrosion rates are possible.

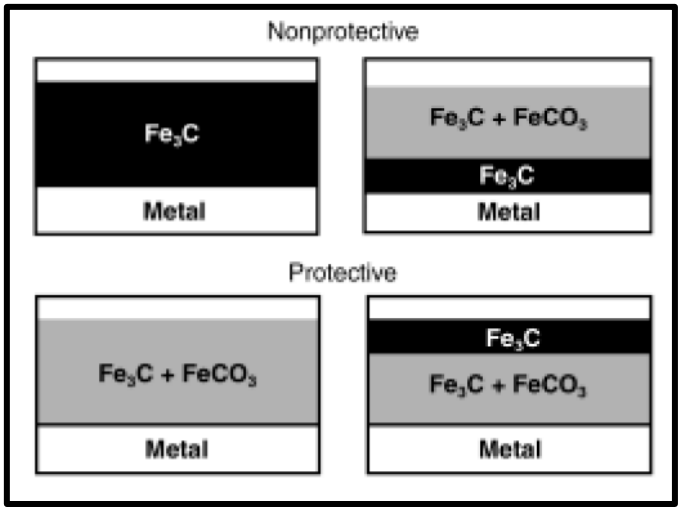

Figure 2-5: Different morphologies observed for protective and non-protective corrosion layers (Crolet et al., 1996)

Effect of Operating Temperature

Temperature strongly influences CO_2 corrosion due to its effect on the rate of scale formation. It is generally agreed that under a given CO_2 partial pressure the corrosion rate increases with increasing temperature, because of higher solubility of the $FeCO_3$ film until a certain temperature, T_{max} is reached as shown in Figure 2-6 (De Waard and Lotz, 1994). Beyond this temperature (around 60-80 °C, for CO_2 partial pressures between 1-3 bar) the iron carbonate layer becomes more adherent to the metal surface and more protective in nature resulting in a decrease of the corrosion rate (Dugstad, 1998; Song, 2010; Videm, 1998). This correlation between temperature and corrosion

rate has been reported by researchers and Ueda et al (1999). attribute the maximum corrosion rate to a critical temperature T_{max} encountered both in carbon and chromium steels. Increasing the CO_2 partial pressure and the pH of the bulk solution tends to lower the scaling temperature and so a protective corrosion film forms earlier with a drop in the corrosion rate. Conversely, a higher flow rate increases the scaling temperature so that a protective corrosion film forms at a much higher temperature.

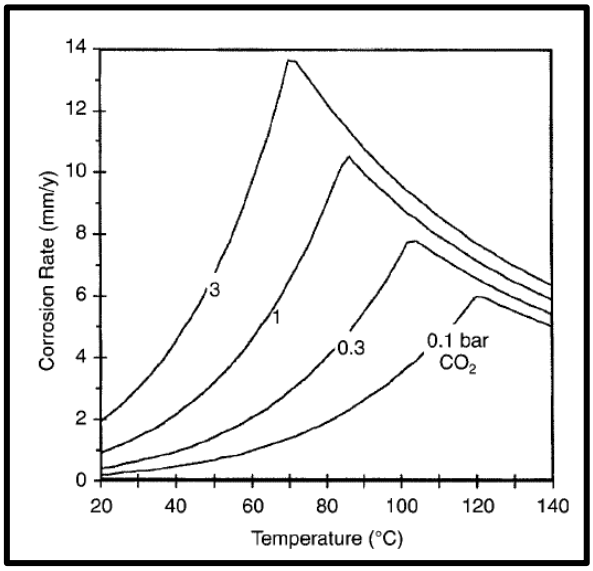

Figure 2-6: Effect of temperature on CO_2 corrosion (De Waard and Lotz, 1994)

Figure 2-6 corroborates the findings of earlier work conducted by Olsen under water condensing conditions to study the CO_2 corrosion of carbon steel. It was observed that in the absence of corrosion inhibitor, black corrosion film consisting primarily of Fe_3C and $FeCO_3$ was formed. At a high temperature (70°C), the films were thin and not easy to remove and resulted in a reduction of the corrosion rate (Olsen and Dugstad, 1991).

De Waard (2004) proposed a predictive tool for CO_2 corrosion rates (mm/y) as a function of both CO_2 pressure (bar) and temperature (^oC) that is widely accepted. Figure 2-7 shows the tool represented in a simple nomogram. The correction factor, (Scale Factor) could be considered as the synergistic effect of protective corrosion product layers, partial dissociation of carbonic acid, corrosion products contamination and operational conditions of the different oil wells. For instance, the estimated sweet

corrosion of carbon steel in aqueous solution with CO_2 partial pressure of 1 bar and temperature of 23°C is 0.9 mm/y.

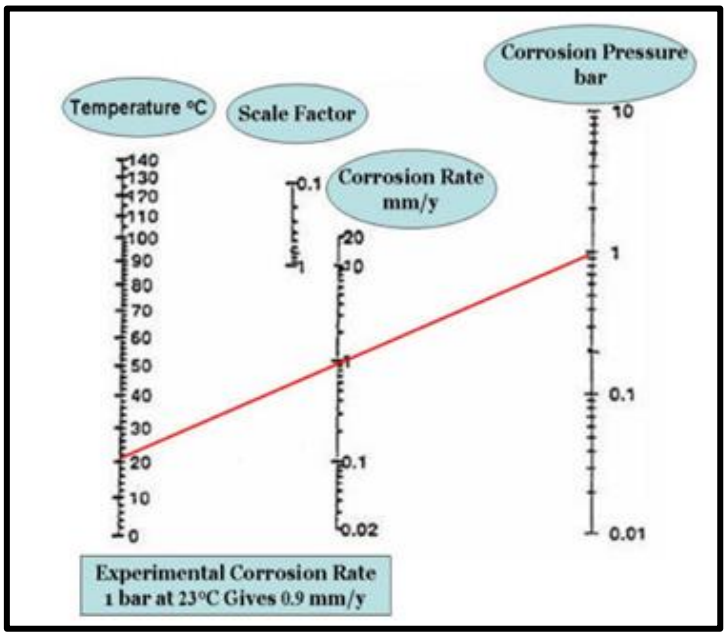

Figure 2-7: Nomogram for predicting CO_2 corrosion of carbon steel (De Waard, 2004)**.**

2.2.5 Flow Accelerated Corrosion

Flow accelerated corrosion (FAC) is defined as "corrosion resulting from the effect of turbulence due to the flow of a fluid that does not contain solid particles in sufficient concentration and/or size to impinge on the metal surface" (Efird et al., 1993). Flow corrosion accelerated by solid particles is termed 'erosion-corrosion'.

Flow accelerates corrosion through the magnitude of fluid turbulence and the fluctuations in turbulence that occur in the liquid water phase in contact with the metal surface. Efird (2000) is of the opinion that these fluctuations bring corrosive species to the metal surface and remove the products of the corrosion reaction from the metal surface.

2.2.5.1 Erosion Corrosion

In multiphase production pipelines, when sand is produced, sand particles impingement on piping surfaces can decrease the efficiency of corrosion protection systems, such as iron-carbonate scale formation or chemical inhibition, and can result in severe corrosion including pitting. Recent studies by Hu and Neville (2009) and Hussain and Robinson (2007) show that there is a significant increase in the total thickness loss when sand particles are present. Synergistic effect of mechanical erosion and electrochemical corrosion has been reported to be the cause.

Erosion-corrosion of carbon steel pipelines is one of the critical asset integrity issues in multiphase production pipelines. When sand is present in the production line and carbon dioxide is present as the gas phase, the damage to the interior of pipe walls can be severe (Marsh et al., 2009). Erosion-corrosion is tribo-corrosion material loss mechanism, disrupting or thinning the protective film of corrosion product. The nature of erosion-corrosion is such that there are mechanical, electrochemical and interactive processes involved (During, 1997; Roberge, 2000; Heidersbach, 2011). The material loss experienced in erosion-corrosion conditions includes synergism of chemical dissolution (which can be increased by mass transfer at the surface), mechanical erosion caused by flow and/or impingement of particles on the pipe wall and electrochemical corrosion enhanced erosion.

The existence of a synergistic effect between corrosion and erosion has been reported. Levy (1995) asserts that combined erosion-corrosion of metals occurs by a simultaneous formation and removal of scale from the surface by a cracking and chipping mechanism or by a spalling mechanism. In general, synergism between corrosion and erosion is acknowledged in the erosion-corrosion process. The total weight loss $\mathbf{W_T}$ experienced in erosion-corrosion conditions usually comprises of the following components (Stack and Abdulrahman, 2010; Addis et al., 2008; Wang et al., 2004; Rogne et al., 1998):

1. Chemical dissolution (which can be increased by mass transfer at the surface), $\mathbf{W_C}$
2. Mechanical erosion caused by fluid flow and impingement of particles on the pipe wall, $\mathbf{W_E}$
3. Electrochemical corrosion enhanced erosion, $\mathbf{\Delta W_C}$

4. Erosion enhanced corrosion, ΔW_E

Such that:

$$W_T = W_E + \Delta W_E + W_C + \Delta W_C \qquad \textbf{Equation 2-11}$$

Therefore, the total synergism, **S** is made up of:

$$S = \Delta W_E + \Delta W_C \qquad \textbf{Equation 2-12}$$

These contributing processes, as well as their interactions have attracted a lot of industrial attention in determining the contributions to weight loss from these different components in order to understand what processes are controlling the weight loss in different situations.

There are some reported cases of surface materials for combined erosive and corrosive conditions have been evaluated on the basis of separate erosion and corrosion studies, with the consequence that the synergistic effects are left out from the evaluation. Since one or both of these effects are frequently large, the conclusions may be incorrect. The ΔW_C contribution is particularly high for passive materials as the stainless steels; since sand erosion destroys the passive oxide layer, (Wc is normally very low for these materials). ΔW_E is most pronounced for ceramic-metallic materials in which the metal phase has a low corrosion resistance especially for pure cobalt (Co) based phase. This may be the case even if the measured corrosion rate under erosive conditions is a small fraction of the total mass loss rate. Rogne and Solem (1998) argued that this is possible because the binder is located in between the carbide grains, often in narrow areas. Corrosion of the binder may undermine the carbide particles and make them more susceptible to erosion attacks.

Stack and Abdulrahman (2010) investigated the effect of erosion–corrosion on carbon steel in oil field production and mapped the results. Experiments were conducted under different conditions; reservoir water with sand, oil with sand and the combination of both conditions. Erosion–corrosion maps were constructed showing the extent of

wastage, the mechanism of degradation and the synergism / antagonism between the processes as a function of impact angle and particle velocity. Major conclusions of their work include:

- The erosion–corrosion of carbon steel in a range of aqueous / crude oil slurries increases with velocity.
- At low impact angles, the erosion of passive film material is likely to increase up to a critical impact angle and to remain constant or marginally decrease due to a decrease in cutting wear at higher impact.
- The passivation rate in the presence of oil is reduced considerably compared to water only systems, indicating that the presence of the oil must have an effect on the passivation and re-passivation kinetics.

A systematic study on pipeline steel degradation due to erosion-corrosion containing sand in CO_2 saturated environments was conducted in a liquid-solid impingement system by Hu and Neville (2009). The aim of the study was to improve the understanding of erosion–corrosion prediction by identifying critical parameters (temperature, flow velocity and sand content) which change the damage mechanism from a flow-induced corrosion regime to erosion–corrosion regime. For impinging type damage, the rates and trends of material loss were assessed based on a semi-empirical approach. The degradation mechanisms across the surface of API X65 in CO_2 erosion–corrosion conditions were evaluated. Hu and Neville (2009) demonstrated that the effect of corrosion as a means of enhancing erosion (synergy) has the largest contribution to the degradation of pipeline steel in CO_2 erosion–corrosion conditions as illustrated in Figure 2-8. The cut-off conditions at which the material degradation mechanisms make the transition from a flow-induced corrosion dominated regime towards erosion–corrosion were also determined in this study.

Another research aimed at identifying and defining the erosion-corrosion regimes was conducted by Stack et al (1995). They studied the synergistic effect of erosion and corrosion of mild steel (BS6323) in sodium carbonate and bicarbonate solutions at ambient temperatures. A rotating cylinder electrode (RCE) apparatus was used for the erosion-corrosion tests. This enabled electrochemical data to be collected for the single and multiple impacts. Using the electrochemical data, an aqueous erosion-corrosion

map was proposed where the transitions between the aqueous erosion-corrosion regimes are given as a function of erodent velocity and potential as shown in Figure 2-9.

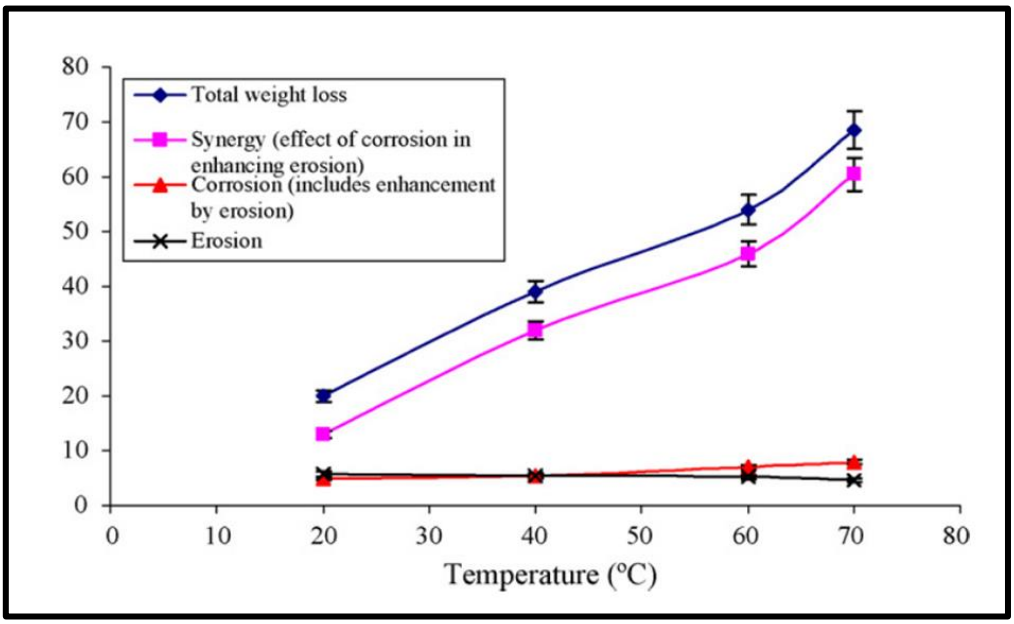

Figure 2-8: Total weight loss and components as a function of temperatures at 20 m/s with 200 mg/L solids in CO_2 saturated solutions (Hu and Neville, 2009)

Figure 2-9, suggests that at relatively negative potentials and low velocities in cathodic conditions, neither erosion nor corrosion occurs. At high velocities, plastic deformation takes place and therefore a transition to "pure' ' erosion occurs. As the applied potential becomes less negative, and dissolution of metal initiates, the transitions between the erosion-dissolution regimes are achieved by variation of particle velocity and applied potential. Increase in velocity shifts the "erosion-dominated" regime to higher potentials since the corrosion rate (the dissolution rate) as a function of increasing potential, increases in this region. It can be seen that a similar phenomenon applies in the passive region, although the boundaries are less dependent on potential because the passive film thickness does not increase significantly with increasing potential in this case.

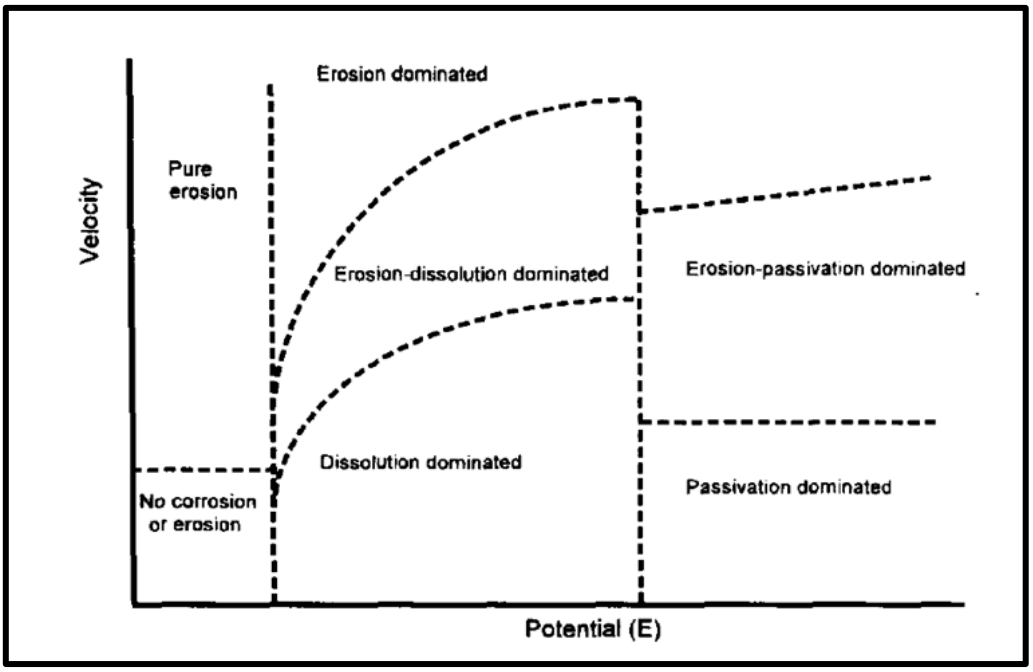

Figure 2-9: Schematic diagram of an aqueous erosion-corrosion map for Fe in $NaHC0_3/Na_2C0_3$ where the transitions between the erosion-corrosion regimes are given as functions of velocity and potential (Stack et al., 1995)**.**

Shadley et al (1996) used a flow loop to study erosion-corrosion of carbon steel elbows (shown in Figure 2-10) in a carbon dioxide environment with sand entrained in the flowing liquid. The results identified three typical behaviour zones whose boundaries were defined by the system erosivity, as illustrated in Figure 2-11:

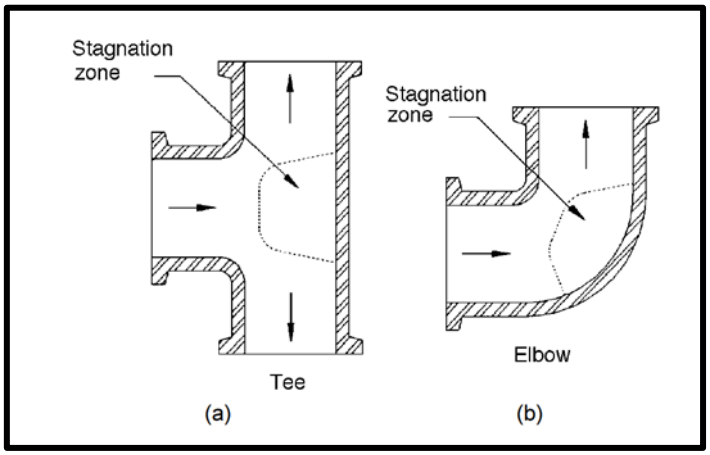

Figure 2-10: Stagnation zone for tee and elbow (Shadley et al., 1996)**.**

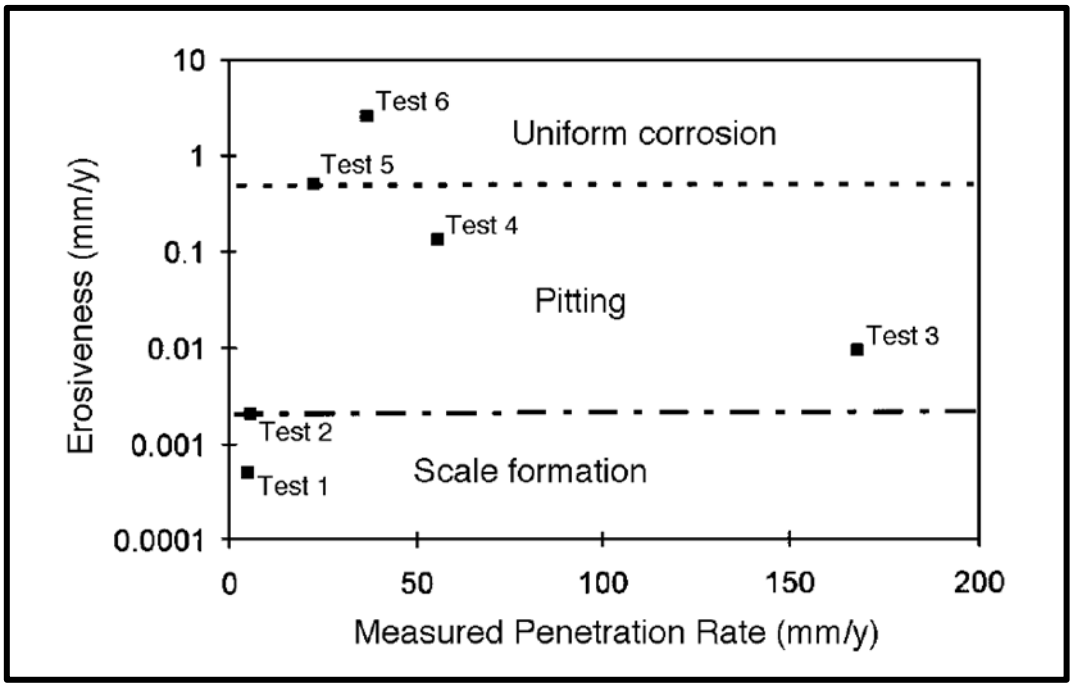

Figure 2-11: Three zones for erosion-corrosion in an elbow (Shadley et al., 1996)**.**

- At low velocities, a protective iron carbonate (FeCO3) scale formed over all surfaces of the elbow, and corrosion rates were very low.
- At high velocities, impingement on elbow surfaces by sand particles entrained in the flow prevented protective scales from forming in the elbow. Corrosion rates were high and uniform over the entire surface.
- At intermediate velocities, protective scales formed over all of the elbow surface except at very localized points, where impinging sand particles prevented scale formation. Deep pits formed at these points, and wall penetration rates were extremely high. These conditions are damaging but can be avoided by reducing or increasing flow velocities.

Effect of Oxygen on Erosion-Corrosion

Figure 2-12 shows the results of an investigation of the role of dissolved oxygen in CO_2 corrosion and erosion-corrosion, using high temperature / high pressure autoclaves and a rotating cage method (Dong et al., 2014). When silica sand of 75 mesh (215~315μm)

and hardness 980 HV was flowed with formation water at 2 m/s and 90°C, the erosion-corrosion rate was 3.8 mm/y in CO_2 saturated solution and 33.8 mm/y in CO_2–O_2 solution compared with 1.8 mm/y and 3.4 mm/y respectively under effect of flow (FAC). This substantiates the argument that erosion significantly enhances erosion-corrosion as well as the importance of the solution chemistry.

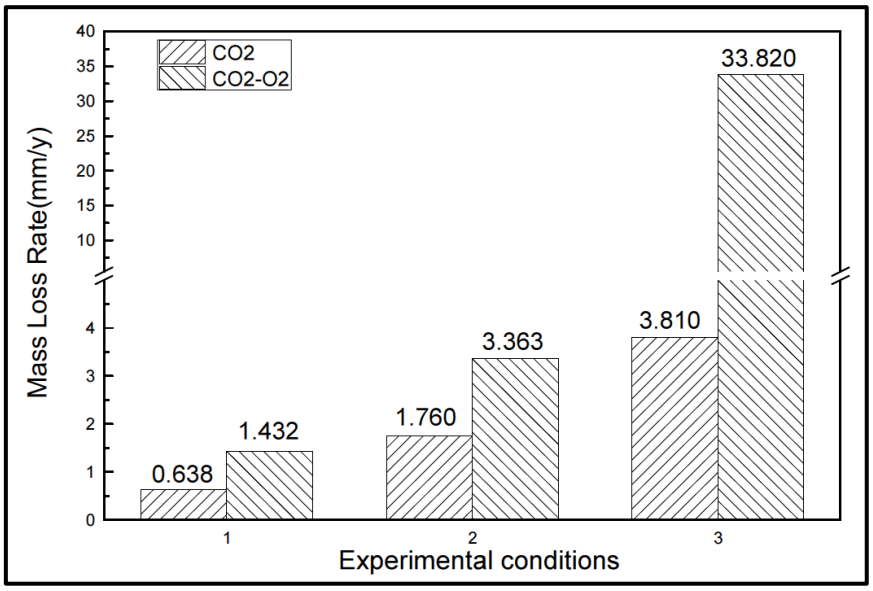

Figure 2-12: Average mass loss rate of N80 under different experimental conditions (1) static condition; (2) flowing condition (2m/s) without sands; (3) flowing condition (2m/s) with sands (Dong et al., 2014)

2.2.5.2 Nature of Turbulent Flow

Fluid flow is turbulent in virtually all situations where flow accelerated corrosion occurs (Meng and Jovancicevic, 2008; Efird, 2006; Hausler and Schmitt, 2004), so the physical structure of turbulent flow is of primary consideration. Fully developed turbulent flow consists of a turbulent core where the mean velocity is essentially constant and a boundary layer near the solid/fluid interface. The majority of the changes in fluid stress, turbulence, mass transfer and fluid interaction with the wall occur within this boundary layer. An illustration of the general structure of the turbulent boundary layer is presented in Figure 2-13 (Efird, 2006). This shows the energy, momentum and mass

transfer (diffusion) that occurs within the boundary layer and how the various layers within the boundary layer interact.

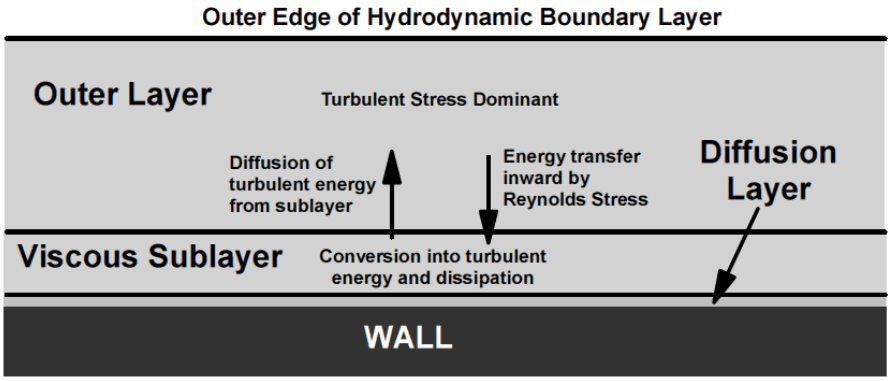

Figure 2-13: The general structure of the hydrodynamic boundary layer showing the energy, momentum and mass transfer within the various layers (Efird, 2006)**.**

The nature of the turbulent boundary layer dictates that this is where the processes that control corrosion and film formation will occur. One of the main conclusions by Praturi and Brodkey (1978) is that all movements of the corroding species to the wall and of corrosion products from the wall, and all chemical reactions with the wall, must occur in this region. Consequently, they suggested that any disturbance in the turbulent boundary layer, particularly within the viscous region, must be a primary factor affecting the corrosion process.

Disruption of the boundary layer in turbulent flow occurs primarily by the formation of turbulent bursts and sweeps. The turbulent burst is an ejection of fluid from the wall, which also causes fluid to impinge on the wall by the simultaneous formation of sweeps, or movement of fluid toward the wall. Turbulent bursts and sweeps occur through the formation of vortices and the lift-up of wall streaks.

One of the early proposals of the formation of shear layer vortices and evolution into a turbulent burst by Praturi and Brodkey (1978) is illustrated in Figure 2-14. The vortex moves with the flow and is increasingly tilted by the mean shear in the viscous region (Stages (a) to (d)). At some point the vortex becomes unstable and a strong ejection

occurs along with a rapid sweep of fluid into the viscous region (Stage (e)). It is evident that severe pressure fluctuations must occur with the formation of a turbulent burst and during the rapid ejection of fluid.

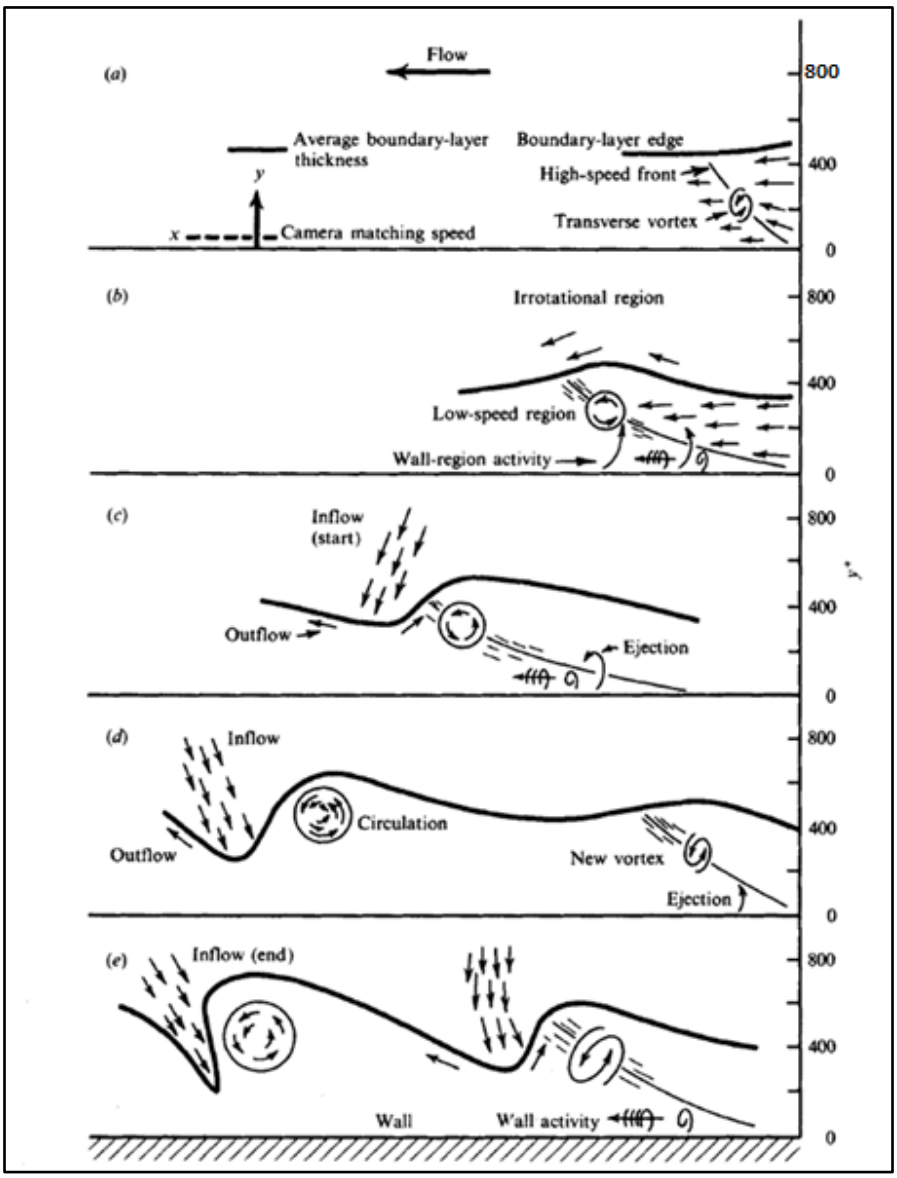

Figure 2-14: Progression of flow (Praturi and Brodkey, 1978)

The interaction of the solid surface with the violent, rapidly fluctuating nature of turbulent flow in the viscous region and diffusion boundary layer is the primary reason

that mass transfer and wall shear stress are the fundamental hydrodynamic factors that define the effect of flow on corrosion.

Some authors, (Efird, 2000; Hausler and Schmitt, 2004; Fang and Liu, 2004; Schmitt and Mueller, 1999) agree that the processes control corrosion and film formation occur in the viscous region of the hydrodynamic boundary layer and the diffusion boundary layer. All movement of corroding species to the wall, and of corrosion products from the wall, and all chemical reactions at the wall, must occur in these regions. Consequently, disturbances in these layers control the corrosion process. The violent, rapidly fluctuating nature of turbulent flow in the viscous region and diffusion boundary layer, and its interaction with the solid surface, is the primary reason that mass transfer and wall shear stress are the fundamental hydrodynamic factors that define the effect of flow on corrosion.

It is imperative therefore, that fluid flow must be expressed in terms related to flow parameters common to all hydrodynamic systems to allow the application of laboratory test data to operating systems (Efird et al., 1993). The parameters, calculated from empirical equations developed to characterize flow are wall shear stress, $\boldsymbol{\tau}_{\omega}$, and mass transfer coefficient, K_d.

2.2.5.3 Wall Shear Stress

Wall shear stress is a direct measure of the viscous energy loss within the turbulent boundary layer, and is related to the intensity of turbulence in the fluid acting on the wall. It is not a force on the wall from the fluid, but a force in the fluid at the wall.

The wall shear stress is defined as the isothermal pressure loss in a moving fluid within an incremental length due to fluid friction from contact with a stationary wall. The total shear stress in a fluid moving past a fixed wall is the sum of the viscous and Reynolds stresses expressed as Equation 2-13 (Efird, 2000).

$$\boldsymbol{\tau} = \boldsymbol{\upsilon}\left(\frac{\partial U}{\partial y}\right) - \mathbf{U_x U_y}$$

Equation 2-13

Where U = fluid velocity (m/s) and υ = fluid kinematic viscosity (m^2/s).

The Reynolds stresses (U_xU_y) go to zero at the wall, leaving only the viscous stress in the fluid. The wall shear stress is defined as this viscous shear stress at wall, (where $U_x = U_y = 0$), expressed as Equation 2-14:

$$\tau_\omega = \upsilon \left(\frac{\partial U}{\partial y}\right)_{y=0}$$

Equation 2-14

2.2.5.4 Mass Transfer Coefficient

Efird (2006) expressed the mass transfer coefficient, K_d (m/s) as the ratio of diffusion coefficient to the displacement as given in Equation 2-15:

$$K_d = \frac{D_J}{\delta d}$$

Equation 2-15

Where D_J = diffusion coefficient for species J in the bulk solution (m^2/s)

δd = diffusion boundary layer thickness (m)

2.2.5.5 Interrelationship of Mass Transfer Coefficient and Wall Shear Stress

The mass transfer coefficient is intimately linked to wall shear stress, and the two cannot be practically separated either experimentally or mathematically. Thus, changes in flow parameters that affect one parameter result in changes in the other parameter. Efird (2006) argued that the link is not totally independent of geometry. However, the relationship between mass transfer and wall shear stress may change from one flow geometry to another. The diffusion coefficient is related to the wall shear stress through the Chilton Colburn analogy, as in Equation 2-16:

$$K_d \approx \left(\frac{\tau_\omega}{\rho}\right)^{0.5}$$

Equation 2-16

This relationship is more precisely defined as Equation 2-17:

$$K_d = 17.24\left(\frac{\tau_\omega}{\rho}\right)^{0.5} Sc^{2/3}$$

Equation 2-17

Where **Sc** is the dimensionless Schmidt number, defined as the ratio of the viscosity (**μ**), to the product of the density (**ρ**), and diffusion coefficient (**D**), for the active species, **j**.

For **Sc** > 100:

$$Sc = \frac{\mu}{\rho D_j}$$

Equation 2-18

2.2.5.6 Flow Effects on Corrosion

The magnitude of the effect of hydrodynamics on corrosion, or flow accelerated corrosion, is determined by mass transfer and wall shear stress existing in the liquid phase (without solid particles in sufficient concentration and/or size) contacting the solid wall. An increase in the rate of corrosion under the influence of flow from 0.64 mm/y to 1.8 mm/y in CO_2 saturated formation water at 90^{o}C as presented in Figure 2-12 (Dong et al., 2014) represent a typical characteristic of FAC. It is widely agreed that the fluid flow would accelerate the mass transfer process and degrade the protective corrosion scale formed on the steel surface (Zhang and Cheng, 2010; Silva et al., 2004; Efird et al., 1993; Efird, 2000; Alawadhi and Robinson, 2010; Davies, 1972; Efird, 2006; M.Martinez et al., 2011). A study on hydrodynamic effects on corrosion by Fang and Liu (2004) shows a typical increase in the corrosion rate with fluid flow velocity as presented in Figure 2-15.

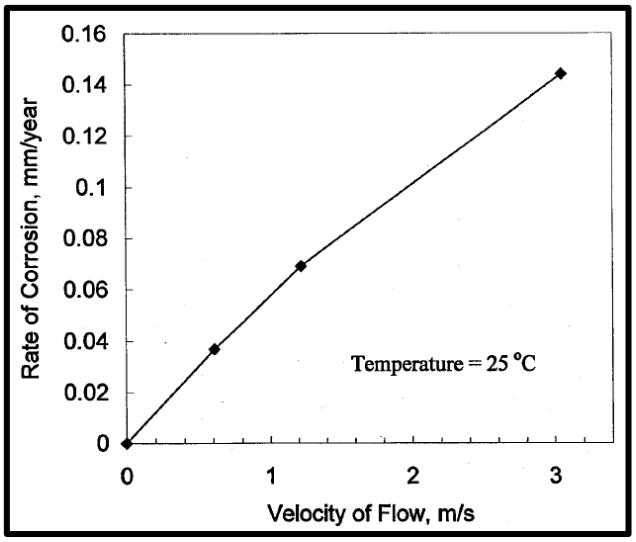

Figure 2-15: Rate of corrosion in fully-developed flow region (Fang and Liu, 2004)

One of the attempts to accurately predict flow enhanced CO_2 corrosion in steel produced a model which shows good correlation between the calculated and measured corrosion rates in low shear stress flow environments. This mechanistic model of CO_2 corrosion that takes into account the electrochemical reaction kinetics, mass transport and fluid flow, chemical reaction (hydration of CO_2), and corrosion product scale growth kinetics (Nesic et al., 1996; Nesic et al., 2003; Nordsveen et al., 2003). Nevertheless, this model did not take turbulent effect or momentum transfer into consideration and is not able to explain the mechanical film removal and its effect on flow enhanced localized corrosion. The force responsible for the mechanical film removal is considered to relate to fluctuations in turbulence. Based on the theoretical calculations and experimental measurement using a micro technique, another study proposed that near-wall waves have enough energy to break down the protective corrosion product layer, therefore leading to flow enhanced localized corrosion such as pitting (Nesic and Lee, 2003; Hausler and Schmitt, 2004).

Corrosion failures often occur in areas where steady state flow patterns are disrupted, termed regions of disturbed flow. Typical regions / locations in oil and gas production pipeline systems include:

- downstream of weld beads
- at pre-existing pits

- downstream of hard shell fouling
- heat exchanger tube inlets
- partial blockage in heat exchanger tubes
- downstream of valves
- at bends and elbows
- at threaded joints and upsets

2.2.6 Corrosion of High Strength Low Alloy Steel Weldments

The corrosion behaviour of carbon steel welds varies, depending on parameters such as the composition of the parent and filler metal, the welding process, welding procedure employed and the nature of the corrosive environment (Mahajanam and Joosten, 2011; Lee and Woollin, 2005; Kakooei et al., 2012). As a result of the metallurgical transformations across the weld and HAZ, microstructures and morphologies become significant. The range of microstructures formed depend on the welding energy input, preheat temperature, metal thickness, weld bead size and reheating due to multi-pass welding. Hence, the filler metal microstructures are often different from that of the parent and HAZ, due to the chemical composition, weld inclusions and welding thermal control. Consequently, in a suitable electrolyte, the weldment shows characteristic features of a typical galvanic couple. The modes of preferential corrosion commonly found in the offshore oil and gas industry, as well as in chemical plants, are shown in Figure 2-16 (Dawson et al., 1999). Severe localised corrosion of the weld metal, the fusion zone and the heat-affected zone are predominant. The preferential attack may be in any or a combination of the weldment zone, reducing the effective area of the cross section of the joint and causing premature failure of the joint, which can result into loss of production and/or life, environmental degradation and economic consequences.

The integrity of welds could be undermined by preferential weld corrosion and this remains a potential operational challenge in the offshore oil and gas industry. Furthermore, the presence of oxygen in brine containing carbon-dioxide (CO_2) worsens the problem, as it is thought to be responsible for intense high PWC rate, resulting in premature failure with concomitant effects. This subject has (not been researched) just

attracted the attention of the offshore exploration industry and requires a focused attention.

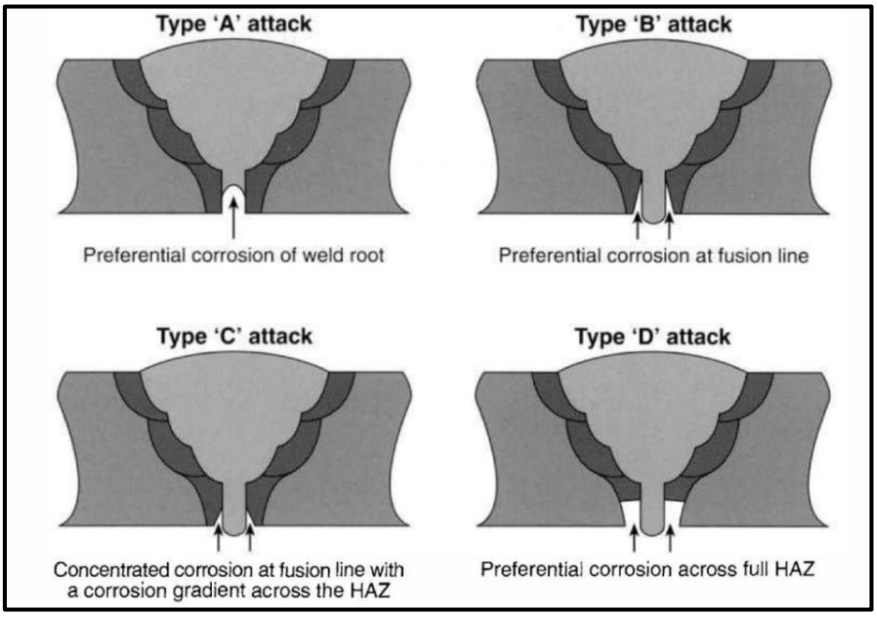

Figure 2-16: Typical morphologies of preferential weld corrosion. (Dawson et al., 1999)

In practice, it is difficult to determine the mechanisms and cause of preferential weld corrosion, even with vast amounts of information and industrial experience. It can also be challenging to predict the rate of preferential weld corrosion that could be experienced, the exact location of attack (weld material or HAZ) and the performance of corrosion inhibitors on the different regions (Queen et al., 2004).

If applied correctly, corrosion inhibition can contribute towards reducing preferential weld corrosion. However, there is evidence to suggest that certain corrosion inhibitors may increase preferential weld corrosion under certain conditions (Martinez et al., 2011).

Figure 2-17 is a typical preferential weld corrosion (PWC) test coupon assembly referred to as "hockey puck". This proven technique can provide a practical, rapid and sensitive response to study galvanic effects between the PM, the HAZ and the WM. Each specimen in the "hockey puck" coupon has an electrical wire attached, and all the

conducting cables can be connected to a multichannel electrochemical instrument, which allows measurement of both the self-corrosion rate or the effect of the galvanic coupling of the different weldment zones in a stimulated stagnant test solution.

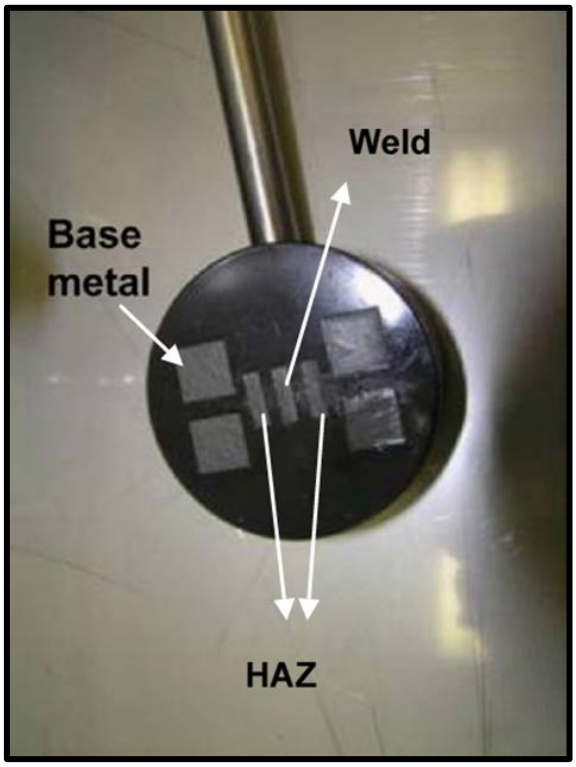

Figure 2-17: Typical configuration of the electrodes on PWC "hockey puck" coupon (McIntyre et al., 2014)**.**

The most accepted explanation of selective corrosion is difference in composition and microstructure across the weldment. However, it is still impossible to predict whether attack will be concentrated on the heat-affected zone (HAZ), weld metal WM), or both areas in susceptible conditions. Care is also required in the transfer of remedial measures to different applications because of the complexity of the interacting factors that may lead to additional problems. Therefore, corrective measures need to be applied once a problem is identified. Hence laboratory testing is essential for applications where preferential attack is anticipated (Mahajanam and Joosten, 2011; Winning et al., 2004; Olsen et al., 1997).

2.2.6.1 Preferential Corrosion of the Weld Metal

Corrosion in welds may in part be due to differences in the composition of individual welding electrodes of filler wire. Micro-galvanic cells can form if one of the root passes is more noble than another and bay regions can develop where previous weld root passes have re-melted. Preferential corrosion of the weld may occur, if the filler metal is less alloyed than the parent metal, and may therefore have a lower potential. Kermani and Smith (1997) argued that in such instance, the large cathode (parent metal), and the small anode (weld) would accelerate the weld attack further, since the cathodic reaction is usually rate determining. Poor corrosion resistance can also be found in welds of similar composition and hardness to the parent, which may be due to the flux used to coat the electrode. Rutile (TiO_2) fluxes provide superior corrosion resistance to basic ones, although not to the standard of the parent metal (Olsen et al., 1997). Variations in flux composition may cause this and heat treatment unfortunately has little effect at remedying it.

To counter preferential attack, alloying small quantities of Cu, Cr, Mo, Nb, Ti, Al, V and Ni with the intention of making the weld more noble has been tested successfully even with basic electrodes. The addition of these elements must be treated with caution as it is the synergistic behaviour of selected elements together that is more beneficial rather than assuming that optimum performance can be gained by adding all of them to a filler metal (Mahajanam and Joosten, 2011; Lee and Woollin, 2005).

The effect of the environment where the weld is in service is also very crucial. In aqueous solution containing CO_2, accelerated corrosion of the weld is possible when the pH is low, due to increase in bicarbonate concentration (HCO_3^-) and when hydrodynamic regime changes. High turbulent flow gives high fluid to wall shear stresses and enhance mass transfer of the corroding species, hence higher corrosion rate. The effect of turbulent flow rates and their detrimental effect on welds have been known for many years, since high corrosion rates were noted in welds on the hulls of ships (Emenike, 1993).

2.2.6.2 Preferential Corrosion of the Heat-Affected Zone

Corrosion of the HAZ has been reported in aqueous environments between pH 7-8. It is apparent that the HAZ will corrode more severely than the parent metal; as a result of microstructural changes that accompanied the welding process in the vicinity of the weld (Tebbal and Hackerman, 1993).

Mahajanam and Joosten (2011) reported that addition of low levels of Cu and Ni (>0.1%) to the PM and using a 1% Ni filler metal has resulted in selective corrosion of the HAZ, especially in low-energy input welds. This was attributed to the WM and the PM areas becoming very cathodic, thereby shifting the anodic sites to the HAZ. De Waard (1993) also submits that manganese, silicon, carbon and decreasing welding energy can reduce the likelihood of PWC of the HAZ.

2.2.7 Flow Accelerated Preferential Weld Corrosion Incidents

The preferential weld corrosion shown in Figure 1-1 is a carbon steel flowline joint in a multiphase (oil/gas/water) offshore field, which failed after 15 months in service (Mahajanam and Joosten, 2011). The weld was produced by gas tungsten arc welding (GTAW) root-run followed by flux-cored arc welding (FCAW) process.

Another example of perferential weld corrosion in a multiphase production carbon steel pipeline containing hydrocarbon and brine saturated with carbon-dioxide is shown in Figure 2-18 (Winning et al., 2004). The nickel content of the weld metal was more than 1%w, nevertheless, PWC occurred contrary to assertions based on previous researches and field experiences (Copson, 1945). The severity of the PWC was attributed to poor anodic to cathodic ratio.

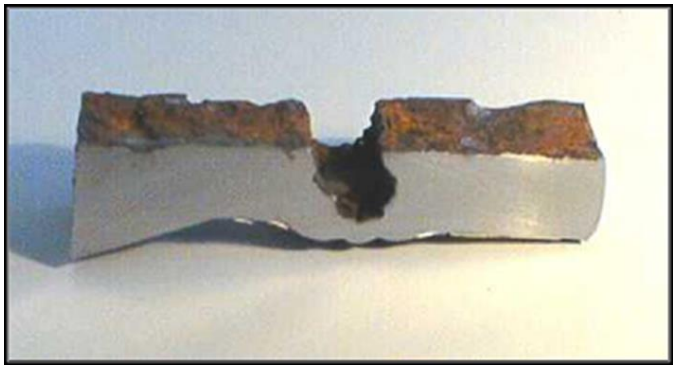

Figure 2-18: Severe PWC in carbon steel pipeline carrying inhibited oil and gas (Winning et al., 2004)**.**

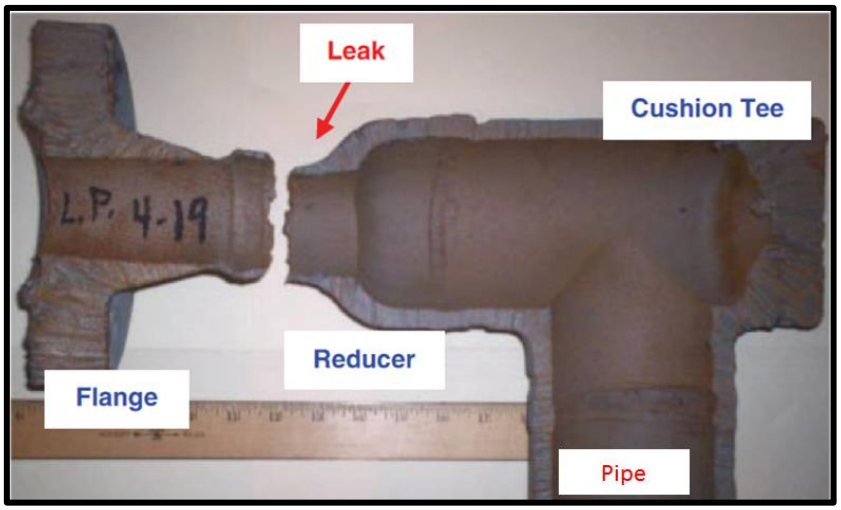

Figure 2-19: Corroded flowline section. (Mahajanam and Joosten, 2011)

Figure 2-19 shows a corroded flowline section with pinhole leaks in the weld from bulk oil/gas/water off wellhead at an offshore field in the Gulf of Mexico. The carbon steel flowline had been in service for 30 months.

Figure 2-20 shows an example of preferential corrosion in the HAZ of a carbon steel weldment (Gooch and Hart, 1986). This phenomenon has been observed in a wide range of aqueous environments, the common link being that the environments are highly conductive while attack has usually, but not invariably, occurred at pH values below approximately 7 to 8.

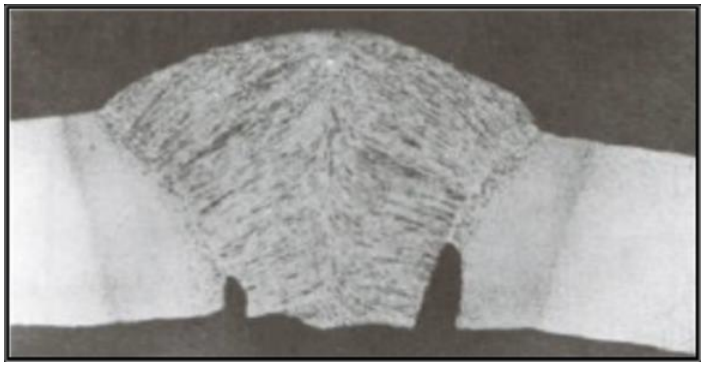

Figure 2-20: Preferential corrosion in the HAZ of a carbon steel weldment after service in an aqueous environment (Gooch and Hart, 1986)

2.3 Corrosion Control Methods

The four main methods for controlling the corrosion of a material or component are:

1) Materials selection and structural design
2) Environmental modification
3) Electrochemical control
4) Application of a protective coating

These methods may be used either individually or in combination and generally, the choice is often based on the most cost-effective option able to achieve the required performance and lifetime characteristics.

Successful materials selection is based upon identifying and delivering the key materials property / performance requirements of the product that is being designed in relation to:

1. Functionality – appropriate combinations of physical, thermal, mechanical, electrical and/ or magnetic properties in combination with appropriate formability and ease of fabrication.
2. Appearance – appropriate formability and ease of fabrication with surfaces amenable to appropriate finishing that might include processes such as colouring, patterning and texturing.
3. Durability – predictable resistance to fracture, wear, corrosion, or other deterioration processes throughout the design life of the product.

4. Economy – acceptable cost and availability.

Practically, cost-effective corrosion control often requires the use of a relatively cheap material that serves the required mechanical or physical function (e.g. a carbon or low-alloy steel). In such cases *in situ* environmental modification is required to control the corrosivity of the environment. There are a variety of technologies available to achieve this end, and selection depends upon the specific details of the particular application, generally driven by the requirement to achieve acceptable performance for minimum cost. The scientific basis behind environmental modification can be divided into two fundamentally different underlying methods:

- Corrosive agent removal: This involves deliberate modification of an environment in order to reduce its chemical and/or electrochemical activity towards a substrate material by removal of specific corrosive reagents.
- Protective barrier inducement: This involves the deliberate addition of a chemical species that interacts in some way with the corroding substrate so as to form a protective barrier that reduces the corrosion rate to an acceptable level.

It is important to note that these strategies may be combined together (and indeed also combined with one of the *ex situ* corrosion control methods; for example, the addition of corrosion inhibitors into paints) in order to achieve the desired performance.

Electrochemical corrosion control generally involves the application of a cathodic potential to a material so that the net anodic reaction rate is reduced (and, consequently the net cathodic reaction rate is increased); a method known as cathodic protection. This may be achieved either by the use of a sacrificial anode such as zinc to protect carbon steel or by application of an external potential from a direct current (DC) power supply. In the latter case the potential may, in principle, be made sufficiently negative such that the material is driven into its immunity regime. However, a likely result is that the cathodic hydrogen is generated, which can result in undesirable embrittlement of materials. For materials that may be passivated in an appropriate environment, then an anodic potential may be applied in order to ensure that the passive film is successfully formed. This method, known as anodic protection, is only feasible where a passive oxide is stable over a sufficiently large range of potential but can be used in a range of environments.

2.4 Corrosion Inhibitors

A corrosion inhibitor is a chemical substance or combination of substances that, when present in the environment, prevents or reduces corrosion (Baboian, 2002).

One of the most practical methods to reduce the effect of corrosion of carbon steel pipelines, storage and pressure systems in the oil and gas industry is the application of corrosion inhibitors. A number of authors, including (Dayalan et al., 1998; Hausler and Schmitt, 2004; Ahmad, 2006; Gulbrandsen and Dugstad, 2005) agree that when the corrosive environment is extremely aggressive or the scales formed on the steel are non-protective, then the application of corrosion inhibitors is preferred. Corrosion inhibitors have therefore proven to be an effective method for mitigating corrosion, and in many cases, reducing the corrosion rates to acceptable limits as reported by Papavinasam (2000).

Corrosion inhibitors are used to protect metals from corrosion, including temporary protection during storage and / or transport. An efficient inhibitor is compatible with the environment, is economical for application, and produces the desired effect when present in small concentrations (During, 1997; Papavinasam, 2000). The authors are also of the opinion that in the case of pipelines, corrosion inhibitors can be applied when a new pipeline is commissioned or at any other time within the operation of the pipeline.

Nesic (2007) in his review of key issues in internal corrosion of oil and gas pipelines submits that though inhibitors have been successfully used to mitigate internal corrosion, the mechanism of operation has not been fully understood. Other researchers agree with the fact that there is no known mechanism of the inhibition process but that protection is achieved by surface coverage due to the formation of a protective film (Zhang et al., 2011; Foss et al., 2009). They believe that the inhibitor adsorbs onto the steel surface preventing any water or corrosive agents from having direct contact with the metal and so slows down one or more electrochemical reactions. According to Fontana (1987), the action of slowing down the corrosion rate is achieved by the following processes:

- Increasing the anodic or cathodic polarisation behaviour

- Reducing the movement or diffusion of ions to the metallic surface
- Increasing the electrical resistance of the metallic surface

Meng and Jovancicevic (2008) demonstrated that inhibitor effectiveness depends on factors, such as steel composition and microstructure, water chemistry, pH, organic acids, water/oil ratio, temperature, CO_2 and H_2S partial pressure, flow regimes and flow geometry.

Inhibitor efficiency, **P**, is given as

$$\mathbf{P} = \left(1 - \frac{CR}{CR_o}\right) x\ 100 \qquad \textbf{Equation 2-19}$$

where $\mathbf{CR_o}$ is the corrosion rate in the absence of inhibitor, and **CR** is the corrosion rate in the same environment with the inhibitor added (Baboian, 2002; Papavinasam, 2000).

2.4.1 Types of Corrosion Inhibitors

Corrosion inhibitor selection is based on the metal and the environment. Figure 2-21 shows classification of corrosion inhibitors into two broad categories: environmental conditioners and interface inhibitors (Papavinasam, 2000).

2.4.1.1 Environmental Conditioners

Environmental conditioners, also called scavengers, are corrosion inhibitors which act by scavenging the aggressive substances (species) from the environment. Examples of scavengers include sodium sulphite which removes dissolved oxygen from near-neutral and alkaline solutions, thereby decreasing oxygen reduction (cathodic reaction), as represented in Equation 2-20.

$$\mathbf{2Na_2SO_3 + O_2 \rightarrow 2Na_2SO_4} \qquad \textbf{Equation 2-20}$$

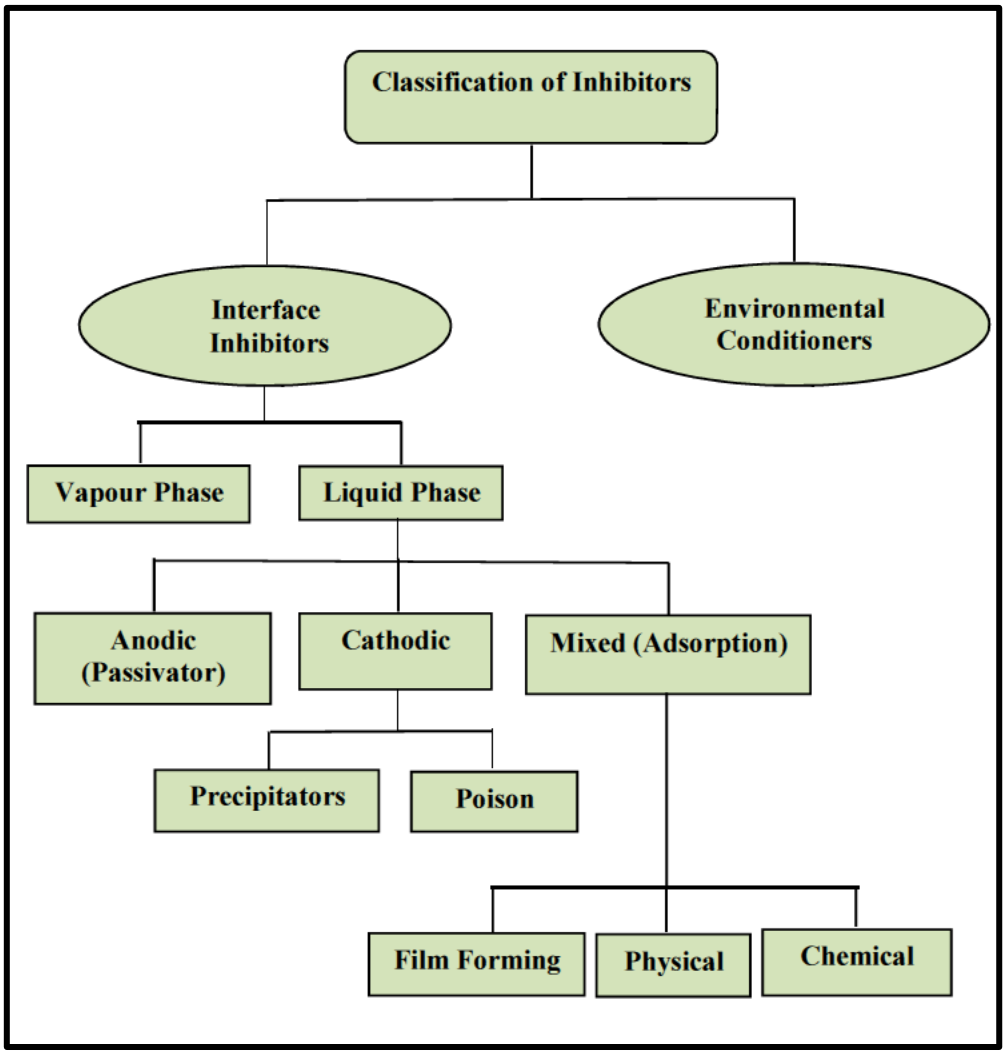

Figure 2-21: Classification of inhibitors. (Papavinasam, 2000)

2.4.1.2 Interface Inhibitors

Interface inhibitors form a diffusion barrier on the metal/environment interface to give rise to resistance of the anodic and cathodic reactions. They can be classified into liquid and vapour-phase inhibitors.

Liquid-Phase Inhibitors

Liquid-phase inhibitors are generally categorized on the basis their chemical functionality in the electrochemical reactions concerned in the corrosion process. Hence, these inhibitors are classified as anodic, cathodic or mixed inhibitors, indicating the inhibited electrochemical reaction(s) respectfully.

Anodic Inhibitors

Anodic inhibitors also called passivating inhibitors work by causing a large anodic shift in the corrosion potential in the noble direction thereby bringing the metallic surface into the passivation range. There are two types of these effective and consequently the most widely used inhibitors, namely:

- Oxidizing anions, such as chromate, nitrite and nitrate that passivates the steel surface in the absence of oxygen.
- Non-oxidizing ions such as phosphate, tungstate and molybdate that requires the presence of oxygen to passivate the steel surface.

Passivating inhibitors are usually used in near-neutral solutions where sparingly soluble corrosion products, such as oxides, hydroxides, or salts, are formed. Papavinasam (2000) argues that the anodic inhibitors form, or facilitate the formation of passivating films that inhibit the anodic metal dissolution reaction. He is also of the view that the critical concentration of these inhibitors for effective inhibition in any corrosive medium depend on the nature and concentration of the aggressive ions. A number of authors also agree that inadequate concentration of anodic inhibitor may accelerate the rate of corrosion rather than reducing it (Roberge, 2000; Ramachandran et al., 2000; Papavinasam et al., 2003).

An inhibitor may decrease the rate of the anodic process, the cathodic process, or both processes. The change in the corrosion potential on addition of the inhibitor is often a useful indication of which process is retarded. Displacement of the corrosion potential in the positive direction indicates mainly retardation of the anodic process (anodic control), whereas displacement in the negative direction indicates mainly retardation of the cathodic process (cathodic control). Little change in the corrosion potential suggests that both anodic and cathodic processes are retarded.

An anodic inhibition mechanism is illustrated in Figure 2-22 which shows an increase in the polarisation of the anode where a positive corrosion potential displacement (shift in the noble direction) accompanied by significant reduction in the corrosion current flow. Adsorption of the inhibitor on the anodic areas also plays a part in the process because it

decreases the current density required for the anode to reach the critical passive potential.

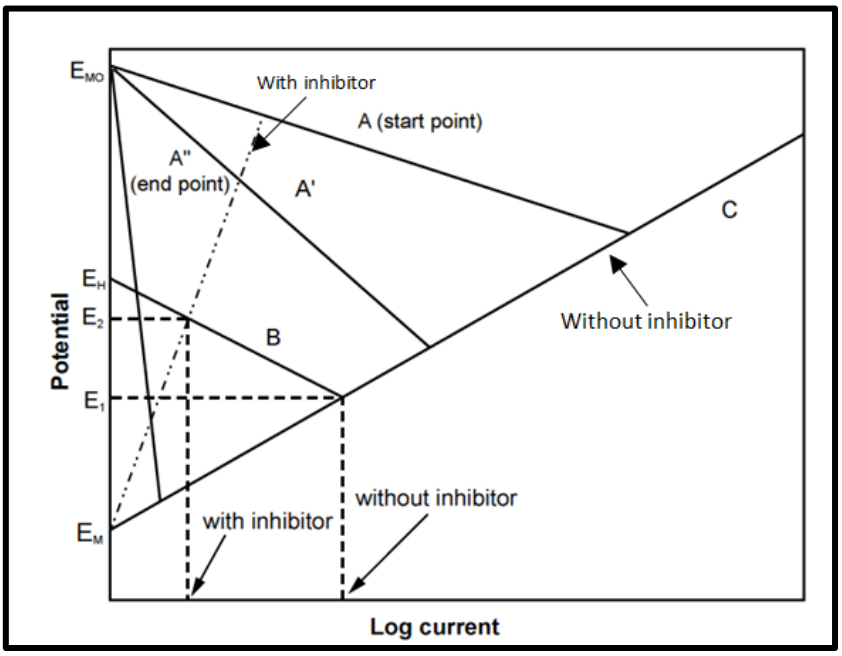

Figure 2-22: The effect of an anodic inhibitor on the dissolution rate of iron and iron oxide (Roberge, 2000)**.**

Cathodic Inhibitors

Cathodic inhibitors control corrosion by either slowing the cathodic reaction process or by selectively precipitating on the cathodic areas to increase the surface impedance and so limit the diffusion of cathodic species to these sites. Cathodic inhibitors can provide inhibition by making the recombination and discharge of hydrogen more difficult or by catalysing cathodic ions such as zinc, calcium to precipitates as oxides on the metal surface.

Inhibition by polarisation of the cathodic reaction can be achieved in several ways such as oxygen scavengers, cathodic poisons and cathodic precipitates. A major drawback in the use of cathodic poisons is that they sometimes cause hydrogen blistering and an increase in hydrogen embrittlement, especially in acid solutions (Papavinasam et al., 2003).

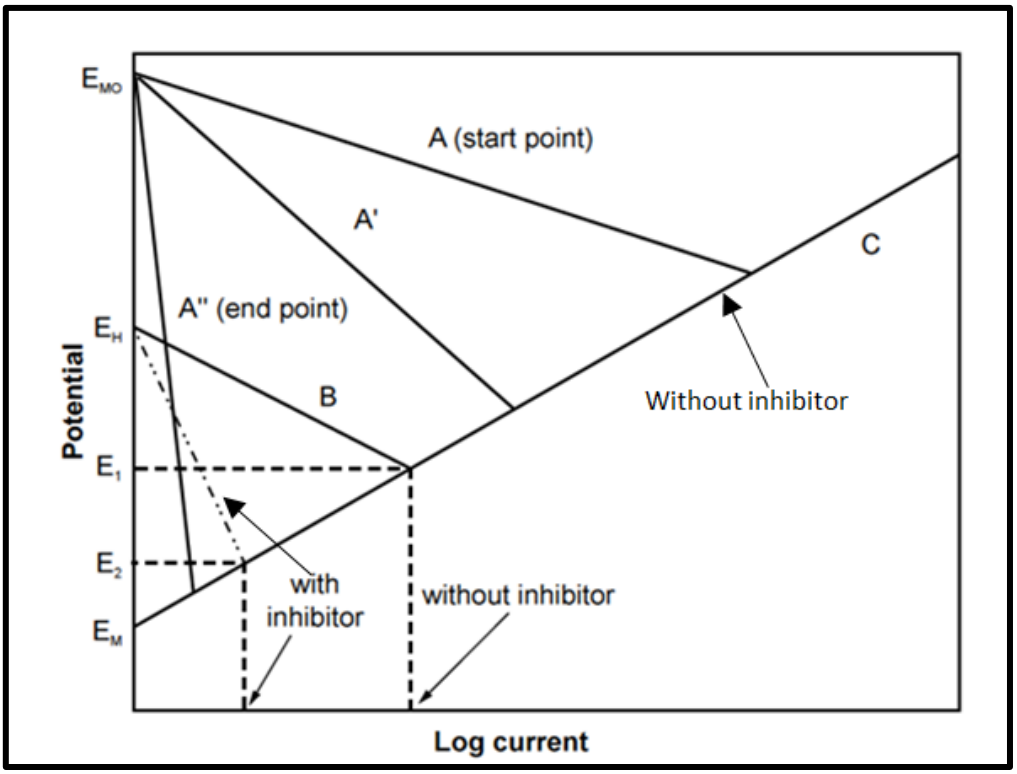

Figure 2-23: The effect of a cathodic inhibitor on the dissolution rate of iron and iron oxide (Roberge, 2000)**.**

Figure 2-23 is a simplified illustration of cathodic inhibition mechanism (Roberge, 2000) which shows a negative corrosion potential displacement (shift in the active potential direction) of the polarization curves, accompanied by significant decrease in the cathodic reduction reaction.

Mixed (Organic) Inhibitors

Mixed (organic) inhibitors suppress the anodic and the cathodic reactions involved in the corrosion process by adsorbing on the metal surface forming a protective layer. It is essential that this inhibitor be present in sufficient concentration for effective inhibition since it is adsorbed unto both anodic and cathodic sites of the metal of concern. Their effectiveness also depends on chemical composition, molecular structure and their affinities for the metal surface (Papavinasam, 2000; Gulbrandsen and Granå, 2007).

Vapour-Phase Inhibitors

These are similar to the organic adsorption-type of inhibitors and possess a very high vapour pressure. They are also called volatile corrosion inhibitors (VCIs), which are transported in a closed system to the site of corrosion by volatilisation from the source. When in contact with a metal surface, the inhibitor vapour condenses and is hydrolysed by any moisture present to liberate nitrite, benzoate and bicarbonate ions. They are usually effective in closed vapour spaces such as shipping containers and boilers because they would be lost rapidly through any leaks in the package or container

2.4.2 Factors Affecting Corrosion Inhibitor Performance

Palmer, Hedges and Dawson (2004) in their report on corrosion inhibition in oil and gas industry assert that selection of effective corrosion inhibitor cannot be achieved without any of following factors, among others:

1. **Partial pressures of CO_2 and H_2S** - the concentrations and total pressures of these gases control fluid corrosivity, rates of general corrosion, sour service criteria and materials selection.
2. **Fluid chemistry** - important factors are scaling tendency, pH and presence of organic acids in sweet systems that may induce pitting corrosion.
3. **Temperature** - higher temperatures influence the degree of scaling and corrosion rates and decrease the adsorption ability of inhibitors.
4. **Fluid composition** - water cut, hydrocarbon gas and condensate contents and oil density and viscosity influence conductivity, holdup, and wetting of steel surfaces.
5. **Flow conditions** - stratified flow, slugging and gas phase flow considerations influence the onset of erosion-corrosion, impingement and erosion that may limit the effectiveness of inhibitors.
6. **Project life cycle costs and perceived risks** - these determine the choice between the use of corrosion resistant materials compared with C-Mn steel plus corrosion inhibition.

7. **Corrosion allowance** - provides an extended time window of operation, a standard mitigation method that requires trending of corrosion inspection and monitoring data when used in conjunction with inhibition in high risk systems.
8. **Management of corrosion control programmes** - most system failures are the result of human error and poor management control procedures.

The performance of a corrosion inhibitor is influenced by many factors including flow rate (wall shear stress), temperature, and surface condition of the pipe. The presence of oxygen has a significant negative influence on the inhibitor effectiveness. In addition, the presence of oxygen in produced fluids or in glycol/methanol injected to control hydrate formation can adversely affect the performance of oilfield inhibitors.

Major factors that are critical to the performance of chemical inhibitors in the offshore oil and gas operations are considered below.

2.4.2.1 Flow conditions

Hydrodynamic characteristics of the pipelines are essential, since the flow patterns (stratified or slugging), pressure drops, water hold-up and water condensation rate, play significant roles in the availability of the chemical inhibitor on the surface of the metal that is being protected. Particular concerns are the development of slugging flow that can adversely affect inhibitor performance, and sand particle impact, that may cause erosion. Slug flow is a transient flow disruption, in that each time a slug passes a point the flow is violently disturbed, but then re-establishes after the slug passes. Efird (2011) simulated this process in the jet impingement test by initiating a step change in the jet flow rate. The change in rate of corrosion was monitored with variation in flow. The results presented in Figure 2-24, for assessment of two chemical inhibitors on carbon steel in a typical offshore service condition, show that large step increase in wall shear stress is accompanied by sharp escalation of corrosion rate. An effective asset management program using chemical inhibitor therefore demands that the flow characteristics or type of flow patterns anticipated throughout the lifetime of the pipe have to be assessed and the shear stress range determined.

Nesic et al (2002) corroborate the observation of Efird (2011). They reported that intense flow can mechanically remove protective corrosion film, resulting in increase of corrosion rate and in addition, localised corrosion may also take place.

Mora-Mendoza et al. (2002) reported higher corrosion rates when flow velocity was increased using a rotating cylinder electrode (RCE) in the presence of an inhibitor. They concluded that when the rotation speed increases, changes in the corrosion potential (E_{corr}) to more positive values could create a positive charge on the metal surface that forces the inhibitor to be removed, especially if the inhibitor was adsorbed by electrostatic attraction.

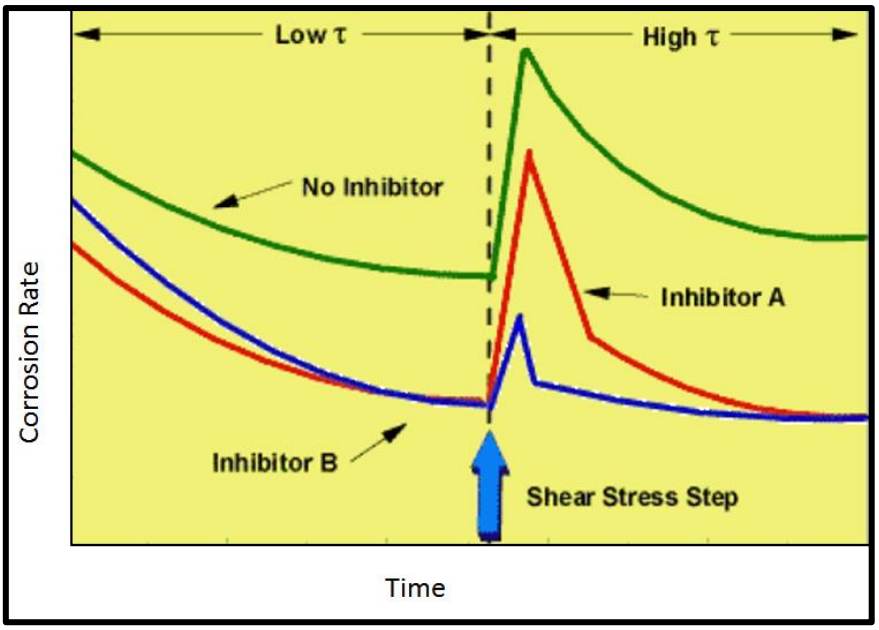

Figure 2-24: Effect of a large step increase in wall shear stress on corrosion rate (Efird, 2011)**.**

In another related study, it was found that the efficiency of corrosion inhibitors in flowing media depends on local flow intensities (Schmitt et al., 2002), which can be quantified in terms of wall shear stress. Critical flow intensities can be defined as the highest wall shear stress up to which no flow induced localised corrosion occurs under specific system conditions. The critical flow intensity varies from one inhibitor to another depending on the adsorption strength of the inhibitor to the metal surface.

Figure 2-25(a) shows that above critical flow intensities the inhibitors lose their efficiency. Under these conditions the materials surface is subject to flow induced localized corrosion. Figure 2-25(b) shows that critical flow intensities initiation can also depend on the inhibitor concentration, which is determined by the chemical structure of inhibitor compounds and formulation of inhibitor packages.

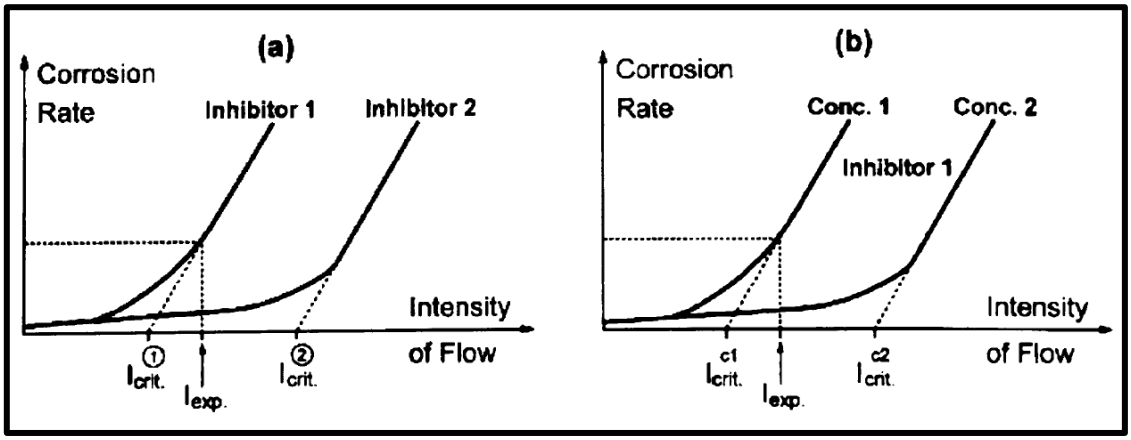

Figure 2-25: Effect of flow intensity on corrosion inhibitor performance (Schmitt et al., 2002)**.**

2.4.2.2 Inhibitor Concentration

It is essential that corrosion inhibitor be available in sufficient quantity all over the surface of the facility being protected throughout the service life in order to ensure adequate protection of the asset. This minimum concentration is required to be maintained both for the initial operation and also during the service life so that inhibitor depletion will not lead to localised corrosion attack. Research has shown that insufficient inhibitor can lead to corrosion that is more severe than if no inhibitor was in place (Nešić, 2007). Inhibitor concentration depends on factors such as economics, disposal problems and availability of devices for monitoring inhibitor concentration (Roberge, 2000; Heidersbach, 2011; Papavinasam, 2000). The importance of hydrodynamic characteristics on the availability of inhibitor had been shown in Figure 2-25(b).

The effect of sequential increases in the concentration of corrosion inhibitor at constant wall shear stress on the corrosion rate of steel as observed by Efird (2011) is shown in Figure 2-26. The corrosion inhibitor reduces the corrosion rate differently for the two corrosion inhibitors shown as the corrosion inhibitor concentration increases. The minimum corrosion inhibitor concentration with a reasonable efficiency, or giving the maximum allowable corrosion rate, is the critical corrosion inhibitor concentration required for the system under test.

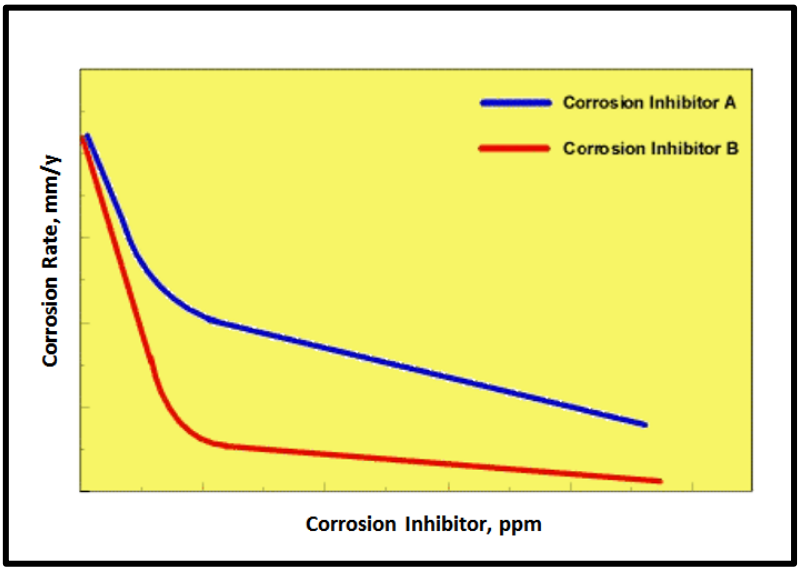

Figure 2-26: Effect of sequential increases in corrosion inhibitor concentration at a fixed wall shear stress (Efird, 2011)**.**

Altoe et al (1996) studied the persistence of the inhibitor film in flowing media containing CO_2 with electrochemical impedance spectroscopy. They concluded that the stability of the inhibitor film is flow dependent and is strongly affected by the residual concentration of the inhibitor in the solution. The latter suggests that it is essential to regenerate the inhibitor film, especially at high flow velocities for effective inhibitor performance.

2.4.2.3 Nature of the Metal

The importance of carbon and low alloy steel chemical composition and microstructure on the inhibition of CO_2 corrosion has been widely recognized. Nevertheless, the effect of these variables on the corrosion product film formation and properties on inhibitor efficiency are far from being understood (Palmer et al., 2004). Several authors have studied the influence of steel microstructures on the corrosion process in aqueous solutions containing CO_2; but there is no general agreement on this issue (Roberge, 2000). This is mainly due to the complexity of the mechanisms involved as reported by Lopez and Simison (2005) . In addition, test conditions also vary widely, making them almost impossible to compare (Ramachandran et al., 2000).

Steel microstructure and surface features are mainly determined by the chemical composition and on the fabrication process. The resulting array of microstructural phases (predominantly: ferrite, pearlite, bainite, martensite) can affect the mechanical properties as well as the corrosion resistance of the material and inhibitor efficiency (Nešić, 2007).

Lopez and Simison (2005) analysed the microstructural characteristics (morphology, thickness and composition) of corrosion layers formed on carbon steel with two different microstructures (annealed, and quenched and tempered). Their conclusion is that the microstructure of steel influences inhibitor efficiency, the morphology of the corrosion layers, and the quantity of the various chemical compounds that are present. They also demonstrated that not only the molecular structure of the inhibitor molecule is important when determining its performance in chloride media saturated with CO_2, but also the microstructure of the steel to be used as the working material.

Paolinelli, Perez and Simison (2008), investigated the role of steel microstructure and nature of the metal surface. In order to evaluate the susceptibility of carbon steel sweet corrosion and inhibitor performance, The experimental condition was a ‘pre-corrosion’ period of 72 hours and addition of 1%Cr content. The results show that pre-corrosion and Cr addition have detrimental effect on corrosion inhibitor, due to the presence of chromium-rich compounds which slows down the inhibitor adsorption and hence inhibitor efficiency. Other authors (Mora-Mendoza et al., 2002; Gulbrandsen et al., 1998; McNaughtan and Winning, 2004) have alluded to this and shown that pre-

corrosion has a remarkable detrimental effect on the performance of commercial inhibitors.

Turgoose and Palmer (2005) in a related work pointed out that the major factor affecting the inhibitor performance on the weld metal is the pre-corrosion time and not the test geometry. The experimental methodology involves 4 days of pre-corrosion in a thin film set-up and for 4 hours of pre-corrosion in a bubble test cell. The results showed that after 4 days of pre-corrosion, in thin film tests the inhibitor did not protect the weld. However, bubble tests with only a few hours of pre-corrosion did give protection of the weld metal. To clarify the cause of this, the authors carried out bubble tests with long-term pre-corrosion, and again the inhibitor failed to sufficiently protect the weld metal. Severe selective attack on the weld metal was observed while the other regions of the weld remained protected. This can occur with under dosing of the inhibitor, and is therefore significantly affected by the extent of pre-corrosion of the weldment before inhibitor addition.

Surface finish of the metal (smoothness and cleanliness) can also affect the performance of the inhibitor. For instance, clean and smooth surfaces usually require a lower concentration of inhibitor for a good protection compared to dirty or rough surfaces. In addition, the presence of oil, wax, grease or corrosion products on metal surfaces will influence the concentration of inhibitor required optimum corrosion rate of the metal and therefore it is important to consider these effects so as to prevent localised corrosion attack (Heidersbach, 2011).

In a research at Cranfield University, Omonua (2004) investigated the effects of environmentally-friendly inhibitors under stagnant conditions. The study showed a change in the direction of corrosion current flow when inhibitor was added to polished and pre-corroded surfaces, leading to PWC of the weld metal and HAZ with respect to the parent metal. He argued that the change in polarity can be attributed to the nature of the corrosion product from general and galvanic corrosion, where the inhibitor.

Corrosion inhibitors may often be less effective in corroded pipelines, particularly those that are old or heavily pitted, and in pipelines that contain large amounts of debris, such as corrosion products, sand and scales. In these cases cleaning by scraper pigs and use of high dosage rates of inhibitor are often required.

2.4.2.4 Temperature

Temperature is an important factor that influences inhibitor performance due to its affects not only on the inhibitor but also the medium, and the corroding material. Temperature affects the physical as well as the chemical structure of inhibitors. Gulbrandsen et al. (1998) observed that inhibitor performance was impaired with increasing pre-corrosion time and increasing temperature. The commercially available water soluble corrosion inhibitors for CO_2 corrosion have been tested in the laboratory on carbon steel specimens that were corroded for up to 18 days in the medium prior to inhibitor addition. The tests were performed at 20-50ºC, pH 5, 1 bar CO_2, 1-3 wt% NaCl in glass cells and a glass loop. The results show that inhibitor performances were impaired with increasing temperature and pre-corrosion time.

In general, inhibition should not be a problem in systems with low pressures, low temperatures and low flow rates, the exceptions being under-deposit corrosion and bacterial induced corrosion in low velocity pipelines. Systems with high temperatures, high velocities or high CO_2 pressures have lower inhibitor efficiencies and require high inhibitor availability and the use of more 'tenacious' inhibitors.

2.4.3 Evaluation of Carbon Dioxide Corrosion Inhibitors

Corrosion inhibition is conventionally used to mitigate preferential weld corrosion (PWC) in service environments containing CO_2; nevertheless, many studies have advanced some evidences to prove that some corrosion inhibitors may increase preferential weld corrosion (Winning et al., 2004; Alawadhi and Robinson, 2011; Marsh et al., 2009; Palmer et al., 2004; Mora-Mendoza et al., 2002; Paolinelli et al., 2008; Nesic et al., 2004). For instance, Palmer et al (2004) are of the opinion that failures of nickel containing weldments in aqueous CO_2 service environment are primarily a consequence of the inability of some inhibitors to penetrate a nickel rich corrosion product on the weld metal in comparison to effective protection of unalloyed parent pipe. The consequent potential difference between the unprotected weld and the adjacent inhibited parent metal can lead to rapid localised attack of the weld metal. An example of this type of problem is reported by Palmer (2006) as illustrated in Figure

2-27. The figure shows weldments from a high water cut pipeline in which preferential attack of the weld metal occurred downstream of the inhibitor injection point, while welds upstream of inhibitor injection corroded uniformly.

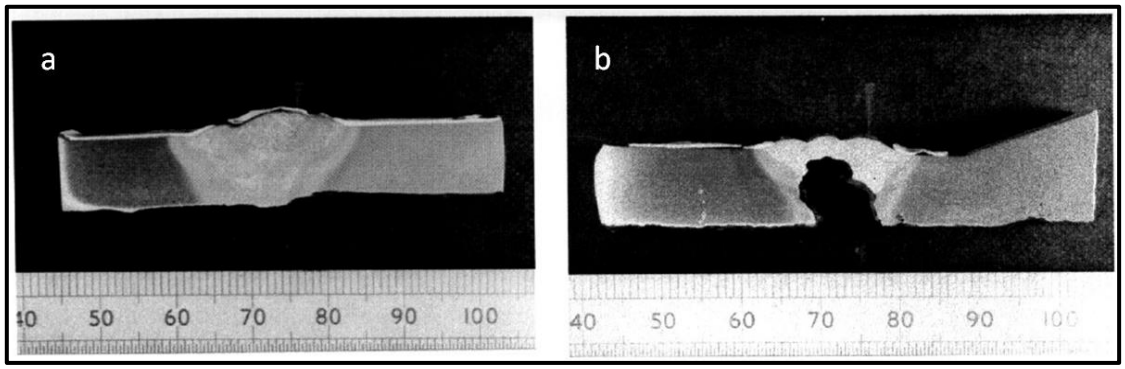

Figure 2-27: Preferential corrosion of a weld downstream of inhibitor injection (b) compared to uniform attack upstream of the injection point (a). (Palmer, 2006)

Furthermore, many studies on the performance of preferential weld corrosion inhibitors suggest that it is not possible to differentiate between those systems that are prone to PWC and those that are not or to understand the apparent ineffectiveness of some corrosion inhibitors at high flow rates (Mahajanam and Joosten, 2011; Lee and Woollin, 2005; Barker et al., 2013).

McIntyre et al (2014) studied corrosion inhibition of PWC of X65 carbon steel water injection pipeline using the metallurgical condition of the welds and the inhibitor concentration as independent variables. The study used Tafel polarisation and electrochemical noise tests on multi-electrode assemblies fabricated from sections of the PM, the HAZ and the WM (Figure 2-17) in simulated seawater treatment system sparged with natural gas, 2% CO_2 and 150 ppm of H_2S. In welds susceptible to PWC, adequate corrosion inhibitor concentration is effective in reducing galvanic corrosion, due to the shifts in the relative corrosion potentials. However the inhibitor efficiency depends on the inhibitor dosage, while under-dosage increased the corrosion rate. Low energy weld was also found to be less susceptible to galvanic corrosion compared with high energy weld, since segregation increases with dendrite in high energy input mode.

2.5 Corrosion Evaluation Techniques

Corrosion tests are performed to determine the suitability of equipment, materials, and chemicals among others, for use in field applications. Evaluation of operating procedure and / or process may also be conducted to effectively manage corrosion rate of the system or a specific component. These tests are often performed in laboratories, but may also involve field trials.

Performance in a specific environment requires simulation of that environment as accurately as possible. The constraints of time and test equipment often make this difficult. The issue then becomes, what criteria are required for the flow accelerated corrosion (FAC) testing that effectively simulates the effect of flow in the operating system.

2.5.1 Correlation of Laboratory Data with Field Service Conditions

Fluid velocity has long been used as the primary parameter for comparison of laboratory test results to field applications, but this concept began to change in 1977 when Efird published the first data relating the calculated hydrodynamic parameter of wall shear stress to corrosion for copper alloys in flowing water (Efird, 1977). It is now generally accepted that FAC must be expressed in terms of geometry-independent fluid flow parameters common to all hydrodynamic systems to allow application of laboratory test data to operating systems (Zhang and Cheng, 2010; Hausler and Schmitt, 2004; Efird, 2011; Schmitt and Bakalli, 2010). The parameters used most frequently are the wall shear stress, (τ_ω) and the mass transfer coefficient, (k_d), which can be calculated from empirical equations developed to characterize fluid flow.

Figure 2-28 shows the fundamental process of relating laboratory fluid flow corrosion data to field applications (Efird et al., 1993). To allow correlation with operating systems in the field, laboratory corrosion tests must be conducted in a manner that allows calculation of the basic geometry independent hydrodynamic parameters such as, mass transfer coefficient and wall shear stress. The laboratory corrosion rates are then

applied to the facility operating system for identical calculated parameters. The basic assumptions are that:

- the parameter calculation is valid,
- the calculated parameters are those controlling corrosion or are directly related to them,
- the structure of the turbulence in the laboratory system is similar to that of the field system, and
- the scale up of these parameters to facility operations with respect to flow accelerated corrosion is valid.

Both wall shear stress and mass transfer coefficient meet these basic criteria. Furthermore, it is essential that experimental test design and techniques be carefully planned to allow accurate calculation of the hydrodynamic parameters for effective study of flow accelerated corrosion.

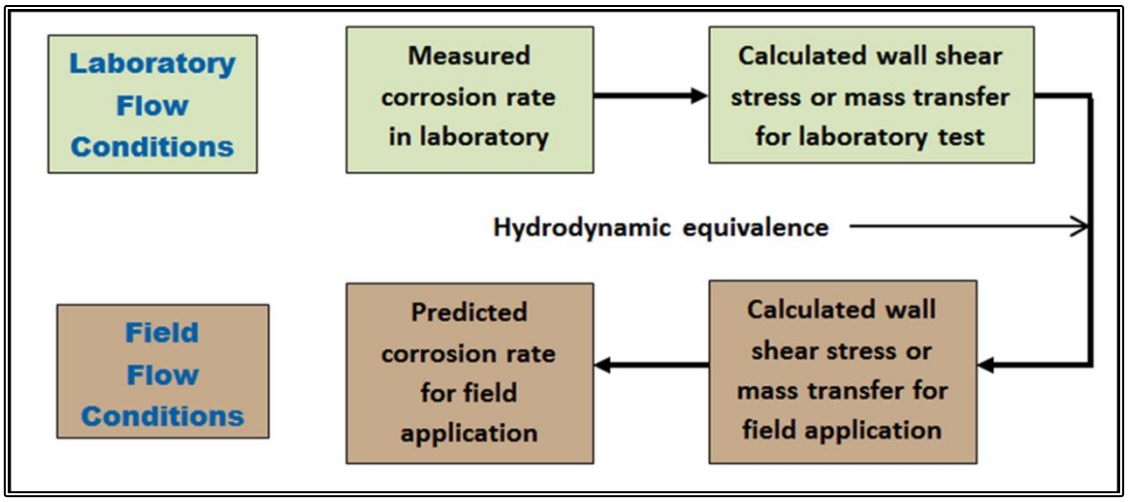

Figure 2-28: The process of relating laboratory data to field corrosion rate using hydrodynamic conditions (Efird et al., 1993)**.**

2.5.2 Electrochemical Techniques

Corrosion monitoring techniques can be classified into two major categories: non electrochemical techniques and electrochemical techniques. Traditionally the non-

electrochemical techniques are widely used through the industry due to their simplicity, robustness and reliability. However, the drawback of these techniques is that they do not reveal any details about corrosion mechanisms. Conversely, the electrochemical measurements provide a much more details with regard to the corrosion mechanism. In addition, electrochemical methods are preferred when test (measuring) time, high measurement accuracy, and the possibility of continuous corrosion monitoring are crucial.

Electrochemical corrosion rate monitoring techniques that are commonly used in corrosion studies include:

- Linear polarisation resistance
- Zero-Resistance Ammetry
- Potentiodynamic Polarisation
- Tafel extrapolation
- Electrochemical noise
- AC impedance spectroscopy

Linear polarisation resistance (LPR), zero-resistance ammetry and potentiodynamic polarisation are the techniques used in this work and also reviewed below.

2.5.2.1 Linear Polarisation Resistance

The linear polarisation resistance (LPR) technique is an electrochemical method that uses either three or two sensor electrodes. In this technique, a small potential perturbation (typically of the order of 10-20 mV) is applied to the sensor electrode of interest, and the resulting direct current is measured. A typical hypothetical LPR plot is shown in Figure 2-29. The ratio of the potential to current perturbations, known as the polarisation resistance, is inversely proportional to the uniform corrosion rate. The accuracy of the technique can be improved by measuring the solution resistance independently and subtracting it from the apparent polarisation resistance value.

The polarization resistance of a material is defined as the slope of the potential–current density ($\Delta E/\Delta i$) curve at the free corrosion potential (Figure 2-29). This yields the

polarization resistance Rp, which can be related to the corrosion current using Equation 2-21.

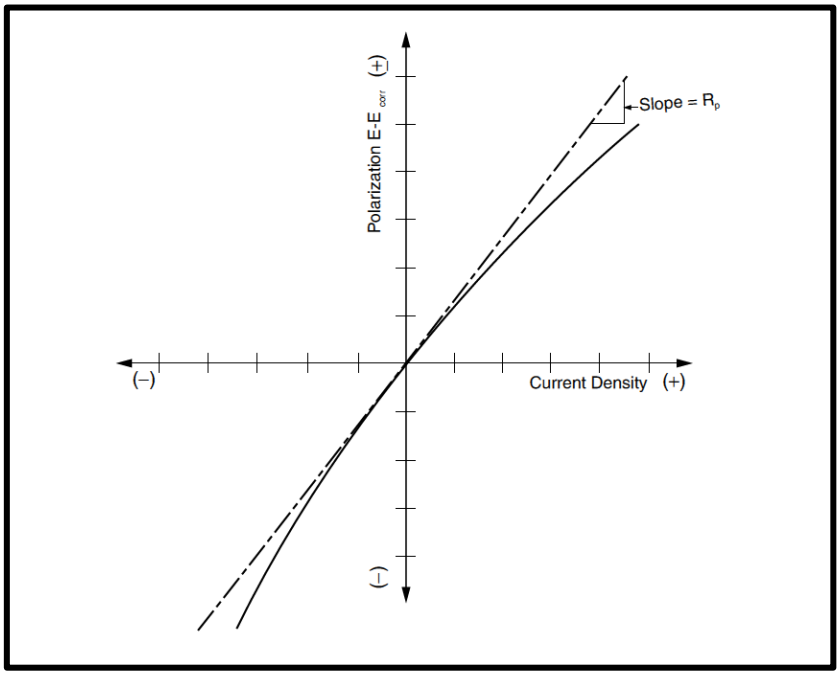

Figure 2-29: Hypothetical linear polarisation resistance plot (Baboian, 2002)**.**

$$\mathbf{R_p} = \frac{\boldsymbol{B}}{\boldsymbol{i_{corr}}} = \frac{\mathbf{\Delta E}}{\mathbf{\Delta i}}$$

Equation 2-21

Where R_p = polarisation resistance (Ωcm^2)

i_{corr} = corrosion current (A/cm^2)

B = empirical polarisation resistance (Stern-Geary) constant that can be related to the anodic (b_a) and cathodic (b_c) Tafel slopes with Equation 2-22:

$$\mathbf{B} = \frac{\mathbf{b_a b_c}}{\mathbf{2.3(b_a + b_c)}}$$

Equation 2-22

The Stern-Geary constant is dependent on the corrosion system and can also be directly measured in separate experiments (Hedges et al., 2006).

The corrosion current evaluated from Equation 2-21 is usually expressed in penetration rates using Faraday's law Equation 2-23:

$$\textbf{Corrosion Rate} = \frac{\mathbf{0.0033\ i_{corr}\ EW}}{\mathbf{d}}$$

Equation 2-23

EW = the equivalent weight of the element (material) being oxidised,

d = density of the element (material) being oxidised.

Such that for carbon steel (Fe) oxidised to Fe^{2+}, the corrosion rate

$$\mathbf{1\ \mu A/cm^2 \equiv 0.012\ mm/y}$$

Equation 2-24

Linear polarisation resistance (LPR) measurements are widely used in corrosion assessments, including the following:

- Studies of the effect of environment variables on corrosion rate. These include changes in composition, velocity, and temperatures.
- Evaluation of inhibitors in controlling corrosion.
- Comparison of the corrosion rates of various alloys of similar composition in a given environment.
- Determination of changes in corrosion rate with time, including studies of underground structures as well as materials in aqueous solutions.
- It also may be possible to evaluate the condition of coatings in service which cannot be inspected by visual methods.

However, there are complications associated with performing polarization measurements. According to Roberge (2000), the major difficulties include:

- **Effect of scan rate**. The rate at which the potential is scanned may have a significant effect on the amount of current produced at all values of potential.

The rate at which the potential is changed, the scan rate, is an experimental parameter over which the user has control. If not chosen properly, the scan rate can alter the scan and cause a misinterpretation of the features.

- **Effect of solution resistance**. The distance between the Luggin probe (of the salt bridge to the reference electrode) and the working electrode is purposely minimized in most measurements to limit the effect of the solution resistance.
- **Changing surface conditions**. Since corrosion reactions take place at the surface of materials, when the surface is changed as a result of processing conditions, active corrosion, or other reasons, the potential is usually also changed. This can have a strong effect on the polarization curves.
- **Determination of pitting potential**. In analysing polarization curves, the appearance of a hysteresis (or loop) between the forward and reverse scans is often thought to denote the presence of localized corrosion (pitting or crevice corrosion). This observation is particularly valid when the corrosion potential is higher or more noble than the pitting potential.

2.5.2.2 Zero Resistance Ammetry (ZRA)

In zero-resistance ammetry (ZRA), galvanic currents are usually measured between dissimilar materials. The dissimilarities between the sensor elements may be related to different compositions, heat treatments, stress levels, or surface conditions. The technique may also be applied to nominally identical electrodes, to indicate changes in the corrosive environment and serve as a broad indicator of changes in corrosion rate.

However, the measured currents may not represent actual (service field) galvanic corrosion rates, as this form of corrosion is highly dependent on the anode / cathode area ratio. In addition, an increase in current readings is not always directly associated with an actual increase in corrosion rates. Hence, galvanic measurements should be used with data from other techniques.

2.5.2.3 Potentiodynamic Polarisation

This method is best known for its fundamental role in electrochemistry in the measurement of Evans diagrams. A three-electrode corrosion probe is used to polarise the electrode of interest. The current response is measured as the potential is shifted away from the free corrosion potential. The basic difference from the LPR technique is that the applied potentials for polarization are normally stepped up to levels of several hundred millivolts. These polarization levels facilitate the determination of kinetic parameters, such as the general corrosion rate and the Tafel constants. The formation of passive films and the onset of pitting corrosion can also be identified at characteristic potentials, which can assist in assessing the overall corrosion risk.

A major advantage of this technique is that kinetic information and an overall picture of the material's corrosion behaviour can be obtained relatively quickly (compared to, say, coupon exposures). However, these techniques are usually limited to laboratory studies, as specialized skills are required to interpret the data. The applied polarization levels may change the sensor surface irreversibly, especially if pitting damage is induced in the anodic cycle. These measurements are generally applicable only to fully immersed probes in conducting solutions.

2.6 Techniques for Evaluation of Flow Accelerated Localized Corrosion

Generally, there are two reasons for conducting flow corrosion tests. The first is to make a comparison under high turbulence conditions. The second is to simulate the flow turbulence in an operating system. The former is fairly straight forward in that only the generation of high turbulence in the test is required. The second is much more complex as it requires flow simulation.

There are a number of test methods that have been employed over the years to investigate the effects of flow on corrosion. For the purpose of this work, only test methods that are conventionally used are considered. These are:

- Recirculating Flow Loops
- Rotating Cylinder

- Rotating Cage
- Submerged Jet Impingement

2.6.1 Recirculating Flow Loops

Recirculating flow loops are the most basic tests for investigating flow effects in piping systems since they essentially duplicate pipe flow. They consist of piping systems that recirculate the test fluid from a reservoir through a designed test section. The test section contains the coupons and/or electrochemical electrodes to measure the effect of the flow on corrosion. The electrically insulated coupons/electrodes may be full pipe sections or plugs mounted in the pipe wall. The primary requirement in the design of the test section is that the test coupons/electrodes are in an area of established flow. Equations for mass transfer and wall shear stress are well established, however, the construction and operating costs are high.

2.6.2 Rotating Cylinder Electrode

The rotated cylinder electrode (RCE) can be arranged as a free rotating cylinder or as a rotating cylinder in a static coaxial housing. The rotated cylinder has the advantage that the complete flow regime from laminar to turbulent can be tested in the same arrangement.

Figure 2-30 shows the RCE assembly used recently by Alawadhi and Robinson (2011) for the study of preferential weld corrosion of X65 pipeline steel in flowing brines containing carbon dioxide. The RCE consisted of hollow cylindrical samples, which were machined from each region of the weld (parent material, heat affected zone and weld metal) and has wires attached to carry the electrochemical signals. The three component parts were electrically isolated from each other by polytetrafluoroethylene (PTFE) spacers assembled onto an insulated shaft and secured with a retaining nut.

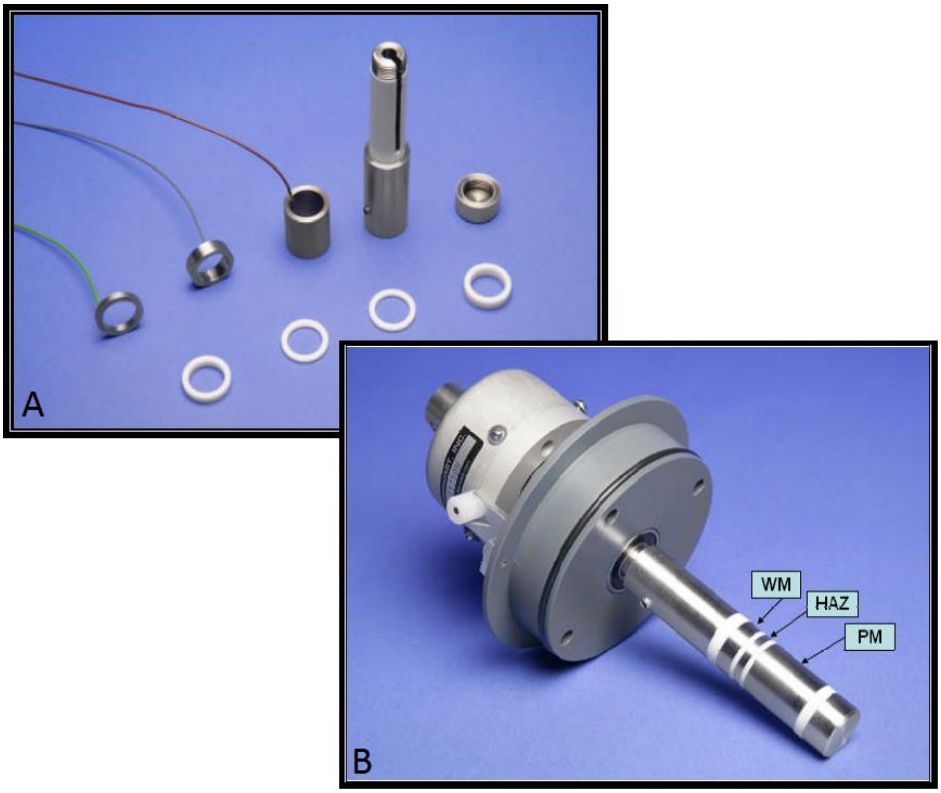

Figure 2-30: Rotating cylinder electrode showing (A) component parts and (B) complete assembly (Alawadhi and Robinson, 2011)**.**

2.6.3 Rotating Cage

This test method is widely used as a screening tool for corrosion inhibitor evaluation for resistance to high turbulence conditions. The rotating cage provides a "worst case" scenario, since it provides very high turbulence conditions, including leading and trailing edge turbulence.

The rotated cage arrangement of coupons has the advantage that different alloy compositions (up to eight) could be tested in the same experiment with the same inhibitor under high pressure and elevated temperatures. Major weaknesses of rotating cage are:

- Electrochemical tests cannot be used
- Equations for mass transfer and wall shear stress are not available.

2.6.4 Submerged Jet Impingement Test

Submerged jet impingement is used for flow corrosion testing due to the hydrodynamic characteristics of a jet impinging on a flat plate as shown in Figure 2-31. The fluid flow across the flat surface contains characteristic flow regions that are mathematically definable, and the equations for mass transfer and wall shear stress are well established. Placing the working electrode of the test probe at a specific radial location in the jet allows measurement of the corrosion rate under those specific conditions. The result when the test ring is properly placed is the ability to accurately and reproducibly measure corrosion rates under defined wall shear stress conditions.

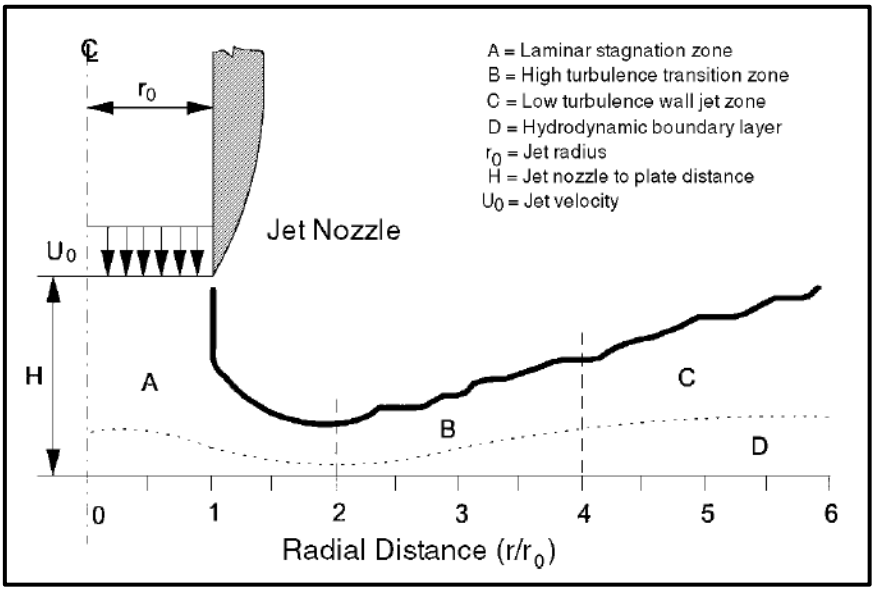

Figure 2-31: Hydrodynamic characteristics of jet impingement on a flat plate showing the four typical flow regions (Efird, 2000)**.**

2.6.4.1 Hydrodynamic Characteristics of Submerged Jet Impingement

Submerged jet impingement is one of the major techniques used to study flow accelerated corrosion. Figure 2-31 shows the four characteristic flow regions when a circular submerged jet impinges on a flat plate with its central axis normal to the plate surface (Efird, 2000). The distinct hydrodynamic regions are:

i. The Laminar Stagnation Region

Flow is laminar near the surface of the plate and the major velocity component is changed from axial to radial with a stagnation point at the centre. This region extends from the centre axis to the point of maximum velocity and minimum jet thickness at about r/r_o (radial distance) ≈ 2 (where r_o equals the jet radius).

ii. The High Turbulence Transition Region

The laminar flow rapidly develops into a wall jet, with the principal flow vector parallel to the plate surface. This region extends to a radial distance of about 4, and is characterised by high turbulence, a large velocity gradient at the wall, and high wall shear stress. Dawson et al, (1999) reported that the shear stress and the mass transfer coefficient reach maximum values within this transition region. Secondly, the fluid flow momentum is transferred toward the pipe wall in contrast to the one transferred away from the wall in the wall jet region C. This was corroborated in a study conducted by Efird et al (1993) as shown in Figure 2-32,. Region B is therefore of utmost importance for appraising the effect of flow on corrosion in high turbulence areas.

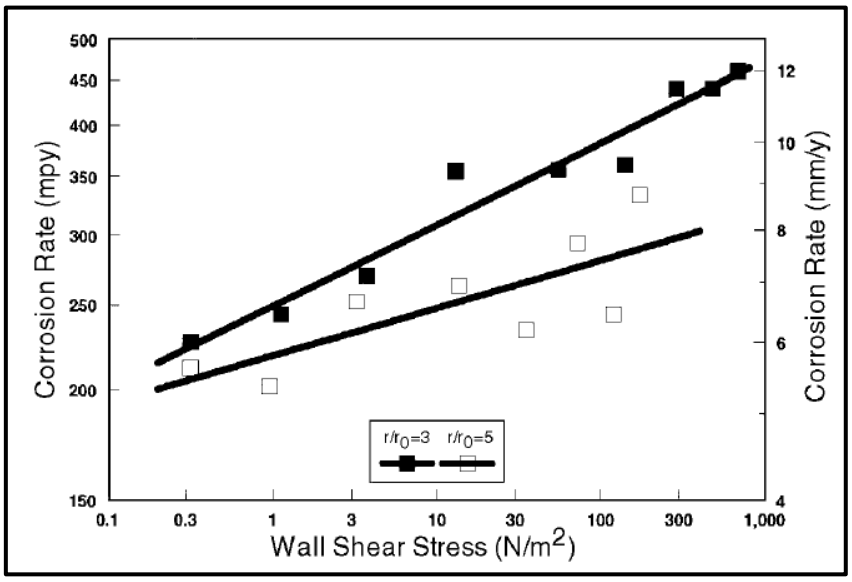

Figure 2-32: Corrosion rate of the C-steel as a function of τ_ω value for jet impingement with test rings at r/r_o = 3 and r/r_o = 5 (Efird et al., 1993)**.**

iii. The Low Turbulence Wall Jet Region

In region C as shown in Figure 2-31, the bulk flow rate and turbulence decrease rapidly as the thickness of the wall jet increases, momentum is transferred away from the plate, and the surrounding fluid is entrained in the jet.

iv. The Hydrodynamic Boundary Layer

The hydrodynamic boundary layer (region D) near the solid / fluid interface is where majority of changes in fluid stress, turbulence, mass transfer and fluid interaction with the wall occur.

2.6.4.2 Computational Fluid Dynamics Simulation of Submerged Jet Impingement

Zhang and Cheng (2010) investigated a computational fluid dynamics (CFD) simulation of flow-accelerated corrosion of an X65 pipeline steel on micro-electrodes installed on an impingement jet system. The CFD simulation was performed using a commercial software package of "Solidworks 2009". Figure 2-33 shows the experimental set-up of the micro-electrodes for the FAC test at various impact angles. The fluid was assumed to be incompressible, and a k-ε turbulent model was used to numerically solve all simulation, where k refers to the turbulent kinetic energy and ε refers to its local rate of dissipation. Turbulence intensity was set at 10%. The turbulent kinetic energy, k, was set as 1 J/kg and the turbulent dissipation, ε, was 1 Wkg for simulation. The initial and boundary conditions for CFD simulation included:

a) Inlet: a flow of aqueous solution with a velocity of 3 m/s.
b) Outlet: an environment pressure of 101,325 Pa.
c) The grid resolution: 0.4 mm.
d) Solid wall: the wall could be approximately considered as an adiabatic wall with a roughness of 10 μm, and the surface of electrode was also set at 10 μm.
e) Flow type: turbulent flow as calculated.

The CFD simulation shows that there are quite distinct flow velocities and shear stresses in different regions along the radial direction under a normal impact of the impinging fluid. The observation agrees with the results obtained in similar studies (Efird, 2000;

Fang and Liu, 2004; Schmitt and Mueller, 1999; G.Schmitt and M.Bakalli, 2009). The electrode under the impinging flow is generally divided into four regions: a central laminar region, a transition region, a wall jet region, and a boundary layer region. In the centric region where the micro-electrode 4 is located, the flow is essentially laminar on the electrode surface, and the principal velocity component is changing from axial to radial, with a stagnation point at the centre. The shear stress, which is the isothermal loss due to fluid friction resulting from contact with a stationary wall, is low at this region, as illustrated in Figure 2 34.

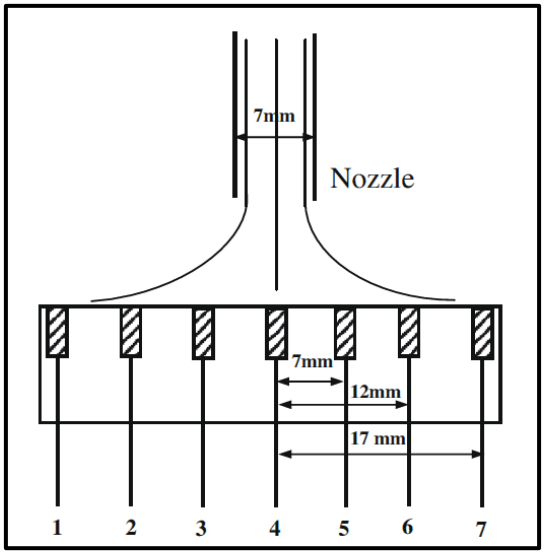

Figure 2-33: Experimental set-up of micro-electrodes under fluid impingement. (Zhang and Cheng, 2010)

Increase in the radial distance to transition region is accompanied with rapid increase in the fluid flow velocity which peaks at about x/d = 1 (x is the radial distance from the centre of the electrode and d is diameter of the jet nozzle). The shear stress increases to a maximum value, with enhanced turbulence intensity over the electrode surface. The flow pattern is featured with a high turbulence, a large velocity gradient at the electrode surface, and a high shear stress. It is therefore unexpected that the mass transfer rate in transition region is higher compared with the laminar stagnation region. Hence, the

transition region is of primary interest for studying fluid flow effects on corrosion in high turbulence areas. In this work, micro-electrodes 3 and 5 are located in this region.

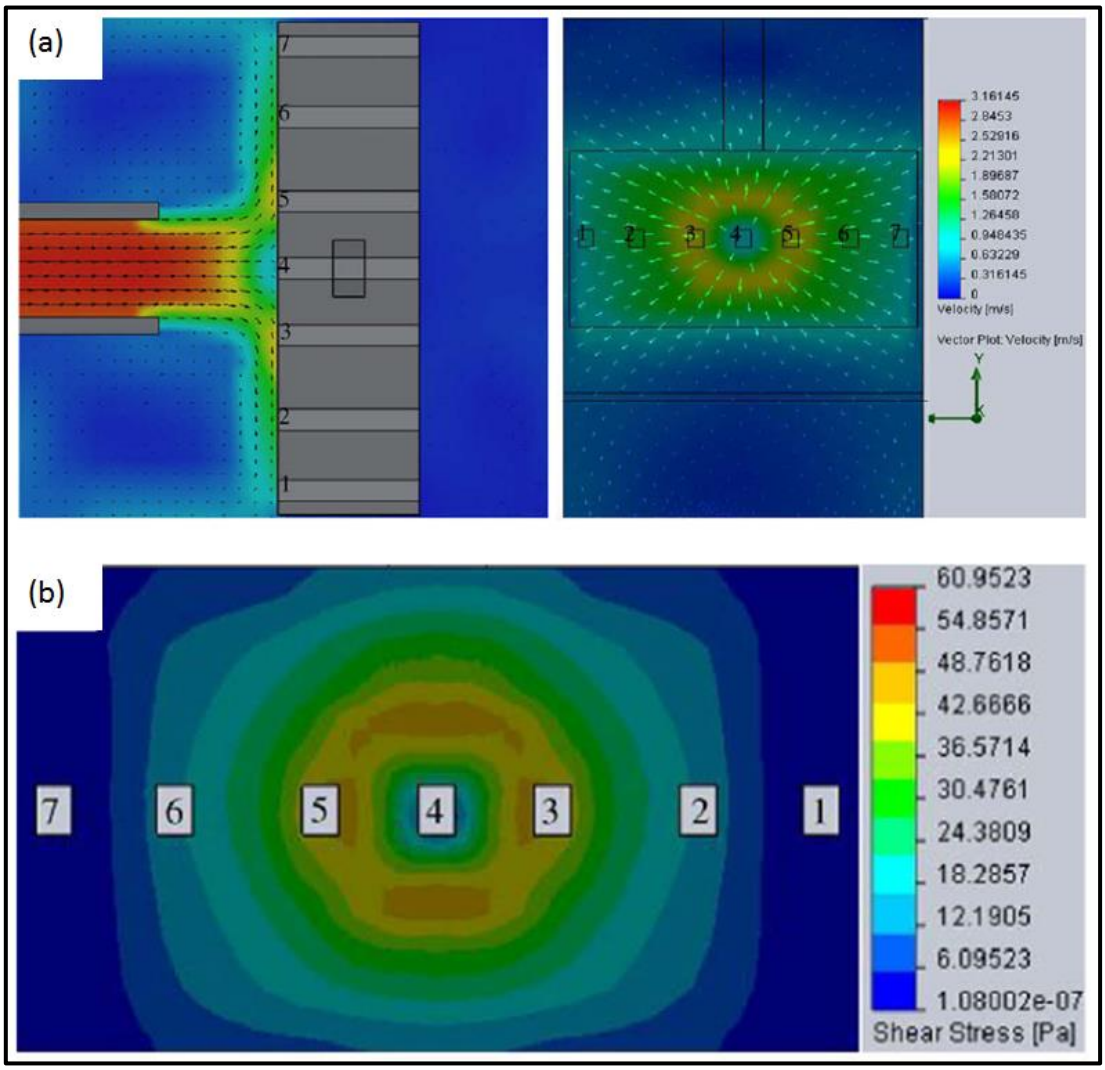

Figure 2-34: (a) fluid flow field distribution and (b) shear stress distribution on the micro-electrodes at 90° impact angle with a flow velocity of 3 m/s (Zhang and Cheng, 2010)**.**

At further radial distances away from the centre, (d > 2), the fluid flow velocity and turbulence intensity decay as the thickness of the wall jet increases and the surrounding fluid is entrained in the jet. The shear stress also decreases with the increase of the radial distance. The decreasing mass transfer rate and shear stress result in a decrease of

corrosion rate of the steel. At the boundary layer region, the flow velocity and the resulting shear stress further decrease, resulting in decreasing corrosion rate of the steel.

2.6.4.3 Flow-Accelerated Corrosion and Wall Shear Stress

Efird et al (1993) studied the relationship between laboratory fluid flow corrosion test techniques to field data and proposed Equation 2-25 as flow-accelerated sweet corrosion rate (R_{corr}) of carbon steel under turbulent flow conditions.

$$R_{corr} = a\tau_{\omega}^{b} \qquad \textbf{Equation 2-25}$$

Where τ_{ω} is the wall shear stress (N/m^2) and the values of the coefficient, a and exponent b, are functions of the specific environment and solution chemistry, (such as the CO_2 partial pressure, ionic strength, pH, Fe^{++}, HCO_3^- and corrosion product film formation). The basic fluid parameters, such as fluid density, viscosity and surface roughness, are included in the τ_{ω} evaluation.

2.7 Chapter Summary

This review emphasizes the importance of this research in providing effective integrity management for oil and gas production facilities. The offshore oil and gas industry continues to rely on the extended use of carbon steels, which are readily available and are able to meet many of the mechanical, structural, fabrication, and cost requirements. However, their integrity in service is limited by corrosion performance in general and preferential corrosion of the welded joint in particular. The need for a veritable predictive tool for this deleterious localised attack is therefore imperative.

CHAPTER 3.
CONCEPTUAL DEVELOPMENT

This chapter provides a concise review of existing methods for assessing flow accelerated corrosion and the basis for the choice of submerged jet impingement as the candidate test method is established. In addition, design and construction of a novel submerged jet impingement target are highlighted, and the wall shear stresses in the high turbulence transition zone under experimental conditions are evaluated.

3.1 Selection of Test Method for the Assessment of Flow Accelerated Preferential Weld Corrosion

A typical oilfield multiphase flow produces a shear stress of 120 Pa (120 N/m^2) on the pipe wall, at maximum production (Craddock et al., 2004). Current research ventures into the challenges of flow accelerated preferential weld corrosion (PWC) of carbon steel have only succeeded in simulating maximum wall shear stress of 70 Pa (70 N/m^2) with flow-accelerated electrochemical test methods (Alawadhi and Robinson, 2011; Martinez et al., 2011; Nešić, 2007; Wang et al., 2008). Therefore, to ensure effective oilfield asset integrity management, the need for a robust and economic technique that accommodates electrochemical measurements and capable of simulating a wall shear stress comparable with field values cannot be over emphasized. In addition, it is essential that the parent metal (PM), the heat-affected zone (HAZ) and the weld metal (WM) be assessed simultaneously under the same hydrodynamic condition. This is the aim of this research.

The strategy adopted in achieving this task includes:

- Selection of a possible standard flow accelerated electrochemical method that could be improved upon
- Revision of the underlining principles of the selected method
- Appraisal of critical parameter(s) and a workable improvement plan proposed
- Design and construction / implementation of the proposal
- Evaluation of the modified component / system

The choice of appropriate corrosion test / evaluation method(s) can be bewildering, due to large number of laboratory methodologies that are available. This is further compounded by the several assumptions made to convert corrosion rate (and hence, inhibitor efficiency) from one geometry to another, the vast variation of field operating conditions, and the possibility of reproducing all field operating conditions in the laboratory. The standard field tests used to create the hydrodynamic and mass transfer conditions were reviewed and the results are presented in Table 3-1. These include Rotating Cylinder Electrode, Flow Loop, Jet Impingement and Rotating Cage (ASTM, 2001).

Table 3-1: Comparison of common methods for flow accelerated corrosion testing (Efird, 2006)

Test Criteria	Flow Test Method				
	Recirculating Flow Loops		Rotating Cylinder	Jet Impingement	Rotating Cage
	Small Diameter	Large Diameter			
Fluid Requirements	High	Very High	Low	Medium	Low
Construction Cost	High	Very High	Low	Medium	Low
Operating Cost	High	Very High	Low	Medium	Low
Test Work Effort	Medium	High	Low	Medium	Low
High pressure operation	Yes	Yes	No	Yes	Yes
Determine k and/or τ	Yes	Yes	Yes	Yes	No
Operation at high τ (> 1000 Pa)	No	Yes	No	Yes	Yes
Multiphase Testing	Yes	Yes	No	Yes	Yes
Scale up – liquid	Yes	Yes	No	Yes	No
Scale up - gas	No	Yes	No	Possible	No
Coupons	Yes	Yes	Yes	Possible	Yes
Electrical resistance Probes	Yes	Yes	Yes	Yes	No
Electrochemical Test Methods	Yes	Yes	Yes	Yes	No

Figure 3-1 shows the major criteria used in the selection of the candidate test method for the evaluation of flow accelerated PWC of carbon steel. As electrochemical testing is preferred, the rotating cage method was not considered (Efird, 2006). The rotating cylinder electrode (RCE) method is limited to single phase liquid for the wall shear stress to be evaluated and, it is also difficult to achieve high shear stresses because of the moving parts. Some of the factors that limit the use of recirculating flow loops in the laboratory include:

- Large fluid requirements for both gas and liquid
- High liquid pumping and / or gas compression requirements
- High construction costs and operating costs
- Obtaining high shear stress is difficult.

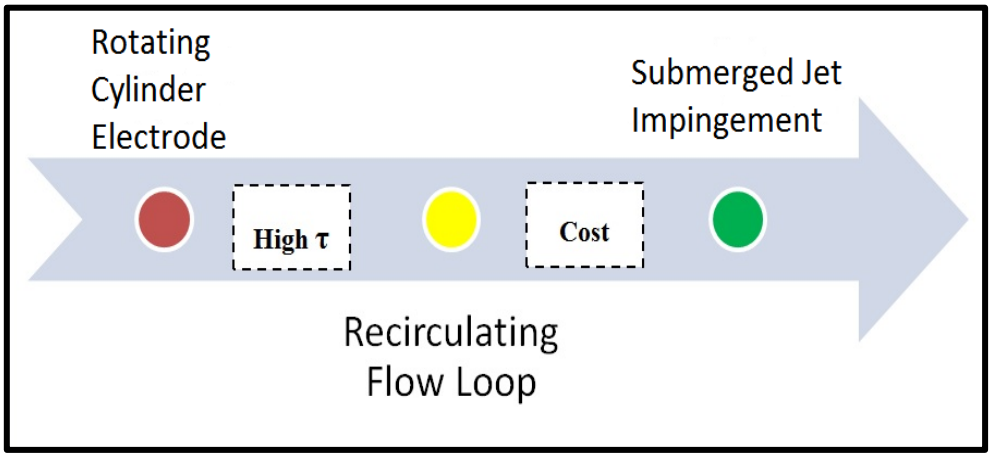

Figure 3-1: Selection criteria for flow-accelerated electrochemical test methods.

A possible candidate flow accelerated corrosion (FAC) test that could be adapted for a more reliable study of PWC and inhibitor evaluation in a typical field service scenario is the submerged jet impingement (SJI) test. The choice of SJI was based on the following desirable attributes:

- Equations for mass transfer and wall shear stress are well established
- Very high wall shear stress (>1000 Pa) is obtainable
- Electrochemical tests can be used
- Multi-phase operation can be employed

Some of the challenges that must be addressed in order to have reliable (accurate and reproducible) measurements which are crucial to the validity of the flow test include:

1. Requirements for pumps, valves and flow control equipment
2. Proper test cell design is critical
3. Sensing element position is critical to obtain valid results

3.2 Experimental Design

In the SJI method, the test fluid is ejected at right angles onto the target surface which is placed directly under the jet nozzle. The fluid then flows across a flat surface with characteristic flow regions that are mathematically definable, and the equations for mass transfer and wall shear stress are well established. A schematic is given in Figure 3-2 (Efird, 2000). It could therefore, be assumed that placing the working electrodes (specimens of the weldment) at specific radial locations on the target will allow measurement of the corrosion rate under those specific hydrodynamic conditions, as indicated in Figure 3-2.

3.2.1 Existing Target Designs

Key findings of a critical review of contemporary SJI layouts, test target designs and techniques for various studies (Figure 2-33, Figure 3-2, Figure 3-3, and Figure 3-4), show that:

1. All working electrodes are in ring form, except those placed directly under the nozzle jet in erosion-corrosion tests, such as shown in Figure 3-4 (Hussain, 2001).
2. All targets, without exception, have only one mounted working electrode; such that tests requiring galvanic measurements are conducted by coupling two working electrodes on different targets (under another nozzle jet), as presented in Figure 3-3 (Barker et al., 2012; Hu and Neville, 2009). It is therefore not surprising that reproducible laboratory conditions of such tests would be uncertain and results unreliable.
3. SJI is mostly used for a freely corroding system; such that one metal is assessed at a time as indicated in Figure 2-24 (Meng and Jovancicevic, 2008; Schmitt and Mueller, 1999; Efird, 2011)
4. In all PWC studies, only two of the three major weld sections were assessed, by coupling the weld section specimens (the WM and the PM) on separate targets, such as shown in Figure 3-3 (Barker et al., 2012; Barker et al., 2013)

Subsequent to these findings, this research seeks to design a SJI target that would be capable of accommodating:

- specimens of three main weldment regions (three working electrodes) and
- the working electrodes in each of the three hydrodynamic zones.

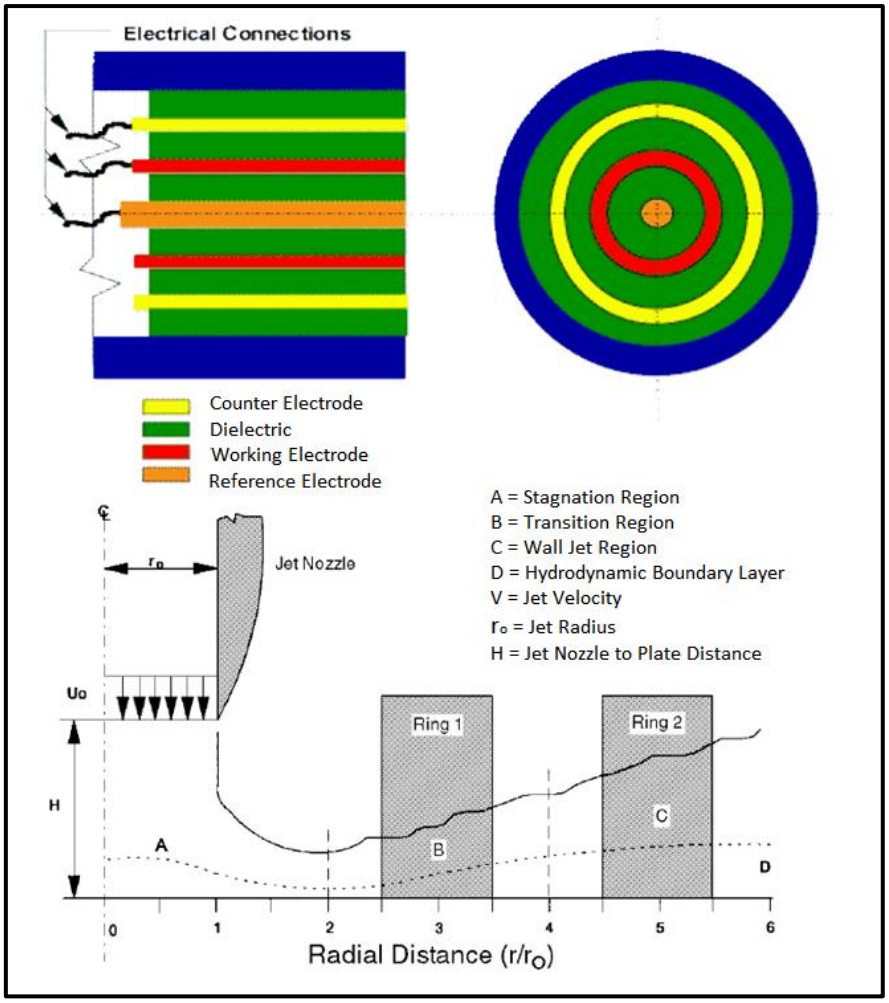

Figure 3-2: Convectional SJI target showing the position of the test ring in the flow field and the characteristic flow regions.(Efird, 2000)

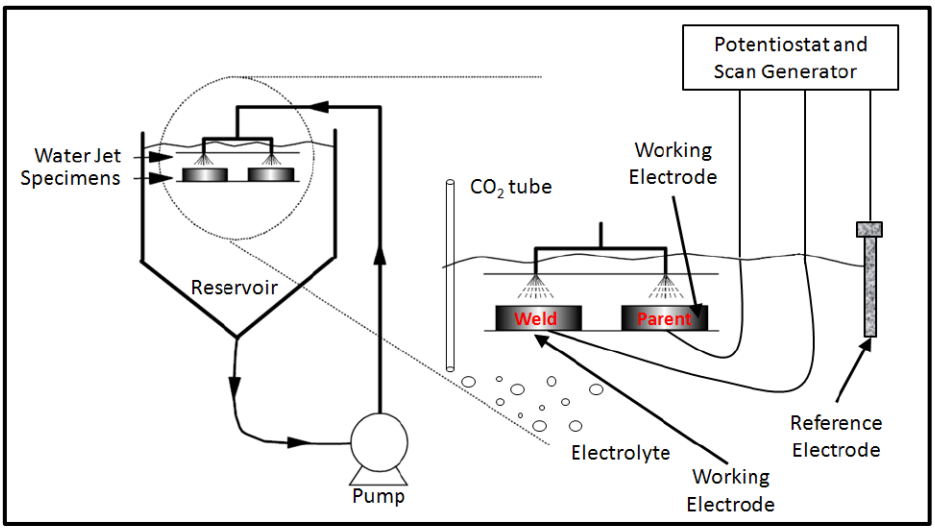

Figure 3-3: Schematic representation of the impinging jet apparatus.(Barker et al., 2012)

Figure 3-4: Targets (a, b and c) for SJI. (Hussain, 2001)

3.2.2 X65 Steel Weldment

All tests were carried out on samples machined from a seam welded X65 steel pipe with the composition shown in Table 3-2 (Alawadhi et al., 2008). The steel had been thermo-mechanical controlled rolling to give a 32 mm wall thickness. Submerged-Arc Welding process was used to weld a double-vee joint preparation. The composition of the weld metal was similar to that of the parent material, except for a higher Ni (0.68%) content. Figure 3-5 shows the macrostructure and microstructures across the weldment.

Table 3-2: Composition of X65 pipeline steel and weld metal (Wt %) (Alawadhi et al., 2008)

	C	Mn	Ni	Cr	Mo	Si	Al	Cu	V	P	S
Pipe	0.08	1.6	0.04	0.02	0.01	0.3	0.04	0.02	0.05	0.009	0.0005
Weld	0.08	1.4	0.68	0.03	0.33	0.3	0.03	0.02	0.04	0.01	-

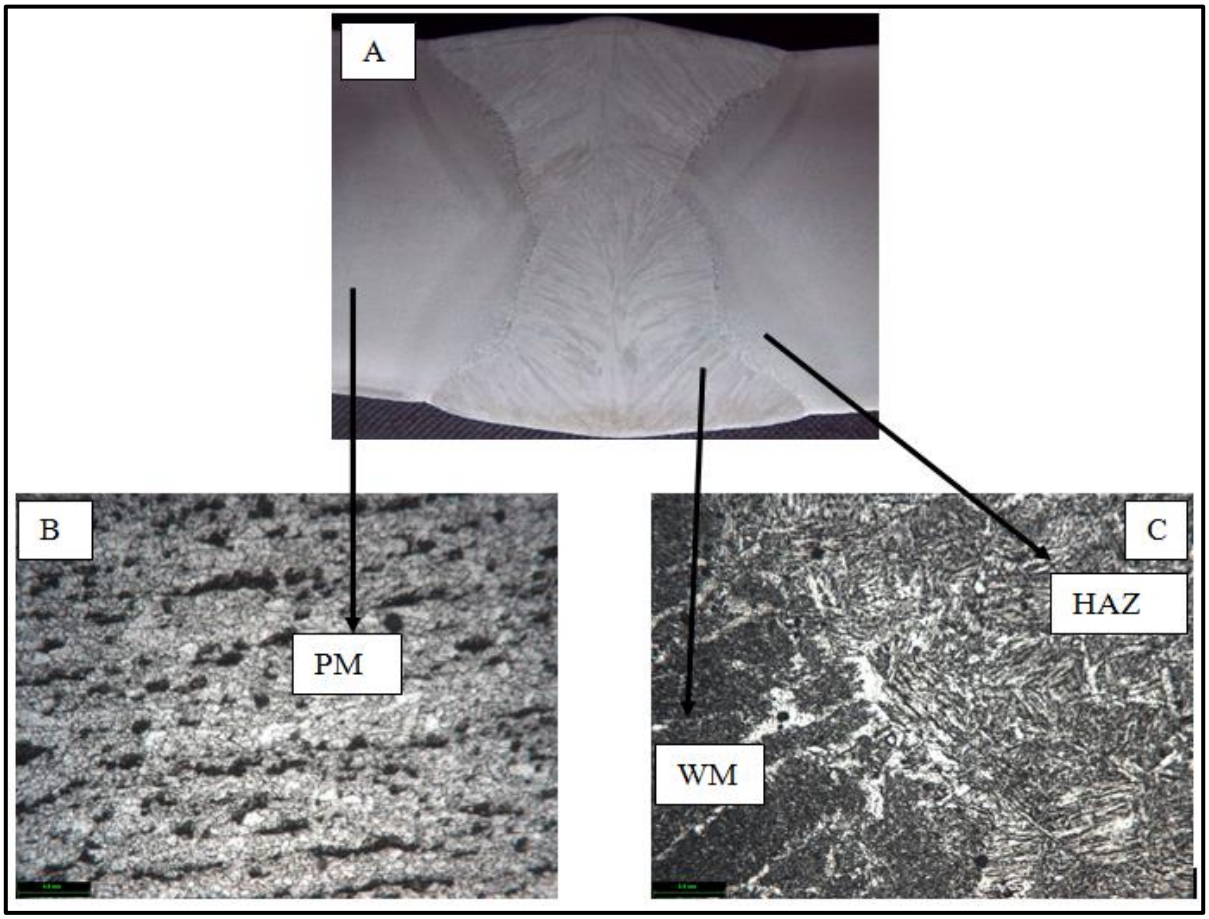

Figure 3-5: (A) macrostructure of X65 C-Mn steel weldment, microstructures of (B) the PM and (C) the WM and HAZ, separated by fusion region; etched in 10% nital.

3.2.3 Design and Construction of Jet Impingement Target

The novel aspect of the present work was the design and construction of the target, which allowed simultaneous electrochemical measurements on all weldment sections within the same hydrodynamic region. It was made up of sections of weld metal, heat affected zone and parent material, machined from the X65 carbon steel pipeline weld by electrical discharge

machining (EDM) to give surface areas in the ratio 2:1:8 respectively, as shown in Figure 3-6. Throughout the cutting, temperature was kept very low to avoid grain growth and the machining tolerance was 0.1 mm.

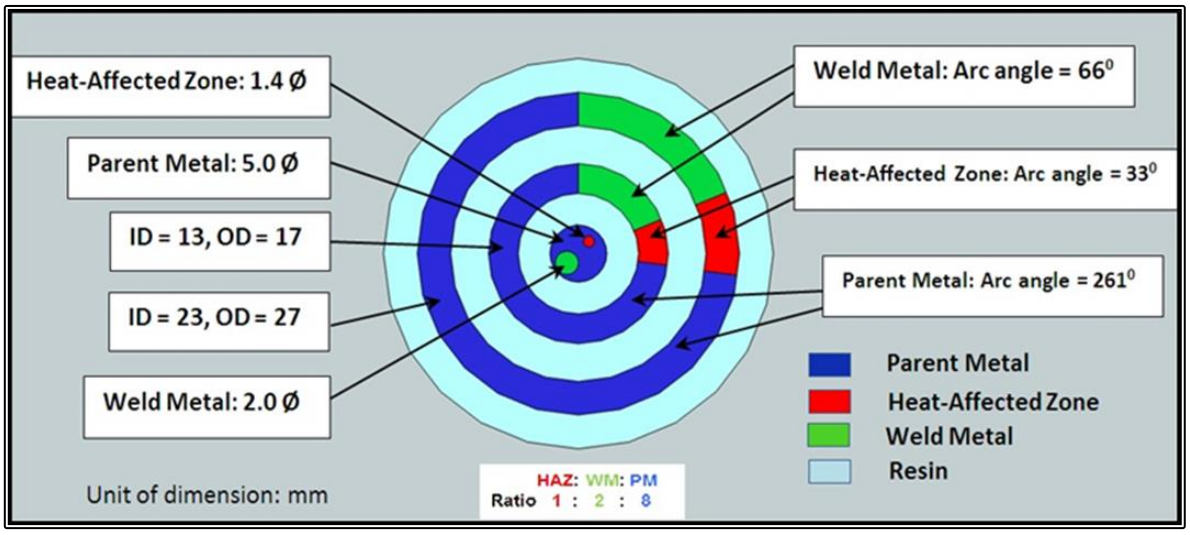

Figure 3-6: Design of the new submerged jet impingement target.

Each weld section was attached to a wire to form an electrode, assembled in position and mounted in non-conducting resin as presented in Figure 3-7. One set of electrodes prepared from the three weld regions was located in the centre of the target, directly under the jet nozzle (5 mm in diameter); where the flow impinged on the surface and was momentarily brought to rest. The two other sets of electrodes were positioned at radial distances of 15 mm (high turbulence hydrodynamic transition region) and 25 mm (low turbulence wall jet region), as shown in Figure 3-8. The hydrodynamic zones on the target surface are defined in Figure 3-9.

Some unique features of this novel submerged jet impingement target include:

- Placement of working electrodes at the centre (the stagnant hydrodynamic zone); as opposed to auxiliary electrode in conventional targets as shown in Figure 3-2 (Cai et al., 2012; Barker et al., 2012; Efird, 2000; Efird, 2011; Barker et al., 2013).
- All convectional SJI targets have one working electrode which is not suitable for comprehensive simultaneous PWC studies enhanced by hydrodynamic changes

(Zhang and Cheng, 2010; Hussain and Robinson, 2007; Menendez et al., 2005; Schmitt and Bakalli, 2006; Schmitt et al., 2004).

Improved reproducibility, time and economic saving are some anticipated benefits of this novel SJI target.

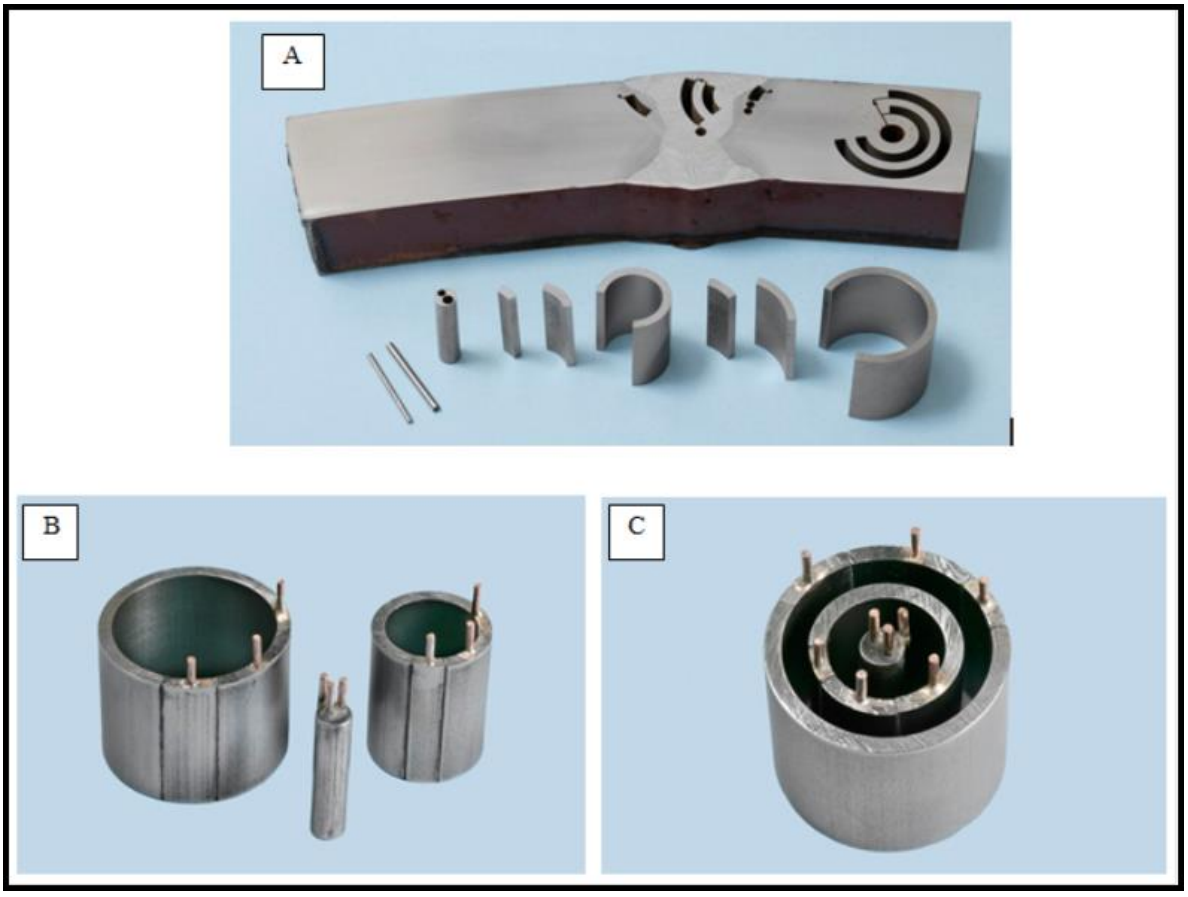

Figure 3-7: Construction stages of test target (a) cutting of test specimens from X65 steel weldment, (b) assembly and (c) setting.

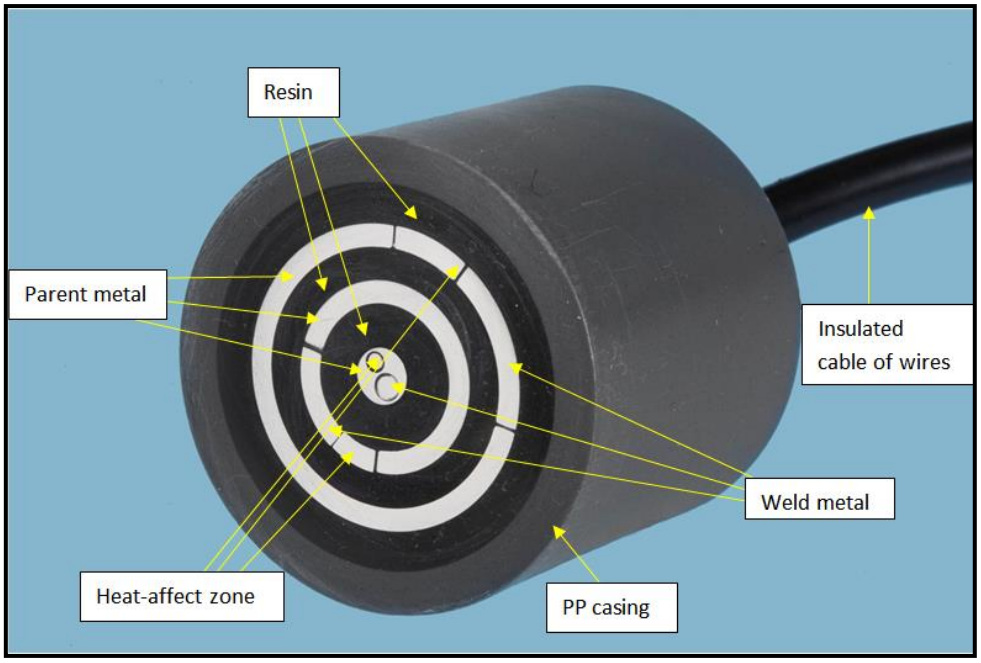

Figure 3-8: Fully assembled novel submerged jet impingement target.

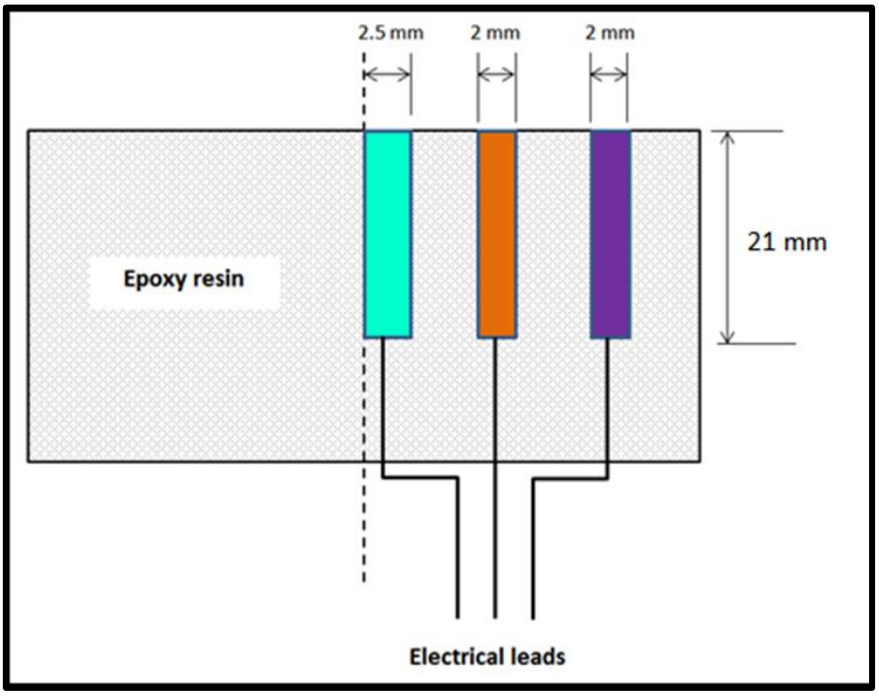

Figure 3-9: Layout drawing of the novel submerged jet impingement target.

3.2.4 Wall Shear Stress of the New Target

An essential requirement of any FAC test is that field conditions must be replicated (or simulated) to have reliable result(s). It was therefore necessary to evaluate the wall shear stress in the high turbulence region of the new target that could be simulated in the laboratory. Conventional empirical expressions, Equation 3-1 and Equation 3-2 were used to calculate the simulated wall shear stress of the modified SJI method (Meng and Jovancicevic, 2008; Efird et al., 1993; Menendez et al., 2005).

The nozzle was 5 mm in diameter ($2r_o$) and positioned at a fixed distance (H) of 5 mm from the target. The wall shear stress, $\boldsymbol{\tau_\omega}$, at the high turbulence transition region (radial distance $r/r_o = 3$), in brine solution with jet velocities of 5 m/s and 10 m/s, at ambient conditions was evaluated from:

$$\boldsymbol{\tau_\omega = 0.179\rho U_o^2 R_e^{-0.182}(r/r_o)^{-2.0}} \qquad \textbf{Equation 3-1}$$

Where the jet Reynolds number is defined as:

$$\boldsymbol{Re = 2r_o U_o(1/\upsilon)} \qquad \textbf{Equation 3-2}$$

Where **r** is the radial distance from the jet centre line and $\mathbf{r_o}$ is the jet radius

$\boldsymbol{\rho}$ is the density of liquid/fluid (seawater) = 1025 kg/m^3

$\boldsymbol{\upsilon}$ is the kinematic viscosity = 1.046 x 10^{-6} m^2/s

Such that, for $\mathbf{U_o}$ (jet velocity) 5 m/s, $\boldsymbol{\tau_\omega} \approx 72$ N/m^2

When $\mathbf{U_o}$ = 10 m/s, $\boldsymbol{\tau_\omega} \approx 253$ N/m^2

The shear stress at a nozzle flow rate of 5 m/s (72 N/m^2) was designed to be comparable with the value of 70 N/m^2 from a previous project on PWC, using a rotating cylinder electrode,

operating at 5000 rpm (Alawadhi et al., 2008). Hence, it expected that the results of the two tests in the same conditions should be similar. Tests were conducted to verify this assertion.

At jet velocity of 10 m/s, a simulated wall shear stress of 250 N/m^2 (250 Pa) was achieved in the high turbulence transition hydrodynamic zone (inner ring) of the new target, which is 100% more than the wall shear stress of 120 Pa (120 N/m^2), produced in a typical oilfield multiphase flow (Craddock et al., 2004). It could therefore be anticipated that this adapted technique would be a capable tool for FAC studies in general and PWC in particular.

3.3 Chapter Summary

The need for a reliable FAC technique was established. The basis for the choice of SJI method for PWC studies was also highlighted. A novel jet-impingement target was designed and constructed from samples of the parent material, heat affected zone and weld metal in a carbon steel weldment, to give a range of hydrodynamic conditions from stagnation to high turbulence. The simulated shear stresses were both comparable with other FAC methods at low stress values and oilfield high wall shear stress.

CHAPTER 4.
EXPERIMENTAL WORK

Concise description of the SJI test rig and electrochemical measurement techniques in typical oilfield conditions to assess the PWC of X65 carbon steel is presented in this chapter. Surface characterisation of corrosion product and potentiodynamic polarisation scans to determine corrosion mechanisms are also highlighted. Major challenges encountered in the course of research are also highlighted and measures to ameliorate experimental conditions are proffered.

4.1 Submerged Jet Impingement Test

4.1.1 Objective

The primary purpose of performing the following flow accelerated electrochemical tests using the improved submerged jet impingement Test (SJI) technique is to appraise the suitability of the adapted target for the study of preferential weld corrosion (PWC) in typical oilfield service conditions.

4.1.2 Materials

Materials used to perform flow accelerated electrochemical measurements using SJI include:

1. X65 pipeline steel weld sections as prepared on the new target with corroding surface areas as presented in Table 4-1 and mounted as shown in Figure 3-8.
2. Sea salt solution prepared from 33.33 g/l of Tropic Marin® Sea Salt. The macro-elements of the sea salt are as shown in Table 4-2.
3. Oxygen-free nitrogen (OFN) gas
4. Carbon dioxide (CO_2) gas
5. Oilfield inhibitor (CORRTREAT 10-569)
6. Natural air

Table 4-1: Surface area of corroding weld specimens

	Weld specimen (cm^2)		
	PM	**HAZ**	**WM**
Centre	0.114	0.016	0.025
Inner Ring	0.914	0.114	0.228
Outer Ring	1.142	0.143	0.286

Table 4-2: Macro-elements per gram of Tropic Marin® sea salt

	%
Calcium (Ca)	1.1
Chlorine (Cl)	49.0
Magnesium (Mg)	3.5
Potassium (K)	1.1
Sodium (Na)	27
Sulphur (S)	2.2

4.1.3 Apparatus and Equipment

The apparatus and equipment used to perform flow accelerated electrochemical tests using the improved SJI technique include the following:

1. Centrifugal pump
2. Peristaltic (tubing) pump
3. Air pump
4. A Zero-Resistance Ammeter, Galvo-Gill 12 connected to a data logging PC (from ACM Instruments, Grange-over-Sands, UK)
5. Computer-controlled potentiostat Gill-AC potentiostat (from ACM Instruments, Grange-over-Sands, UK)
6. A 1.5 L corrosion glass cell with nylon lid
7. Counter (secondary) platinum electrode. The platinum electrode paddle type with gauze wire 0.12 mm, 250 mesh per cm^2 and 2.5 grams in weight and total area of 8.4 cm^2

8. Calibrated saturated calomel electrode (SCE), as reference electrode, with connection into the cell through a Luggin capillary probe
9. Thermometer
10. Gas bubbler (3 units)
11. Micro pipettes
12. Spirit (bubble) level
13. Three equal lengths of 5 mm stainless steel rods

4.1.4 Experimental Conditions

The oilfield simulated conditions under which the experiments were performed are summarised in Table 4-3. CO_2 partial pressure of 1 bar was maintained and test solution pH value of 4.5 was observed in all the experiments. In no-flow conditions, ambient temperature (18 – 20^{o}C) was maintained, while the temperature steadily rose to 50^{o}C in flowing conditions. Air was deliberately introduced into the loop in some SJI tests at a flow rate of 2.2 ml/litre/min, to simulate specific oilfield condition in which oxygen and CO_2 are dissolved in seawater.

Table 4-3: Experimental environment and flow conditions

	Uninhibited brine		**Inhibited brine**	
	Saturated with CO_2	**Containing CO_2 and O_2**	**Saturated with CO_2**	**Containing CO_2 and O_2**
No-flow (Stagnant)	✓	✓	✓	✓
Flowing at 5 m/s	✓	✓	✓	✓
Flowing at 10 m/s	✓	✓	✓	✓

4.1.4.1 Preparation of Inhibitor

One of the objectives of this study is to assess the effectiveness of a typical oilfield inhibitor (CORRTREAT 10-569) supplied by Clariant Oil Services UK. CORRTREAT 10-569 is an environmentally acceptable ethoxylated amine containing corrosion inhibitor in a water/glycol based solvent package, although, the exact composition remains confidential.

Corrosion inhibitors are conventionally applied in parts-per-million (ppm) (Meng and Jovancicevic, 2008). Hence, in all inhibited brine solutions the CORRTREAT 10-569 inhibitor concentration used was 30 ppm by volume; typical of industry accepted levels (Gulbrandsen and Dugstad, 2005; Gulbrandsen et al., 2005).

The quantity of inhibitor required to make a concentration of 30 ppm is 30×10^{-6} or 0.03 ml per litre. Therefore for a 4 litre solution of brine in the corrosion cell, 0.12 ml of inhibitor was required to make up a concentration of 30 ppm for the test. As standard Health Safety and Environment (HSE) management demands, this quantity of the inhibitor was drawn from its container with a micro-pipette in the fume cupboard and safely stored.

4.1.5 Experimental Setup and Procedure

The novel target constructed in this research, as shown in Figure 3-8, was used throughout the SJI tests. The hydrodynamic zones on the target surface are as defined in Figure 4-1. The target was wet-ground to 1200 silicon carbide abrasive paper, rinsed with distilled water, degreased with iso-propanol, and dried before starting each experiment.

All experiments were performed on the same weldment samples. Between each experiment, the target was re-polished and tested again and this procedure ensured that the results were obtained on materials with a consistent surface preparation. The jet nozzle to target distance of 5 mm and submerged depth of 40 mm was maintained throughout the SJI experiments. The electrolyte was artificial seawater, saturated with carbon dioxide at 1 bar pressure. Each experiment was carried out in static conditions and also at nozzle flow rates of 5 and 10 m/s. In some cases, a typical oilfield corrosion

inhibitor (CORRTREAT 10-569) was added to the brine and in other experiments a small quantity of air (2.2 ml/litre/min) was bubbled into the cell to simulate the effects of a leaking pump or valve.

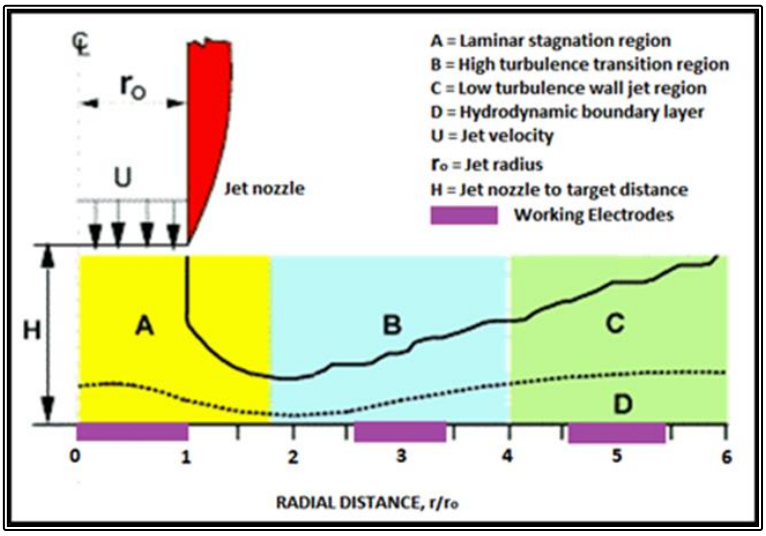

Figure 4-1: Hydrodynamic characteristics of jet impingement on the novel target indicating the positions of the working electrodes.

Prior to starting every experiment, the brine solution, contained in a plastic storage container, was sparged with oxygen-free nitrogen (OFN) for 2 hours and CO_2 for 4 hours to achieve saturation with CO_2.

A "Totton" multistage magnetically coupled centrifugal pump (GP20/18 230-1-50) with 15 mm ports was used for recirculation of the test solution. This pump is fitted with a ceramic spindle for minimising heat transfer to the pumped fluids and to prevent contamination of the test fluid. At the end of each experiment, the test (uninhibited and inhibited) solutions were safely turned into separate waste plastic containers and subsequently disposed.

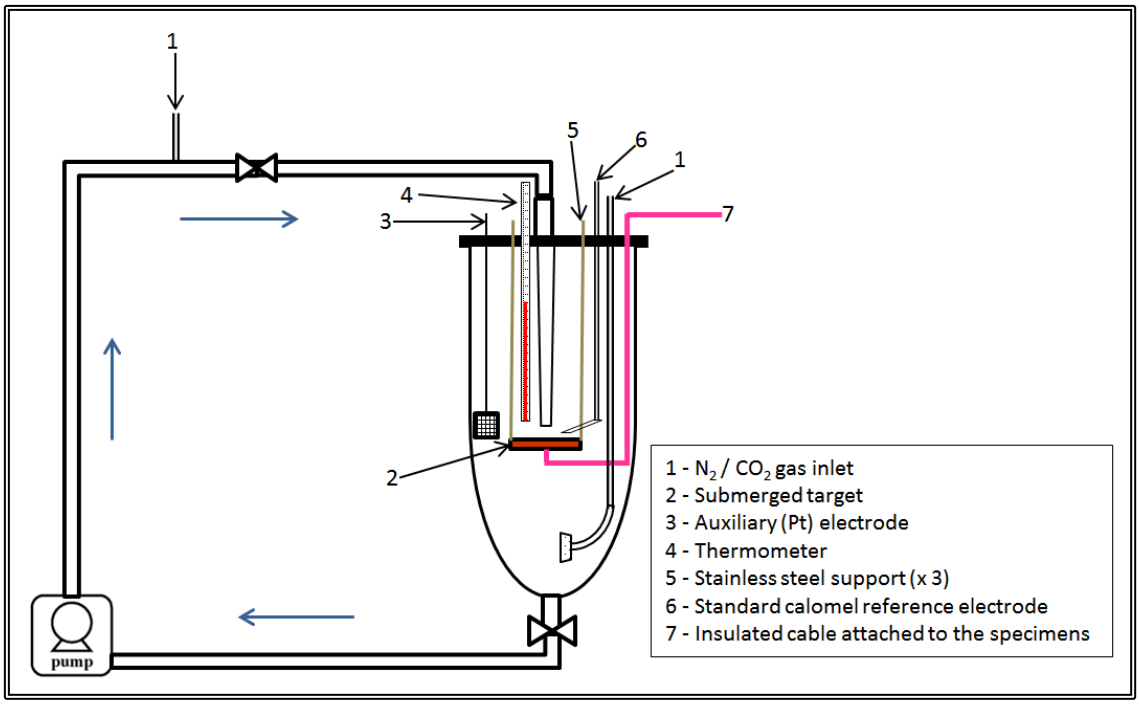

Figure 4-2: Submerged jet impingement experimental layout.

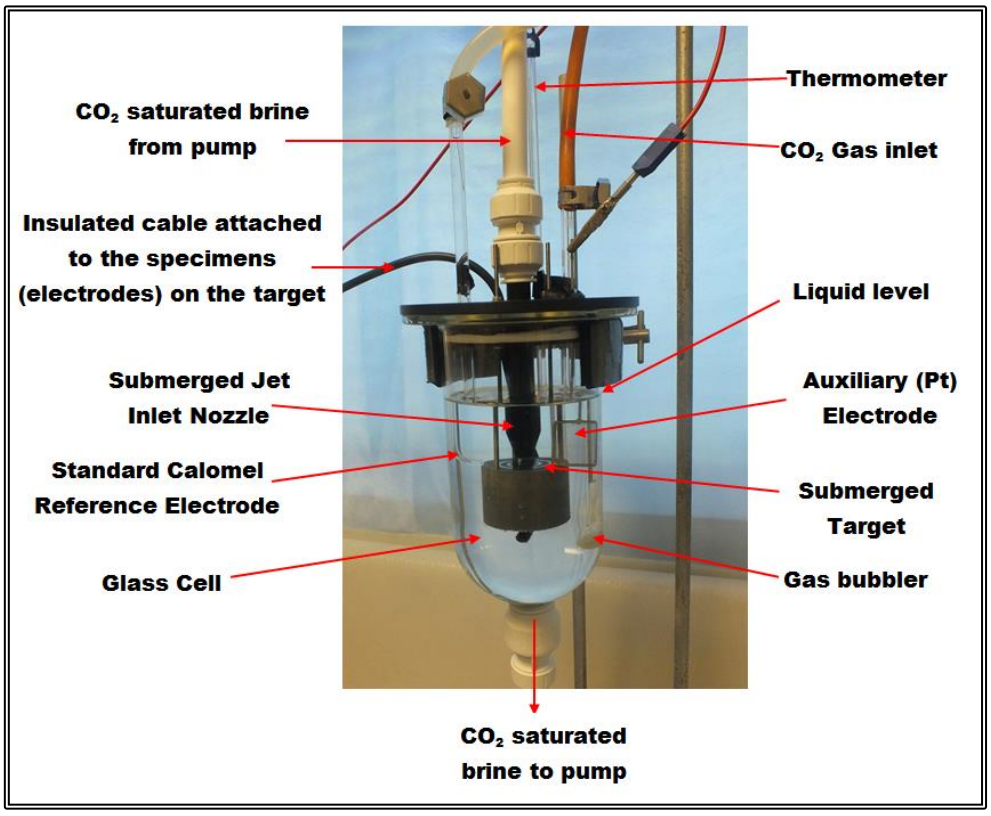

Figure 4-3: Submerged jet impingement experimental setup.

4.1.5.1 Submerged Jet Impingement (SJI) Test Procedure

Figure 4-2: is a sketch of the experimental layout of the submerged jet impingement used throughout this study. An illustration of the set-up is shown in Figure 4-3. The SJI test procedure is outline as follows:

1. Install the constructed target under the SJI nozzle with three equal and equidistant stainless steel rods
2. Install the electrodes (reference and counter), thermometer and the gas bubbler on the nylon lid
3. Lower the lid and seal the corrosion glass cell using rubber washers and metal clips
4. Connect gas vents with (second) gas bubbler lowered into fresh water in a beaker
5. Connect the glass cell to the flow loop via the recirculating centrifugal pump
6. Connect the insulated electrical cable attached to the working electrodes to Zero-Resistance Ammeter (ACM Instrument Galvo-Gill 12)
7. Sparge solution (in the storage container) and the loop (incorporating the corrosion glass cell and the recirculating pump) with oxygen-free nitrogen for 2 hours followed by CO_2 gas for 4 hours. Run the circulating pump for about 30 seconds at 20 minutes interval during sparging in order to ensure complete deaeration of the entire system
8. Transfer brine saturated with CO_2 gas into the corrosion glass cell using the peristaltic pump, with continuous CO_2 sparging
9. Begin data logging of galvanic corrosion measurements in static (no-flow) condition and continue for at least 10 hours
    - In tests involving oxygen, sparge air into the glass cell through the third gas bubbler, with continued CO_2 sparging

10. Set the control valve to give desired flow rate (5 or 10 m/s) and start the recirculation pump, without stopping galvanic current measurement data logging
11. Calibrate the computer-controlled potentiostat (Gill-AC) at 500 Ohms
12. Stop galvanic corrosion data logging after 6 hours in flowing condition, but continue recirculation and sparging (with CO_2 or CO_2 and air, as required)
13. Disconnect working electrodes and the reference electrode (SCE) from the ZRA
14. Connect the SCE, counter (platinum) electrode and one working electrode to the Computer-controlled potentiostat
15. Measure the linear polarisation resistance (LPR) by scanning 10 mV (SCE) below and above the open circuit potential (OCP) at the rate of 10 mV per minute
16. Repeat the previous procedure for all the working electrodes in turns, with continuous recirculation and appropriate gas sparging
17. Stop recirculation and disassemble the setup.
18. Turn solution into waste liquid plastic container and store away for disposal
19. Clean the apparatus and flush the loop with deionised water
20. Clean the target and prepare the surface for another test

4.1.6 Electrochemical Measurements

Electrochemical techniques give information about the corrosion rate and in some cases, the corrosion mechanism. Electrochemical methods are sensitive to the nature of the surface of the material and generally provide very consistent results when used for corrosion measurements (Abayarathna and Naraghi, 2001).

4.1.6.1 Galvanic currents

The galvanic currents between each weld region were recorded every 60 seconds during the test using a multi-channel zero resistance ammeter (ZRA) (ACM Instrument Galvo-Gill 12), connected to a data logging PC. For weld sections in each hydrodynamic region of the target, currents from the parent material (PM) to the heat-affected zone (HAZ) and from the weld metal (WM) to the HAZ were recorded on two channels of the ZRA. The working electrodes were coupled, with the HAZ short-circuiting both channels. The reference electrode (SCE) was connected in the same manner as the HAZ, as shown in Figure 4-4. Since the three working electrodes (PM, HAZ and WM) were in the short-circuit condition, the algebraic sum of their individual galvanic currents will be zero; such that their individual galvanic currents were established from the following relationship:

$$I_{PM} + I_{HAZ} + I_{WM} = 0 \qquad \textbf{Equation 4-1}$$

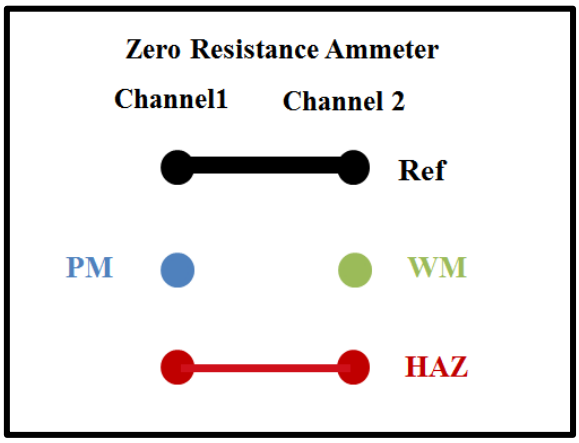

Figure 4-4: Electrical connection of the electrodes to Zero resistance ammeter (ZRA).

At first, galvanic measurements were interrupted for linear polarisation resistance (LPR) measurements at 6 hours intervals. These resulted in disturbance of galvanic current flow and polarisation of the corroding surface, as described in Chapter 5 (Preliminary Results and Discussion). It was therefore resolved that LPR measurements be

performed at the end of galvanic current measurements in order to avoid these undesirable effects.

4.1.6.2 Self-Corrosion Rates

The linear polarisation resistance (LPR) technique is the most frequently used, being both quick and easy. A small sweep from -10 mV to +10 mV, around the rest potential was performed, at 10 mV per minute. The resulting current/voltage plot usually exhibits a straight line the inverse slope of which is proportional to the corrosion rate.

Self-corrosion rates of each weld section, in the three hydrodynamic regions of the SJI target, were evaluated from linear polarisation resistance measurements of each working electrode. The LPR was measured by uncoupling each electrode in turn and carrying out LPR measurements using a platinum gauze secondary electrode, a standard calomel reference electrode (SCE) and a low noise potentiostat, Gill-AC. 'Long term -LPR sweep' technique was used to scan each uncoupled electrode from 10 mV (SCE) below the open circuit potential (OCP) to 10 mV (SCE) above the OCP. 60 seconds was allowed for 'cell settle time' before every scan. ACM software display of the LPR measurement is as shown in Figure 4-5. The uncoupled electrode rapidly established its open circuit potential and the potential was then scanned at a rate of 10 mV min^{-1} , and the current response was recorded.

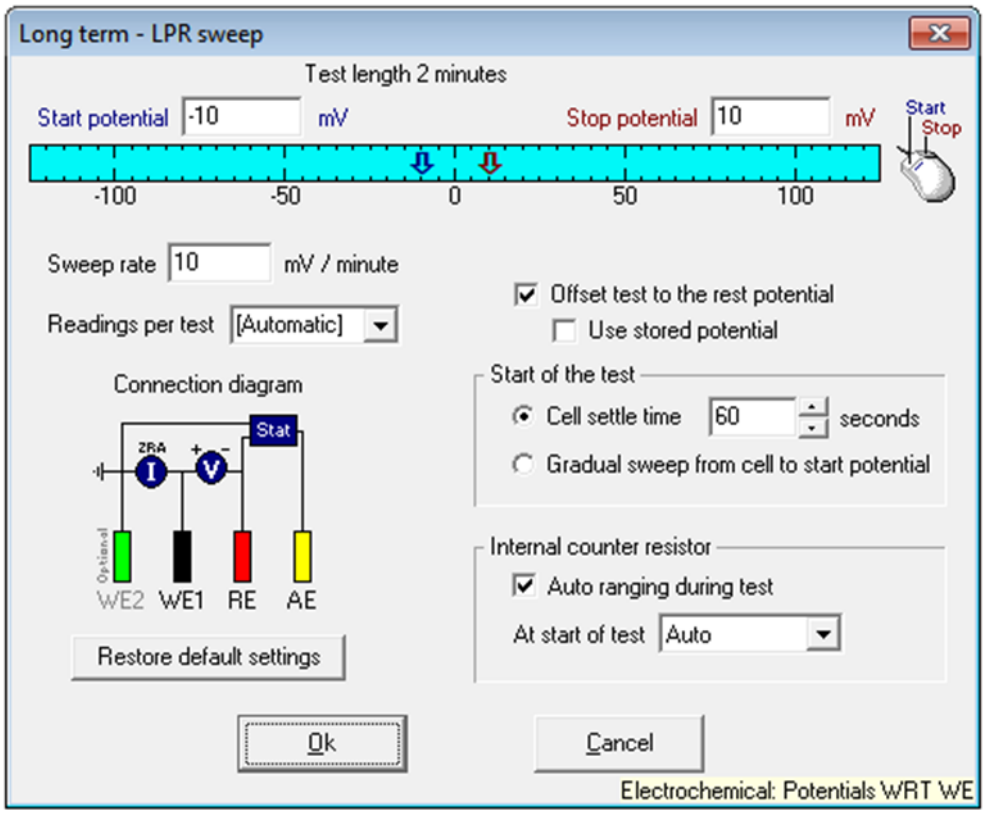

Figure 4-5: Long-Term LPR Sweep parameters used in preliminary experiments.

The polarisation resistance, Rp, was obtained from the best-fit gradient of the potential/current graph and the corrosion current, I_{CORR}, was then found from the Equation 4-2.

$$I_{CORR} = B / R_p \qquad \textbf{Equation 4-2}$$

where B is the LPR constant for the material and its environment, taken as 13 mV (Martinez et al., 2011). The use of a fixed value of B may result in some inaccuracies in the calculation of self-corrosion rates due to variations in polarisation characteristics, especially for anodic reactions when surface films are present. The very small potential perturbation applied makes the polarisation resistance method repeatable over long periods without changing the behaviour of the steel significantly from its freely corroding condition.

4.1.6.3 Total Corrosion Rates

The total corrosion rate (CR_{Total}) of each weld zone in the three hydrodynamic regions was evaluated from the sum of their galvanic corrosion (CR_{Galv}) and self-corrosion (CR_{Self}) rates as shown in Equation 4-3.

$$\mathbf{CR_{Galv} + CR_{Self} = CR_{Total}} \qquad \textbf{Equation 4-3}$$

4.2 Surface Characterisation

Characterisation of the corroded surface and the adjoining substrate were performed in order to assess the nature of the corrosion product film and the roles of the corroding environment and the metallurgical features of the weldment. Specimen for microscopy was machined from the same X65 carbon steel pipeline weld from which the SJI target specimens were selected, using electrical discharge machining (EDM) technique as shown in Figure 4-6. The specimen measuring (5 x 30) mm^2 cross sectional (corroding) area was mounted on electrically conductive bakelite.

4.2.1 Scanning Electron Microscopy

Examination and analyses of the thickness and morphology of the corrosion product film were performed after 2 hours of exposure to uninhibited brine containing CO_2 and air, flowing at 10 m/s, using a scanning electron microscope (SEM), Philips-XL30 ESEM with energy–dispersive x-ray (EDX). Pure copper was used for the calibration of the SEM equipment used for these analyses.

The cross-section analyses of the corrosion layers were performed with energy dispersive X-ray (EDX). Mapping of C, O and Fe was carried out to investigate the distribution of these elements on the surface and to calculate the relative concentration values of each element in the corrosion layers. Samples were prepared by etching the SEM cross-sections with a focused ion beam (FIB), FEI-FIB 200 equipment.

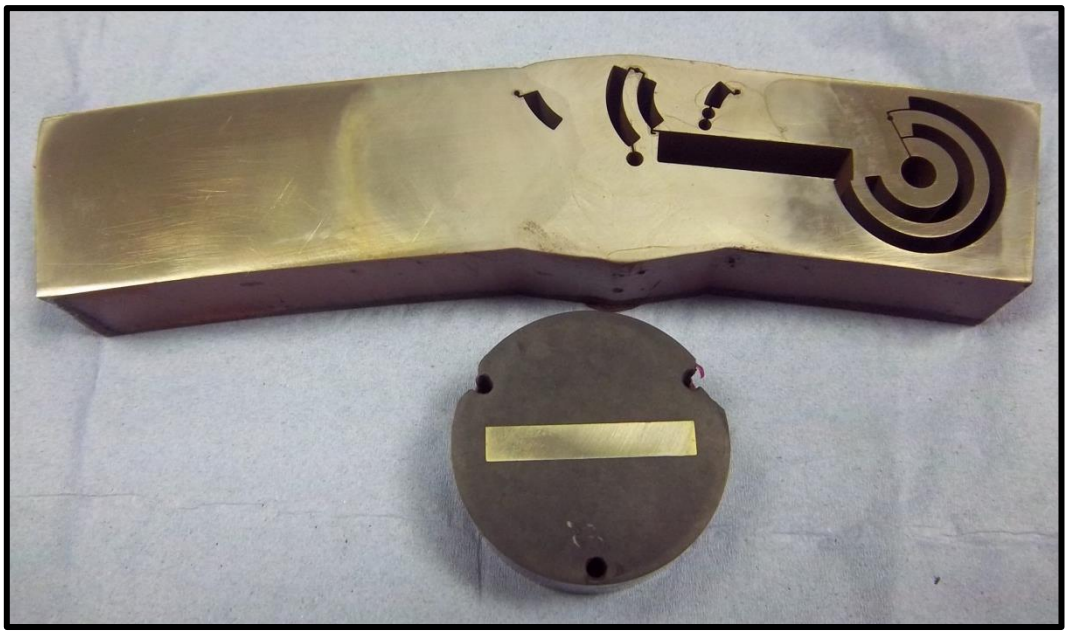

Figure 4-6: Cutting and assembly of target for surface characterisation.

4.2.2 X-Ray Diffraction (XRD)

An X-Ray Diffraction (XRD) instrument (Siemens D5005) was used for direct XRD measurements of the corrosion film with chromium wavelength of 2.291A. The determination of chemical composition was carried out by comparison of experimental lines with standard data obtained from the XRD database.

4.3 Potentiodynamic Polarisation Scanning

Polarisation scans were performed to verify the electrochemical reactions involved in the corrosion process in various environments under consideration.

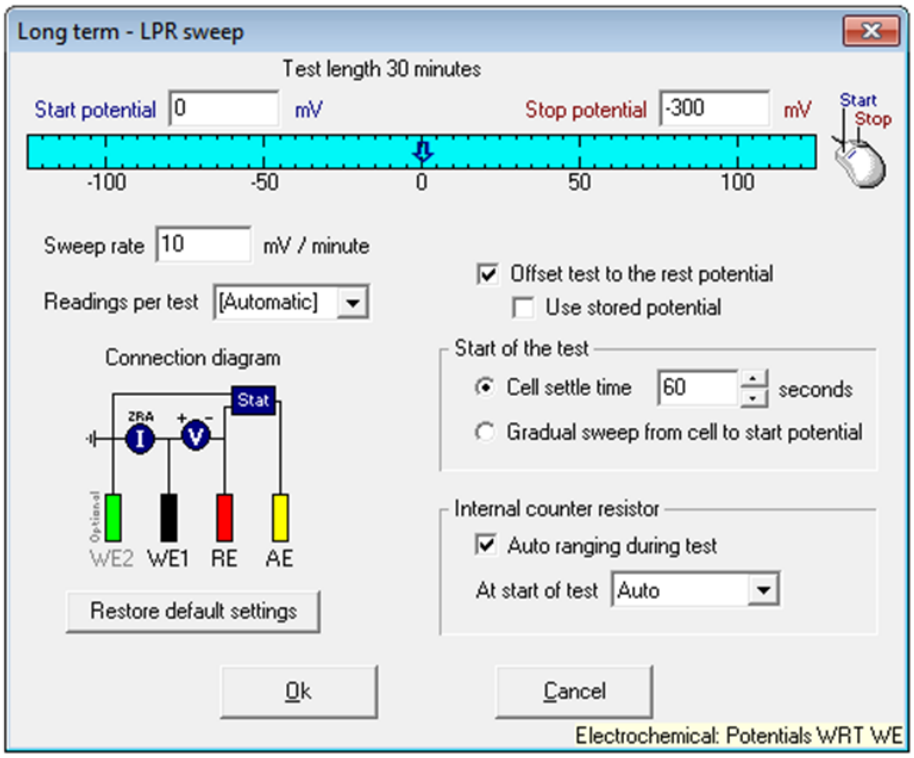

Figure 4-7: Cathodic scanning parameters

Cathodic polarisation tests were conducted on a 3-electrode cell using a computer-controlled Gill-AC potentiostat with the PM on the inner ring as the working electrode, SCE as reference electrode and platinum mesh as the counter electrode. The potential was swept from the open circuit potential, 0 to -300mV (SCE) at 10mV /min and the polarisation recorded in different test solution environments. The scanning parameters are as shown in Figure 4-7. A similar configuration was used for anodic polarisation scans performed for the same PM on the inner ring from 0 to +300 mV (SCE).

4.4 Observations from Experimental Methodology

Potential source of errors and measures taken to prevent or mitigate limitations are highlighted as follows:

- All working electrodes in the novel SJI target were mounted without electrical contact with each other to prevent 'electrical short-circuit'. Electrical contact test was also conducted before the commencement of corrosion experiments.
- The same set of working electrodes were used in all the tests following surface preparation (grinding and polishing) using 1200 silicon carbide abrasive paper and thus ensure consistent surface preparation.
- Before each experiment, the target was visually examined for structural damage of the epoxy insulation, especially at the epoxy/metal interface. Necessary repairs were done when required. Thereafter, the target was tested for ionic conductivity.
- Spirit-level was used to ensure that the target was perpendicular to the nozzle.
- Brine solution used throughout this research was prepared from the same production batch / package and deaerated with oxygen-free-nitrogen gas.
- Deaerated solution was transferred into the corrosion cell, which had been previously sparged with OFN and CO_2, with the aid of peristaltic pump. Furthermore, CO_2 was sparged into the solution throughout each test.
- Single sourced vapour withdrawal cylinders of carbon dioxide were used in all the experiments.
- Calibration of the standard calomel reference electrode (SCE) before each experiment.
- Calibration of "ACM Gill-AC" was conducted before each LPR measurement.

4.5 Chapter Summary

Flow accelerated electrochemical tests were performed using submerged jet impingement test to assess the suitability of the novel target to study preferential weld corrosion. Galvanic and linear polarisation measurements were conducted in typical oilfield environment and flow conditions. Corrosion film products were appraised by

surface characterisation techniques while the corrosion mechanisms involved were assessed by potentiodynamic polarisation scanning. Major sources of error, as well as, mitigating measures were also highlighted.

CHAPTER 5.
PRELIMINARY RESULTS AND DISCUSSION

The suitability of the novel SJI target and the developed technique for the study of flow accelerated corrosion (FAC) of weldments are discussed in this chapter. The exploratory tests are conducted in no-flow and flowing conditions to replicate typical offshore oilfield conditions of commissioning / shut-down and production, respectively. Electrochemical measurements from the weld sections in each of the three hydrodynamic regions are also appraised.

5.1 Uninhibited No-Flow Condition

In these exploratory tests, galvanic measurements were performed while deaeration of the brine solution with oxygen-free-nitrogen (OFN) was carried out in no-flow condition. After 400 minutes, the brine solution was sparged with CO_2 and galvanic measurements were interrupted by linear polarisation resistance (LPR) measurements over the next 1000 minutes. Ambient temperature of 20^{o}C was maintained throughout these tests.

5.1.1 Galvanic Current Measurements

In the deaeration stage, weld sections placed in the inner ring of the target show that the HAZ stabilized as anodic current; protecting the PM and WM at ambient temperature, as shown in Figure 5-1. Galvanic currents decreased gradually throughout this stage, as well as, the coupled potentials of the weld sections, Figure 5-2. This could be attributed to stable, but partially protective corrosion product film on the working electrodes.

Sparging the deaerated solution with gaseous CO_2 reduced each coupled (PM-HAZ and WM-HAZ) potential to about -740 mV (SCE), (as presented in Figure 5-2). Reduction in the corrosion potential of the couple was accompanied by galvanic current reversal of the PM, from being cathodic to anodic current. This shows that, when CO_2 was

dissolved in brine, the WM was protected by the anodic currents of the PM and the HAZ. This was expected, since the PM and HAZ are essentially of the same elemental composition and only differ in microstructures. Furthermore, the WM was the most noble in brine saturated with CO_2, as indicated by the highest open circuit potential (OCP) in Figure 5-4. It is worth noting that the total galvanic current exchanged in this stage is higher than in the deaerated stage, indicating that the X65 steel weldment is more susceptible to galvanic corrosion in brine containing CO_2 compared with deaerated brine solution.

Sudden changes in galvanic currents at intervals of about three hours in Figure 5-1 are associated with uncoupling of the working electrodes for LPR measurements, used for evaluation of self-corrosion rate of each weld section. In this instance, galvanic current measurements of all the working electrodes were continued except the one being assessed for LPR. Stabilization of galvanic currents was disturbed during LPR measurements. This disturbance raises a concern on the steadiness of the galvanic current and hence a fair measurement of the corrosion rate.

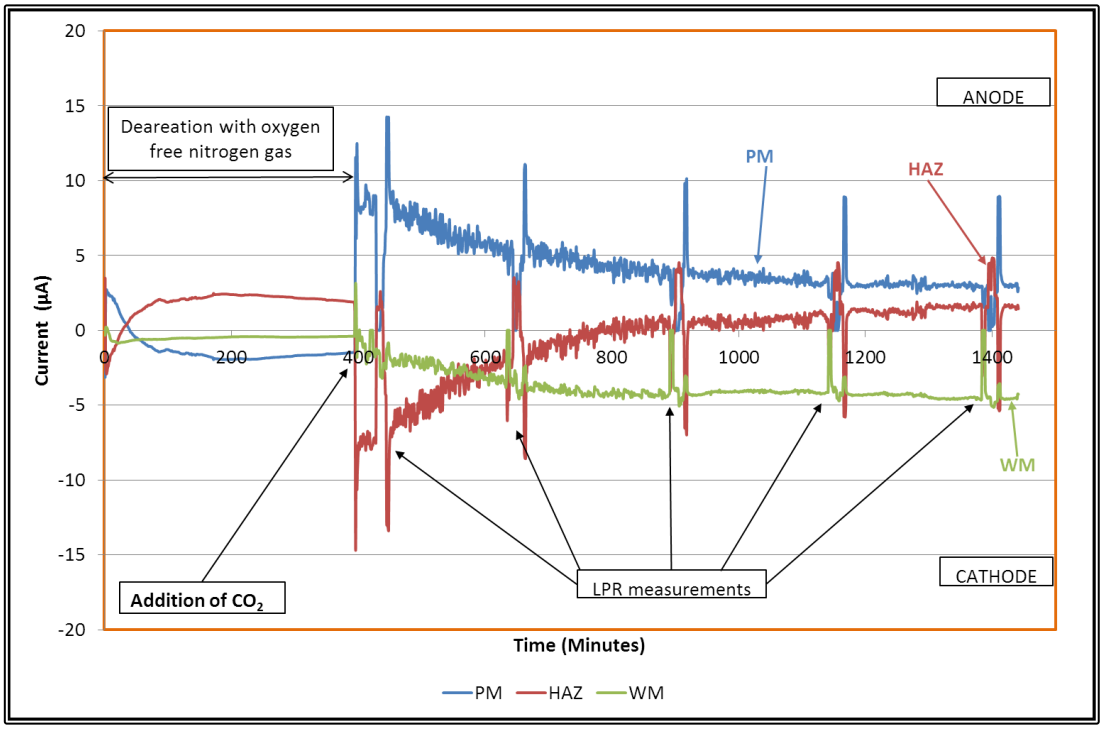

Figure 5-1: Galvanic currents in the weld sections, placed in the inner ring of the target, in no-flow uninhibited brine saturated with CO_2.

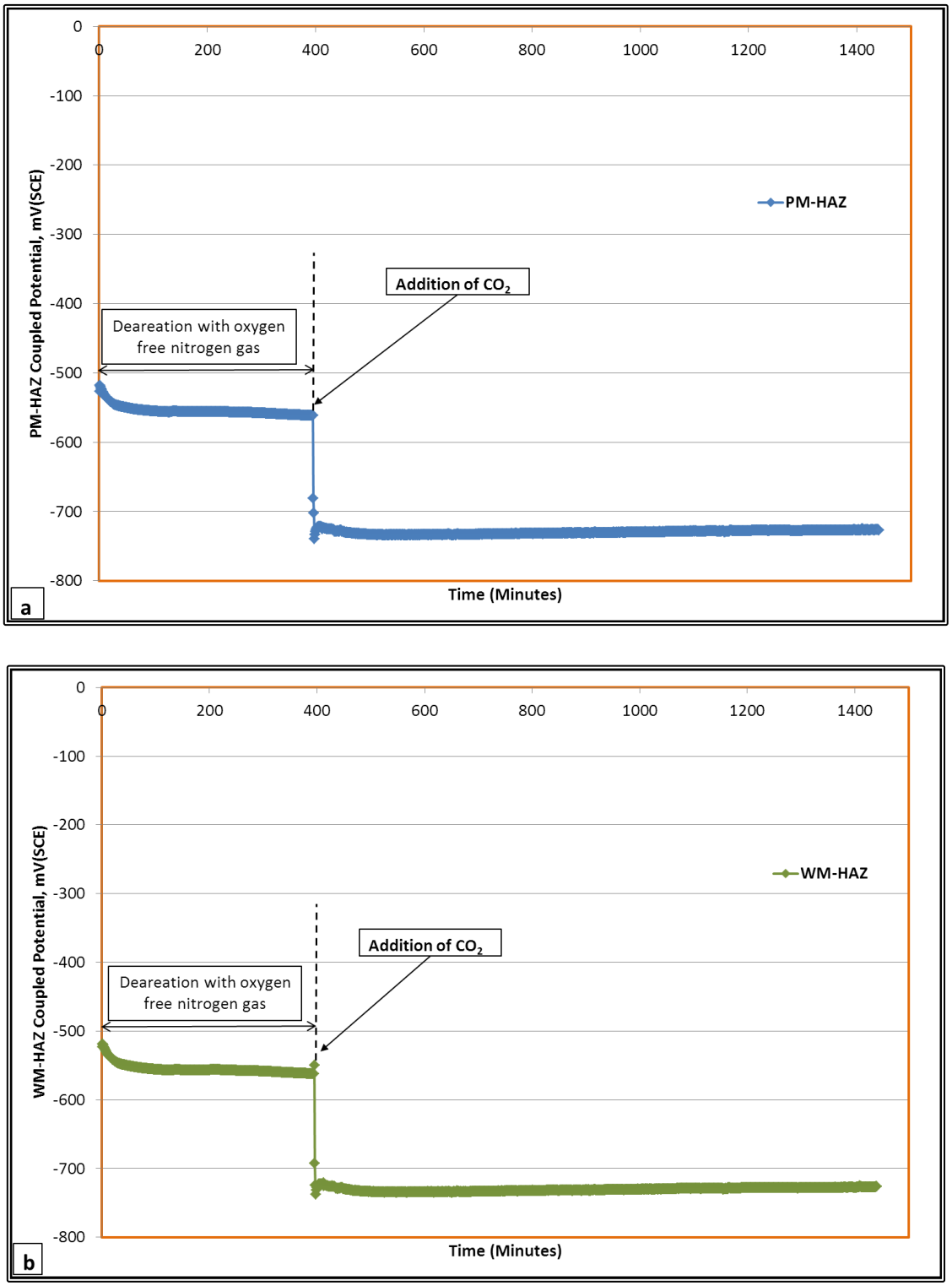

Figure 5-2: Corrosion potential of (a) PM-HAZ and (b) WM-HAZ galvanic couples in uninhibited no-flow brine saturated with CO_2.

In no-flow condition, the galvanic current characteristics of each weld section are expected to be same, regardless of where placed on the target. This was not the case in the experiments conducted in no-flow condition, as shown in Figure B-1. The HAZ specimen in the outer ring was anodic, while similar specimens (HAZ) in inner ring and at the centre were cathodic. Such change could have resulted from difference in composition and / or microstructure, occasioned by variance in production and / or fabrication factors.

5.1.2 Self-Corrosion Rates

Calibration plot at 500 Ohms for Gill AC data acquisition equipment used for the LPR measurement of is shown in Figure 5-3.

Self-corrosion rates were evaluated from linear polarisation resistance (LPR) measurements of each working electrode in uncoupled state. 'Long term sweep' technique was used to scan each uncoupled working electrode from 10mV (SCE) below the open circuit potential (OCP) to 10mV (SCE) above the OCP. 60 seconds was allowed for 'cell settle time' before every scan All LPR measurements were preceded by calibration of the data acquisition equipment used (Gill AC).

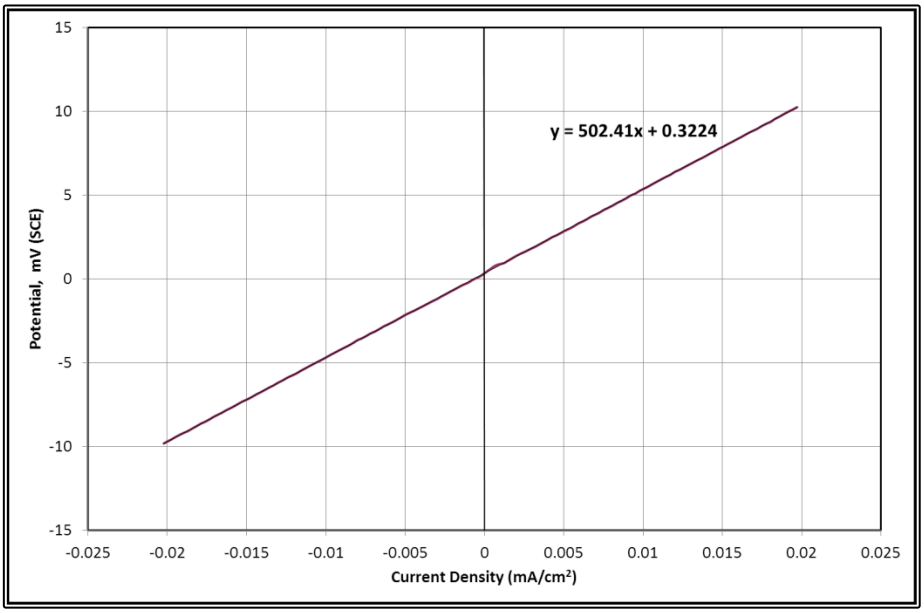

Figure 5-3: Calibration plot for the LPR measuring device (Gill AC) at 500 Ohms.

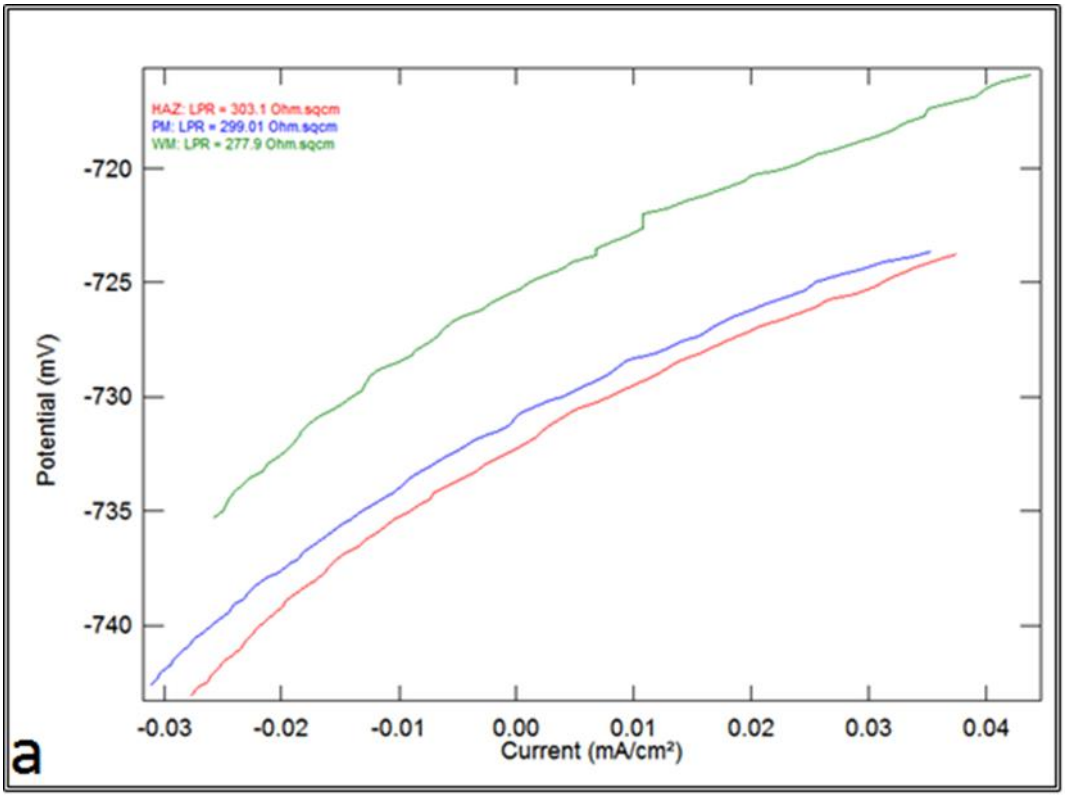

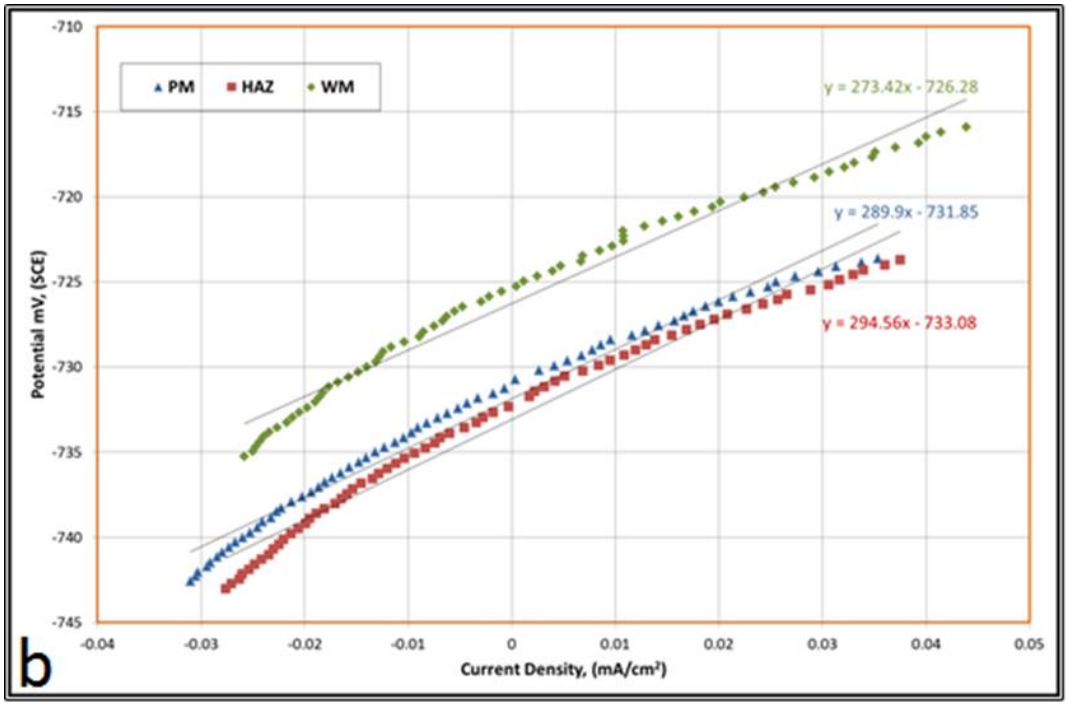

Figure 5-4: (a) Gill AC output and (b) Microsoft Excel plot of Long Sweep LPR measurements for the weld sections in the inner ring in no-flow uninhibited brine saturated with CO_2.

Typical plots of changes in current (ΔI) corresponding to change in potential (ΔE) for the weld specimens in the inner ring are as shown in Figure 5-4. The Gill-AC software output is presented in Figure 5-4(a), while the Microsoft Excel plot is shown in Figure 5-4(b). The slope of the linear regression is called the Polarisation Resistance (R_p), which is inversely related to the corrosion current density (I_{CORR}), given by Equation 4-2.

The WM was the noblest component of the three weld sections as characterised by its highest OCP value, as shown in Figure 5-4. The OCP and polarisation resistances of the HAZ and PM being close are not surprising since they are essentially of the same chemical composition but differ only in microstructures.

In an ideal metal or welded joint, the self-corrosion rates of similar weldment segment would be the same in a no-flow system, regardless of where the electrode was positioned. All the working electrodes behaved differently (as shown in Figure B-2), presumably due to composition and / or microstructural differences, as explained previously for galvanic current measurements.

5.1.3 Total Corrosion Rates

The total corrosion rates of the three weld sections in each hydrodynamic zone of the target were evaluated from the sum of the arithmetic mean of galvanic corrosion rates and self- corrosion rates towards the end of the experiment, as shown in Figure B-2. They are expressed as current densities but can be converted to metal loss from the relationship that:

$$\mathbf{1\ \mu A/cm^2 \equiv 0.012\ mm/y} \qquad \textbf{Equation 2-24}$$

Figure 5-5 shows the contributions of the mean of galvanic corrosion and the mean of self-corrosion to the total corrosion rates of each weld segment in the inner ring (high turbulence hydrodynamic transition zone) in uninhibited brine saturated with in no-flow condition. The overall galvanic protection (negative corrosion current) of the WM

resulted into lower total corrosion current compared with the self-corrosion current. The WM exhibited the least total corrosion rate while the HAZ was the highest. This implies that the X65 carbon steel welded joint has high propensity to preferential weld corrosion (PWC) failure, since the thickness of HAZ would be severely reduced compared with other weldment zones. Similar trend was observed in the weld segments at the centre, as shown in Figure 5-6. Also, WM showed the least total corrosion rate in the three sets of weldment samples; presumably due to the improved composition of the weld metal, as presented in Table 3-2.

In no-flow condition, the galvanic current characteristics of each weld section is expected to be same, regardless of where placed on the target, however, this was not the case, as shown in Figure B-1. Also anticipated is similar self-corrosion rates and hence, comparable total corrosion rates of each weld section/zone on the target in no-flow condition. This was not the case, as presented in Figure 5-6 and Figure B-2. The three PM specimens were anodic while all the WM specimens also exhibited cathodic galvanic current in the three hydrodynamic regions. However, the HAZ was anodic at the centre and the inner ring but cathodic in the outer ring, as shown in Figure B-1, resulting into higher PM anodic current. Hence, PM total corrosion rate was higher than total corrosion rate of HAZ in the outer ring. These differences could be attributed to composition, microstructure and stresses (thermal and structural) associated with each section. Also important is the non-uniformity of these features within a particular zone and therefore in the selected specimens.

Apart from the aspects described in the paragraph above, all the results of tests performed using this technique and conditions were consistent. Therefore, it could be presumed that the new target provides opportunity for flow accelerated electrochemical measurements using SJI.

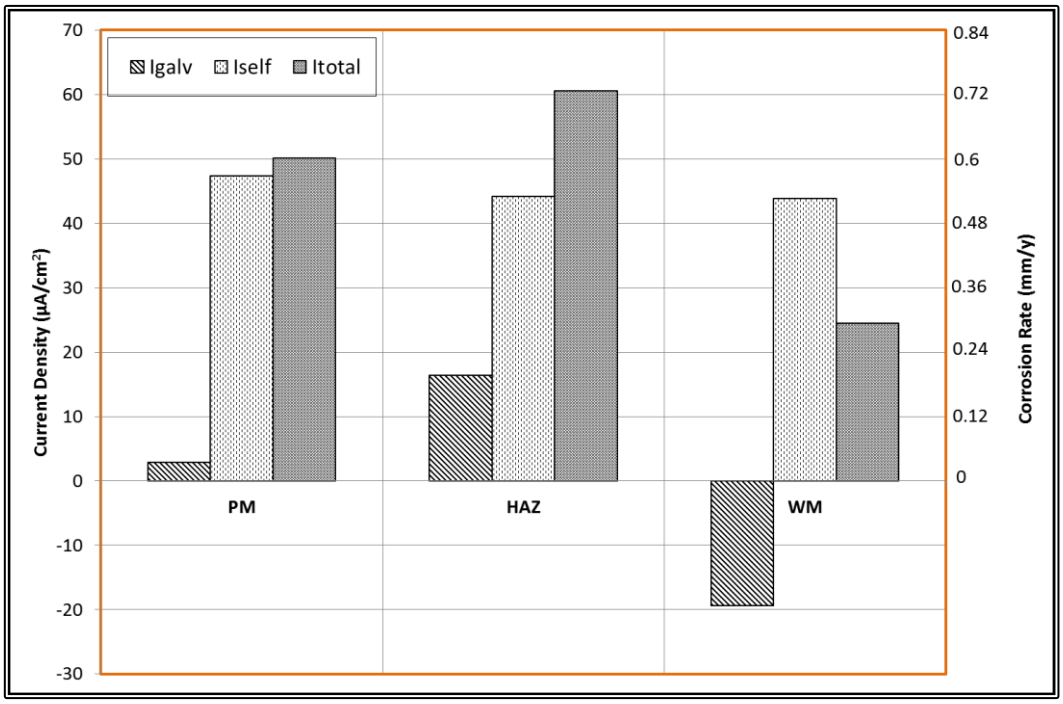

Figure 5-5: Total corrosion (I_{total}) currents for each weld section in the inner ring of the target in stagnant uninhibited brine saturated with CO_2.

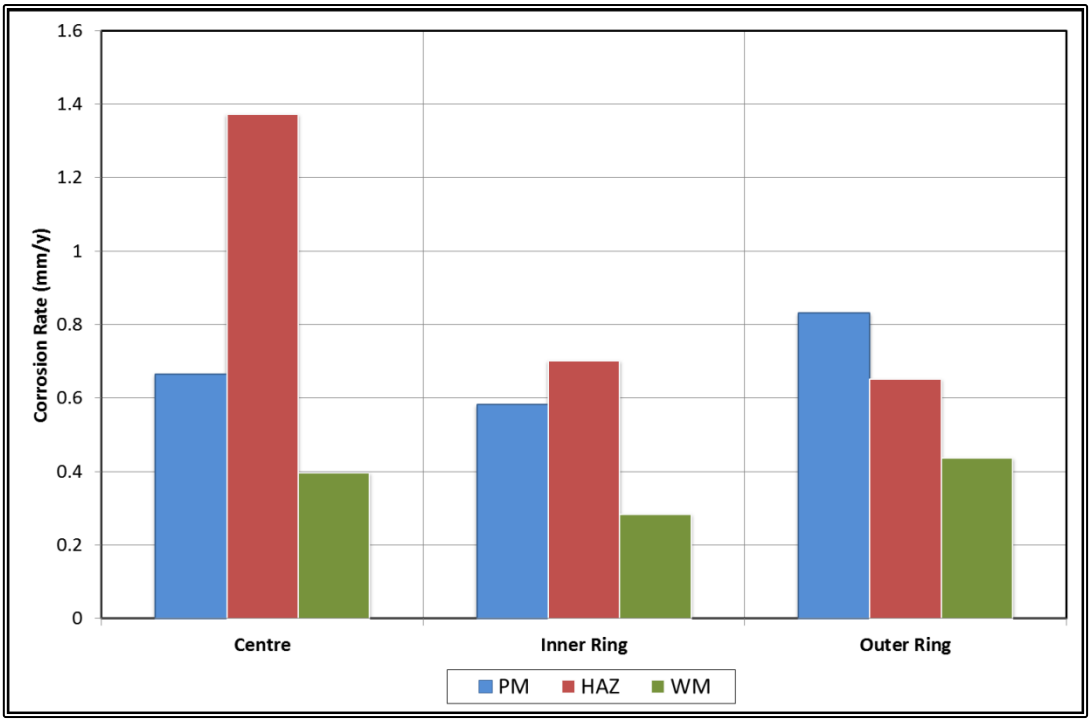

Figure 5-6: Total corrosion rates for each weld section in the three hydrodynamic zones in stagnant uninhibited brine saturated with CO_2.

5.2 Uninhibited Flowing Condition

In these trial tests, brine solution was flowed at nozzle jet velocity of 10 m/s. The first stage involved deaeration of the solution in the flow loop with OFN for about 700 minutes. In the second stage, CO_2 gas was sparged into the loop. Galvanic measurements were performed in both stages, but were interrupted by LPR measurements in the second stage of the test. The solution temperature rose from 20^oC, at the beginning of the experiment, and stabilized at 42^oC as the test progressed.

5.2.1 Galvanic Current Measurements

Plots of typical galvanic current measurements for weld segments in the inner ring are shown in Figure 5-7. In the deaeration stage, the WM and PM were protected by the HAZ anodic current. Galvanic current exchange value increased steadily as flow progresses. A sharp decrease after about 200 minutes could be attributed to formation of a partially protective and stable corrosion product film on the working electrodes. CO_2 sparging into the solution resulted into galvanic current reversal, with the HAZ being protected by the large anodic currents of PM and WM. A second current reversal was observed as the current settles, with the anodic current of HAZ protecting the PM and WM. The low galvanic current value is a characteristic response to partial protection offered by the surface corrosion product to the substrate metal. Interruptions of the galvanic measurements when LPR was performed could also be noticed in the same Figure 5-7.

Figure 5-8 shows the corresponding galvanic current densities of the weld sections in the inner ring (high turbulence transition region) of the target in uninhibited brine solution saturated with CO_2 and flowing at 10 m/s jet velocity. These were evaluated from the current and the corroding surface areas of the working electrodes. It could be presumed that the anodic nature of HAZ in the couple predisposes such welded joint to localised attack of HAZ and hence, PWC and risk of premature failure in flowing brine containing CO_2.

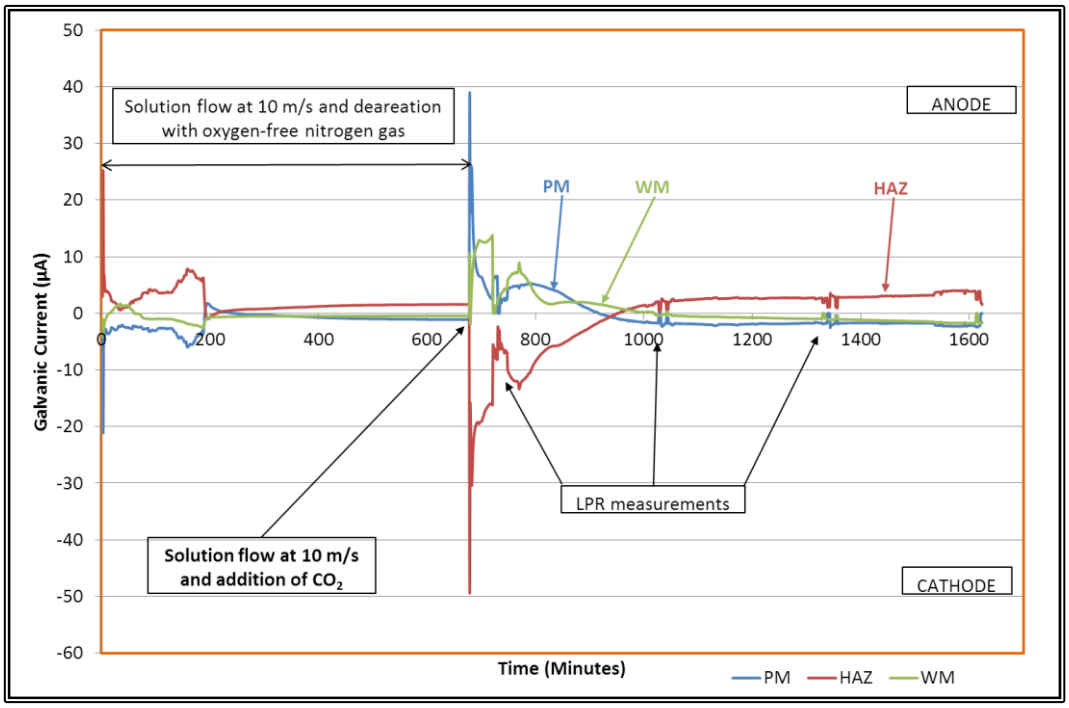

Figure 5-7: Galvanic currents of weld sections in the inner ring in uninhibited brine solution saturated with CO_2 flowing at 10 m/s.

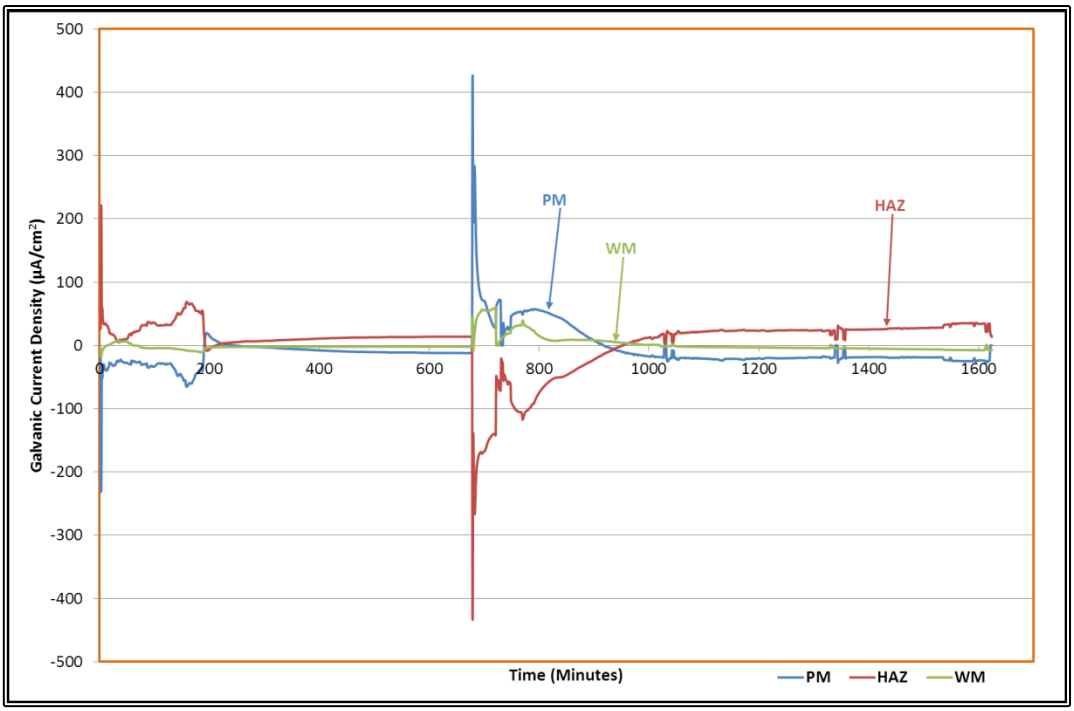

Figure 5-8: Galvanic current densities of weld sections in the inner ring in uninhibited brine solution saturated with CO_2 flowing at 10 m/s.

5.2.2 Self-Corrosion Rates

Figure 5-9 shows a typical ACM software generated results of Long Sweep LPR measurements, similar to the plots presented in Figure 5-4. The trends in evaluated self-corrosion rates at 4 hours intervals for the weld sections in the inner ring are presented in Figure 5-10. The PM and the HAZ displayed similar self-corrosion rates / trends. This is comparable to self-corrosion rates in no-flow conditions (Figure 5-4 and Figure 5-5), and could also be attributed to their same chemical composition but different microstructures. However, the WM exhibited higher self-corrosion rate than the PM and the HAZ in contrast to the situation in no-flow condition. This change in corrosion rates underscores the roles of the environment, especially, change in hydrodynamics, on corrosion rates (Mahajanam and Joosten, 2011; Lee and Woollin, 2005; Fang and Liu, 2004; Avendano-Castro et al., 2009).

Description	Value
File name	C:\Users\c067307\Documents\ADEGBITE M\RESULTS\Baseline\RUN5\RUN5 - LPR\1Rip
Test type	LPR sweep
Instrument serial number	1249
Physical channel	1
Sequence number	1
ZRA Number	n/a
Time and Date	07:11:20 18/Jul/2012
Data points	67
Area (cm²)	0.914
Rest Potential (mV)	-710.53
Metal	Mild Steel
Metal factor	1159
LPR (Ohm.cm²)	1186.2
Ba (mV)	60
Bc (mV)	60
Icorr (mA/cm²)	0.0109959
Corrosion Rate (mm/year)	0.1274425
Corrosion rate (mils/yr)	5.0174
Intercept (mA/cm²)	0
Intercept corrosion rate (mm/year)	0
Intercept corrosion rate (mils/yr)	0
IR Compensation value (Ohm.cm²)	N/A
Start Potential	-10 mV
Stop Potential	10 mV
Sweep Rate	10 mV/min
Readings Per Test	100
Gradual Sweep From Cell to Start Potentia	No
Cell Settle Time	60 seconds
Oversample	On
Count Resistor At Start	Auto
Count Resistor During Test	Auto
Offset To Rest Potential	Yes

Figure 5-9: Gill-AC computer out of Long Sweep LPR measurements for the PM in the inner ring in uninhibited brine containing CO_2, flowing at 10 m/s.

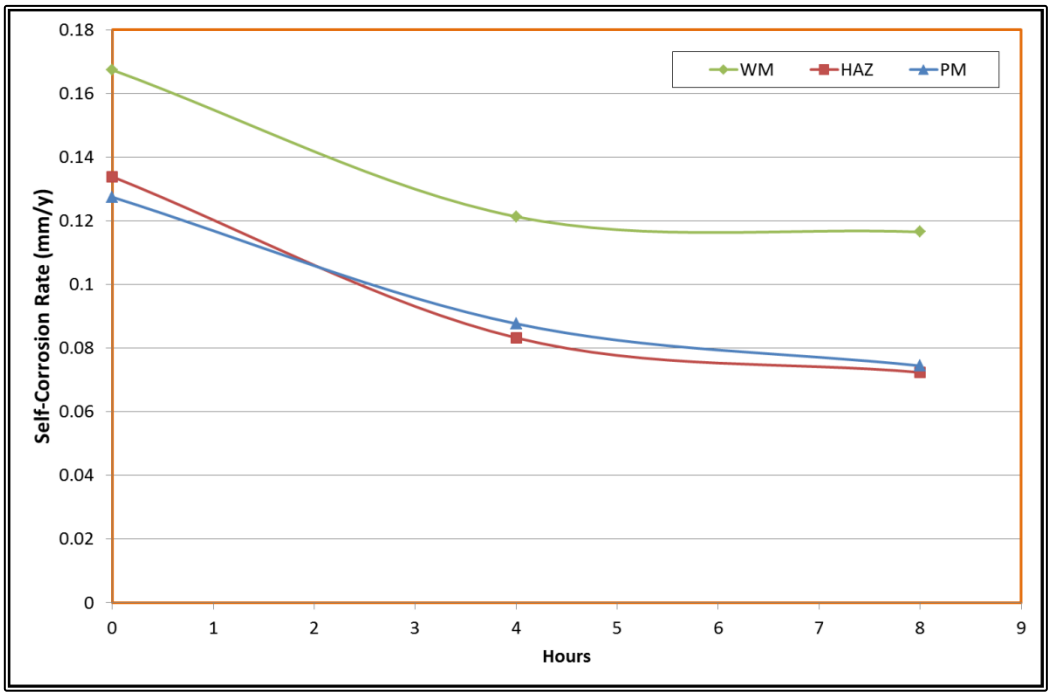

Figure 5-10: Self-corrosion rates of weld sections in the inner ring in uninhibited brine solution saturated with CO_2 flowing at 10 m/s.

5.2.3 Total Corrosion Rates

The total corrosion rate of each weld section can be considered to be the sum of its galvanic corrosion and self-corrosion rates. Figure 5-11 shows the total corrosion rates as the sum of the galvanic corrosion and the self-corrosion. The total corrosion rates of weld sections in the high turbulence transition region of the target show that the HAZ and the WM were significantly more than the PM. This intense selective attack of HAZ and WM predisposes the joint to PWC.

The total corrosion rates in other hydrodynamic regions were calculated as above and the total corrosion rates in uninhibited brine solution saturated with CO_2 and flowing at 10 m/s are presented in Figure 5-12. Local attacks of the HAZ and /or the WM in each region of the target indicate propensity to PWC in flowing uninhibited brine containing CO_2.

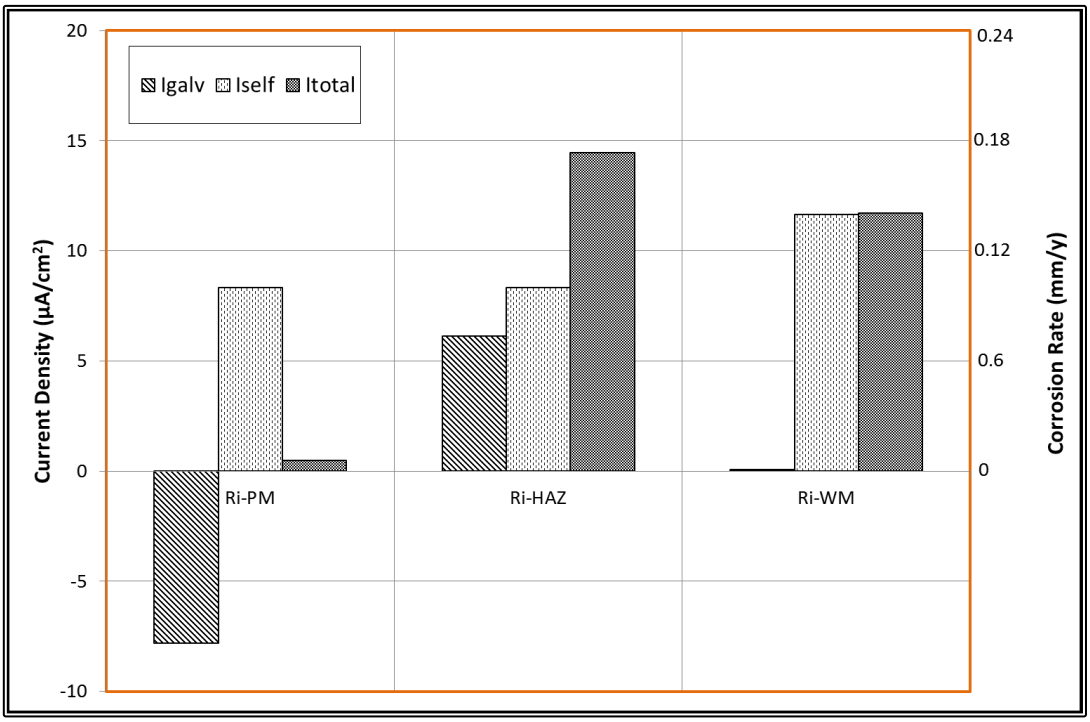

Figure 5-11: Total corrosion rates of weld sections in the high turbulence region in uninhibited brine solution saturated with CO_2 flowing at 10 m/s.

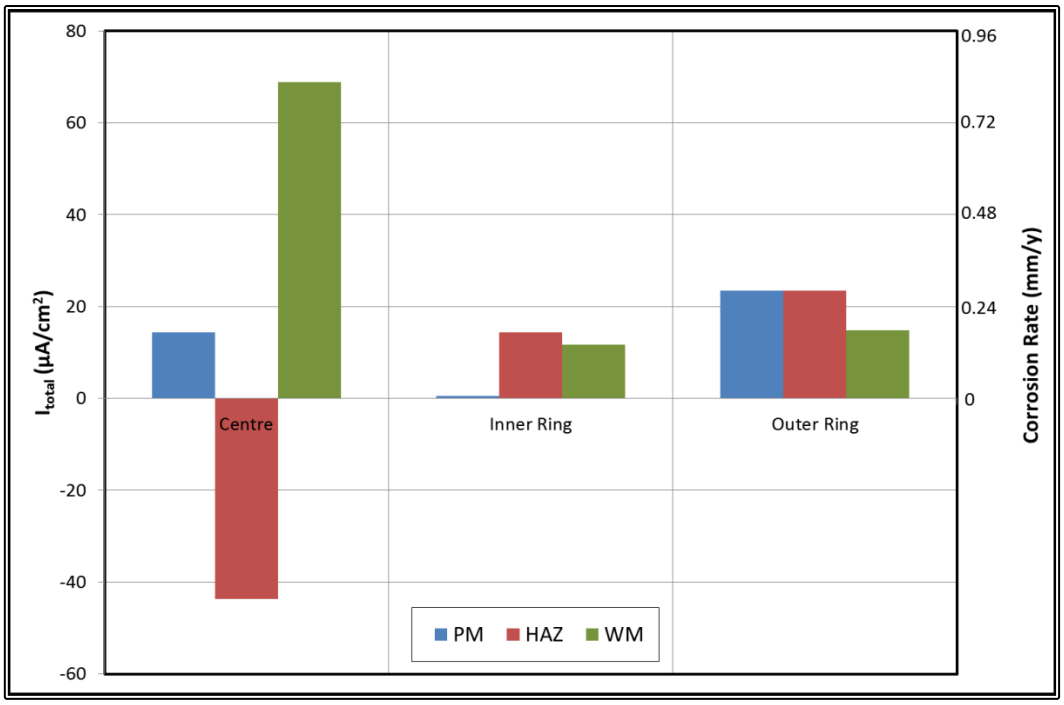

Figure 5-12: Total corrosion rates of weld sections in uninhibited brine solution saturated with CO_2 flowing at 10 m/s.

5.3 Chapter Summary

Galvanic current exchange between sections of the weld and LPR measurement of each weld section are presented and assessed to check the variability of this novel SJI technique for evaluation of FAC studies.

- Novel SJI target is suitable for electrochemical studies of weldments
- It was possible to simultaneously record measurements in all the three working electrodes in the three different hydrodynamic regions in a single test, thereby ensuring the same test environment, and saving time and other economic resources.
- Tests in stagnant (no-flow) conditions are expected to produce the same results, regardless of where placed on the target; since all the weld sections are exposed to the same hydrodynamic (stagnant) condition. However, this was not the case. The differences in galvanic current characteristics may therefore be attributed to variation in the metallurgical features of the weld sections.
- The inner ring of the target (high turbulent transition region), corresponding to the most critical region in pipeline flow, was chosen as the focus of study for flow accelerated PWC in X65 pipeline steel in subsequent tests.
- Interruption of galvanic measurements when LPR measurements were conducted produced undesirable disturbance in the galvanic response, hence the decision to perform LPR at the end of the test.
- Linear polarisation resistance (LPR) measurements of each working electrode in uncoupled state, using ‘cyclic sweep’ technique, instead of ‘Long term sweep’ technique, from 10mV (SCE) below the open circuit potential (OCP) to 10mV (SCE) above the OCP and back (one cycle).

CHAPTER 6.
RESULTS AND DISCUSSION

In this chapter the microstructural analysis and micro hardness distribution across the weldment are presented. The high turbulence transition region (inner ring), being characterized by high turbulence, a large velocity gradient at the wall, and high wall shear stress, was of primary interest for studying the effects of hydrodynamic changes. The total corrosion rate of each weld section in the inner ring was calculated from galvanic and self-corrosion rates and the susceptibility to PWC were evaluated for different oilfield scenarios. Evaluations of corrosion products and reaction mechanisms were performed with a view to ascertaining the influence of the weld metallurgy, environment and flow conditions.

6.1 Welded Pipeline Steel

Micrographs and micro-hardness profile of the weld zones are shown in Figure 6-1. The microstructure of the parent metal (PM) consisted of fine equiaxed ferrite with small amounts of pearlite; giving hardness of 200 – 210 $HV_{(0.2)}$. The fine-grained heat-affected zone (HAZ) was similar in appearance to the PM, having slightly larger equiaxed ferrite and a small quantity of pearllite. The coarse grained HAZ displayed acicular ferrite that had formed throughout the enlarged prior-austenite grains. In the weld metal, primary ferrite had formed on prior-austenite grain boundaries, with a finer aligned microstructure within the grains; giving hardness of 223 – 230 $HV_{(0.2)}$ (Alawadhi and Robinson, 2011).

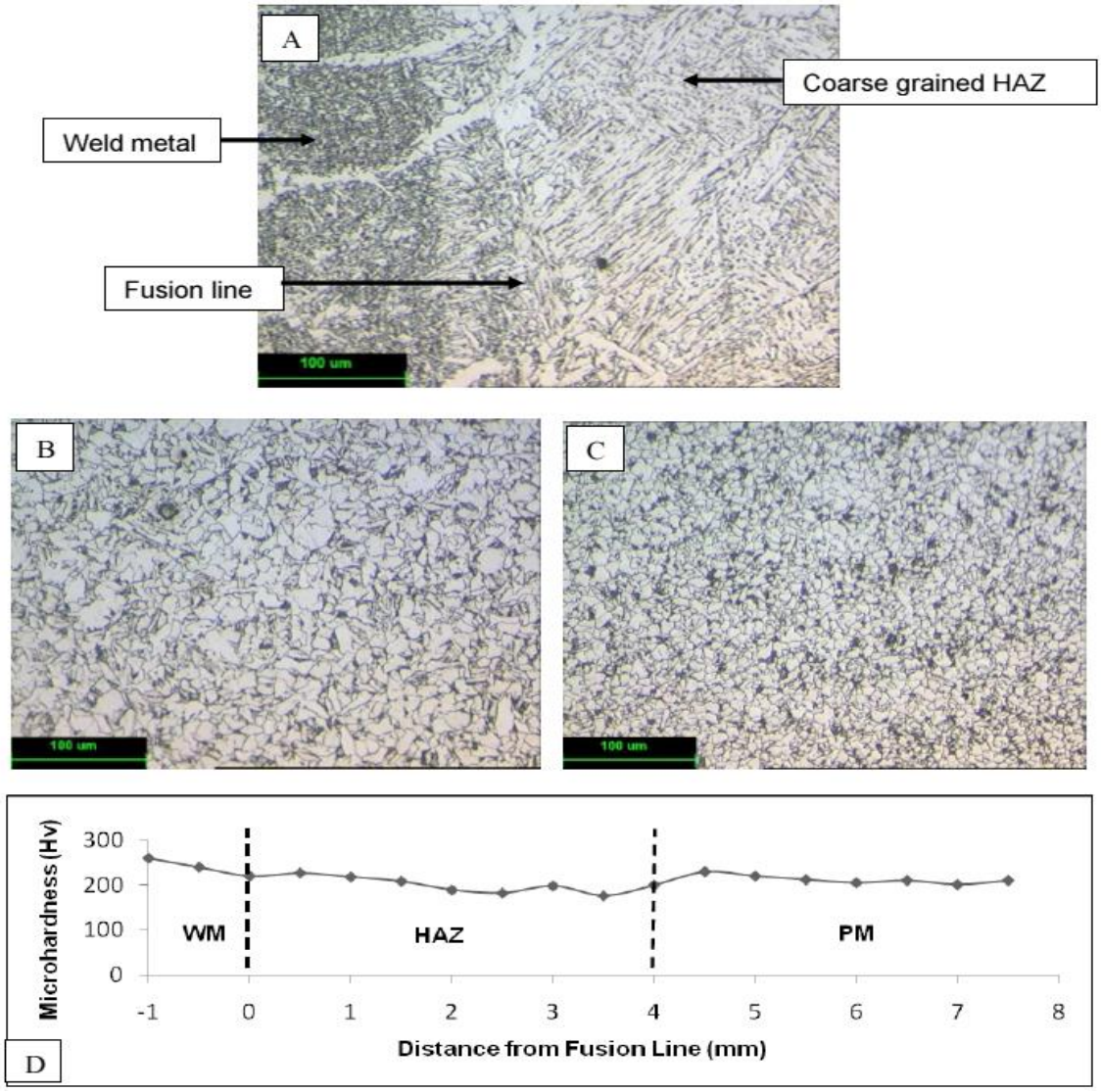

Figure 6-1: Microstructures of (a) fusion region of weld, (b) fine grained HAZ and (c) PM; (d) corresponding micro-hardness profile.

6.2 Corrosion Rates in Uninhibited No-Flow Condition

The primary purpose of this test was to investigate how corrosion rates in the weld sections (parent metal, heat-affected zone and weld metal) compromised the X65 high strength low alloy (HSLA) steel welded joint performance, in terms of preferential weld corrosion (PWC), in uninhibited brine saturated with CO_2 in the no-flow and ambient conditions.

6.2.1 Galvanic Current Measurements

The galvanic current exchange among the specimens in the high turbulent transition zone (inner ring) is shown to gradually decrease with exposure time in Figure 6-2. The decline in galvanic currents was accompanied by formation of transparent grey film on the surface of each working electrode (specimen), which appeared to be partially protective.

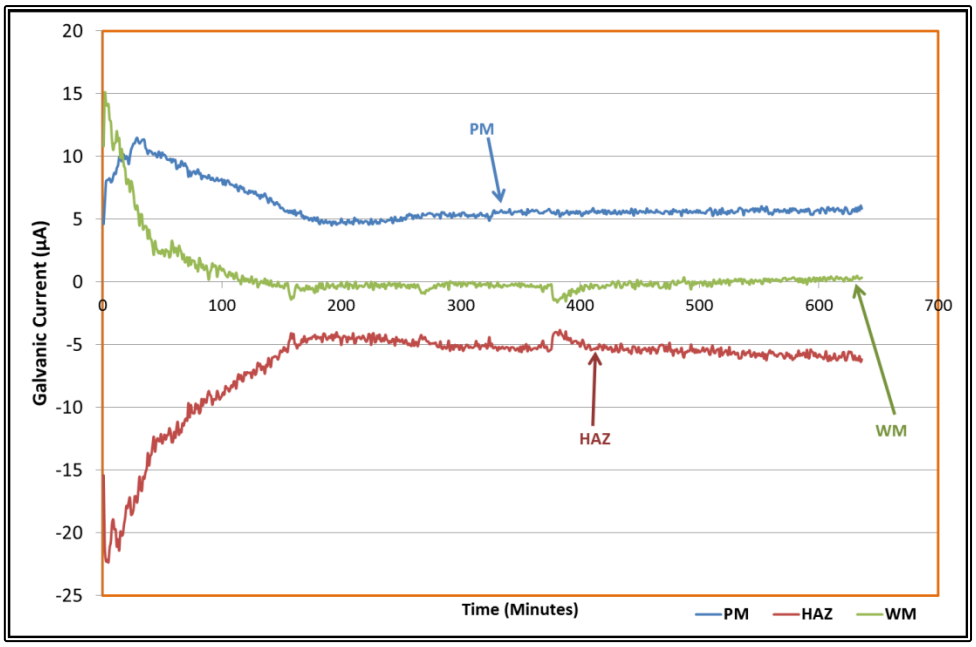

Figure 6-2: Galvanic current measurements of X65 steel weldment specimens in the inner ring in the uninhibited no-flow condition.

The galvanic current measurements show that the HAZ was protected by the anodic current of the PM. The PM was anodic (positive current) and the HAZ was cathodic (negative current) throughout the duration of this test. However, the weld metal (WM) galvanic current was essentially zero. Figure 6-3 shows the average anodic currents leaving the PM and the WM, and cathodic current arriving the HAZ within the last few minutes of the test. More current arriving HAZ indicates higher cathodic protection. Figure 6-4 shows the variations in current densities of the same weld sections. It was clearly favourable for the PM to be the anodic component in the couple, as this condition ensures that its corrosion offers sacrificial protection to other weld regions in

uninhibited brine saturated with carbon-dioxide at ambient temperature and no-flow conditions. Furthermore, since there was no accumulation of electrical charges, the total current arriving every point equals total current leaving the same point, according to Equation 4-1.

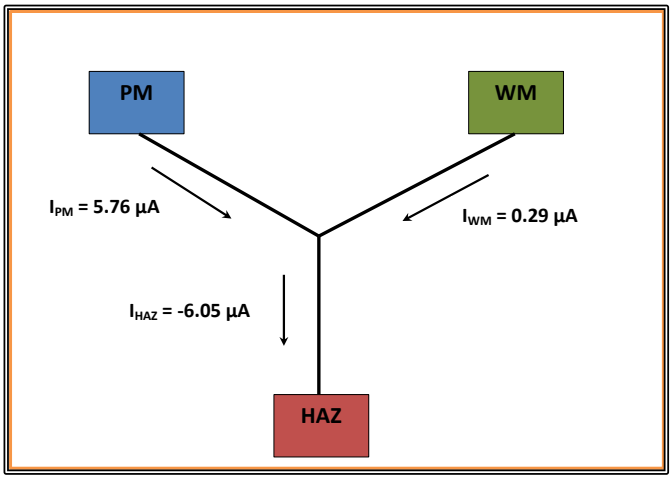

Figure 6-3: Average galvanic current in the uninhibited no-flow condition.

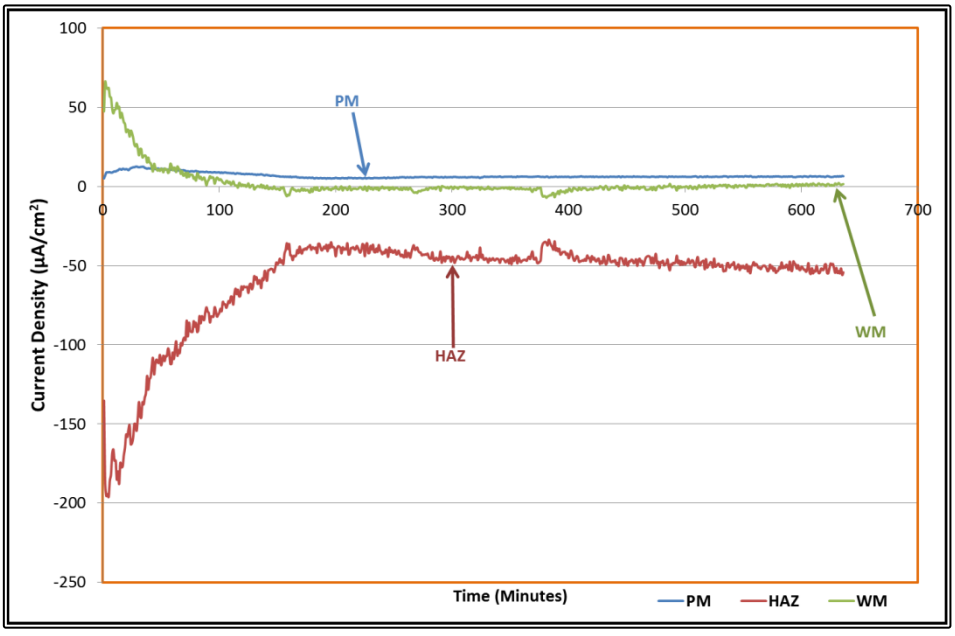

Figure 6-4: Galvanic current densities of X65 steel weldment specimens in the inner ring in the uninhibited no-flow condition.

6.2.2 Self-Corrosion Rate Measurements

The self-corrosion current, I_{corr} of each weldment segment (working electrode) in all hydrodynamic zones was evaluated from the linear polarisation resistance (LPR) data (all taken at the end of the experiment), using the Stern-Geary Equation 4-2.

Figure 6-5 compares self-corrosion rates of the electrodes in the inner ring and shows that in the uninhibited no-flow condition, the HAZ corroded faster than the WM and PM. As expected, the WM was the most resistant to self-corrosion since it contains higher nickel (Ni) (0.68%) content as shown in Table 3-2 and this was corroborated by the highest open circuit potential as given in Table 6-1. These results were substantiated by previous related studies (Mahajanam and Joosten, 2011; Queen et al., 2004; Copson, 1945; Ciolkowski et al., 2012) which reported that nickel (Ni) in structural steels promotes formation of insoluble passive corrosion film in marine environment, thereby limiting the formation of soluble iron chloride salt.

Table 6-1: Open circuit potentials in the uninhibited brine saturated with CO_2.

	E_{CORR}, mV (SCE)		
	PM	HAZ	WM
No-flow	-723.52	-719.72	-716.69
Flowing at 5 m/s	-696.58	-695.4	-701.1

The HAZ was observed to be more noble in the test solution in the no-flow and ambient conditions compared with the PM (Table 6-1), however the rate of self-corrosion was higher. The expected cathodic curve is illustrated in Figure 6-6, in which the PM corrosion current (i_{PM}) is greater than the corrosion current of the HAZ (i_{HAZ}).It could be reasoned that since the HAZ would be partially protected when coupled (most noble) it would have less corrosion of the surface. When uncoupled, this uncorroded surface would have initially displayed a high corrosion rate, followed by a gradual reduction in the rate of corrosion of the surface. In contrast, the PM which acted as anode (Figure

6-3) would be more corroded and on uncoupling, its self-corrosion rate would be low to the presence of corrosion film/product (formed in the coupled state) on the surface.

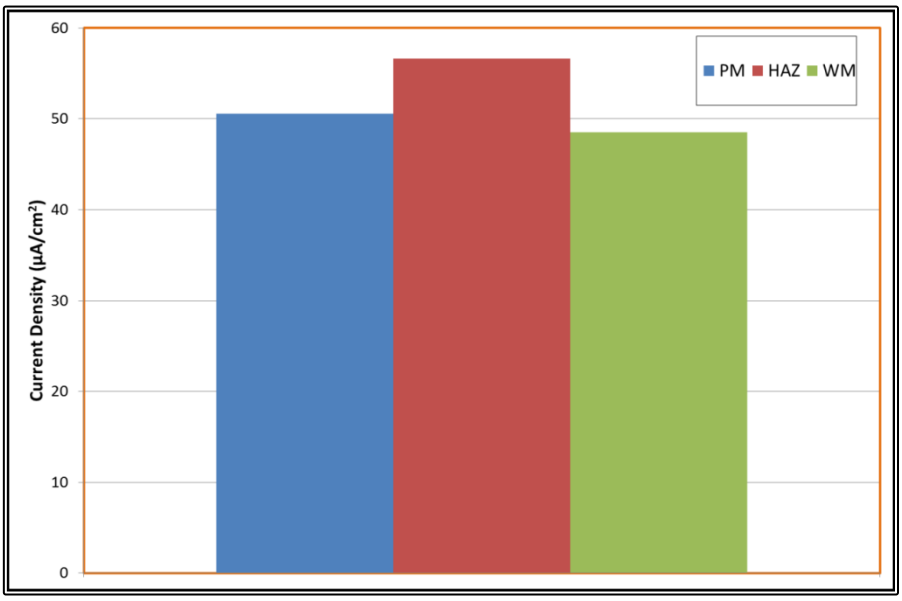

Figure 6-5: Self-corrosion currents of specimens in the inner ring in the uninhibited no-flow condition.

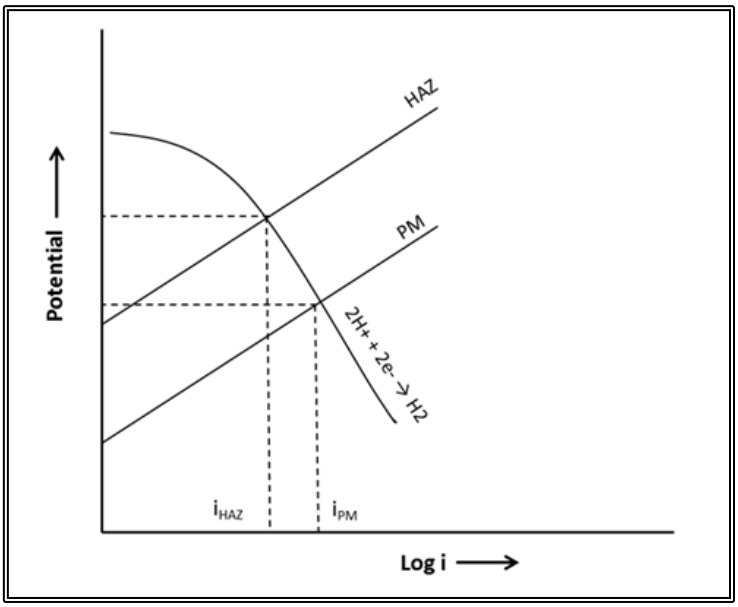

Figure 6-6: Schematic Evans diagram showing the expected cathodic curve in uninhibited brine saturated with CO_2 in the no-flow condition.

6.2.3 Total Corrosion Rates

The total corrosion rate of each weld region was calculated from the sum of the galvanic and self-corrosion current densities using Equation 2-24. Figure 6-7 shows the galvanic and self-corrosion contributions in the total corrosion rates for the weld sections in the inner ring for uninhibited brine saturated with CO_2 in the no-flow condition.

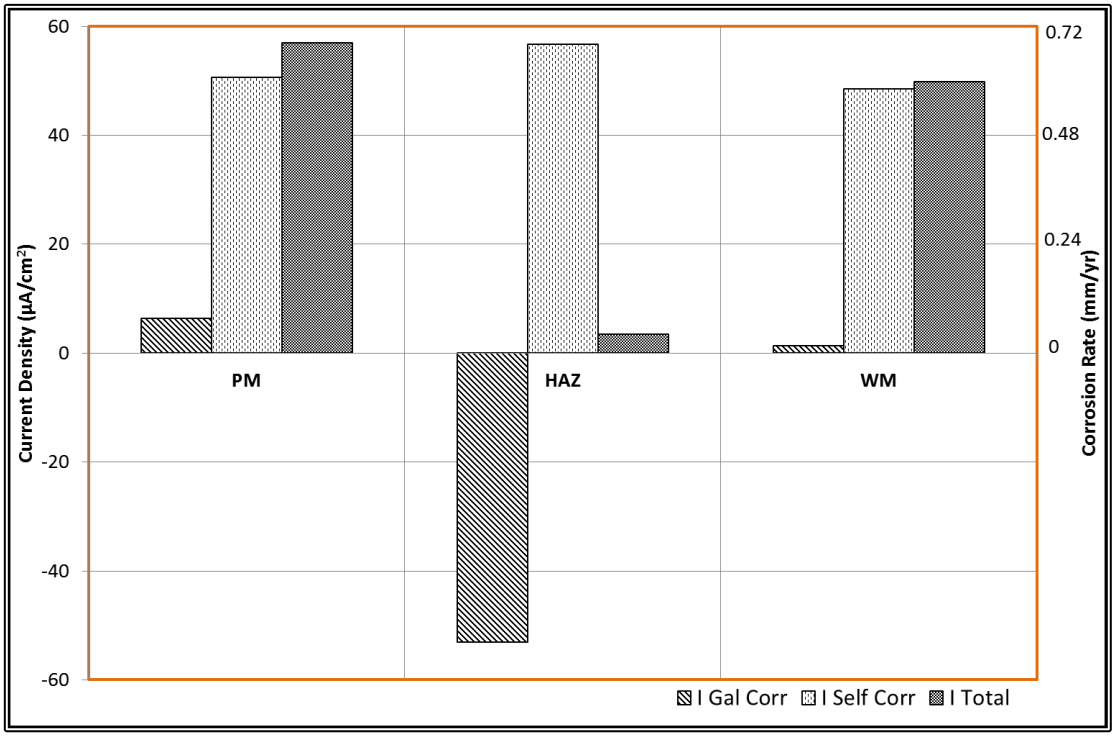

Figure 6-7: Total corrosion rates of weld sections in the inner ring in the no-flow condition.

In general, higher Ni content in the weld metal confers greater resistance to self-corrosion in no-flow condition, as noted in Figure 6-5 and supported by previous studies (Lee and Woollin, 2005; Turgoose and Palmer, 2005; Gulbrandsen and Dugstad, 2005). However, this may not guarantee protection against PWC, as susceptibility to localised corrosion may shift to the HAZ, as previously experienced in some oilfields, (Shifler, 2006; Howell, 1997).

In the no-flow condition, the self-corrosion contribution was more significant to the total corrosion rate. This is not unexpected as carbon-manganese steel is inherently

susceptible to high self-corrosion rates in carbonic acid, whereas the small compositional and microstructural differences between the weld regions would not have caused large galvanic differences (Cranfield University, 2003; Queen et al., 2004; Gulbrandsen et al., 2005; Billingham et al., 2011; Moon et al., 2013).

In summary, in uninhibited brine solution saturated with carbon-dioxide in no-flow ambient conditions, it was a favourable situation for the weld metal galvanic current to be essentially zero and the heat-affected zone to be sacrificially protected by the parent metal. This is a necessary condition for prevention of preferential weld corrosion. The contributions of self-corrosion rate were more predominant in the total corrosion rates compared with the galvanic corrosion.

6.3 Uninhibited Flowing Conditions

In uninhibited brine solution saturated with CO_2 at ambient conditions and flowing at 5 m/s, the WM was more anodic as indicated by high galvanic current leaving the electrode compared with the PM and the HAZ, (Figure 6-8). This condition predisposes such welded joint to preferential weld corrosion (PWC) in flowing uninhibited brine saturated with CO_2 with the attack localised on the WM. The corresponding galvanic current densities in the high turbulence transition zone are presented in Figure 6-9.

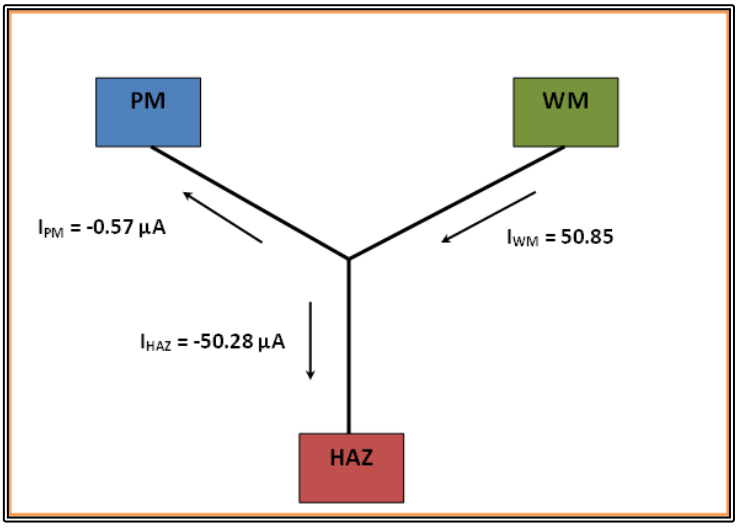

Figure 6-8: Galvanic current exchange in brine saturated with CO_2 flowing at 5 m/s.

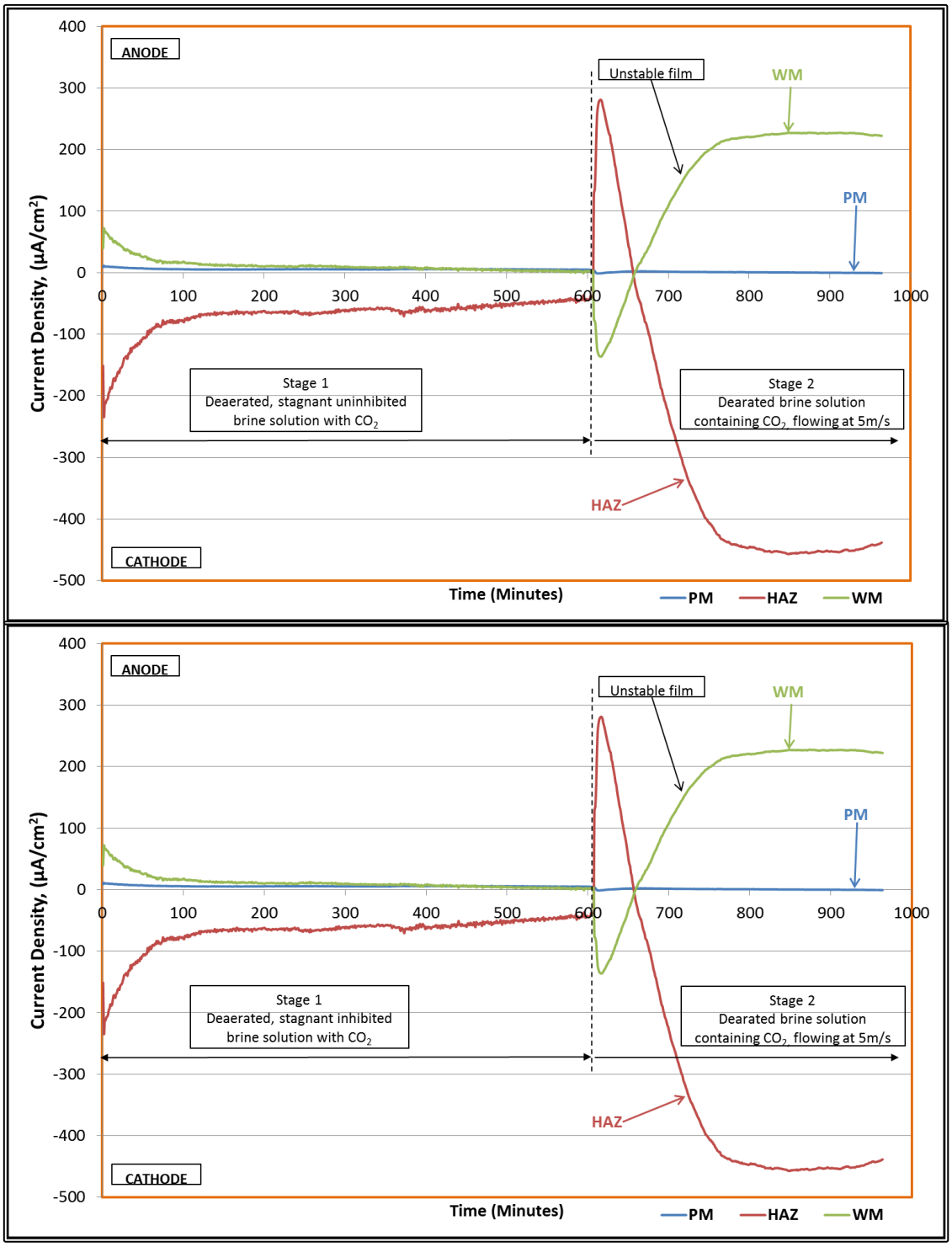

Figure 6-9: Galvanic current densities in uninhibited brine saturated with CO_2 flowing at 5 m/s.

Under a submerged jet velocity of 5 m/s, (wall shear stress of about 72 N/m^2), the WM galvanic current increased steadily due to removal of an unstable corrosion film, protecting the HAZ. Remarkably, the PM galvanic current remained essentially zero. It is significant that the galvanic currents remained higher at wall shear stress of 72 N/m^2 when the film had been thinned or removed than they had been before the flow commenced, indicating that the film had been partially protective. This is consistent with published results of related studies (Alawadhi and Robinson, 2011; Schmitt et al., 2002; Craddock et al., 2004; Schmitt et al., 1992; Chaal et al., 2009).

Linear polarisation resistance (LPR) measurements were conducted in the same solution and flowing condition at the end of galvanic measurements, as previously explained. Subsequently, the self-corrosion rate of each weld section was evaluated from the LPR plots as shown in Figure 6-10.

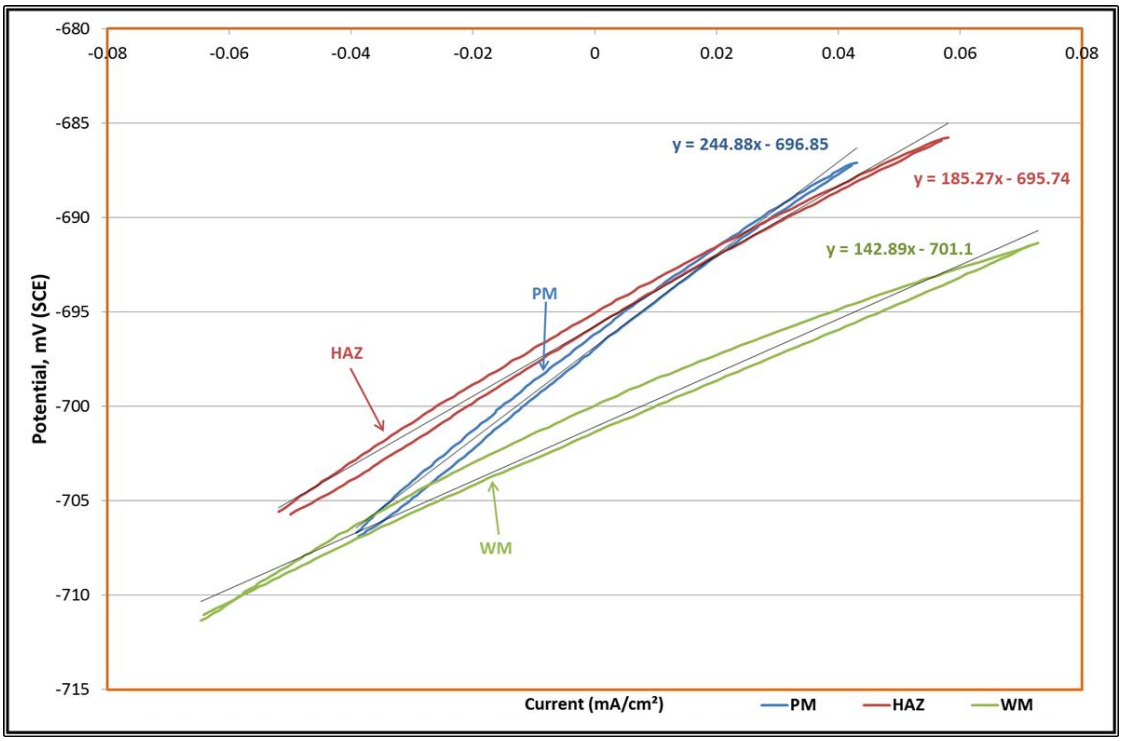

Figure 6-10: LPR cyclic sweep in uninhibited brine saturated with CO_2 flowing at 5 m/s.

Total corrosion rates of the working electrodes in the high turbulence hydrodynamic region were then calculated and presented in Figure 6-11. This figure shows that, in flowing uninhibited brine saturated with CO_2, the HSLA steel welded joint would be

subjected to severe PWC, with local attack of the WM. Hence, it could be ascertained that flowing of brine containing CO_2 has two principal effects on film formation and corrosion rate. First, it prevents the film formation and slows down its growth by reducing the local supersaturation of precipitating ions. Second, flow can damage the film locally to cause localized corrosion. When the surface corrosion film is poorly adhered to the surface, the effect of flow rate on localized corrosion has been shown to result in deleterious consequences (Dugstad, 2006; Dugstad, 1998; Videm, 1998; Dugstad et al., 2006; Sun et al., 2012; Vagapov, 2010).

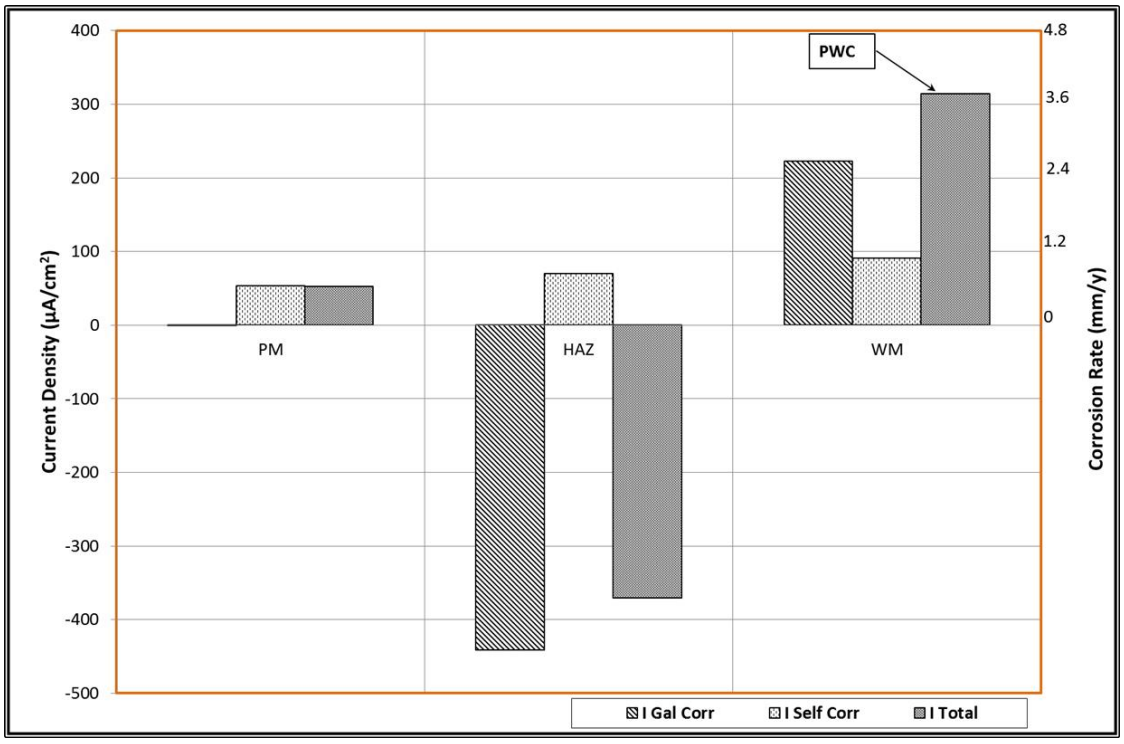

Figure 6-11: Total corrosion rates in uninhibited brine solution saturated with CO_2, flowing at 5 m/s.

6.3.1 Effect of Flow on Uninhibited Brine

A comparison of the self-corrosion rates in the no-flow and flowing (at wall shear stress of 72 N/m^2) conditions are shown in Figure 6-12. The total corrosion rates of the weld segments in the same environment and hydrodynamic conditions are also presented in Figure 6-13.

A slight increase in self-corrosion and considerable increase in galvanic corrosion were noticeable in flowing condition as shown in Figure 6-13. These may be attributed to the high shear stress accompanied by an increase in mass transport with flow, increased instability of the partially protective film, as well as reduced passivity of corrosion product on the working electrodes (Schmitt et al., 1999b; Schmitt and Mueller, 1999; Mora-Mendoza et al., 2002; Schmitt et al., 2005).

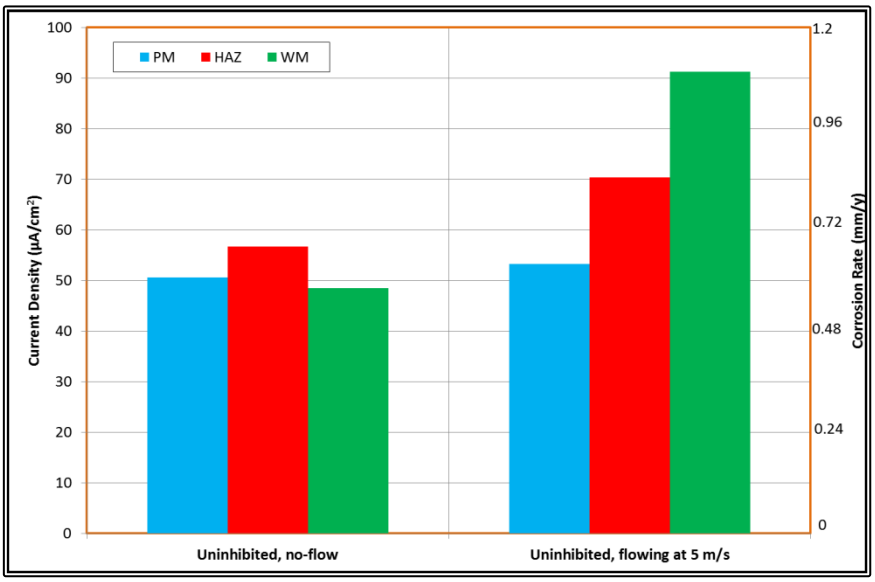

Figure 6-12: Effect of flow on self-corrosion rates in uninhibited brine solution saturated with CO_2.

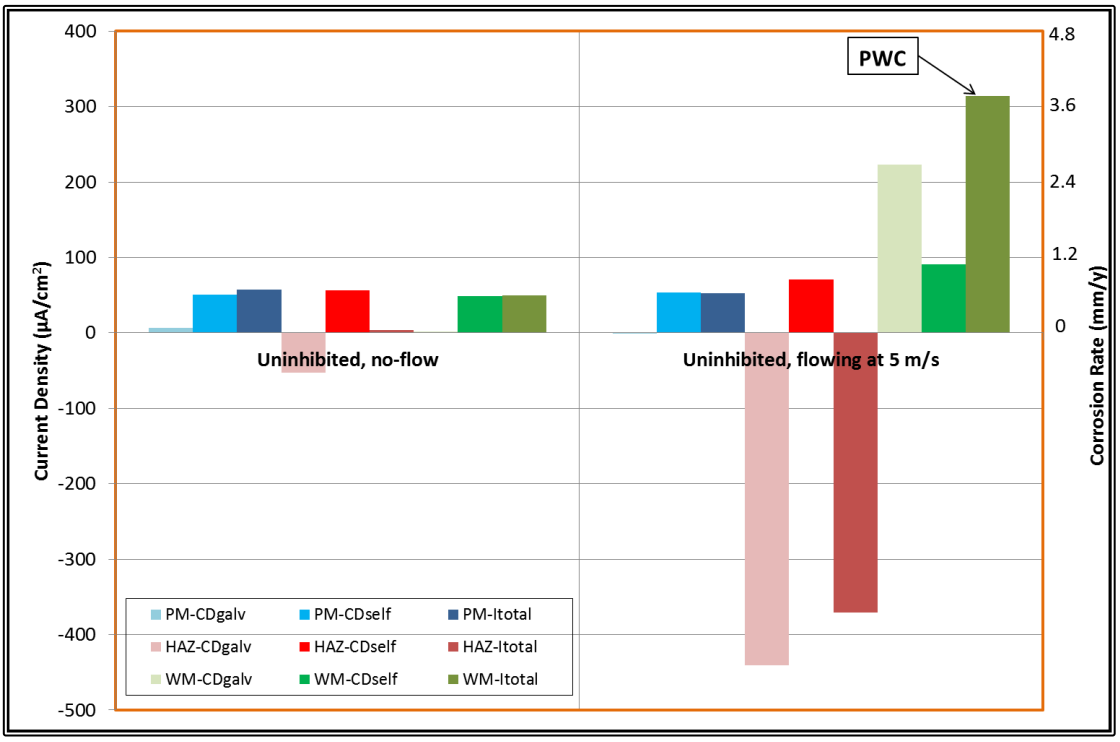

Figure 6-13: Effect of flow on total corrosion rates in uninhibited brine solution saturated with CO_2.

The HAZ was significantly protected by the sacrificial galvanic corrosion of the WM, resulting in negative total corrosion rate; meaning that the HAZ was fully protected from corrosion, under this condition. This was corroborated by the lack of corrosion of the HAZ resulting in a silver-grey appearance of the HAZ after the test. Similar observation had been reported by Martinez et al (2011). Conversely, severe localised corrosion of the WM resulted in PWC in flowing uninhibited brine saturated with CO_2.

Mahajanam and Joosten (2011) proposed an empirical term, **Δ (**Equation 6-1) as a predictive tool for the nature of the galvanic corrosion of the WM-PM couple in an aqueous medium. **Δ** defined as a Cu-Ni equivalent between the WM and the PM compositions. Positive **Δ** values indicate that the PM is the cathode while negative **Δ** values indicate that the WM is the cathode.

$$\Delta = 3.8\,(\%Cu_{base} - \%Cu_{weld}) + 1.1\,(\%Ni_{base} - \%Ni_{weld}) + 0.3 \qquad \textbf{Equation 6-1}$$

The **Δ** value evaluated for the weldment used is -0.4 (from Equation 6-1 and compositions from Table 3-2). The negative value of **Δ** suggests that the WM would behave as the cathode in the galvanic corrosion of the weldment. This was not observed in corrosion tests conducted in uninhibited brine saturated with CO_2. This emphasises the greater importance of the synergism between materials and service parameters, such as the metallurgical, nature of the environment, the flow rate and film attachment. It could therefore be argued that the environmental effects on the galvanic corrosion (and PWC) override the chemical composition and microstructure tendency as reported by Shifler (2006) and Mahajanam and Joosten (2011).

It could therefore be affirmed that the magnitude of the potential difference between the dissimilar materials (including PM-HAZ and HAZ-WM couples) cannot be used to predict the severity of galvanic corrosion because electrochemical potentials are a function of the thermodynamics and not of the reaction kinetics that may occur. It is the surface kinetics that determines the severity of galvanic corrosion (Roberge, 2000; Queen et al., 2004; Ramachandran et al., 2000; Gulbrandsen et al., 2005). For instance, Shifler (2006) reported that a difference of 50 mV between select dissimilar materials can lead to severe corrosion while a potential difference of 800 mV has been successfully coupled. This is possible when the galvanic current is limited by oxygen diffusion to the cathode. Under this (cathodic control) condition, the galvanic current rate is directly proportional to the cathode area and independent of the anode area. Therefore, very small cathode/anode area ratio should enhance better long term performance.

6.4 Corrosion Rates in Inhibited Brine Solution Saturated with CO_2

The galvanic corrosion and self-corrosion rates that resulted from the addition of 30 ppm oilfield inhibitor CORRTREAT 10-569 are presented for the weldment segments in the high turbulence flow zone (inner ring). Total corrosion rates in inhibited brine saturated with CO_2 were evaluated and discussed for no-flow and flowing (at nozzle jet velocities of 5 m/s and 10 m/s) conditions.

6.4.1 Effect of Chemical Inhibition in No-Flow Condition

In static (no-flow) uninhibited conditions, the highest total corrosion rate of 0.66 mm/y was observed in the PM (as presented in Figure 6-7 and Figure 6-13). Addition of a typical oilfield inhibitor (CORRTREAT 10-569) was effective in reducing the total corrosion rate of the PM to 0.08 mm/y (approximately 12% of the uninhibited value) as shown in Figure 6-14. The propensity for PWC to occur in no-flow condition is negligible, as the total corrosion rates of the WM and the HAZ were very low and less than that of the PM. The inhibitor film on the weld segments appears to be stable and protective (Figure 6-16), forming a partial barrier between the corroding metal surfaces and electrolyte. Hence, it could be deduced that inhibition in the static and ambient conditions was beneficial.

Table 6-2 is a comparison of the free corrosion potentials in brine solution saturated with CO_2 with and without chemical inhibitor (CORRTREAT 10-569) in the no-flow and ambient conditions. The OCP were recorded during the 'settling-time' preceding the LPR measurements in uncoupled state. It could be observed that addition of the chemical inhibitor resulted in change of the free corrosion potential into positive (noble) direction. A little increase in the OCP is accompanied by a large reduction in corrosion current as illustrated in Figure 6-15. This suggests that the inhibitor was adsorbed on each weld segment forming a partial protective film and reducing the rate of corrosion reaction on the metal surface.

It is noteworthy that oilfield inhibitors are usually formulated as mixed inhibitors, which reduce both anodic and cathodic reactions. The noble shift in potential therefore indicates that CORRTREAT 10-569 is more effective on the anodic sites.

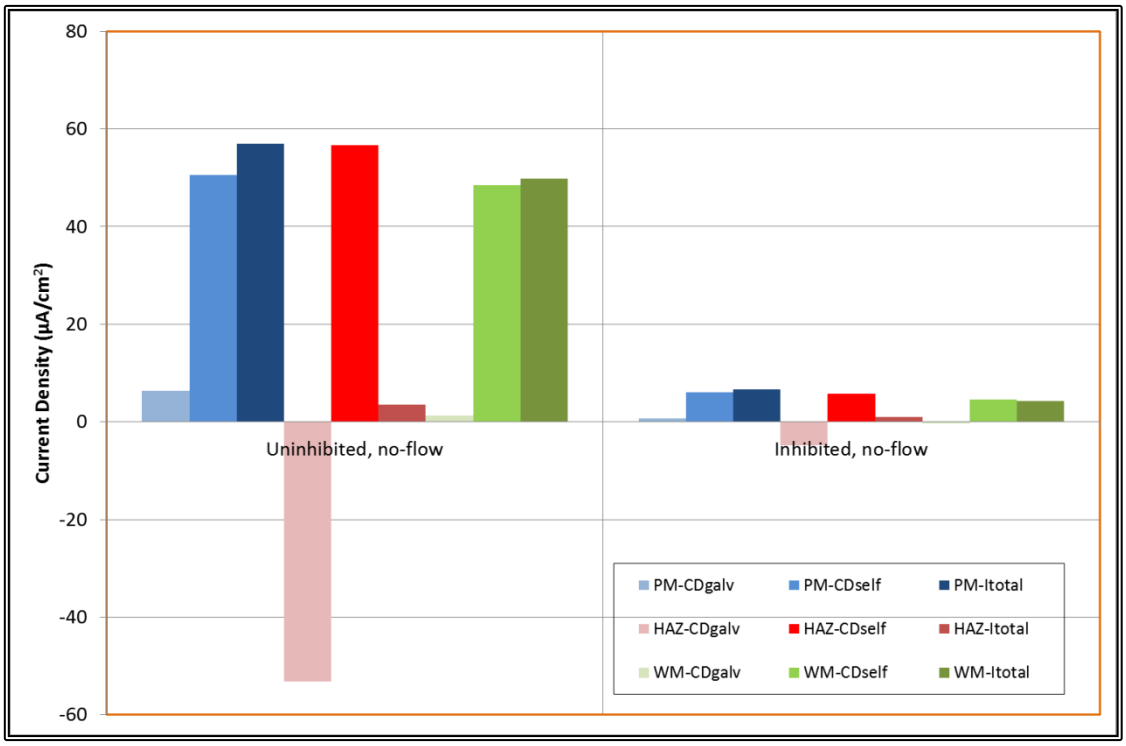

Figure 6-14: Effect of inhibitor, (CORRTREAT 10-569) on corrosion rates in brine saturated with CO_2 in no-flow condition.

Table 6-2: Open circuit potentials of brine solution saturated with CO_2 in the static condition.

	E_{CORR}, mV (SCE)		
	PM	HAZ	WM
Uninhibited solution	-723.52	-719.72	-716.69
Inhibited solution	-649.59	-656.85	-646.10

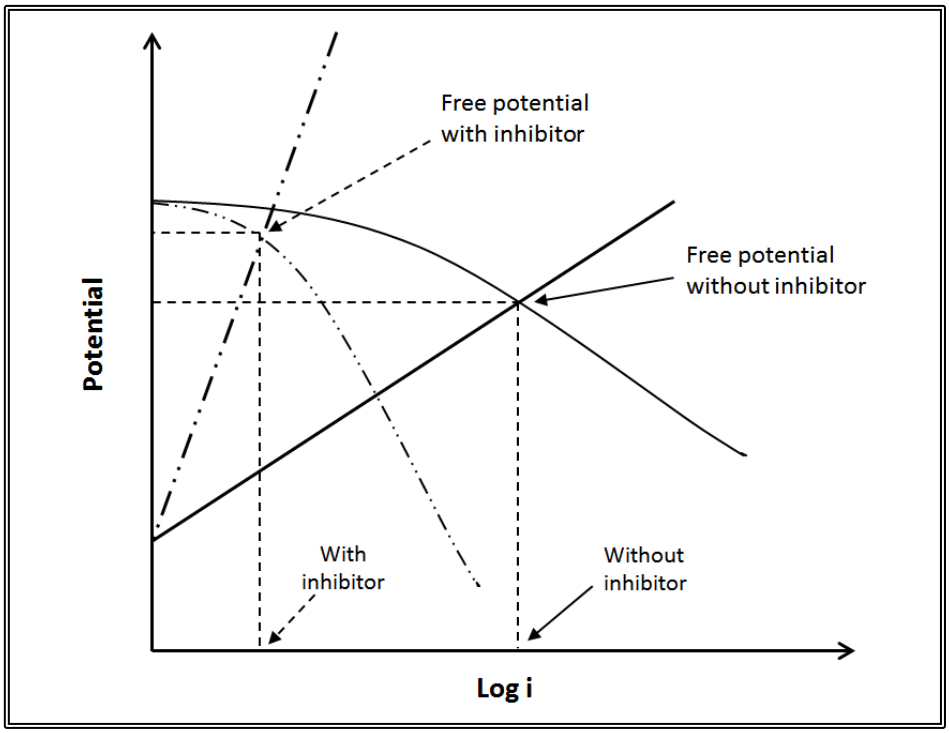

Figure 6-15: Schematic of free corrosion potential with and without chemical inhibitor in no-flow condition.

Consequently, CORRTREAT 10-569 applications in produced water storage facilities and in 'shut-in' condition in the offshore oilfield systems should effectively mitigate the corrosion rate of the HSLA steel infrastructure.

6.4.2 Effect of Flow on Chemical Inhibition

The galvanic currents that resulted from the addition of 30 ppm oilfield inhibitor CORRTREAT 10-569, for weldment segments in the high turbulence flow zone are presented. The total corrosion rates were calculated from the galvanic corrosion and self-corrosion rates. Comparisons were made with similar tests in the same hydrodynamic conditions, as well as experiments conducted with a rotating cylinder electrode (RCE).

6.4.2.1 Flow Jet Velocity at 5 m/s

A typical example of the galvanic current between each weld region is presented in Figure 6-16. The HAZ and the WM were both anodic (positive currents), while the PM was cathodic (negative current) and therefore partially protected from corrosion. It could be noticed that the sum of the anodic currents equals the cathodic current. Under static conditions, the initial galvanic currents decreased rapidly over the first three hours of the test as inhibitor films developed on the electrode surfaces. This suggests that the inhibitor film is protective.

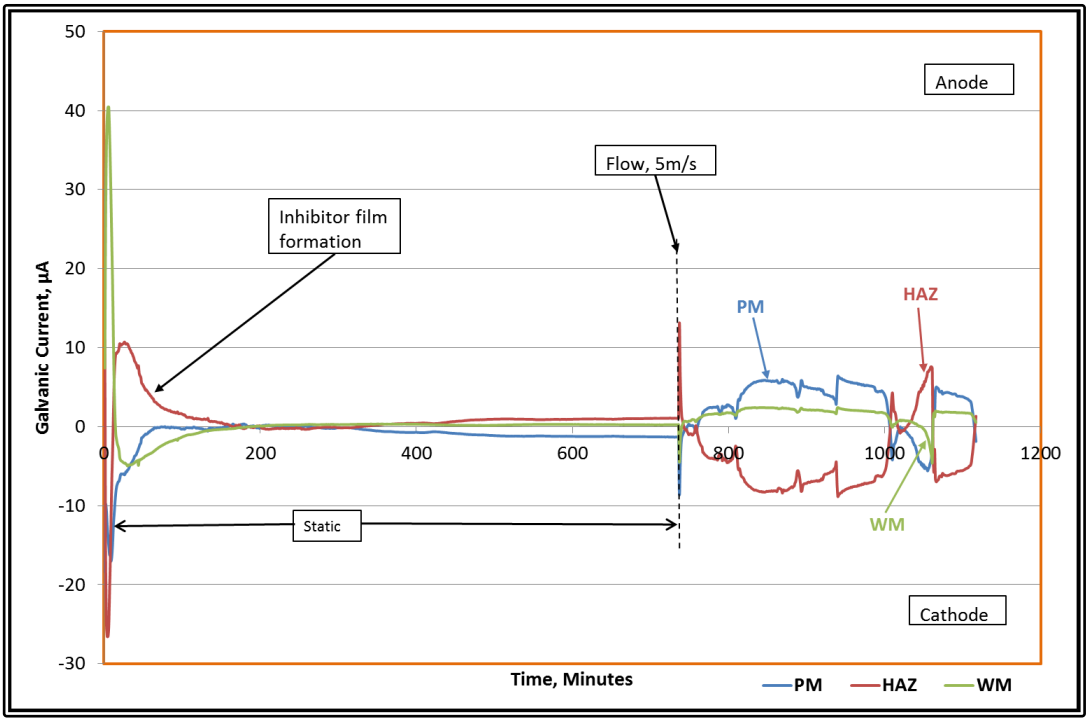

Figure 6-16: Galvanic corrosion currents in inhibited (CORRTREAT 10-569) brine saturated with CO_2 flowing at 5 m/s.

When the brine was flowed at 5 m/s, after the static test period, the PM and WM were also initially anodic. However, after about four hours under flowing conditions there was a current reversal and the HAZ became anodic. A further current reversal occurred later in the test. It is thought that at this intermediate flow velocity, which corresponded to a surface shear stress of 72 N/m^2, the inhibitor was removed more easily from one

weld region; in this case the HAZ. This resulted in a small active shift in the potential of the affected metal surface and the directions of the galvanic currents were reversed as a consequence.

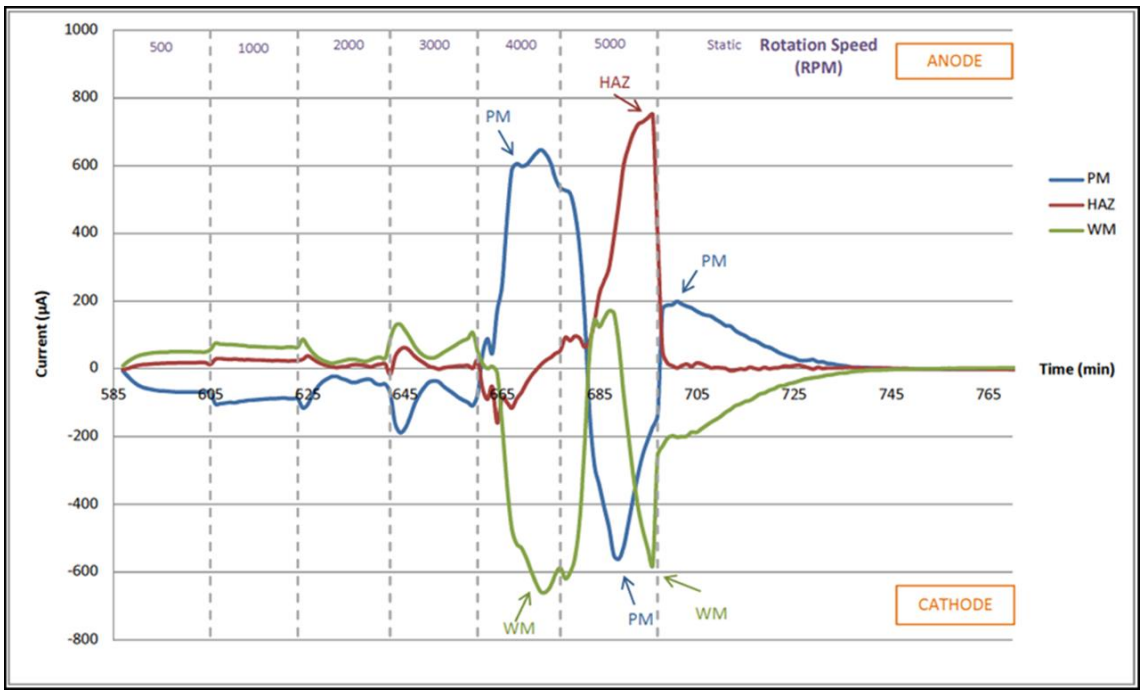

Figure 6-17: Galvanic currents with inhibitor 10-569 displaying current reversals at 4000 and 5000 rpm. (Martinez et al., 2011; Alawadhi et al., 2008)

Similar current reversals have been reported for experiments conducted with a rotating cylinder electrode, as shown in Figure 6-17 (Martinez et al., 2011; Alawadhi et al., 2008), in which samples of the same weldment were tested in CO_2 saturated brine containing the same corrosion inhibitor. The surface shear stresses are comparable in the two tests (72 N/m^2 for the present study and 70 N/m^2 for the RCE results). In both studies, the preferential removal of a surface inhibitor film from one weld region provides a satisfactory explanation for the anomalous role of inhibitors in PWC (Mahajanam and Joosten, 2011; Lee and Woollin, 2005; Barker et al., 2012; Craddock et al., 2004; Fan et al., 2011). Furthermore, this similarity supports the suitability of the novel SJI target for the study of PWC enhanced by change in hydrodynamics and inhibitor efficiency investigations.

Figure 6-18 shows the total corrosion rates at the end of the experiment. This demonstrates the likelihood of the occurrence of PWC since the WM selectively goes into solution compared with other weldment zones.

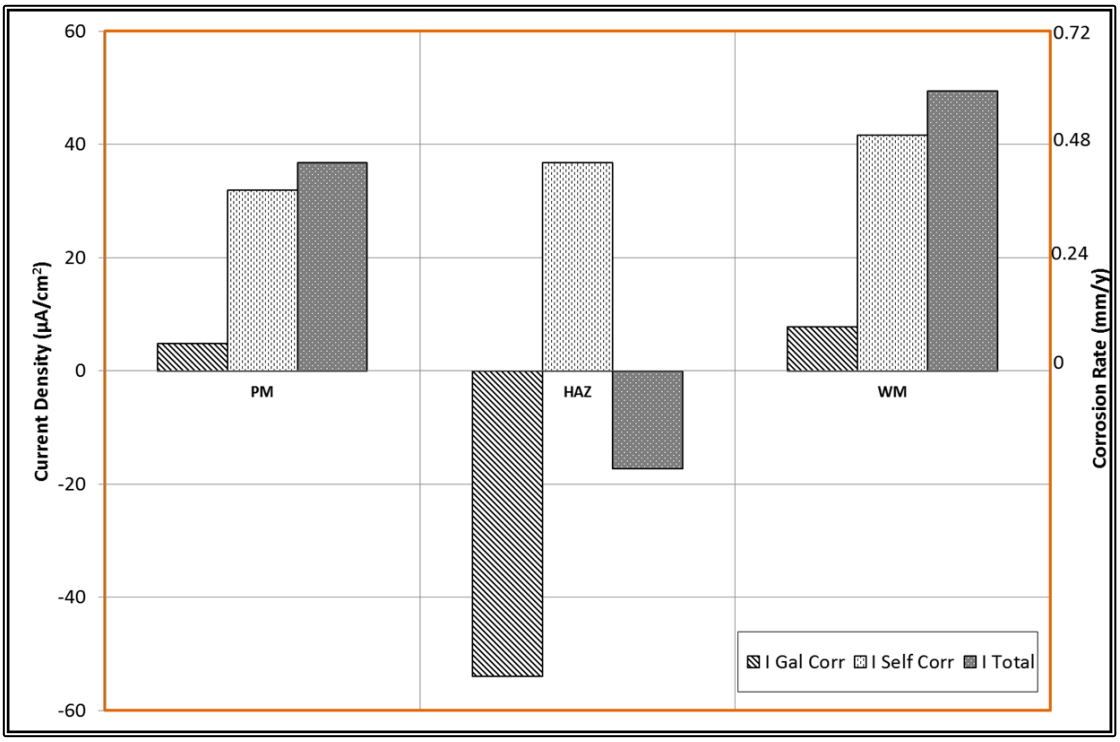

Figure 6-18: Total corrosion rates in inhibited (CORRTREAT 10-569) brine solution saturated with CO_2, flowing at 5 m/s.

6.4.2.2 Flow Jet Velocity at 10 m/s

An overview of the galvanic current density effect of inhibition with CORRTREAT 10-569 and fluid flow rate of 10 m/s is shown in Figure 6-19. Again, it could be deduced that inhibition in static condition is beneficial. However, this measure is inadequate in high shear stress flowing condition, since the protective inhibitor film was removed. Also, the galvanic measurements are proving to be variable and more confidence can be placed on the self-corrosion rate measurements.

The galvanic current behaviour at a flow velocity of 10 m/s differs in an important way from that at 5 m/s as shown in Figure 6-19. Again, there was a reduction in the currents

in the first three hours due to inhibitor film formation. After 10 hours of static conditions, the pump was started to give a flow rate at the nozzle of 10 m/s. The currents increased and the PM and WM remained anodic and the HAZ cathodic. Under these conditions, the highest metal loss from galvanic corrosion occurred on the weld metal (equivalent to 1.6 mm/y). Conversely, this observation is not consistent with some related studies which demonstrated that in offshore oilfield operations PWC could result from the pits developed in the anodic sites under the action of high velocity flow (Alawadhi et al., 2013; Hausler et al., 2004).

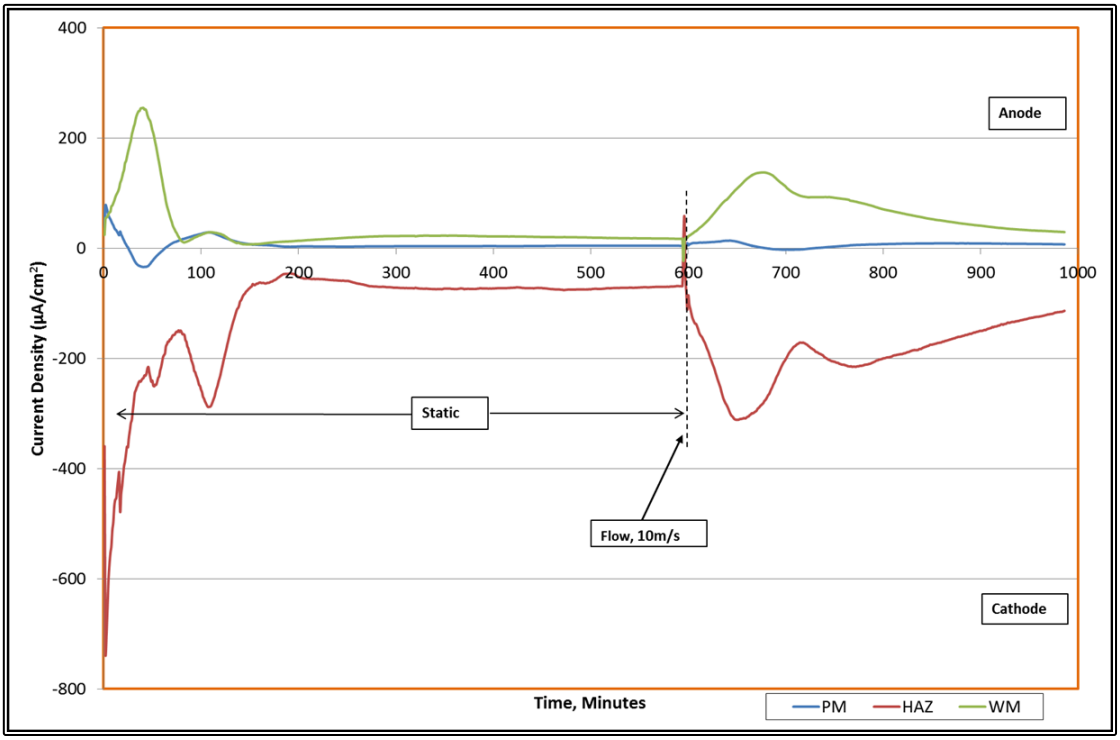

Figure 6-19: Galvanic current densities in inhibited (CORRTREAT 10-569) brine saturated with CO_2 flowing at 10 m/s.

A summary of the total corrosion rates on each weld region in the high turbulence transition zone in uninhibited and inhibited solutions is shown in Figure 6-20. The total rate was the sum of the galvanic rate, (described in Figure 6-19) and the self-corrosion contribution, obtained from LPR measurements. In static uninhibited conditions, the highest corrosion rate of 0.83 mm/y was observed on the PM. Addition of a typical

oilfield inhibitor (CORRTREAT 10-569) was effective in reducing the static corrosion rates to approximately 20% of their uninhibited values. However, at a flow rate of 10 m/s, the inhibited corrosion rates were comparable with those in the uninhibited brine. It appears that in these severe flow conditions, with a surface shear stress of 250N/m^2, the inhibitor was removed from the surface of each weld region. Under this condition, the higher corrosion rates were measured on the HAZ and WM, indicating the occurrence of preferential weld corrosion.

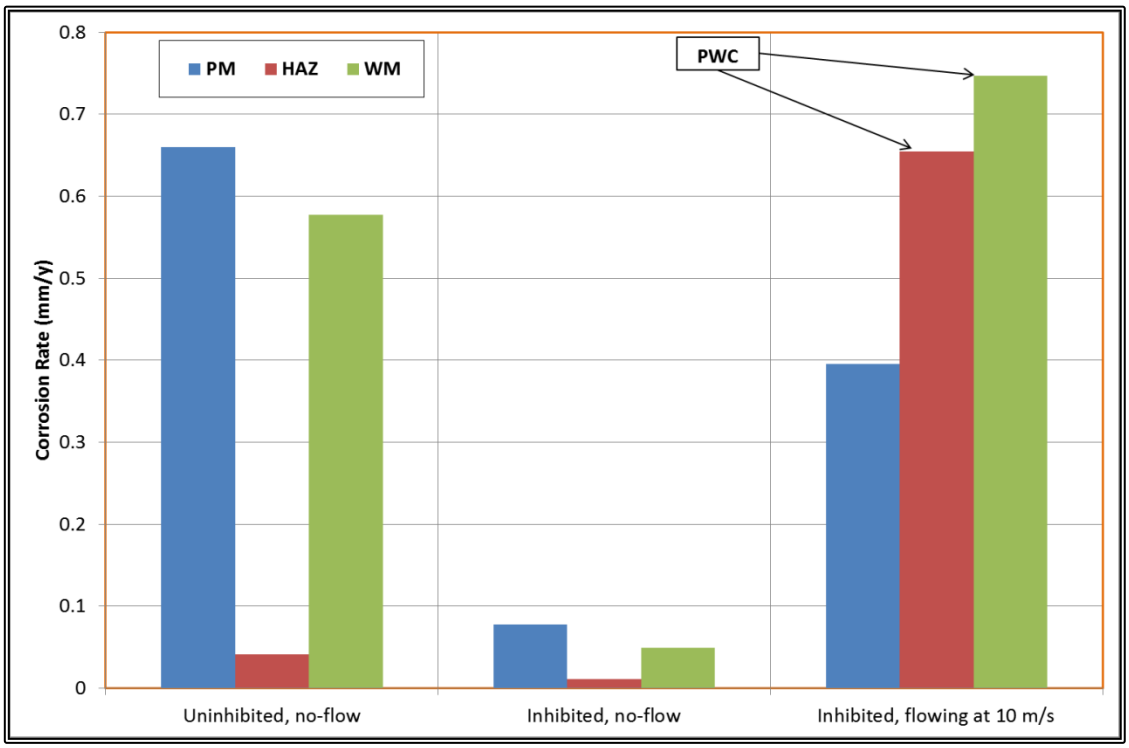

Figure 6-20: Effect of flow and chemical inhibition on corrosion rates in brine saturated with CO_2.

The practical implication of this in offshore oil field applications is the high possibility of premature failure resulting from preferential weld corrosion due to severe desorption of the surface chemical inhibitor product, under the high flow rate / high wall shear stress, causing high galvanic current exchange, with the WM being anodic to the PM and HAZ. This view is corroborated by field and laboratory research reports on the effects of hydrodynamic change on the performance of chemical inhibitors on carbon

steel weldments in offshore applications (Barker et al., 2012; Gao et al., 2011; Gao et al., 2008; Hara et al., 1998). Such that, in addition to the expected benefit of chemical inhibitor being lost, the propensity to PWC failure is very high.

6.5 Corrosion Rates in Brine Solution Containing Carbon-Dioxide and Oxygen

In oil and gas field operations it is possible that the water phase will contain not only dissolved carbon dioxide but oxygen may also be present, as a result of inadvertent leaks or insufficient deaeration of the system. In addition, laboratory studies of pipeline corrosion and inhibitor efficiency, using flow loops, rotating cylinder electrodes and other flow accelerated corrosion methods may also be subjected to the effects of oxygen ingress. For this reason, some jet impingement experiments were carried out in which air was deliberately admitted to the flow loop to investigate its effect. Air was bubbled at a controlled rate of approximately 2.2 ml/litre/min into the uninhibited and inhibited, carbon dioxide saturated brine.

6.5.1 Effect of Dissolved Oxygen in Uninhibited Brine Containing CO_2

In no-flow condition, the effect of air was negligible. Figure 6-21 shows the galvanic current exchange when air was admitted into uninhibited brine saturated with CO_2 in static and flowing (at 10 m/s) conditions. The presence of air reduced the amount of galvanic current exchanged in static (no-flow) condition, suggesting that a more protective corrosion film was formed at this stage. The HAZ was protected by the sacrificial anodic currents of PM and WM. Large galvanic current was observed when flow commenced at 10 m/s. Again, it appears that with flow at wall shear stress of about 250 N/m^2, the protective film was removed from the surface of each weld region. The intensity of anodic current densities of WM and HAZ indicates occurrence of severe PWC as shown in Figure 6-22.

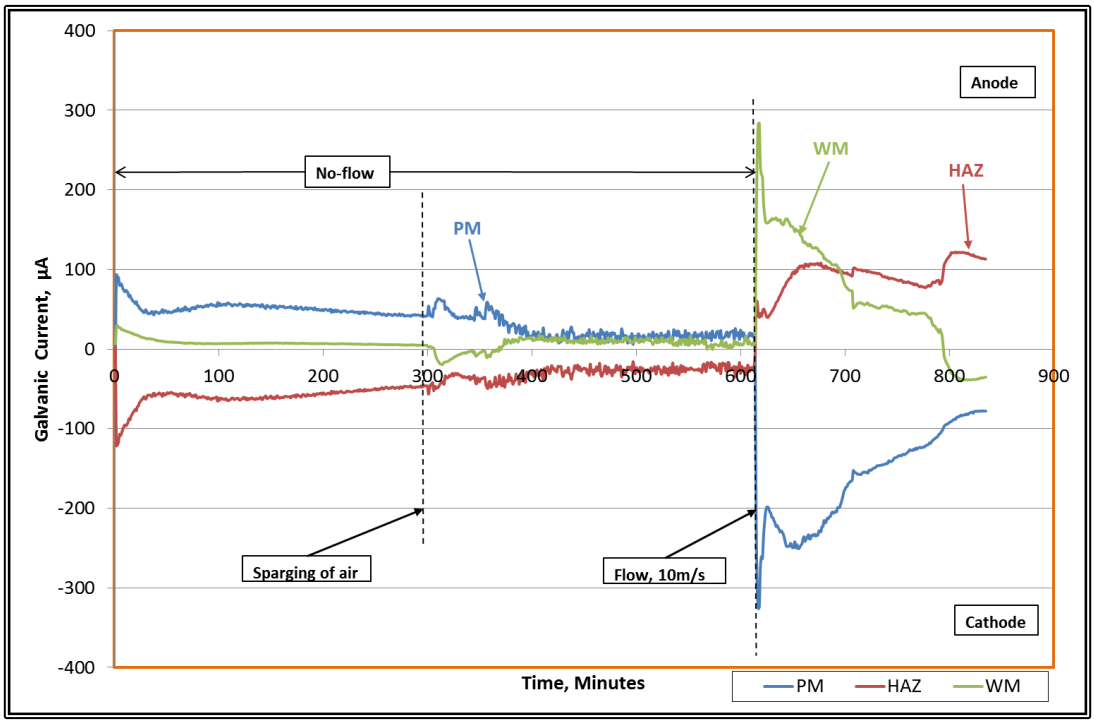

Figure 6-21: Galvanic currents in uninhibited brine containing CO_2 and oxygen.

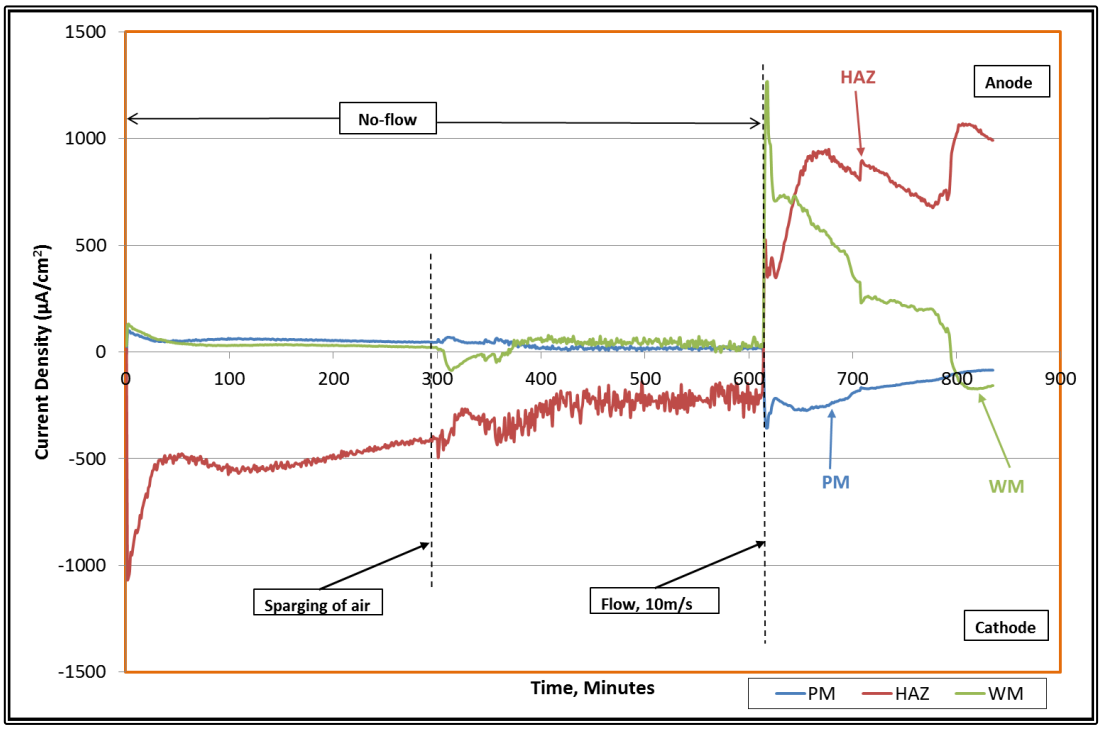

Figure 6-22: Galvanic current densities in uninhibited brine containing CO_2 and oxygen.

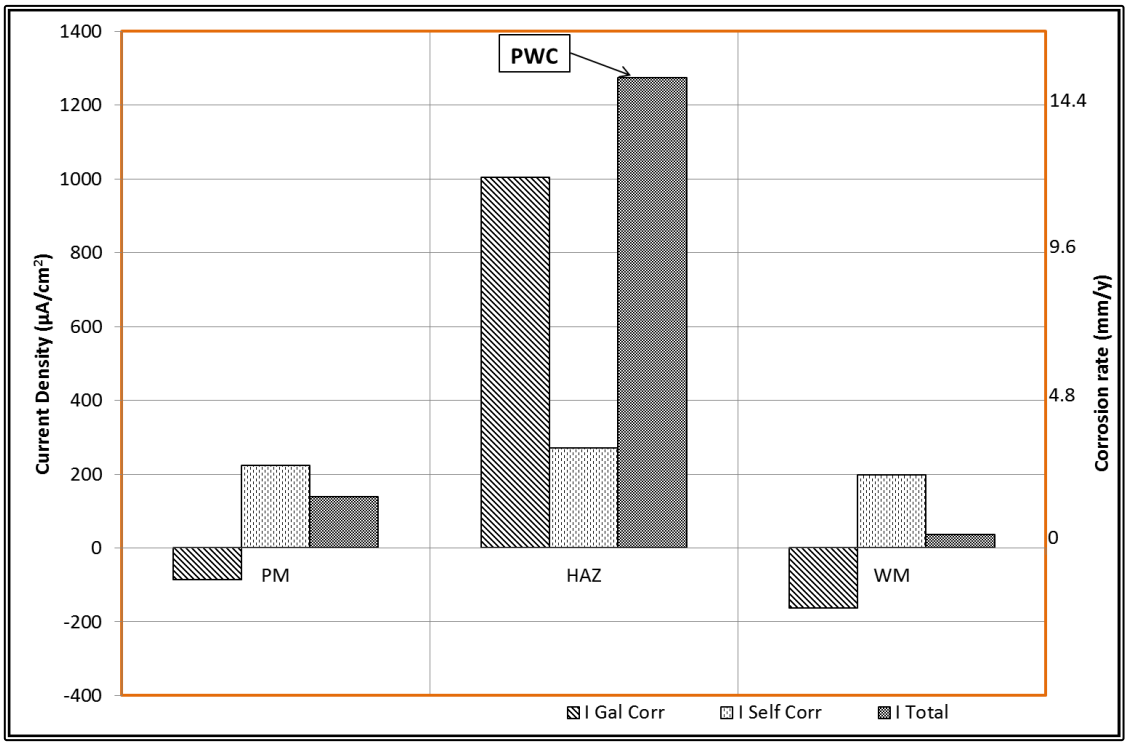

Figure 6-23: Total corrosion rates in uninhibited brine containing CO_2 and oxygen flowing at 10 m/s.

The total corrosion rates for the weldment sections in the high turbulence transition region (inner ring) were evaluated from the galvanic and self-corrosion contributions and presented in Figure 6-23. The likelihood of premature failure due to extreme PWC in uninhibited brine containing CO_2 and air (oxygen) was observed in this figure. This further emphasises the important role of the environment in ensuring pipeline system integrity.

Table 6-3 shows the free corrosion potentials in the uncoupled state in brine solution flowing at 10 m/s. The readings were taken during the 'settling time' preceding each LPR measurement was made. The open circuit potentials (OCP) in aerated uninhibited brine solution were more positive (noble) compared with the values in deaerated uninhibited solutions; however, the corrosion rates were greater. While the OCP values are good indicators for predicting the galvanic corrosion, self-corrosion rate is not not necessarily related to the potential, such that, the most noble does not always display the lowest corrosion rate.

Under the high wall shear stress, (about 250 N/m^2) the corrosion rate is mainly dependent on the mass transfer of the corroding species as well as, the formation, protectiveness and stability of surface film. The observed higher corrosion rates in the aerated solutions therefore, suggest that there is an additional corrosion reaction(s) in the presence of oxygen. In aerated uninhibited brine solution containing CO_2 under wall shear stress of about 250 N/m^2, the HAZ demonstrated the highest self-corrosion rate, while the WM has the least as shown in Figure 6-23.

Table 6-3: Effect of aeration on open circuit potentials in brine containing CO_2 flowing at 10 m/s.

	E_{CORR}, mV (SCE)		
	PM	HAZ	WM
Uninhibited	-713.32	-710.38	-710.94
Aerated Uninhibited	-646.44	-654.59	-641.73
Inhibited	-594.99	-600.99	-602.53
Aerated inhibited	-601.99	-603.9	-585.96

Considering the relative potentials of the weldment sections (as shown in Table 6-3) and the rates of galvanic corrosion in flowing aerated brine containing CO_2 and air (as presented in Figure 6-23), it is apparent that the magnitude of the potential difference between the dissimilar materials cannot be used to predict the severity of galvanic corrosion because electrochemical potentials are a function of the thermodynamics and not of the reaction kinetics that may occur. It is the surface kinetics that determines the severity of galvanic corrosion. A difference of 50 mV between select dissimilar materials can lead to severe corrosion while a potential difference of 800 mV has been successfully coupled. (Shifler, 2006; Francis, 2001)

6.5.2 Effect of Dissolved Oxygen in Inhibited Brine Containing CO_2

Figure 6-24 shows the galvanic current density of the weld segments in aerated inhibited brine containing CO_2. In static conditions, the effect of the added air was minimal. However, at a flow velocity of 5 m/s, a large increase in galvanic current occurred, with several reversals. At the end of the 6 hour flowing test period, the current was highest in the WM and corresponded to a galvanic corrosion rate of approximately 4.4 mm/y.

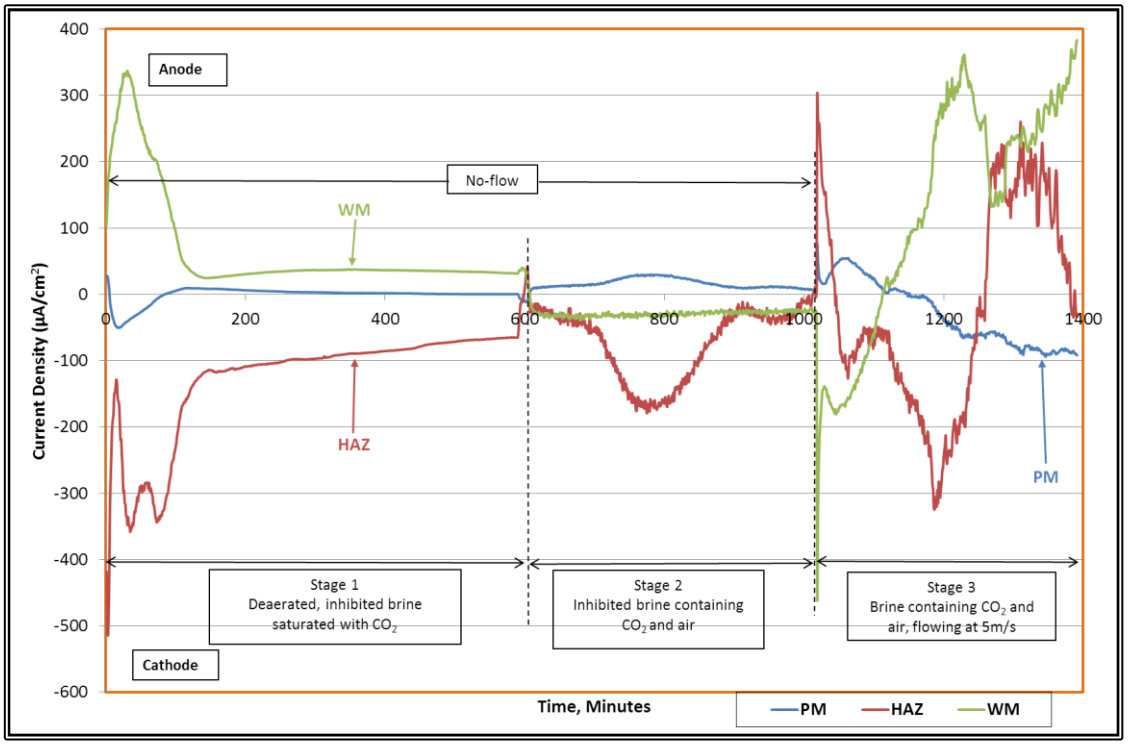

Figure 6-24: Galvanic current density in aerated inhibited brine containing CO_2 flowing at 5 m/s.

Similar large increases in galvanic current occurred when the inhibited brine containing carbon dioxide and air was flowed at a velocity of 10 m/s as shown in Figure 6-25 However, no further current reversals were observed and the HAZ remained anodic. The PM and WM were both cathodic in the flowing conditions and were protected from galvanic corrosion by the preferential attack on the HAZ. The anodic current on the

HAZ corresponded to a galvanic corrosion rate of approximately 18 mm/y. Clearly this represents a very high rate of PWC.

The total corrosion rates with air present at flow rates of 5 and 10 m/s as recorded at the end of the experiments are shown in Figure 6-26. In some cases, the total corrosion rate for a particular region of the weld was less than its self-corrosion rate due to it being partially protected by a cathodic (negative) galvanic contribution. This partial protection of a weld section agrees with previous studies (Alawadhi and Robinson, 2011; Martinez et al., 2011; Akbar et al., 2011), as well as field experience (Lee and Woollin, 2005; Martin, 2003; Ahmad, 2006; Asrar, 2010). At a flow rate of 5 m/s, the highest corrosion rate was on the WM, whereas at 10 m/s the highest rate was on the HAZ. In both cases, the corrosion rate of the PM was relatively low.

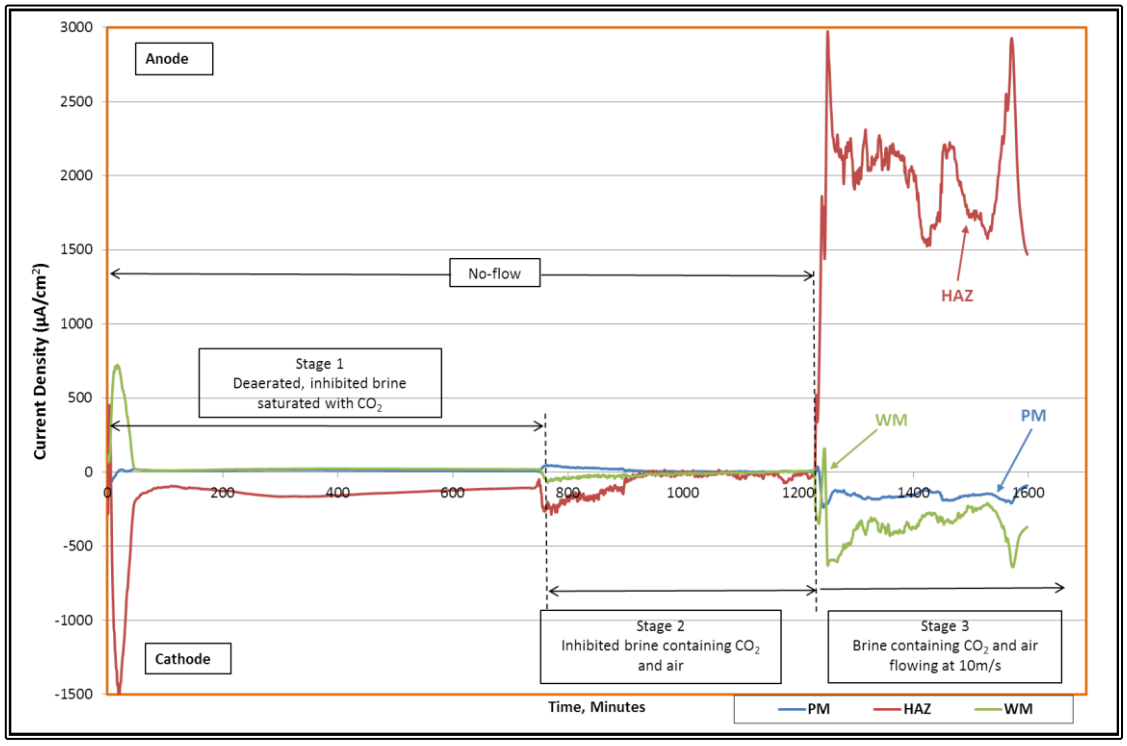

Figure 6-25: Galvanic current densities in aerated inhibited brine containing CO_2 flowing at 10 m/s.

The severe PWC in aerated inhibited brine solution containing CO_2 under a high wall shear stress of 250 N/m^2 being higher than at lower wall shear stress of 70 N/m^2

suggests that more corrosion reactions and / or faster rate of corrosion occur at higher jet velocity. The local corrosion rate that increases with flow rate was expected due to increase in mass transport with flow, increased instability of the partially protective film, as well as reduced passivity of corrosion product on the working electrodes (Alawadhi and Robinson, 2011; Martinez et al., 2011; Schmitt et al., 1992; Chaal et al., 2009; Ruzic et al., 2006). Corrosion reaction mechanisms were investigated to assess corrosion reactions in aerated and deaerated conditions, and the results presented in Section 6.7.

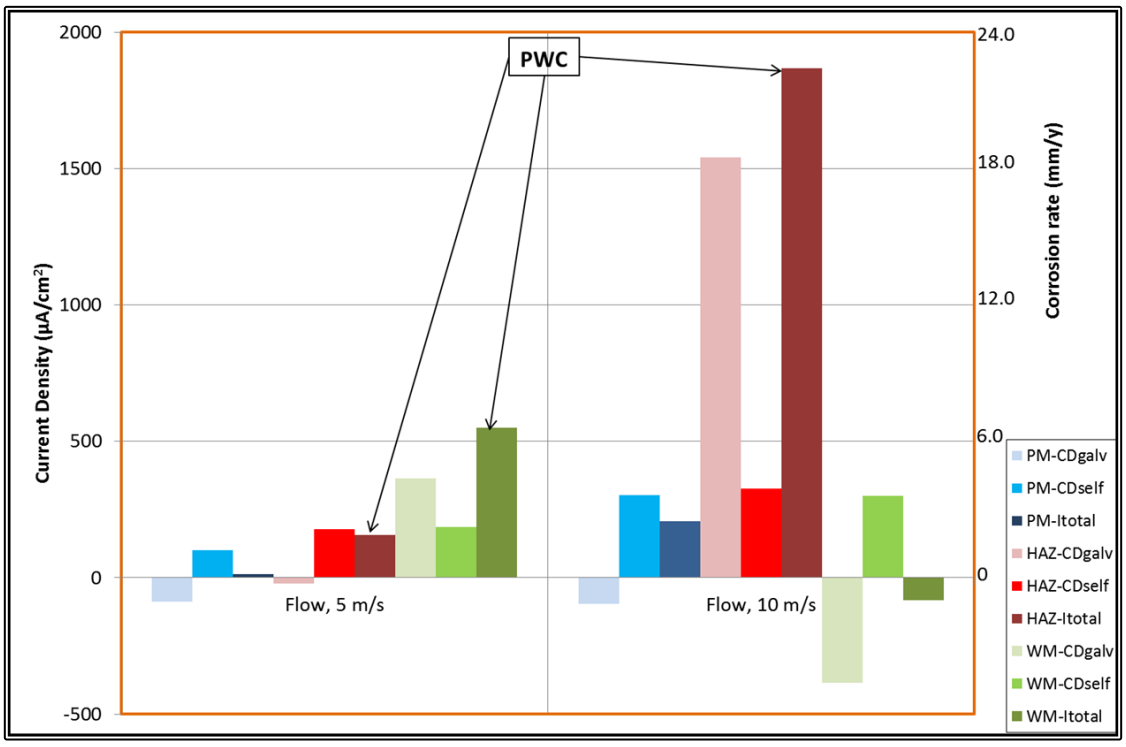

Figure 6-26: Effect of flow on corrosion rate in aerated inhibited brine containing CO_2.

In conclusion, small additions of air to carbon dioxide saturated brine to simulate a leaking pump or valve, and / or ineffective deaeration of the system caused very high corrosion rates in the weld metal and/or heat affected zone, leading to severe PWC as shown in Figure 6-27.

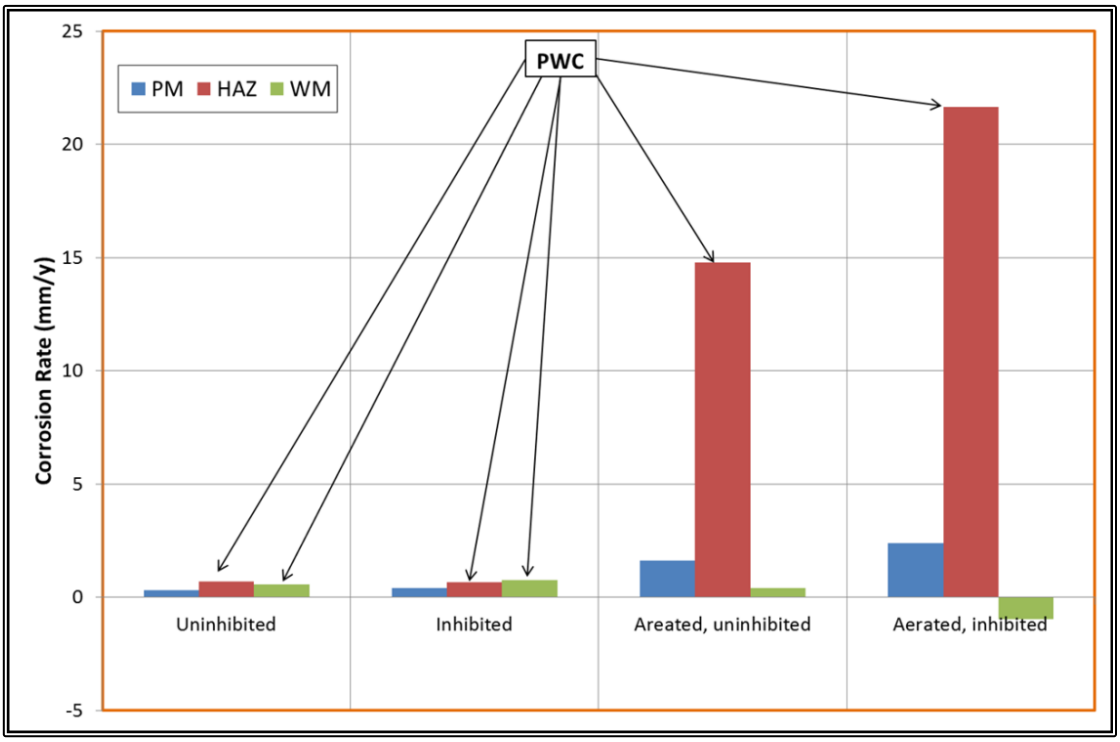

Figure 6-27: Effect of inhibitor and aeration on total corrosion rates of X65 steel weldment in brine containing CO_2 flowing at 10 m/s.

6.6 Corrosion Products

The structures of the corroded WM surfaces were examined after they had been exposed to brine saturated with carbon dioxide, with and without the deliberate addition of air. This was done by first etching a trough through the surface film, down to the substrate, using a focussed ion beam (FIB) and then viewing the wall of the trough in a scanning electron microscope (SEM). Figure 6-28 shows the back-scattered micrographs across the sections of the weldment.

Figure 6-29 shows a typical structure of the grey film that formed in brine containing carbon dioxide alone (Alawadhi and Robinson, 2011). The film consisted only of cementite (Fe_3C), the ferrite phase in the microstructure having been removed by corrosion (Alawadhi and Robinson, 2011; Martinez et al., 2011; Alawadhi et al., 2008). No $FeCO_3$ was detected in the film as there was insufficient Fe^{2+} present in the test solution for this product to form.

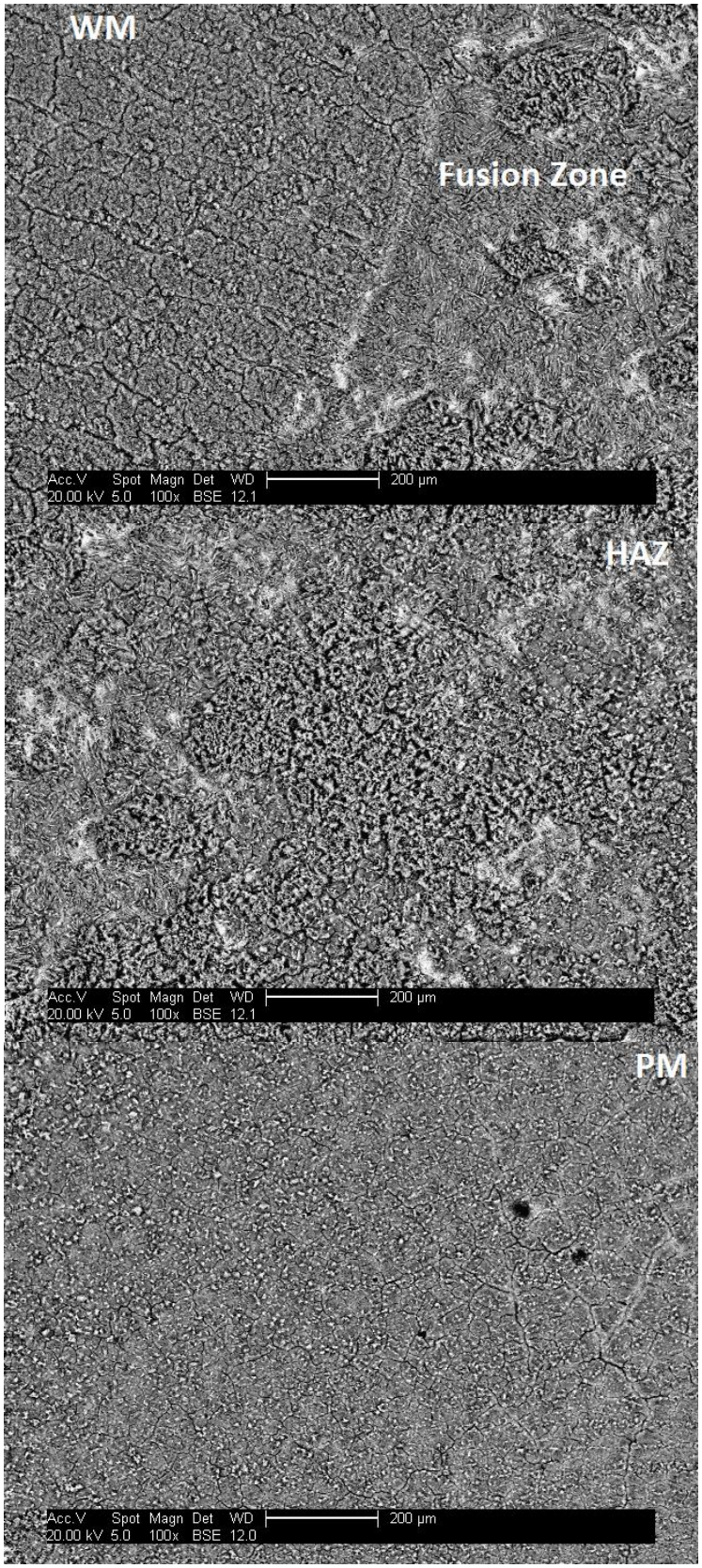

Figure 6-28: Back-scattered SEM of X65 weldment after exposure to aerated uninhibited brine containing CO_2 flowing at 10 m/s.

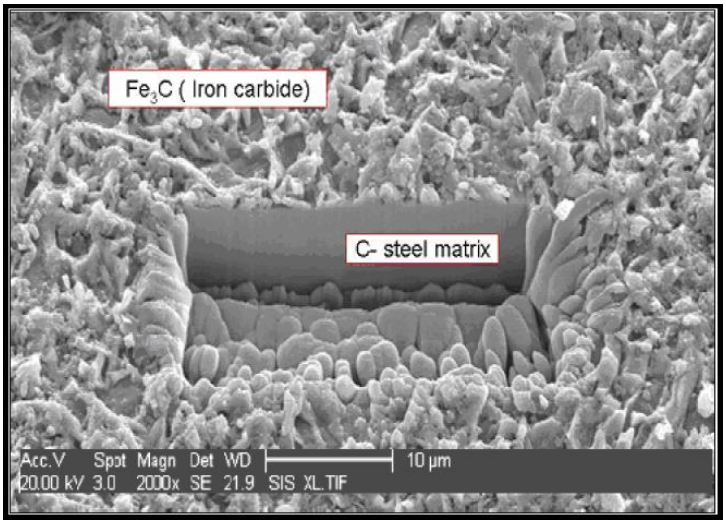

Figure 6-29: SEM micrograph of WM after 5 days in static, uninhibited brine containing CO_2 at 70°C (Alawadhi and Robinson, 2011)**.**

It is well known that the microstructure of low alloy steel is composed of proeutectoid ferrite and pearlite, while pearlite is composed of lamellar eutectoid ferrite and cementite. The observed structure in Figure 6-29 suggests that cementite has a more noble potential than ferrite, which resulted in the selective dissolution of ferrite (both the proeutectoid ferrite and eutectoid ferrite) on the weld specimen (Alawadhi and Robinson, 2011; Zhang et al., 2011; Dayalan et al., 1998; Videm, 1998; Sun et al., 2012; Olsen et al., 2005; Nyborg, 2010; Paolinelli et al., 2007; Alink et al., 1999).

In contrast, the film that formed on WM when air was added was dark brown in colour and relatively thick, as shown in Figure 6-30. However, it was essentially porous in structure and many slightly different fissures were visible when viewed from the surface and in the cross-section. The porous structure indicates that the film would be non-protective to the substrate and this is consistent with the very high corrosion rates measured when this film was present (Martin, 2001; Gulbrandsen et al., 2005; Rosli et al., 2014; Asrar, 2010; Kvarekval et al., 2005). As expected, energy dispersive X-ray (EDX) spectrum and analysis of the film showed that oxygen was present as shown in Figure 6-31 and Figure 6-32.

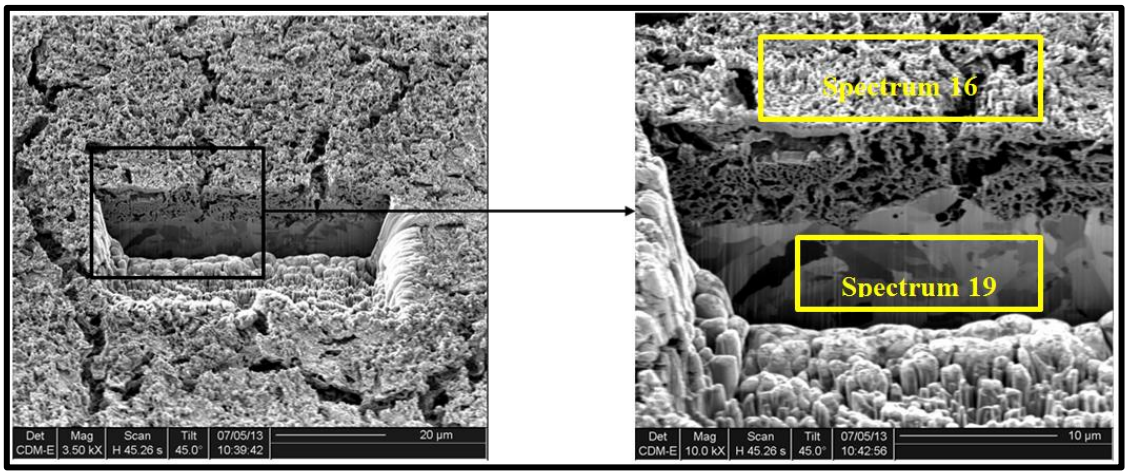

Figure 6-30: FIB micrographs of the WM after 2 hours exposure to aerated uninhibited brine containing CO_2 flowing at 10 m/s.

Figure 6-33 shows similar micrographs for the PM after 2 hours exposure to aerated uninhibited brine containing CO_2 and flowing at 10 m/s. Mud cracks were also observed on the surface film, indicating that it was non-protective. The surface film on the PM is comparable with the WM surface film. The EDX spectrum and analysis are presented in Figure 6-34 and Figure 6-35 revealed iron-system substrate and oxide-rich surface film as expected.

The X-ray diffraction (XRD) patterns of the WM and PM, after 2 hours exposure to uninhibited brine flowing at 10 m/s, containing CO_2 and air, revealed that the two corroded weld segments consist of hematite (Iron-III- oxide, Fe_2O_3) and iron crystalline systems as presented in Figure 6-36 and Figure 6-37.

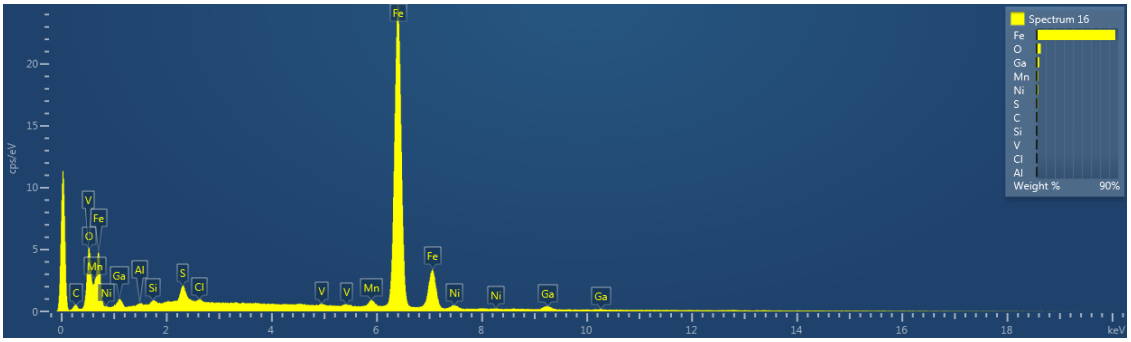

Spectrum 16	Line Type	Apparent Concentration	k Ratio	Wt%	Wt% Sigma	Atomic %	Standard Label	Factory Standard
C	K series	2.11	0.02111	0.68	0.09	2.73	C Vit	Yes
O	K series	73.66	0.24789	4.6	0.08	13.91	SiO2	Yes
Al	K series	1.05	0.00755	0.17	0.03	0.3	Al2O3	Yes
Si	K series	2	0.01585	0.3	0.03	0.51	SiO2	Yes
S	K series	8.75	0.0754	1.2	0.04	1.81	FeS2	Yes
Cl	K series	1.87	0.01634	0.26	0.03	0.35	NaCl	Yes
V	K series	2.24	0.02239	0.29	0.05	0.28	V	Yes
Mn	K series	10.66	0.10664	1.6	0.07	1.41	Mn	Yes
Fe	K series	608.3	6.08296	89.31	0.17	77.38	Fe	Yes
Ni	K series	10.05	0.10052	1.6	0.09	1.32	Ni	Yes
Total				100		100		

Figure 6-31: EDX spectrum and analysis (print-out) of the corrosion product film on the WM after 2 hours exposure to aerated uninhibited brine containing CO_2 flowing at 10 m/s.

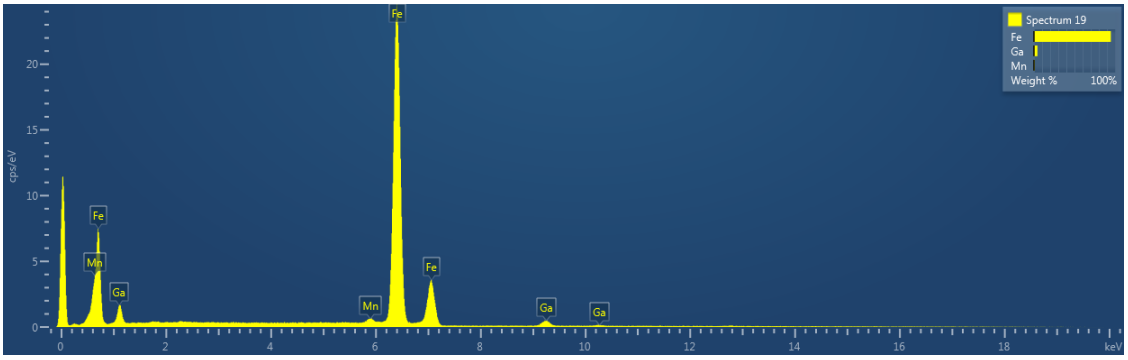

Spectrum 19	Line Type	Apparent Concentration	k Ratio	Wt%	Wt% Sigma	Atomic %	Standard Label	Factory Standard
Mn	K series	6.35	0.06348	1.06	0.07	1.07	Mn	Yes
Fe	K series	607.05	6.07051	98.94	0.07	98.93	Fe	Yes
Total				100		100		

Figure 6-32: EDX spectrum and analysis (print-out) of the WM substrate after 2 hours exposure to aerated uninhibited brine containing CO_2 flowing at 10 m/s.

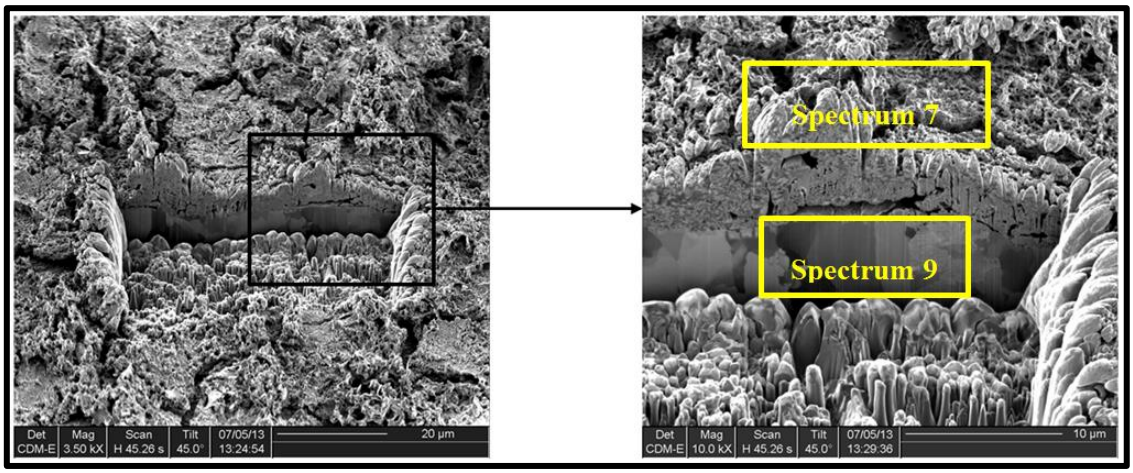

Figure 6-33: FIB micrographs of the PM after 2 hours exposure to aerated uninhibited brine containing CO_2 flowing at 10 m/s.

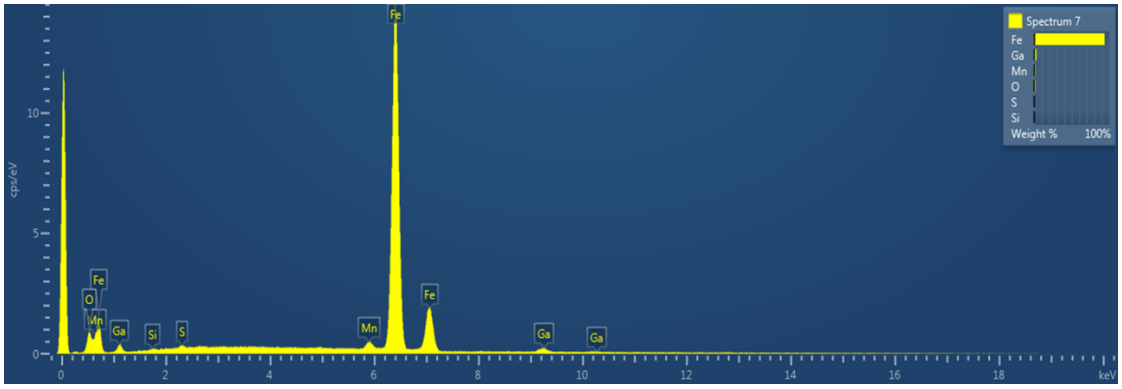

Spectrum 7	Line Type	Apparent Concentration	k Ratio	Wt%	Wt% Sigma	Atomic %	Standard Label	Factory Standard
O	K series	13.64	0.04592	1.61	0.06	5.39	SiO2	Yes
Si	K series	0.31	0.00246	0.09	0.03	0.17	SiO2	Yes
S	K series	0.66	0.00571	0.17	0.03	0.29	FeS2	Yes
Mn	K series	6.01	0.0601	1.68	0.1	1.64	Mn	Yes
Fe	K series	351.82	3.51817	96.44	0.12	92.51	Fe	Yes
Total				100		100		

Figure 6-34: EDX spectrum and analysis of the corrosion product film on the PM after 2 hours exposure to aerated uninhibited brine containing CO_2 flowing at 10 m/s.

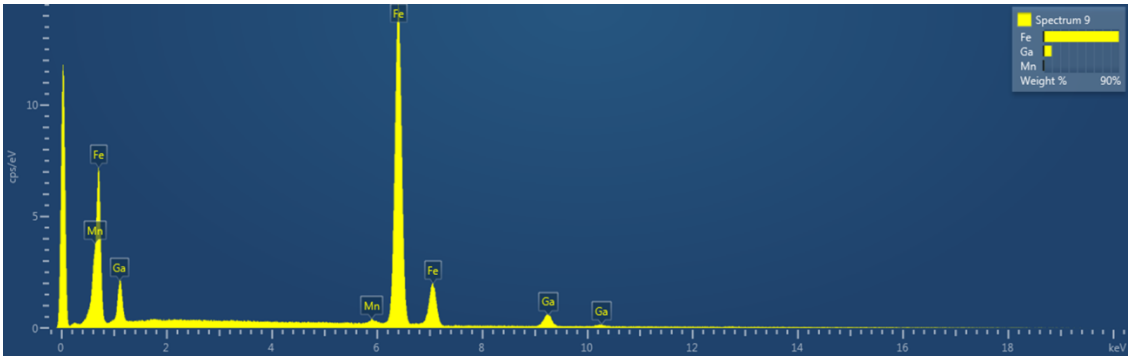

Spectrum 9	Line Type	Apparent Concentration	k Ratio	Wt%	Wt% Sigma	Atomic %	Standard Label	Factory Standard
Mn	K series	3.22	0.03225	0.92	0.1	0.94	Mn	Yes
Fe	K series	353.23	3.53235	99.08	0.1	99.06	Fe	Yes
Total				100		100		

Figure 6-35: EDX spectrum and analysis of the PM substrate after 2 hours exposure to aerated uninhibited brine containing CO_2 flowing at 10 m/s.

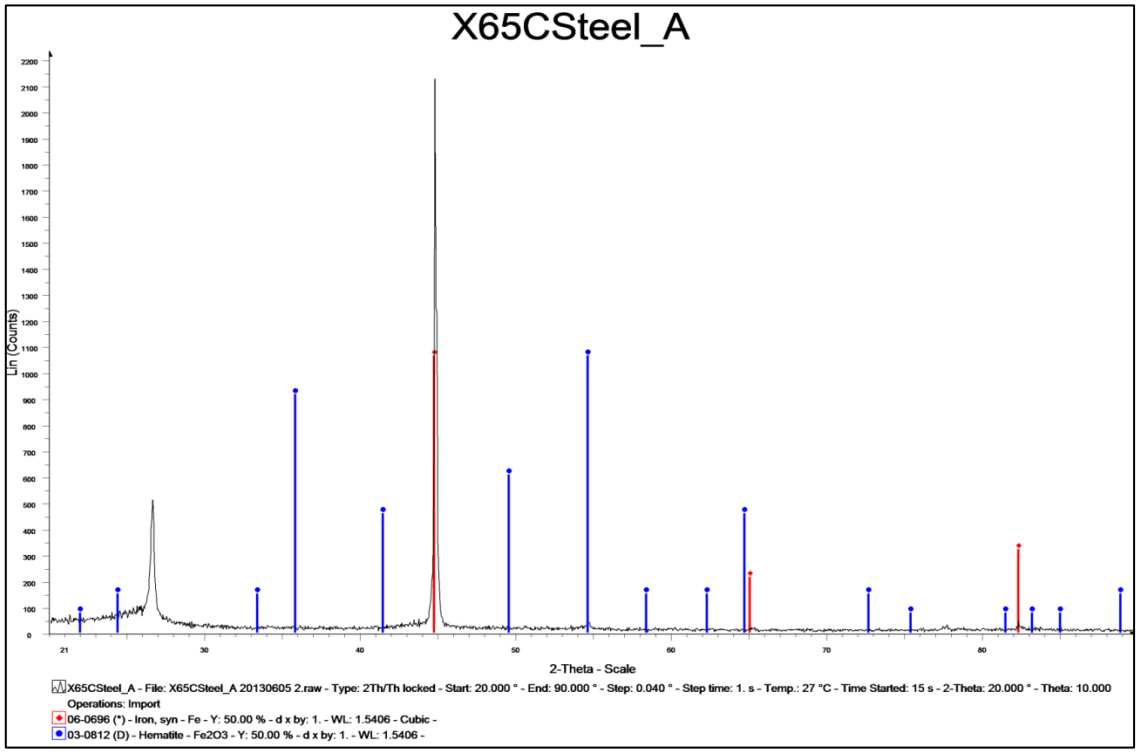

Figure 6-36: XRD of the WM after 2 hours exposure to aerated uninhibited brine containing CO_2 flowing at 10 m/s.

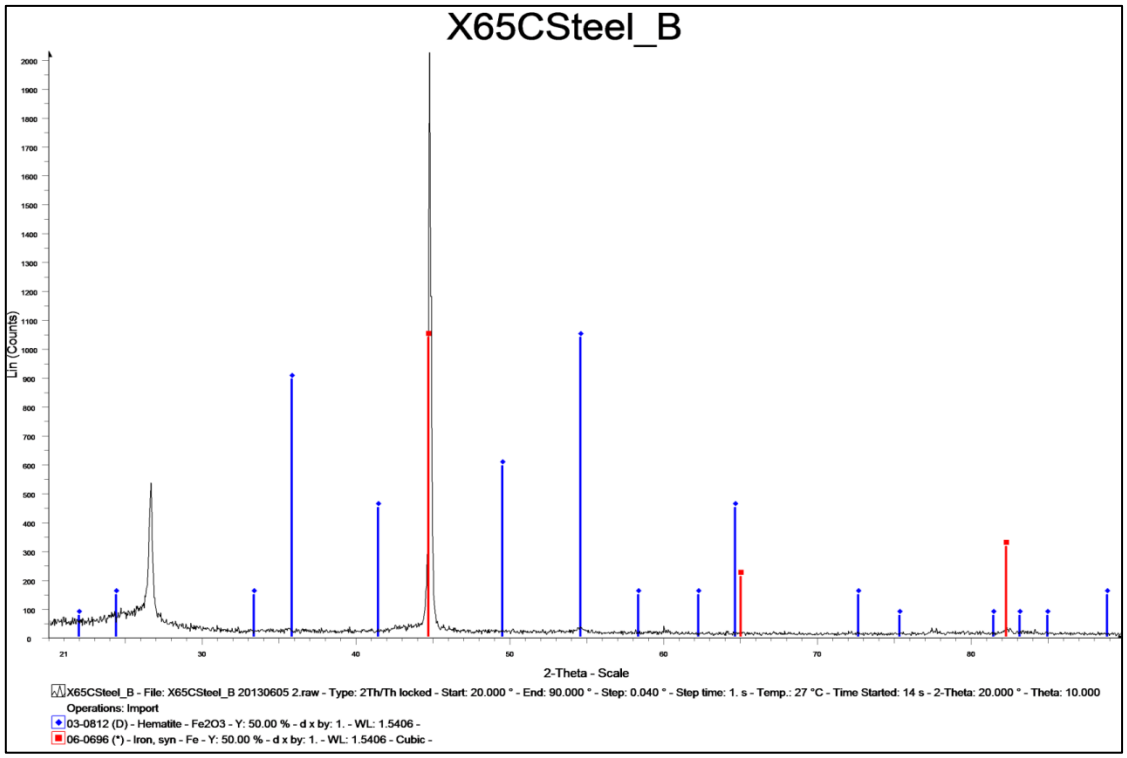

Figure 6-37: XRD of the PM after 2 hours exposure to aerated uninhibited brine containing CO_2 flowing at 10 m/s.

6.7 Corrosion Reaction Mechanisms

In order to investigate the mechanism of the increased corrosion rate caused by the addition of air, cathodic and anodic potentiodynamic scans were carried out, as shown in Figure 6-38 and Figure 6-39 respectively. In uninhibited brine saturated with carbon dioxide alone and flowing at 10 m/s, the open circuit potential of the sample was at an active value close to -700 mV(SCE), indicating that a very low level of oxygen was present. When air was bubbled into the cell, the cathodic curve was strongly depolarized. The open circuit potential rose by almost 470 mV(SCE) and the current densities increased by more than two orders of magnitude. These results are consistent with other work reported in the literature (Dugstad, 2006; Martin, 2002; Martin, 2001; Gulbrandsen et al., 2005; Choi and Nešić, 2010; Ruhl and Kranzmann, 2012) and support the view that the corrosion rate in CO_2/air mixtures was under oxygen mass transport control (Gulbrandsen et al., 2005; John et al., 2008; Foss et al., 2009;

Gulbrandsen and Granå, 2007; Dugstad et al., 2006; Hu et al., 2013; John et al., 2007; John et al., 2007; Endo et al., 1997).

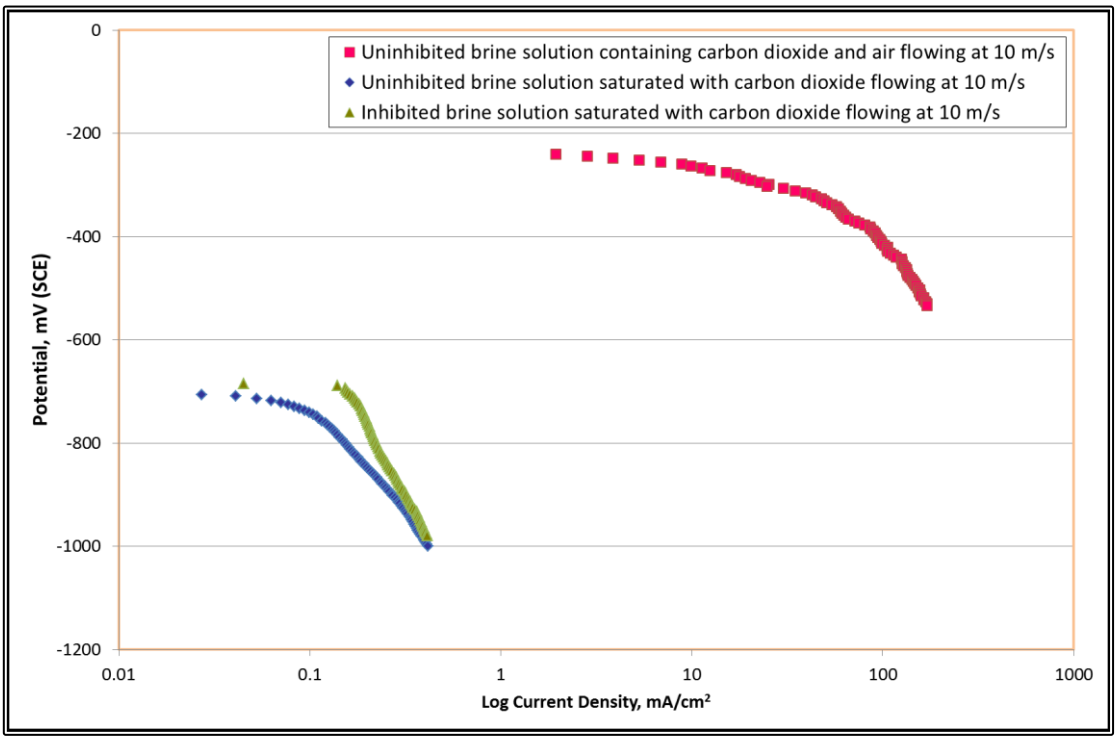

Figure 6-38: Cathodic potentiodynamic scans for PM in brine containing CO_2 flowing at 10 m/s.

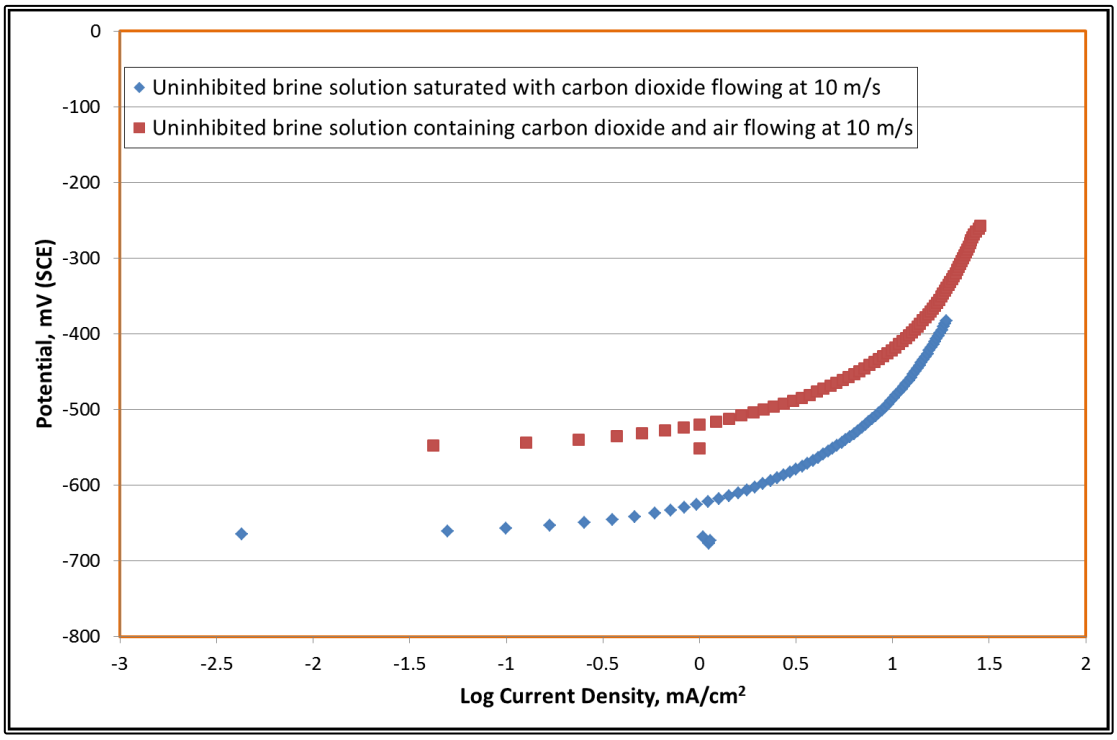

Figure 6-39: Anodic potentiodynamic scans for PM in uninhibited brine saturated with CO_2 flowing at 10 m/s and with the addition of air.

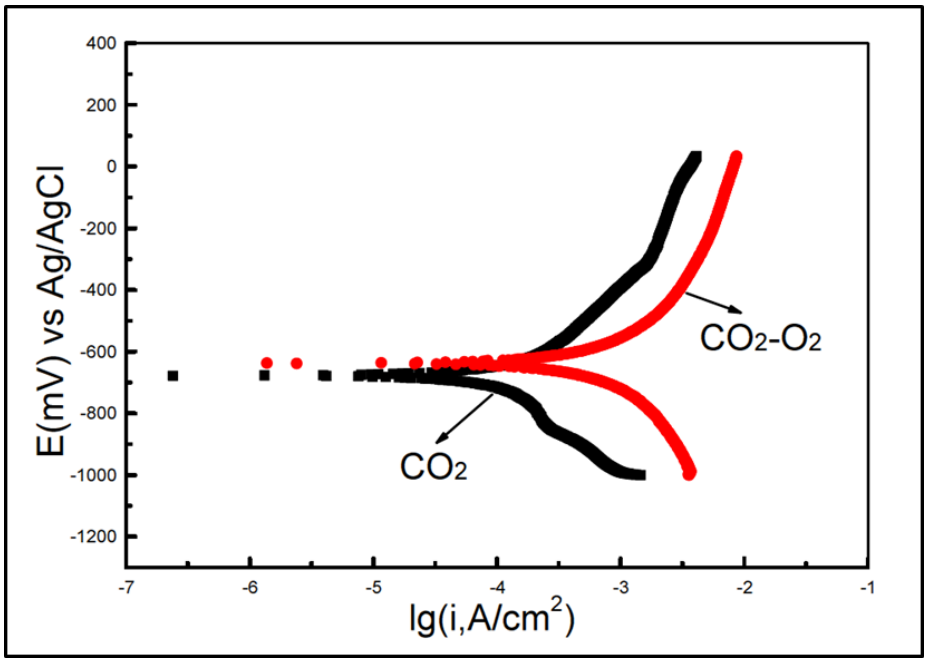

Figure 6-40: Polarization curves of N80 steel in two corrosive environments under static condition (Dong et al., 2014)

The polarization curves, reported in a recent research (Dong et al., 2014), of N80 steel in two corrosive environments under static condition are presented in Figure 6-40. As shown, when 0.05MPa O_2 was added, the corrosion potential increased by 41mV (Ag/AgCl), and the corrosion current density was increased by 3 orders of magnitude compared with absence of oxygen; the polarization resistance (Rp) in CO_2 saturated environment was 2.8 times higher than that under CO_2-O_2 environment. When the solution was flowed at 2 m/s in a rotating cage set-up, the corrosion rates (with and without oxygen) increased significantly, as shown in Figure 2-12. Combined actions of the dissolved oxygen in CO_2 and flow resulted in higher corrosion rate by more than 5 orders. This corroborates the observed direct proportional total corrosion rates with jet flow rates (with or without dissolved oxygen) in the work.

6.8 Chapter Summary

The likelihood of risk to premature failure due to preferential weld corrosion is very negligible in static / no-flow and ambient conditions. Conversely, in both inhibited and uninhibited solutions under flowing condition, HSLA steel welded joint could be subjected to severe PWC due to the high shear stress accompanied by an increase in mass transport with flow. A characteristic feature that was observed at intermediate wall shear stress of 70 N/m^2 is galvanic current reversal in inhibited aerated and deaerated solutions. It is thought that at this intermediate jet velocity (of 5 m/s), the surface film was removed more easily from one weldment region, causing a shift in the potential of the affected metal surface and the direction of the galvanic current was reversed as a consequence. Such preferential removal of a surface film from one weld region provides a satisfactory explanation for the anomalous role of inhibitors in PWC. An increase in corrosion rates and hence PWC risk in the presence of air may be attributed to additional cathodic reduction of oxygen.

All the tests conducted in flowing conditions showed that the galvanic corrosion contributed very significantly to the total corrosion rate, with the HAZ and / or WM being anodic. Since the anode current density is inversely proportional to the surface area ratio of the cathode, a very small anode (HAZ and / or WM) will therefore corrode much faster than one that is much larger relative to the cathode, resulting into PWC.

CHAPTER 7.
GENERAL DISCUSSION

Major findings and implications of results in offshore oil and gas HSLA pipeline steel selection, fabrication and integrity management are outlined. Operational (commissioning, production and shut-down / shut-in) measures that could be taken to mitigate preferential weld corrosion are also highlighted, as well as, effective applications of conventional corrosion control techniques. Preventive and mitigating measures are proffered, especially in the presence oxygen. The suitability of SJI test as a tool for flow accelerated corrosion investigation; particularly at high wall shear stress is also appraised.

7.1 Preferential Weld Corrosion of Offshore Pipeline

Flow accelerated preferential weld corrosion (PWC) is one of the dominant integrity issues affecting the internal section of offshore production and service pipelines. The severity of this deleterious selective corrosion of either the weld metal (WM) and/or heat affected zones (HAZ) rather than adjacent parent metal (PM) depends on the synergism of the metallurgical characteristics of the welded joint, the nature of the environment and the operation parameters. Chemical inhibitors are used to control this internal corrosion with a lot of reservation since it is still impossible to predict the preferential corrosion rate that may be experienced, the exact location of attack (such as, weld metal and/or heat affected zone), or the effectiveness of corrosion inhibitors. Premature failures of the high strength low alloy (HSLA) pipeline steel are being reported and research efforts have demonstrated that the possibility of inconsistent galvanic nature of HAZ and / or the WM with respect to the PM. Understanding and effectively managing the integrity of the pipelines is necessary to predict, prevent and detect the presence of any loss of integrity. The aim of this research is not to examine all possible the integrity issues, but to evaluate the suitability using a novel target in the submerged jet impingement technique to study flow accelerated preferential weld corrosion.

7.2 Effect of Flow

A typical North Sea field, The Curlew Field, produces oil and gas with wall shear stress of 120 N/mm^2 at maximum production flow velocity (Craddock et al., 2004). The simulated hydrodynamic conditions used in this study ranged from static (no-flow) to very high turbulent flow, corresponding to wall shear stress range of 0 to about 250 N/mm^2.

7.2.1 Effect of Flow in CO_2 Saturated Brine Solution

Wall shear stress is conventionally used as a parameter in the studies of the influence of flow on performance of chemical inhibitors and other flow related studies, and was therefore used in this study. The wall shear stress is one of several factors that can be used to describe flow conditions and it is suitable in some applications because it is directly related to the friction pressure loss (Efird, 2006; Schmitt and Mueller, 1999). Mass transfer coefficient is another major flow parameter that is used to describe the influence of flow on corrosion. Efird (2000) discussed the scientific basis for using the wall shear stress and the mass transfer coefficient in flow assisted corrosion studies, and points out that these two parameters are intimately related.

The electrochemical evaluation of the weldment specimens was conducted under submerged jet impingement with and without chemical inhibitor in both deaerated and aerated brine solution containing CO_2.

7.2.1.1 Uninhibited Brine Solution Saturated with CO_2

In no-flow conditions, the heat-affected zone (HAZ) was cathodic to both parent metal (PM) and the weld metal (WM) as shown in Figure 6-2. The gradual decrease in the galvanic current was due to the formation of partially protective transparent corrosion film on the surface of weldment segments. The average anodic current of the WM was minimal (1.3 $\mu A/cm^2$) compared with that of the PM (6.3 $\mu A/cm^2$). The influence of the corrosion product film on the anodic electrode is illustrated in Figure 7-1. The anodic curve is displaced in the positive direction due to the effect of thin film formation of the

electrode with corrosion product with a corresponding reduction in the current density/corrosion rate. This is expected because of the assumed formation of a corrosion film as discussed in the previous reports (Alawadhi and Robinson, 2011; Martinez et al., 2011; Schmitt and Bakalli, 2006).

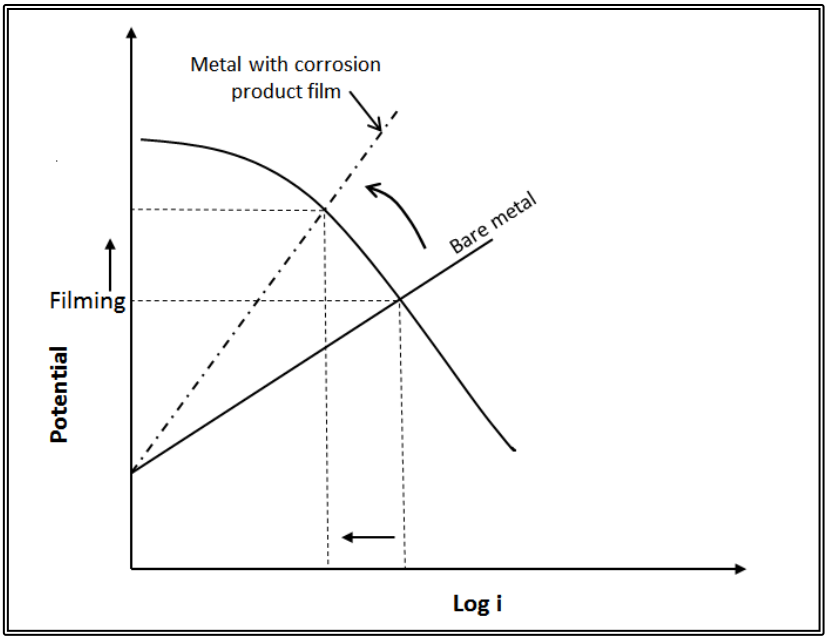

Figure 7-1: Schematic of the effect of corrosion product film on an anodic electrode

The WM also demonstrated the least self-corrosion rate (Figure 6-5) as a result of the composition effect (higher nickel content) compared with the PM (Mahajanam and Joosten, 2011). Furthermore, since HSLA steel is inherently susceptible to high self-corrosion rates in carbonic acid (Billingham et al., 2011) the corrosion rates of the weldment segments in the uncoupled state were quite significant in the total corrosion rates, as shown in Figure 6-7.

In contrast, under a submerged jet velocity of 5 m/s, the WM displayed a strong anodic characteristic, with high galvanic current leaving the electrode, protecting the PM and the HAZ as shown in Figure 6-9. It is noteworthy that the galvanic currents remained higher at wall shear stress of 72 N/m^2 when the film had been thinned or removed than they had been before the flow commenced, indicating that the film had been partially

protective. This result corroborates the findings of Alawadhi and Robinson (2011), Chaal et al (2009) and Schmitt et al (1992).

The Evans schematic in Figure 7-1 can be used to explain the observed trend under flow. Removal of the corrosion product film due to high wall shear stress will cause a negative displacement of the anodic curve, such that the corrosion potential is reduced with corresponding increase in the corrosion current.

In line with previous result (Fang and Liu, 2004) on the influence of flow velocity on the corrosion rate (Figure 2-15), the self-corrosion rates of the weld sections, under flow velocity of 5 m/s, increased compared with static condition (Figure 6-12). Again, it could be asserted that the quantity of the corrosion current depends on the mass transfer of the electrochemically active species to the electrode surface, since the steady state electrochemical process had been disrupted by the moving fluid, thinning and / or removing the corrosion product film, and bringing fresh corrosives into contact with the exposed metal surface. Consequently, the high jet flow rate is accompanied by increased instability of the partially protective film, as well as reduced passivity of corrosion product on the working electrodes, leading to high galvanic corrosion rate. Comparable results had been reported by Efird (2006) and Schmitt et al (2005).

The total corrosion rates of each weld section could be considered as the algebraic sum of the galvanic corrosion and the self-corrosion. In the absence of chemical inhibitor, the total corrosion rates of the weld sections were dominated by the self-corrosion in the no-flow condition while the galvanic corrosion was dominant under flowing condition as shown in Figure 6-13.

The effect of flow at jet velocity of 5 m/s on the total corrosion rate is summarised in Figure 7-2. Severe selective corrosion of the WM resulted in PWC. Conversely, the HAZ was fully protected from corrosion, under this condition, being considerably protected by the sacrificial galvanic corrosion of the WM, resulting in negative total corrosion rate. This was substantiated by the silver-grey appearance of the HAZ after the test. Similar observation had been reported by Martinez et al (2011).

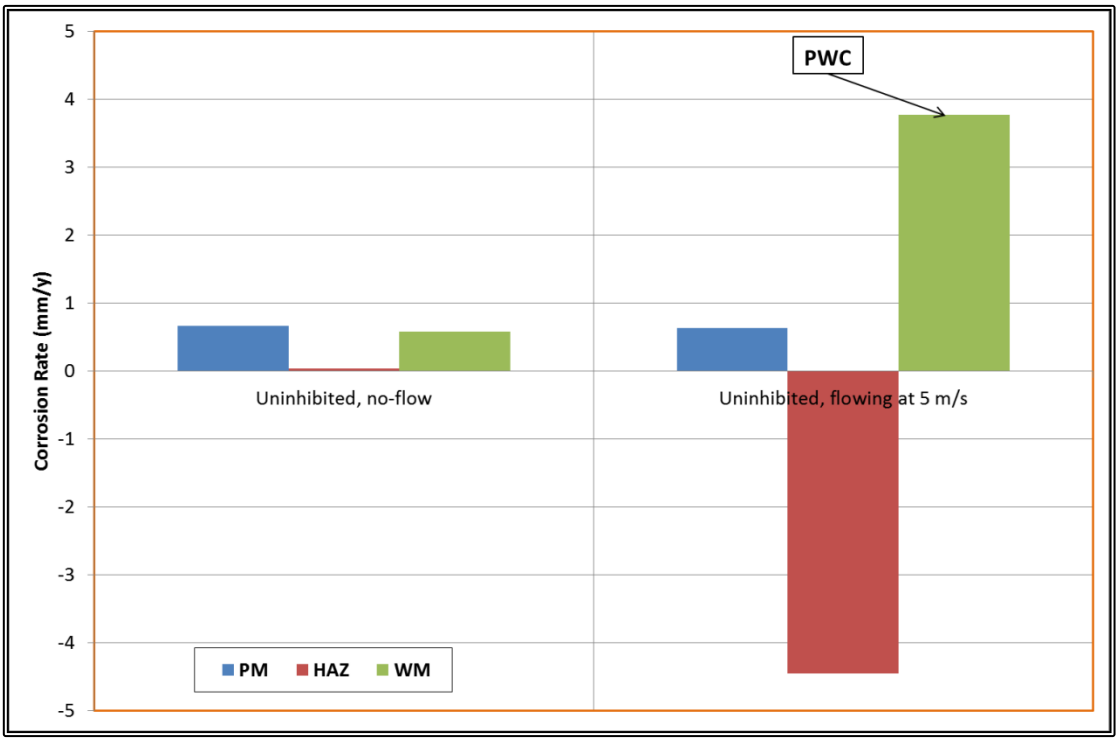

Figure 7-2: Effect of flow rate in uninhibited brine solution saturated with CO_2.

The severe localised corrosion of the WM, the Cu-Ni equivalence of the WM and the PM (Equation 6-1) notwithstanding, demonstrates the greater influence of the service environment on the rate of galvanic corrosion (Mahajanam and Joosten, 2011).

Therefore, in uninhibited brine solution saturated with carbon dioxide, it could be reasoned that:

- The HSLA steel welded joint is not predisposed to PWC in static and ambient conditions. Similar result was reported by Moon et al (2013) and Queen et al (2004). This suggests that the likelihood of PWC is minimal in offshore storage systems and 'short-down' / 'short-in' production condition without using chemical inhibitor. However, it is essential to apply suitable chemical inhibitor for effective control of the corrosion rate.
- Under flowing condition, HSLA steel welded joint is highly susceptible to severe selective corrosion of the WM and hence, premature failure due to PWC

7.2.1.2 Inhibited Solution

Static (No-Flow) Condition

Figure 6-14 shows the effect of addition of 30 ppm of a typical oilfield inhibitor (CORRTREAT 10-569) in the no-flow and ambient conditions. The propensity for PWC to occur in no-flow condition is negligible, as the total corrosion rates of the WM and the HAZ were very low and less than that of the PM. The action of the chemical inhibitor is illustrated in Figure 6-15, with the anodic curve being displaced positively accompanied by reduction in corrosion current. An affirmation of this is shown in Figure 6-16, with the inhibitor film on the weld segments forming a partial barrier between the corroding metal surfaces and electrolyte. Similar reduction in corrosion current was recorded in LPR measurements used to evaluate the self-corrosion rates. Hence, it could be deduced that inhibition in the static and ambient conditions is beneficial.

Flow at Jet Velocity of 5 m/s

Under impinging jet velocity of 5 m/s, corresponding to wall shear stress of about 72 N/mm^2, the galvanic currents increased and multiple galvanic current reversals of the HAZ occurred (Figure 6-16). The total galvanic current exchanged was higher compared with the no-flow condition as substantiated by the illustration of the effect of jet velocity on the polarisation of metal surface in Figure 7-3. This result indicates that, under high wall shear stress, the chemical inhibitor film was thinned / partially removed or de-adsorbed, leading to reduced protectiveness. In addition, the galvanic current reversals show that the inhibitor film was unstable and could be removed selectively from the HAZ and the WM, leading to a condition that would cause severe preferential weld corrosion.

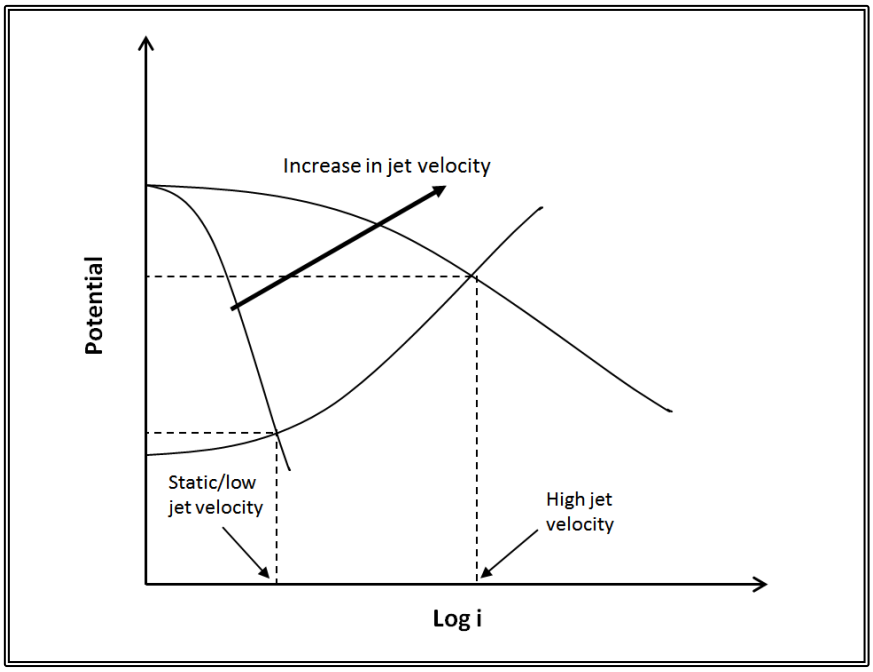

Figure 7-3: Schematic polarisation curve for the effect of jet velocity on the metal surface.

Martinez et al (2011) and Alawadhi et al (2008) reported similar current reversals for related studies conducted with a rotating cylinder electrode, as shown in Figure 6-17, in which samples of the same weldment (used in this study) were tested in CO_2 saturated brine containing the same corrosion inhibitor. The surface shear stresses are comparable in the two tests (72 N/m^2 for the present study and 70 N/m^2 for the RCE results). In both studies, the preferential removal of a surface inhibitor film from one weld region provides a satisfactory explanation for the anomalous role of inhibitors in PWC. Furthermore, this similarity supports the suitability of the novel submerged jet impingement target for the electrochemical study of preferential weld corrosion enhanced by change in hydrodynamics and inhibitor performance / selection studies.

In the uncoupled state, the self-corrosion rates increased significantly under hydrodynamic wall shear stress of about 72 N/mm^2, regardless of the presence of chemical inhibitor. The effects of inhibition with CORRTREAT 10-569 and flow at jet velocity 5/m are summarised in Figure 7-4. The following are obvious from this figure:

- In both uninhibited and inhibited brine solution saturated with CO_2, fluid flow (in the absence of solid particles) results in increase in self-corrosion rate.

- The benefit of the applied chemical inhibitor was demonstrated by significant reduction in the self-corrosion rates, especially in no-flow and ambient conditions.
- Under flowing condition, the efficiency of the chemical inhibitor was reduced by instability of the partially protective inhibitor film and reduced passivity of corrosion product on the working electrodes as well as, rapid desorption of the inhibitor film.
- The self-corrosion rate of HSLA steel in brine saturated with CO_2 is predominantly determined by the synergism of the environmental parameters and less influenced by the metallurgical nature of the steel, as indicated by the trend of corrosion rates of the WM (Mahajanam and Joosten, 2011).

The action of hydrodynamic change on the chemical inhibitor films had been adduced earlier for galvanic corrosion and is also applicable to self-corrosion.

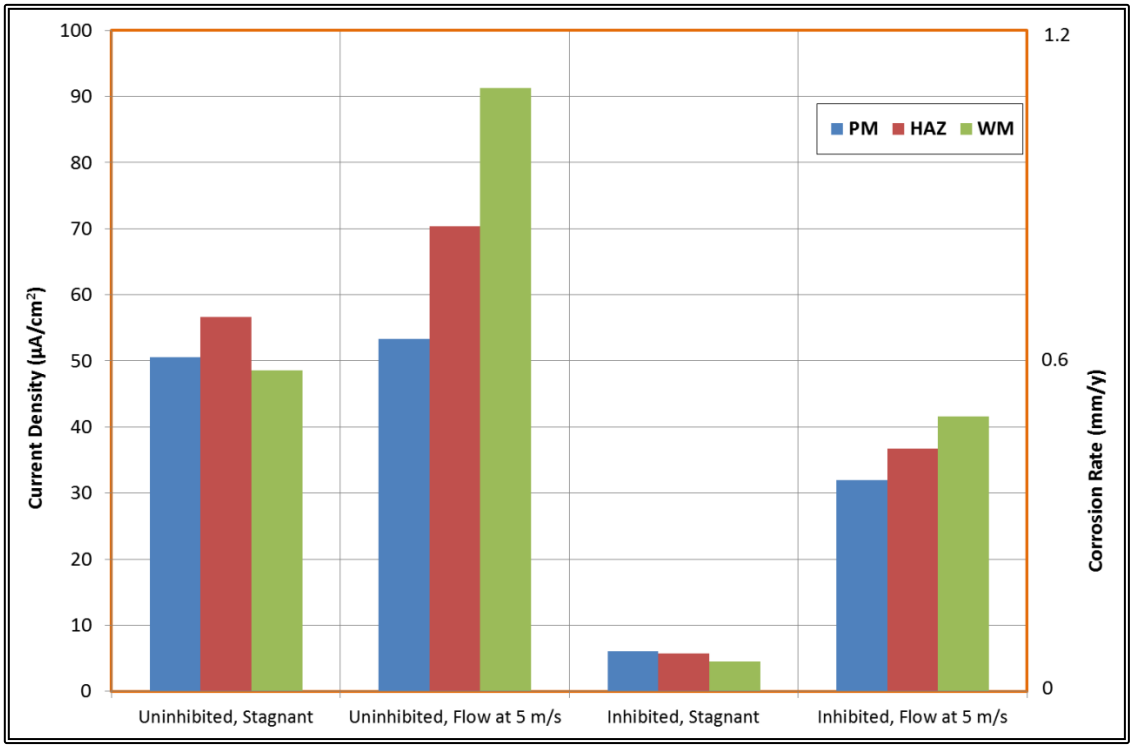

Figure 7-4: Effect of flow and inhibition on self-corrosion in CO_2 saturated brine solution.

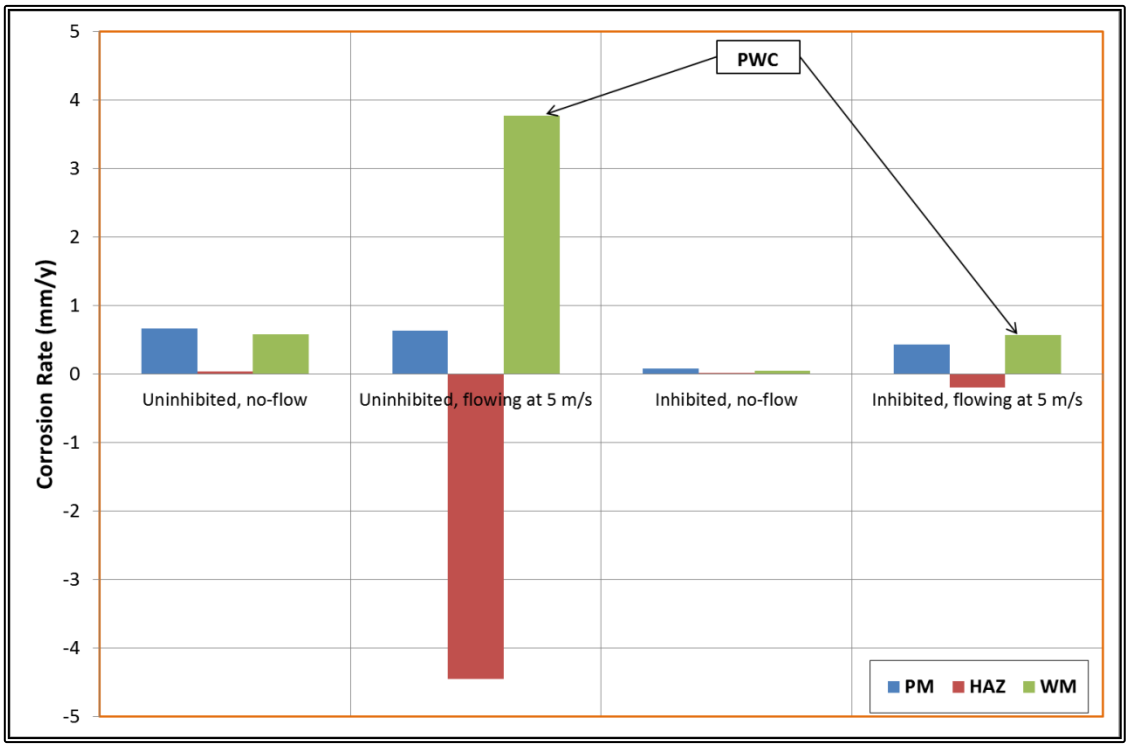

Figure 7-5: Effect of flow and inhibition in CO_2 saturated brine solution.

Using Equation 2-19, the efficiency of the inhibitor on the total corrosion rate of the WM was evaluated in no flow and flowing (at 5 m/s) conditions. The efficiency was found to slightly reduce from 91.53 to 84.82 under flowing condition, demonstrating quite good inhibitor performance.

An overview of the role of influence of flow under wall shear stress of about 72 N/mm^2 on the total corrosion rate of each weldment segment is shown in Figure 7-5. It is evident that at this simulated wall shear stress, X65 steel weldment showed high risk of premature service failure arising from preferential weld metal corrosion. Therefore, at a typical oilfield production rate, corresponding to 120 N/mm^2 (Craddock et al., 2004), it could be anticipated that deleterious oilfield incidents, traceable to PWC, may occur and hence avoided. Such oilfield preferential weld corrosion incidents had been reported by Mahajanam and Joosten (2011), Winning et al (2004) and, Gooch and Hart (1986), among others. Thus, the novel target used in this study is justified as an important improvement, capable of being used as predictive tool for PWC and related studies.

Flow at Jet Velocity of 10 m/s

The galvanic corrosion currents under jet velocity of 10 m/s, corresponding to wall shear stress of 250 N/mm^2 in brine solution saturated with CO_2 in the presence of 30 ppm CORRTREAT 10-569, are shown in Figure 6-19. Again, the inhibitor is beneficial before flow commenced. However, the measure is inadequate under high wall shear stress since the protective inhibitor film was removed. It is noteworthy that the galvanic response at flow velocity 10 m/s differed in significant way from that at 5 m/s. Galvanic current reversal was not observed in all experiments conducted at jet velocity of 10 m/s. The PM and WM remained anodic, with the highest metal loss (equivalent to 1.6 mm/y) from WM.

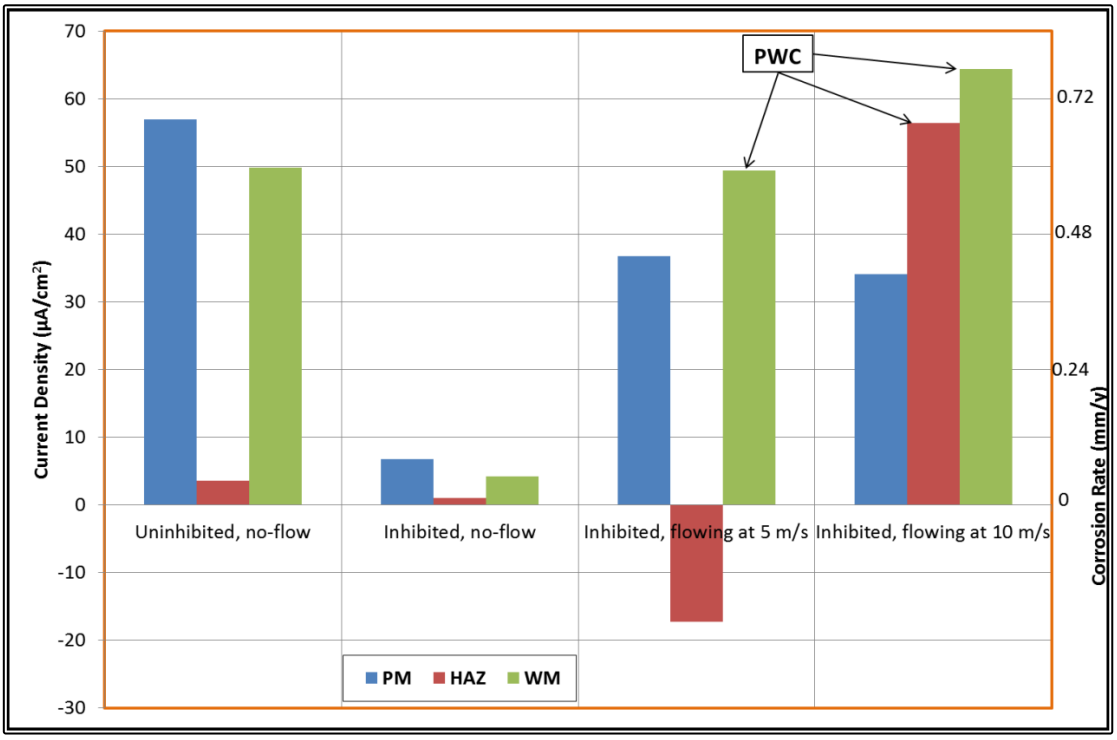

Figure 7-6: Effect of flow on inhibition in brine saturated with CO_2.

Similar high metal loss occurred in the uncoupled state. An overview of the effect of flow velocity of the inhibitor efficiency of 30 ppm CORRTREAT in brine saturated with CO_2 on the total corrosion rates of the weldment is shown in Figure 7-6. It is

evident that with a surface shear stress of 250N/m^2, the inhibitor was removed from the surface of each weld region. Under this condition, the higher corrosion rates were measured on the HAZ (0.65 mm/y) and WM (0.75 mm/y), indicating the occurrence of preferential weld corrosion. In addition, it could be assumed that the risk of PWC occurrence increases with the jet velocity rate, inhibition treatment notwithstanding. This is corroborated by Fang and Liu (2004) as illustrated in Figure 2-15. An effective way of preventing PWC could therefore be to establish the critical flow intensity of the service condition / parameters being and maintaining the service flow rate below this value.

7.2.2 Effect of Aeration of Brine Solution Containing CO_2

There are many circumstances in which air (oxygen) is inadvertently admitted into the oilfield production system or laboratory system. An example of this is in the carbon dioxide enhanced oil recovery (CO_2 – EOR) injection operations facilitated by the development of carbon capture and storage (CCS) technologies. However, captured CO_2 from anthropogenic sources can potentially contain oxygen (Rosli et al., 2014) which will increase the risk of corrosion and therefore preferential weld corrosion. Other oilfield sources include leakage of pump and valve system, and inadequate deaeration of seawater / service system. Furthermore, laboratory studies, especially flow enhanced corrosion investigations, may also be subjected to the effects of oxygen ingress. It is therefore unexpected that information / reports on the role of oxygen in oilfield corrosion are scarce since the presence of air / oxygen is either not realised or ignored. For this reason, jet impingement experiments were carried out in which air was deliberately admitted to the flow loop to investigate its effect. Air was bubbled at a controlled rate of approximately 2.2 ml/liter/min into the carbon dioxide saturated brine solution, with and without inhibition.

7.2.2.1 Uninhibited Aerated Solution

The influence of the presence of oxygen / air in brine solution containing CO_2 on the X65 steel weldments in the inner ring (high turbulence hydrodynamic region) is shown

in Figure 6-21. Galvanic current exchange in the absence of air and no-flow condition is similar to that which had been discussed earlier in Figure 6-2. The ingress of air in the static condition being accompanied by reduction in galvanic current suggests that a more protective corrosion product film was formed. This could be attributed to a noble shift in potential resulting in the decay of the galvanic current as shown in Figure 7-1. The PM and the WM were anodic to the HAZ.

When the solution was flowed at a jet velocity of 10 m/s, large galvanic current was observed, suggesting that the protective film was removed from the surface of each weld segment. However, the HAZ galvanic current was reversed under this severe wall shear stress and remained anodic. This is contrary to the galvanic response of the HAZ in the absence of air as shown in Figure 6-9. In the uncoupled state, the self-corrosion rate of each working electrode was also higher, compared with completely deaerated system as shown in Figure 6-23.

The total corrosion rates of the weldment sections under wall shear stress of 250 N/mm^2 shows that the HAZ corroded at a rate of 14.8 mm/y in the aerated uninhibited system (Figure 6-23). Therefore, the propensity to premature failure under this condition, caused by PWC, is very high. This again supports the vital role of the service environment on the corrosion of HSLA steels.

7.2.2.2 Inhibited Aerated Solution

The reduced galvanic current before the streaming-in of air into the inhibited solution as shown in Figure 6-25, indicates the beneficial role of the applied chemical inhibitor as explained earlier in Figure 7-1. The sparging of air was accompanied by further decay of the galvanic current suggesting that more protective film is being formed on the surface of the weld sections. It is worth noting that the HAZ was cathodic in the no-flow stages. However, when flowed at a jet velocity of 10 m/s, a large increase in the galvanic currents, with the HAZ being anodic to the PM and the WM. The action of change in hydrodynamics is as explained previously in Figure 7-3.

Under a jet velocity of 5 m/s, significant current reversals were recorded as shown in Figure 6-24, similar to the occurrence in deaerated inhibited solution, under the action

of the same wall shear stress. This further corroborates the varying behaviour of the inhibitor under this wall shear stress as explained previously in deaerated solution (Figure 6-16) and also reported by Alawadhi and Robinson (2011) and Martinez et al (2011).

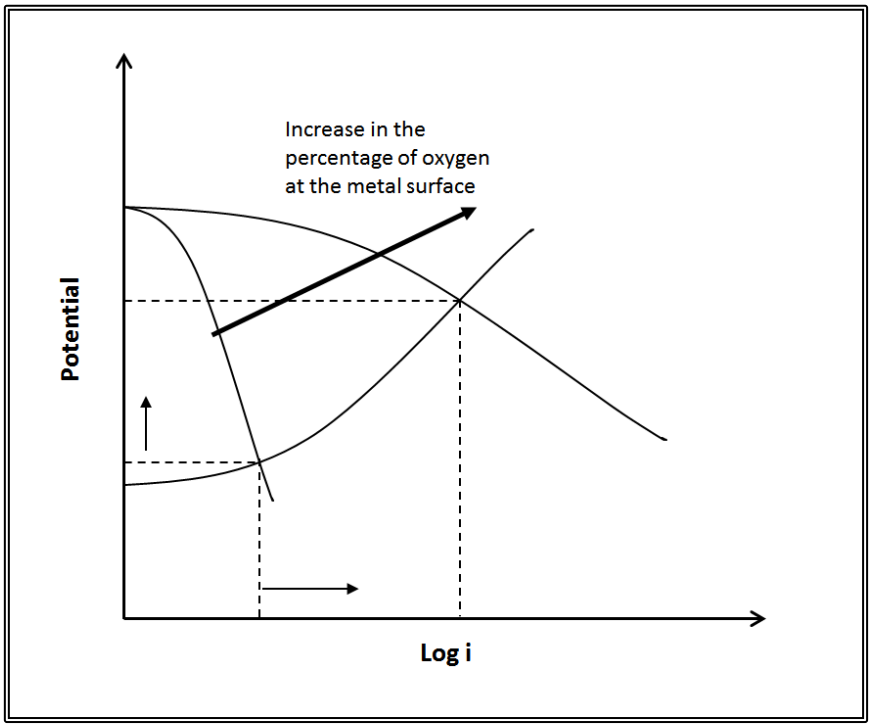

Figure 7-7: Effect of oxygen on the metal surface

The amount of oxygen available at the metal surface increases with flow, causing a noble shift of the cathodic curve as illustrated in Figure 7-7.

In the uncoupled state, the self-corrosion rates increased with the jet velocity and are higher compared with deaerated inhibited solution as shown in Figure 6-26. Furthermore, an appraisal of the total corrosion rates under the two jet velocities shows that:

- In some cases, the total corrosion rate for a particular region of the weld was less than its self-corrosion rate due to it being partially protected by a cathodic (negative) galvanic contribution.

- At a flow rate of 5 m/s, the highest corrosion rate was on the WM (6.39 mm/y), whereas at 10 m/s the highest rate was on the HAZ (21.66 mm/y). In both cases, the corrosion rate of the PM was relatively low.
- The severe PWC in aerated inhibited brine solution containing CO_2 under a high wall shear stress of 250 N/m^2 being higher than at lower wall shear stress of 70 N/m^2 suggests that more corrosion reactions occur at higher jet velocity as illustrated in Figure 7-3.

The effect of inhibition on aerated solution with 30 ppm CORRTREAT 10-569 is shown in Figure 7-8. It could be deduced that under flowing conditions, this inhibitor and / or the dosage is not suitable for the control of corrosion rate and hence, PWC. In addition, the risk of PWC is higher using 30 ppm CORRTREAT 10-569 under this service condition and can lead to premature failure and concomitant costs.

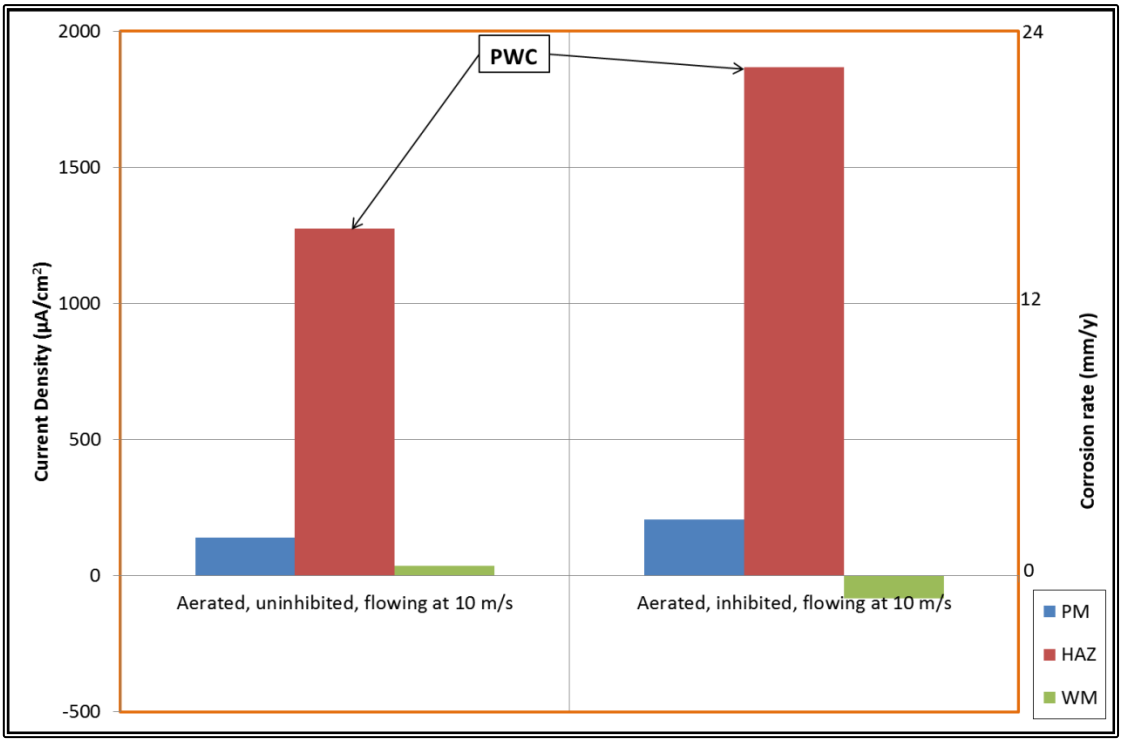

Figure 7-8: Effect of inhibition in aerated brine solution containing CO_2.

Figure 6-27 sums up the effect of dissolution of small quantity of oxygen in brine solution containing CO_2 and can be correlated to a leaking pump or valve, and / or

ineffective deaeration of the system. With or without inhibitor (in this case, 30 ppm CORRTREAT 10-569), the presence of oxygen could be adduced for the very high corrosion rates in the weld metal and/or heat affected zone, leading to severe PWC as substantiated by the noble shift of the potential under cathodic scan in Figure 6-38. This is indicates that additional cathodic reaction occurs, being facilitated by the presence of oxygen. It is imperative therefore, that these deleterious rates be addressed to guarantee the integrity of the infrastructure.

7.3 Effect of Chemical Composition and Microstructure on PWC

The weld metal composition is similar to that of the parent metal (and hence, the heat-affected zone), except for the addition of 0.68% Ni and larger quantities of Cr and Mo as shown in Table 3-2. As explained previously, the Cu-Ni equivalent between the WM and the PM compositions suggests that the WM would be cathodic to the PM, which is a necessary condition for preventing PWC Mahajanam and Joosten (2011). In no-flow condition, the WM demonstrated the least self-corrosion rate with and without chemical inhibition as shown in Figure 6-14. In contrast, under the action of flow (at wall shear stress of 72 N/mm^2 and 250 N/mm^2) the benefit of the WM alloying was lost and the likelihood of PWC increased as shown in Figure 6-20. This affirms that the environmental effects override the influence of the chemical composition and microstructure.

7.4 Industrial Applications of Findings

Prevention and control of PWC is primarily an issue which must be dealt with in the design stage. In the service stage, effective monitoring and satisfactory applications of the following measures should mitigate challenges with PWC and galvanic corrosion related issues:

a) **Specifics**:

- It was demonstrated that the susceptibility to PWC is low in no-flow condition, even without inhibitor. Conversely, inhibited solution demonstrated increased

tendency to PWC with jet velocity. It is therefore essential to establish and maintain service flow rate below the critical flow intensity for the service conditions / parameters being considered.

- ❖ Environmental parameters have been shown to be vital in determining the level of PWC risk, it therefore essential to modify the environment with the aim of achieving effective management of the corrosion rate in general and PWC in particular

b) **General**:

- In offshore applications, prevention of aeration of seawater and other production fluids will certainly reduce the risk of corrosion and therefore occurrence of PWC in pipeline systems.
- A major challenge in assessing the risk of PWC is the difficulty in extrapolating data from one set of environmental conditions to another. In particular, high velocity flow was shown to be a significant influence on the occurrence and location of preferential attack. Hence, a viable field flow rate should be maintained to justify the overall production economics.
- Thermal gradient due to uneven heating or dissipation of heat has a similar effect on the metal as galvanic corrosion. The metal is differentially polarized (or enhanced in weldment), causing preferential attacked at the hot area. Therefore, suitable measure must be taken to avoid local temperature differences caused by uneven heating or cooling. Besides, formation of cold or hot spots, for example due to discontinuities in insulation or coating, must be prevented.
- Adequate chemical inhibitor dosage must be maintained continuously throughout the system.
- Effective monitoring and asset integrity management system should be implemented.

7.5 Chapter Summary

The interactions between the weldment segments and the service environment in achieving effective corrosion control were considered and measures for the prevention

of deleterious preferential weld corrosion were proffered. In static condition, similar to storage and 'shut-in' system, the susceptibility of X65 steel weldment to PWC is negligible. In contrast, PWC risk increases with jet velocity, regardless of the presence of chemical inhibitor. Aerated system, with or without inhibitor, was also shown to pose severe threat to the integrity of an oilfield infrastructure. In particular, the novel submerged impingement target demonstrated suitable capability as a predictive tool for PWC and flow enhanced corrosion studies.

CHAPTER 8.
CONCLUSIONS AND RECOMMENDATIONS

In this chapter, deductions are made from earlier chapters and major contributions of this research are underscored. In addition, critical service conditions outside the scope of this research are highlighted as potential areas for further studies towards predicting and controlling flow accelerated PWC.

8.1 Conclusions

It is essential that general conclusions on the causes and mitigation of PWC must be made with careful consideration of the synergistic metallurgical / service environment effects, however, some practical lessons from this research include:

- The novel submerged jet impingement technique developed in this research was found suitable for investigation of flow accelerated preferential weld corrosion and effective evaluation of corrosion inhibitors in a typical offshore oil and gas pipeline systems.
- A typical oilfield corrosion inhibitor (CORRTREAT 10-569) was effective in reducing the corrosion rate, as well as, preventing preferential weld corrosion (PWC) of X65 pipeline steel weldment in brine solution saturated with carbon dioxide under static (no-flow) and ambient conditions.
- The benefit of the corrosion inhibitor was lost at very high flow rates (shear stress of 250 N/m^2) due to removal of the corrosion inhibitor film from the metal surface.
- In both aerated and deaerated inhibited brine solution, at intermediate flow rates (shear stress of 72 N/m^2) the corrosion inhibitor film was removed preferentially from one weld region, which resulted in a shift in its open circuit potential and a reversal in the galvanic current. Such current reversals provide a satisfactory explanation for the anomalous role of inhibitors in PWC that has been observed in oilfield service.

- Small additions of air to carbon dioxide saturated brine, to simulate a leaking pump / valve or inadequate seawater deaeration, caused very high corrosion rates in the weld metal and/or heat affected zone, leading to severe PWC.
- The corrosion rate in aerated brine solution containing CO_2, with or without inhibition, was reduced in no-flow and ambient condition, but was shown to increase with flow rate.
- Cathodic potentiodynamic polarisation scans confirmed that the corrosion process in aerated solution was under oxygen mass transport control.
- In aerated flowing conditions, the inhibitor used was not only inappropriate but also enhanced the risk of PWC and hence, premature failure.
- Comparable galvanic current reversals were observed in the improved submerged jet impingement technique and the rotating cylinder electrode method in the same inhibited solution and hydrodynamic conditions of about 70 N/m^2 wall shear stress. In addition, electrochemical studies at wall shear stress of 250 N/m^2 were achieved with the novel technique.

8.2 Recommendations for Further Research

This research has demonstrated the suitability of submerged jet impingement, using an improved target to evaluate flow-accelerated preferential weld corrosion. Consequently, opportunity now exists for researches to enable improved predictive capabilities for the effective use and deployment of carbon and low-alloy steel in the offshore oil and gas production, in particular and engineering systems in general. Further focused research areas, requiring systematic studies, for better predicative capabilities include:

- Presence of hydrocarbon phase which plays a vital role in CO_2 corrosion in terms of its phase ratio, its partitioning capability for CO_2, water wetting, and its inhibiting effect on CO_2 corrosion.
- Test environment to include different temperatures as well as different concentrations and sizes of suspended sand to simulate specific down-hole conditions that are very demanding for effective corrosion inhibition.

- Studies on the effective inhibitor concentration (concentration to achieve a specific corrosion rate) in typical field system parameters, such as, interactions with H_2S and acetic acid.
- Flow modelling to better quantify water wetting / shedding can lead to improved predictive modelling, bearing in mind the flow regimes and their changes throughout the life of the field.
- Studies with different welded joint configurations produced with typical oilfield fabrication parameters.
- Studies in characteristic service environments, replicating installation, commissioning, operating and shut down / down-time, among other oilfield scenarios.

REFERENCES

Aagotnes, N. O., Hemmingsen, T., Haarseth, C. A. and Midttveit, I. (1999), "Comparison of Corrosion Measurements by use of AC-Impedance, LPR, and Polarization Methods on Carbon Steel in CO_2 Purged NaCl Electrolytes", 25-30 April 1999, NACE International, USA, Paper 99027.

Abayarathna, D. and Naraghi, A. (2001), "Evaluation of Corrosion Inhibitors for CO_2 Corrosion Using Electrochemical and Non-Electrochemical Techniques" 11-16 March, 2001, Houston, Texas, NACE International, USA, pp1-20, Paper 01060.

Addis, J., Brown, B. and Nesic, S., (2008), "Erosion-Corrosion in Disturbed Liquid/Particle Flow", NACE International, USA, Paper 08572.

Ahmad, Z. (2006), "Corrosion Control by Inhibition", in *Principles of Corrosion Engineering and Corrosion Control*, Butterworth-Heinemann, Oxford, pp. 352-381.

Akbar, A., Hu, X., Neville, A. and Wang, C. (2011), "Flow rate and inhibitor influences on protective scale formed on carbon steel", *Materials Performance,* vol. 50, no. 12, pp. 54-59.

Alawadhi, K., Aloraier, A. S., Joshi, S., Alsarraf, J. and Swilem, S. (2013), "Investigation on Preferential Corrosion of Welded Carbon Steel Under Flowing Conditions by EIS", *Journal of Materials Engineering and Performance*, vol.22 (8), pp. 2403-2410.

Alawadhi, K., Robinson, M., Chalmers, A. and Winning, I. G. (2008), "Inhibition of Weld Corrosion in Flowing Brines Containing Carbon Dioxide", *Corrosion 2008*, 16-20 March 2008, New Orleans, USA, NACE International, Houston, TX, pp. 086221.

Alawadhi, K. and Robinson, M. J. (2011), "Preferential weld corrosion of X65 pipeline steel in flowing brines containing carbon dioxide", *Corrosion Engineering Science and Technology*, vol. 46, no. 4, pp. 318-329.

Alink, B. A., Ramachandran, S., Campbell, S., Outlaw, B. and Jovancicevic, V. (1999), "Mechanism of CO_2 Corrosion Inhibition by Phosphate Esters", 25-30 April 1999, NACE International, USA Paper 99037.

Altoé, P., Pimenta, G., Moulin, C. F., Díaz, S. L. and Mattos, O. R. (1996), "Evaluation of Oilfield Corrosion Inhibitors in CO_2 Containing Media: A Kinetic Study", *Electrochimica Acta,* vol. 41, no. 7-8, pp. 1165-1172.

Amin, M. A. and Ibrahim, M. M. (2011), "Corrosion and corrosion control of mild steel in concentrated H_2SO_4 solutions by a newly synthesized glycine derivative", *Corrosion Science*, vol. vol. 53, no. no. 3, pp. 873-885.

Arivarasu, M., Manikandan, M., Gokulkumar, K., Karthikeyan, S., Devendranath Ramkumar, K. and Arivazhagan, N. (2013), "Studies on weldment corrosion in different corrosive environments", *Journal of Corrosion Science and Engineering*, vol. 16, pp.57-65.

Asrar, N. (2010), "Corrosion control of drilling tools through chemical treatments - Effectiveness and challenges", *Society of Petroleum Engineers - 5th SPE International Conference on Oilfield Corrosion 2010*, pp. 93.

ASTM (2001), *Standard Guide for Evaluating and Quantifying Oilfield and Refinery Corrosion Inhibitors in the Laboratory*, G 170-01a, ASTM International, USA.

Avendano-Castro, C., Galvan-Martinez, R., Contreras, A., Salazar, M., Orozco-Cruz, R., Martinez, E. and Torres-Sanchez, R. (2009), "Corrosion Kinetics of Pipeline Carbon Steel Weld in Aqueous Solution Containing H_2S", *Corrosion Engineering, Science and Technology*, vol. 44, no. 2, pp. 149-156.

Baboian, R. (ed.) (2002), *NACE Corrosion Engineer's Reference Book*, Third ed, NACE International, Texas, USA.

Barker, R., Hu, X. and Neville, A. (2013), "The Influence of High Shear and Sand Impingement on Preferential Weld Corrosion of Carbon Steel Pipework in CO_2-Saturated Environments", *Tribology International, vol. 68, pp. 17-25*.

Barker, R., Hu, X., Neville, A. and Cushnaghan, S. (2012), "Assessment of Preferential Weld Corrosion of Carbon Steel Pipework in CO_2 Saturated Flow-Induced Corrosion Environments", *NACE - International Corrosion Conference Series*, Vol. 3, pp. 2208.

Billingham, M. A., Lee, C., Smith, L., Haines, M., James, S. R., Goh, B. K. W., Dvorak, K., Robinson, L., Davis, C. J. and Peralta-Solorio, D. (2011), "Corrosion and materials selection issues in carbon capture plants", *Energy Procedia*, vol. 4, pp. 2020-2027.

Cai, F., Liu, W., Fan, X., Lu, M., Zhang, J. and Du, Q., (2012), *Electrochemical Corrosion Behavior of X70 Pipeline Steel In Wall Jet Zone Under Jet Impingement at High Temperature And High Pressure CO_2 Environment*, 11-15 March 2012, NACE International, Paper 12141.

Cayard, M.S. and Maldonado, J.G., (2000), "Use and Misuse of Laboratory Tests", 26-31 March 2000, Orlando, Florida, NACE International, Paper 00132.

Chaal, L., Albinet, B., Deslouis, C., Al-Janabi, Y. T., Pailleret, A., Saidani, B. and Schmitt, G. (2009), "Wall shear stress mapping in the rotating cage geometry and

evaluation of drag reduction efficiency using an electrochemical method", *Corrosion Science,* vol. 51, no. 8, pp. 1809-1816.

Choi, Y. and Nešić, S., (2010), "Effect of Impurities on the Corrosion Behaviour of Carbon Steel in Supercritical CO_2 - Water Environments", 14-18 March 2010, San Antonio, NACE International, Paper 10196.

Ciolkowski, M., Neville, A., Hu, X. and Mavredaki, E. (2012), "Influence of brine with different supersaturation ratio on corrosion processes for pipeline material carbon steel X65, scale deposition and performance of combined inhibitor", *Society of Petroleum Engineers - SPE International Conference and Exhibition on Oilfield Corrosion 2012,* pp. 254.

Copson, H. R. (1945), "A Theory of the Mechanism of Rusting of Low Alloy Steels in the Atmosphere", ASTM, USA, , Philadelphia, Pennsylvania, Vol. 45, pp 121-130 .

Craddock, H., Daneilsen, B., Mamann, A. and Caird, S., (2004), "Preferential Weld Protection Corrosion Inhibitor for Topsides Gas Producing Facility under High Shear and Sweet Condition", NACE International, Paper 04425.

Cranfield University (2003), *Review of the Performance of High Strength Steels used Offshore,* 105, Health and Safety Executive, UK.

Crolet, J. L., Thevenot, N. and Dugstad, A. (1999), "Role of Free Acetic Acid on the CO_2 Corrosion of Steels", 1999, Houston, TX, USA, NACE, pp. Paper 99024.

Crolet, J. L., Nesic, S. and Thevenot, N. (1996), "Role of Conductive Corrosion Products on the Protectiveness of Corrosion Layers", 24-29 March 1996, Denver, Colorado, NACE International, Paper 96004.

Davies, J. T. (1972), Turbulence Phenomena: An Introduction to the Eddy Transfer of Momentum, Mass and Heat, Particularly at Surface, Academy Press, New York, pp. 121-174.

Davis, J. R. (ed.) (2006), *Corrosion of weldments,* Davis and Associates, ASM International, OH, USA.

Dawson, J. L., John, G. and Oliver, K. (2010), "Management of Corrosion in the Oil and Gas Industry", in Tony J.A. Richardson (ed.) *Shreir's Corrosion,* Elsevier, Oxford, pp. 3230-3269.

Dawson, J. L., Palmer, J. W., Moreland, P. J. and Dicken, G. E. (1999), "Weld Corrosion - Chemical, Electrochemical and Hydrodynamic Issues, Inconsistencies and Models", in Jackman, P. S. and Smith, L. M. (eds.) *Advances in Corrosion and Materials in Oil and Gas Production: (EFC 26),* European Federation of Corrosion Publications, Maney Publishing, Leeds, UK, pp. 155-169.

Dayalan, E., Shadley, J. R., Rybicki, E. F., Shirazi, S. A. and Moraes, F. D. d. (1998), "CO_2 Corrosion Prediction in Pipe Flow Under $FeCO_3$ Scale-Forming Conditions", 22-27 March 1998, San Diego, California, NACE International, Paper 98051.

De Waard, C., (2004), *Monogram for predicting CO_2 corrosion of carbon steel is based on the deWaard- Milliams equation, accessed 07 March, 2014 from* http://cdewaard.home.xs4all.nl/#CO2.

De Waard, C. and Lotz, U. (1993), "Prediction of CO_2 Corrosion of Carbon Steel", NACE, USA, Paper 93069.

De Waard, C. and Lotz, U. (1994), Prediction of CO_2 Corrosion of Carbon Steel, 13, The Institute of Materials, UK .

De Waard, C. and Milliams, D. E. (1975), "Carbonic Acid Corrosion of Steel", *Corrosion*, vol. 31, no. 5.

Dong, S., Liu, W., Zhang, J., Lin, X., He, J. and Lu, M. (2014), "Effect of Oxygen on CO_2 Corrosion and Erosion-Corrosion Behaviour of N80 Steel under High Temperature and High Pressure", *Corrosion Conference*, 09 - 13 March, 2014, San Antonio, Texas, NACE International, USA, pp. Paper 4198.

Dugstad, A. (1998), "Mechanism of Protective Film Formation During CO_2 Corrosion of Carbon Steel", 22-27 March 1998, San Diego, California, NACE International, Paper 98031.

Dugstad, A. (2006), "Fundamental Aspects of CO_2 Metal Loss Corrosion - Part 1: Mechanism", 12-16 March 2006, San Diego, CaliforniaNACE International, Paper 06111.

Dugstad, A., Kvarekval, J., Nyborg, R., Gulbrandsen, E. and Seiersten, M., (2006), *Corrosion Testing in Multiphase Flow, Challenges and Limitations*, NACE International.

During, E. D. D. (1997), *Corrosion Atlas*, Third, expanded and revised ed, Elsevier, The Netherlands.

Efird, K. D. (1977), "The Effect of Fluid Dynamics on the Corrosion of Copper Base Alloys in Seawater", *Corrosion*, vol. 33, no. 1, pp. 3-8.

Efird, K. D. (2000), "Jet Impingement Testing for Flow Accelerate Corrosion", *NACE Corrosion Conference*, Vol. Paper No. 00052, Houston, Texas, .

Efird, K. D. (2011), *Jet Impingement Testing to Investigate Flow Effects on Corrosion, Efird Corrosion International, Inc., The Woodlands, Texas, USA*, available at: http://efirdcor.com/Jet_Imp_Test.htm (accessed April 10, 2013).

Efird, K. D., Wright, E. J., Boros, J. A. and Hailey, T. G. (1993), "Correlation of steel corrosion in pipe flow with jet impingement and rotating cylinder tests", *Corrosion,* vol. 49, no. 12, pp. 992-1003.

Efird, K. D. (1991), "Predicting corrosion of steel in crude oil production", *Materials Performance,* vol. 30, no. 3, pp. 63-66.

Efird, K. D. (2006), "Flow Accelerated Corrosion Testing Basics", 12-16 March 2006, USA, NACE International, USA, pp. 066891-0668916.

Emenike, C. O. (1993), "The application of knowledge-based systems to corrosion management", *Materials & Design,* vol. 14, no. 6, pp. 331-337.

Endo, S., Fujita, S., Nagae, M. and Iwata, M., (1997), "Prevention of Preferential Corrosion of Welded Joints of Carbon Steel in CO_2 Containing Environment", The International Society of Offshore and Polar Engineers.

Fan, X., Liu, W., Cai, F., Wu, Y., Lu, M., Guo, H. and Du, Q., (2011), *Electrochemical Characterization of Erosion-Corrosion of X70 Pipeline Steel Under Jet Impingement Conditions*, NACE International.

Fang, C. S. and Liu, B. (2004), "Corrosion Induced by Change in Hydrodynamics", NACE International.

Fontana, M. G. (1987), *Corrosion Engineering,* 3rd ed, McGraw-Hill, New York.

Fosbøl, L. P., Thomsen, K. and Stenby, H. E. (2009), "Improving Mechanistic CO_2 Corrosion Models", 22-26 March 2009, Atlanta, Georgia, NACE International, USA, pp. NACE-09561.

Foss, M., Gulbrandsen, E. and Sjöblom, J., (2009), *CO_2 Corrosion Inhibition and Oil Wetting of Carbon Steel with Ferric Corrosion Products*, NACE International.

Francis, R. (2001), "Galvanic Corrosion: A Practical Guide for Engineers", *NACE International, Houston,* 2001, Texas, USA, NACE International, Houston, pp. 5-23.

Gao, M., Pang, X. and Gao, K. (2011), "The Growth Mechanism of CO_2 Corrosion Product Films", *Corrosion Science,* vol. 53, no. 2, pp. 557-568.

Gao, K., Yu, F., Pang, X., Zhang, G., Qiao, L., Chu, W. and Lu, M. (2008), "Mechanical properties of CO_2 corrosion product scales and their relationship to corrosion rates", *Corrosion Science,* vol. 50, no. 10, pp. 2796-2803.

George, K., Waard, K. d., Wang, S. and Nesic, S. (2004), "Modeling of CO_2 Corrosion of Mild Steel in the Presence of High Partial Pressures of CO_2 and Acetic Acid - Electrochemical Modeling and a Modification to the de Waard Corrosion Model", 28 March-1 April 2004, NACE International.

Gooch, T. G. and Hart, P. H. M. (1986), "Review of Welding Practices for Carbon Steel Deaerator Vessels", *Corrosion '86,* Vol. Paper 303, March 1986, Houston, TX, NACE.

Gulbrandsen, E. and Grana, A. (2007), "Testing of carbon dioxide corrosion inhibitor performance at high flow velocities in jet impingement geometry effects of mass transfer and flow forces", *Corrosion,* vol. 63, no. 11, pp. 1009-1020.

Gulbrandsen, E., Miland, H. and Kvarekval, J. (2005), "Effect of Oxygen Contamination on Inhibition Studies in Carbon Dioxide Corrosion", *Corrosion,* vol. 61, no. 11.

Gulbrandsen, E. and Dugstad, A. (2005), "Corrosion Loop Studies of Preferential Weld Corrosion and its Inhibition in CO_2 Environments", 3-7 April 2005, Houston, TX; USA, NACE International, TX, USA.

Gulbrandsen, E., Granaa, A. and Nisancioglu, K., (2005), *How does fluid flow affect performance of CO_2 corrosion inhibitors?,* Society of Petroleum Engineers, Aberdeen, United Kingdom.

Gulbrandsen, E., Nesic, S., Hesjevik, S. M., Skjfrve, S., Sundfer, B., Burchardt, T. and Stangeland, A. (1998), "Effect of Pre-corrosion on the Performance of Inhibitors for CO_2 Corrosion of Carbon Steel", 22-27 March 1998, NACE International, pp. Paper 98013.

Hara, T., Kaneta, H. and Asahi, H. (1998), "Effect of Flow Velocity on CO_2 Corrosion and Galvanic Corrosion Behavior in Oil and Gas Environments", 22-27 March 1998, NACE International.

Hausler, R. H. and Schmitt, G. (eds.) (2004), *Hydrodynamic and Flow Effects on Corrosion Inhibition,* NACE.

Hausler, R.H., Schmitt, G. and Consulta, C., (2004), *Hydrodynamic and Flow Effects on Corrosion Inhibition,* NACE International.

Hedges, B., Chen, H. J., Sprague, K. and Bieri, T. H. (2006), "A Review of Monitoring and Inspection Techniques for CO_2 and H_2S Corrosion in Oil & Gas Production Facilities: Location, Location, Location", 12-16 March 2006, NACE International.

Heidersbach, R. (2011), *Metallurgy and Corrosion Control in Oil and Gas Production,* John Wiley and Sons, USA.

Hong, T., Shi, H., Wang, H., Gopal, M. and Jepson, W. P. (2000), "EIS Study of Corrosion Product Film in Pipelines".

Howell, A. G. (1997), "Under-Deposit Corrosion at Weld Seams in Carbon Steel Piping", 9-14 March 1997, NACE International.

Hu, Q., Liu, J., Zhang, J., Huang, F. and Guo, X., (2013), *Crevice Corrosion Behaviors of X52 Carbon Steel in Chloride Containing Solutions*.

Hu, X. and Neville, A. (2009), "CO_2 Erosion–Corrosion of Pipeline Steel (API X65) in Oil and Gas Conditions—A Systematic Approach", *Wear,* vol. 267, no. 11, pp. 2027-2032.

Hussain, E. A. M. (2001), *An Electrochemical Investigation of Erosion Corrosion of Duplex Stainless Steel in Seawater Containing Sand Particles* (PhD thesis), Cranfield University, UK.

Hussain, E. A. M. and Robinson, M. J. (2007), "Erosion-corrosion of Duplex Stainless Steel in Flowing Seawater Containing Sand Particles ", *Corrosion Science,* vol. Vol. 49, no. 4, pp. 1737-1754.

Jenkins, A. and MacDougall, D., (2013), *Mitigation of Under-Deposit and Weldment Corrosion with an Environmentally Acceptable Corrosion Inhibitor*, NACE International.

John, D., Bailey, S., Kinsella, B. and De Marco, R. (2008), "Effect of trace dissolved oxygen on the cathodic kinetics of carbon dioxide corrosion of carbon steel", *48th Annual Conference of the Australasian Corrosion Association 2008: Corrosion and Prevention 2008,* pp. 347.

John, D., Kinsella, B., Bailey, S. and Marco, R.D., (2007), *Flow Dependence of Carbon Dioxide Corrosion Rates and the Interference of Trace Dissolved Oxygen*, NACE International.

Kakooei, S., Ismail, M. C., Alawadhi, K. and Bataee, M. (2012), "Prediction of Heat Affected Zone (HAZ) Corrosion in CO_2 Environment by Artificial Neural Network", *Australian Journal of Basic and Applied Sciences,* vol. 6, no. 12, pp. 134-140.

Kateřina, K. and Gubner, R. (2010), "Development of Standard Test Method for Investigation of Under-Deposit Corrosion in Carbon Dioxide Environment and its Application in Oil and Gas Industry", *Corrosion Conference*, 14-18 March 2010, NACE International, USA.

Kermani, B. (2014), "Depiction of Metallurgical Parameters as Governing CO_2 Corrosion", *Corrosion Conference*, 09 - 13 March, 2014, San Antonio, Texas, NACE International, USA, pp. Paper 3813.

Kermani, M. B. (1995), *Predicting CO_2 Corrosion in the Oil and Gas Industry,* 34, The Institute of Materials, UK.

Kermani, M. B. and Morshed, A. (2003), "Carbon Dioxide Corrosion in Oil and Gas Production - A Compendium", *Corrosion,* vol. 59, no. 08.

Kermani, M. B. and Smith, L. M. (1997), *CO_2 Corrosion Control in Oil and Gas Production - Design Considerations*, 23, The Institute of Materials, UK.

Kong, D., Wu, Y. -. and Long, D. (2012), "Effects of laser shock processing on electrochemical corrosion properties of X70 pipeline steel welded joints by slow strain rate testing", *Cailiao Kexue yu Gongyi Material Science and Technology*, vol. 20, no. 1, pp. 139-143.

Kvarekval, J., Skjerve, S. and Olsen, S., (2005), *The Effect of O_2 on CO_2 Corrosion in pH Stabilized Gas/Condensate Pipelines*, NACE International.

Lee, C. and Woollin, P. (2005), "Preferential Weld Corrosion: Effects of Weldment Microstructure and Composition", 3-7 April 2005, NACE International.

Lee, H. T. and Wu, J. L. (2009), "Correlation between corrosion resistance properties and thermal cycles experienced by gas tungsten arc welding and laser beam welding Alloy 690 butt weldments", *Corrosion Science*, vol. 51, no. 4, pp. 733-743.

Lee, S., Won, J., Park, D., Kim, Y., Moon, K. and Jeong, J., (2013), *Evaluation of Effect of Welding Methods to Corrosion and Hardness Characteristics of Welded Zone*.

Levy, A. V. (1995), "Erosion and Erosion-Corrosion of Metals", *Corrosion*, vol. 51, no. 11, pp. 872-883.

Llongueras, J. G., Flores, J. M., Duran-Romero, R., Munoz, A. and Hernandez, J. (2005), "Mechanism of $FeCO_3$ Formation on API X70 Pipeline Steel in Brine Solutions Containing CO_2", 3-7 April 2005, NACE International.

Lopez, D. A. and Simison, S. N. (2005), "Inhibitors Performance in CO_2 Corrosion EIS Studies on the Interaction between their Molecular Structure and Steel Microstructure", *Corrosion Science*, vol. 47, no. 3, pp. 735-755.

Suhor,M. F., Mohamed M. F., Nor, A. M., Singer, M. and Nesic, S. (2012), "Corrosion of Mild Steel in High CO_2 Environment: Effect of the $FeCO_3$ Layer", 11-15 March 2012, NACE International.

Martinez, M., Alawadhi, K., Robinson, M., Nelson, G, and MacDonald, A. (2011), "Control of Preferential Weld Corrosion of X65 Pipeline Steel In Flowing Brines Containing Carbon Dioxide", 13-17 March 2011, Texas, USA, NACE International.

Mahajanam, S. P. V. and Joosten, M. W. (2011), "Guidelines for Filler-Material Selection To Minimize Preferential Weld Corrosion in Pipeline Steels", *SPE Projects, Facilities & Construction*, vol. 6, no. 1, pp. 5-12.

Marsh, J., Duncan, P. and MacLeod, I. (2009), "Offshore Pipeline and Riser Integrity - The Big Issues", *2009 SPE Offshore Europe Oil & Gas Conference & Exhibition*, 8

- 11 September 2009, Aberdeen, UK, Society of Petroleum Engineers, pp. SPE 125060.

Martin, R. L., (2001), *Corrosion Consequences of Oxygen Entry into Sweet Oilfield Fluids*, Society of Petroleum Engineers, New Orleans, Louisiana.

Martin, R. L. (2002), "Corrosion Consequences of Oxygen Entry into Oilfield Brines", 7-11 April 2002, Denver, Co, USA, NACE International, pp. 02270.

Martin, R. L., (2003), *Unusual Oilfield Corrosion Inhibitors*, Society of Petroleum Engineers, Houston, Texas.

Martinez, M., Alawadhi, K., Robinson, M., Nelson, G. and MacDonald, A. (2011), "Control of Preferential Weld Corrosion of X65 Pipeline Steel In Flowing Brines Containing Carbon Dioxide", *Corrosion Conference,* 13-17 March 2011, USA, NACE International, USA, pp. Paper 11268.

McIntyre, D. R., Case, R. P., Mahajanam, S., Achour, M. and Singh, P. (2014), "Impact of Corrosion Inhibition on the Mitigation of Preferential Weld Attack in Sea Water Injection Pipelines", *Corrosion Conference,* 09-13 March, 2014, San Antonio, Texas, USA, NACE International, pp. Paper 3847.

McNaughtan, D. and Winning, I. G. (2004), "Comparison of Segmented Weld Corrosion Tests with Short and Long Pre-Corrosion and the Influence of Synergist in Corrosion Inhibitors", *SPE International Symposium on Oilfield Corrosion,* 28 May 2004, Society of Petroleum Engineers, Aberdeen, United Kingdom.

Menendez, C.M., Jenkins, A., Mok, W.Y., Weghorn, S.J. and Ahn, Y.S., (2005), *Electrochemical Evaluations of High Shear Corrosion Inhibitors, Using Jet Impingement Equipment*, NACE International.

Meng, Q. and Jovancicevic, V. (2008), "Electrochemical Evaluation of CO_2 Corrosion Inhibitors in High Turbulence Multiphase Fluid Flow", 16-20 March 2008, NACE International.

Moon, K., Nam, M., Lee, Y., Kim, Y. -. and Jeong, J. (2013), "The Characteristics of Weld Metal Zone Welded with various Filler Metals", *4th International Conference on Manufacturing Science and Engineering, ICMSE 2013,* Vol. 690 693, 30-31, March 2013, Dalian, Advanced Materials Research, China, pp. 2673-2677.

Mora-Mendoza, J. L., Chacon-Nava, J. G., González-Núñez, M. A., Turgoose, S. and Zavala-Olivares, G. (2002), "Influence of Turbulent Flow on the Localized Corrosion Process of Mild Steel with Inhibited Aqueous Carbon Dioxide Systems", *Corrosion,* vol. 58, no. 07.

Nesic, S. and Lee, K. (2003), " A Mechanistic Model for Carbon Dioxide Corrosion of Mild Steel in the Presence of Protective Iron Carbonate Films – Part 3: Film Growth Model", *Corrosion,* vol. 59, pp. 616.

Nesic, S., Nordsveen, M., Nyborg, R. and Stangeland, A. (2003), "A Mechanistic Model for Carbon Dioxide Corrosion of Mild Steel in the Presence of Protective Iron Carbonate Films – Part 2: A Numerical Experiment", *Corrosion,* vol. 59, pp. 489.

Nesic, S., Postlethwaite, J. and Olsen, S. (1996), "An Electrochemical Model for Prediction of Corrosion of Mild Steel in Aqueous Carbon Dioxide Solutions", *Corrosion,* vol. 52, no. 04, pp. 280-294.

Nešić, S. (2007), "Key issues related to modelling of internal corrosion of oil and gas pipelines – A review", *Corrosion Science,* vol. 49, no. 12, pp. 4308-4338.

Nesic, S., Drazic, D., Thevenot, N. and Crolet, J. L. (1996), "Electrochemical Properties of Iron Dissolution in the Presence of CO_2 - Basics Revisited", 24-29 March 1996, NACE International, .

Nesic, S. and Lee, J. K. (2006), "Use and Abuse of EIS in Studying the Mechanisms of CO_2/H_2S Corrosion of Mild Steel", 12-16 March 2006, NACE International, .

Nesic, S., Lee, J. and Ruzic, V. (2002), "A Mechanistic Model of Iron Carbonate Film Growth and the Effect on CO_2 Corrosion of Mild Steel", *Corrosion Conference,* 7-11 April 2002, NACE International, USA, pp. Paper 02237.

Nesic, S., Xiao, Y., Cai, J. and Wang, S. (2004), "Integrated CO_2 Corrosion - Multiphase Flow Model", 28 March-1 April 2004, NACE International, .

Nordsveen, M., Nesic, S., Nyborg, R. and Stangeland, A. (2003), "A Mechanistic Model for Carbon Dioxide Corrosion of Mild Steel in the Presence of Protective Iron Carbonate Films – Part 1: Theory andVerification", *Corrosion,* vol. 59, pp. 443.

Nyborg, R. (2010), "CO_2 Corrosion Models for Oil and Gas Production Systems", 14-18 March 2010, NACE International, USA.

Oldfield, J. W. (1988), "Electrochemical Theory of Galvanic Corrosion", in Hack, H. P. (ed.) *Galvanic Corrosion,* American Society for Testing of Materials, Philadelphia, USA, pp. 5-22.

Olsen, S. and Dugstad, A. (1991), "Corrosion Under Dewing Conditions", *Corrosion,* 1991, pp. Paper No. 472.

Olsen, S., Sundfear, B. and Enerhaug, J. (1997), "Weld Corrosion in C-Steel Pipelines in CO_2, Environments - Comparison Between Field and Laboratory Data", 9-14 March 1997, NACE International.

Olsen, S., Nyborg, R., Lunde, P. G. and Halvorsen, A. M. (2005), "CO_2 Corrosion Prediction Model - Basic Principles", 3-7 April 2005, NACE International.

Omonua, J. O. (2004), *Evaluation of Oilfield Corrosion Inhibitors for Down-Hole Protection of Steels* (MSc thesis), School of Industrial Manufacturing Science, Cranfield University, UK.

Palmer, J. W., Hedges, W. and Dawson, J. L. (eds.) (2004), *EFC 39: The Use of Corrosion Inhibitors in Oil and Gas Production,* Maney Publishing, London, UK.

Palmer, J. W. (2006), "Corrosion Control by Film Forming Inhibitors", 12-16 March 2006, NACE International.

Paolinelli, L. D., Pérez, T. and Simison, S. N. (2008), "The Effect of Pre-Corrosion and Steel Microstructure on Inhibitor Performance in CO_2 Corrosion", *Corrosion Science,* vol. 50, no. 9, pp. 2456-2464.

Paolinelli, L. D., Simison, S. N. and Pérez, T. (2007), "The Influence of Steel Microstructure, Chemical Composition and Precorrosion on CO_2 Corrosion Inhibitor Efficiency", 11-15 March 2007, NACE International, USA.

Papavinasam, S. (2000), "Corrosion Inhibitors", in Revie, R. W. (ed.) *Uhlig's Corrosion Handbook,* Second ed, Wiley, New York, USA.

Papavinasam, S., Attard, M., Demoz, A., Michaelian, K. and Revie, R. W. (2003), "Comparison of Laboratory Methodologies to Evaluate Corrosion Inhibitors for Oil and Gas Pipelines", *Corrosion,* vol. 59, no. 10.

Pereira Farias, J. and Monteiro Quites, A. (1992), *Factors That Influence the Microstructure and Mechanical Properties of Carbon-Manganese and Low-Alloy Steel Weld Metal, SALHS, High strength low alloy steels,* CEP 04038, Associacao Brasileira de Soldagem, Sao Paulo, Brazil.

Praturi, A. K. and Brodkey, R. S. (1978), "A stereoscopic visual study of coherent structures in turbulent shear flow", *Journal of Fluid Mechanics,* vol. 89, no. 02, pp. 251-272.

Queen, D., Lee, C., Palmer, J. and Gulbrandsen, E. (2004), "Guidelines For The Prevention, Control And Monitoring Of Preferential Weld Corrosion Of Ferritic Steels In Wet Hydrocarbon Production Systems Containing CO_2", *SPE International Symposium on Oilfield Corrosion,* 28 May 2004, Society of Petroleum Engineers, Aberdeen, United Kingdom.

Ramachandran, S., Campbell, S. and Ward, M. B. (2000), "The Interactions and Properties of Corrosion Inhibitors with By-product Layers", 26-31 March 2000, NACE International.

Richardson, J. A. and Dawson, J. L. (2010), "Economic Aspects of Corrosion", in Tony J.A. Richardson (ed.) *Shreir's Corrosion*, Elsevier, Oxford, pp. 3040-3051.

Roberge, P. R. (2000), *Handbook of Corrosion Engineering*, McGraw-Hill, USA.

Rogne, T., Solem, T. and Berget, J., (1998), *Effect of Composition and Corrosion Properties of the Metallic Matrix on the Erosion-Corrosion Behavior of HVOF Sprayed WC-Coatings*, NACE International.

Rosli, N. R., Choi, Y. and Young, D. (2014), "Impact of Oxygen Ingress in CO_2 Corrosion of Mild Steel", *Corrosion Conference*, 09-13 March, 2014, San Antonio, Texas, NACE International, USA, pp. Paper 4299.

Ruhl, A. S. and Kranzmann, A. (2012), "Corrosion Behavior of Various Steels in a Continuous Flow of Carbon Dioxide Containing Impurities", *International Journal of Greenhouse Gas Control*, vol. 9, pp. 85-90.

Ruzic, V., Veidt, M. and Nesic', S. (2006), "Protective Iron Carbonate Films Part 1: Mechanical Removal in Single-Phase Aqueous Flow", *Corrosion*, vol. 62, no. 05.

Schmitt, G. and Bakalli, M. (2006), "A critical review of measuring techniques for corrosion rates under flow conditions", *NACE - International Corrosion Conference Series*, pp. 065931.

Schmitt, G., Buschmann, R. and Theunissen, H. (2004), "Evaluation of inhibitor efficiencies in hydraulic fluids", *EUROCORR 2004 - European Corrosion Conference: Long Term Prediction and Modelling of Corrosion*.

Schmitt, G. A., Buecken, W. and Fanebust, R. (1992), "Modeling Micro-turbulences at Surface Imperfections as Related to Flow-Induced Localized Corrosion", *Corrosion*, vol. 48, no. 5, pp. 431-440.

Schmitt, G. A. and Mueller, M. (1999), "Critical Wall Shear Stresses in CO_2 Corrosion of Carbon Steel", 25-30 April 1999, NACE International.

Schmitt, G. A., Papenfuss, M., Strobel-Effertz, E. and Mueller, M. (1999), "Understanding Localized CO_2 Corrosion of Carbon Steel from Physical Properties of Iron Carbonate Scales", 25-30 April 1999, NACE International.

Schmitt, G. and Bakalli, M. (2006), "A Critical Review of Measuring Techniques for Corrosion Rates under Flow Conditions", 12-16 March 2006, NACE International.

Schmitt, G., Bakalli, M. and Werner, C., (2005), *Fluid Mechanical Interactions of Turbulent Flowing Liquids with the Wall - Revisited with a New Electrochemical Tool*, NACE International.

Schmitt, G. and Horstemeier, M. (2006), "Fundamental Aspects of CO_2 Metal Loss Corrosion - Part II: Influence of Different Parameters on CO_2 Corrosion Mechanisms", 12-16 March 2006, NACE International.

Schmitt, G., Schoning, M.J. and Werner, C., (2002), *Microelectrochemical Efficiency Evaluation of Inhibitors for CO_2 Corrosion of Carbon Steel Under High Shear Stress Gradients*, NACE International.

Schmitt, H. G. and Bakalli, M. (2010), "Flow Assisted Corrosion", in Tony J.A. Richardson (ed.) *Shreir's Corrosion,* Elsevier, Oxford, pp. 954-987.

Shadley, J. R., Shirazi, S. A., Dayalan, E., Ismail, M. and Rybicki, E. F. (1996), "Erosion-Corrosion of a Carbon Steel Elbow in a Carbon Dioxide Environment", *Corrosion,* vol. 52, no. 9, pp. 714-723.

Shifler, D. A. (2006), "Understanding and Modeling Galvanic Corrosion in Marine Environments", 12-16 March 2006, NACE International.

Shirazi, S. A., Shadley, J. R., Rybicki, E. F. and Adsani, E. (2006), "Validation of Mass Transfer Coefficient Models used in Predicting CO_2 Corrosion in Vertical Two-Phase Flow in the Oil and Gas Production", 12-16 March 2006, NACE International.

Silva, L. M., Duran, R., Mendoza, J. and Llongueras, J. G. (2004), "Effect of Flow on the Corrosion Mechanism of Different API Pipeline Steel Grades in NaCl Solutions Containing CO_2", 28 March-1 April 2004, NACE International.

Song, F. M. (2010), "A Comprehensive Model for Predicting CO_2 Corrosion Rate in Oil and Gas Production and Transportation Systems", *Electrochimica Acta,* vol. 55, no. 3, pp. 689-700.

Stack, M. M. and Abdulrahman, G. H. (2010), "Mapping erosion-corrosion of carbon steel in oil exploration conditions: Some new approaches to characterizing mechanisms and synergies", *Tribology International,* vol. 43, no. 7, pp. 1268-1277.

Stack, M. M., Zhou, S. and Newman, R. C. (1995), "Identification of transitions in erosion-corrosion regimes in aqueous environments", *Wear,* vol. 186–187, Part 2, no. 3, pp. 523-532.

Stalker, R., Graham, G. M. and Simpson, C. (2004), "The Impact of Inorganic Scale Deposits and Their Removal on General CO_2 Corrosion Rates and Corrosion Inhibitor Performance", *SPE International Symposium on Oilfield Corrosion*, 28 May 2004, Society of Petroleum Engineers, Aberdeen, United Kingdom.

Stout, R. D. and Doty, W. D. (1987), "Weldability of Steels", in Epstein, S. and Somers, R. E (ed.) *Weldability of Steels,* 3rd ed, Welding Research Council, New York.

Sun, J. B., Zhang, G. A., Liu, W. and Lu, M. X. (2012), "The formation mechanism of corrosion scale and electrochemical characteristic of low alloy steel in carbon dioxide-saturated solution", *Corrosion Science*, vol. 57, pp. 131-138.

Szklarska-Smialowska, Z., (1991), *Corrosion of Metals and Hydrogen-Related Phenomena*, Elsevier Science Publishing, New York, USA.

Tebbal, S. and Hackerman, N. (1993), "Liquid film thickness and weak acids in the CO_2 pitting of steel", *Corrosion Science*, vol. 34, no. 11, pp. 1787-1792.

Tobiassen, P. and Pedersen, A. E. (2004), "Experience Feedback on the use of a Carbon Steel Subsea Pipeline for a High Pressure, Sweet Service Gas Field", *Corrosion/2004; New Orleans, LA; USA; 28 Mar.-1 Apr. 2004; Corrosion/2004*, 28 Mar.-1 Apr. 2004, New Orleans, LA; USA, NACE International, P.O. Box 218340, Houston, TX, 77218, USA, pp. 13.

Turgoose, S. and Palmer, J. W. (2005), "Preferential Weld Corrosion of 1% Ni Welds: Effects of Solution Conductivity and Corrosion Inhibitors", 3-7 April 2005, NACE International.

Ueda, M. and Takabe, H. (1999), "Effect of Environmental Factor and Microstructure on Morphology of Corrosion Products in CO_2 Environments", *CORROSION '99*, 1999, NACE International, Houston, Tx, USA.

Vagapov, R. K. (2010), "Corrosivity of the Produced Fluids with Regard to Equipment and Pipelines in Oil and Gas Industries", *European Corrosion Congress*, Vol. 4, pp. 3701.

Videm, K. (1998), "The Influence of Composition of Carbon Steel on the Anodic and Cathodic Reaction Rate in CO_2 Corrosion", 22-27 March 1998, NACE International.

Wang, C., Neville, A. and Ramachandran, S. (2004), "Understanding the Action of Inhibitors in Mitigating Erosion-Corrosion in Impinging Flows", 28 March-1 April 2004, NACE International.

Wang, H., Fell, D. and Bailey, S. (2008), "Corrosion and Inhibition Study for a H_2S Containing Water Injection System: A Field Investigation Using Electrochemical Techniques", *Corrosion Conference*, 16-20 March 2008, NACE International, USA.

Winning, I. G., Mcnaughtan, D. and Bretherton, N. (2004), "Evaluation of Weld Corrosion Behavior and the Application of Corrosion Inhibitors and Combined Scale/Corrosion Inhibitors", 28 March-1 April 2004, NACE International.

Zhang, G. A. and Cheng, Y. F. (2010), "Electrochemical Characterization and Computational Fluid Dynamics Simulation of Flow-Accelerated Corrosion of X65

Steel in a CO_2-Saturated Oilfield Formation Water", *Corrosion Science*, vol. 52, pp. 2716-2724.

Zhang, Y., Gao, K. and Schmitt, G., (2011), Inhibition of Steel Corrosion Under Aqueous Supercritical CO_2 Conditions, NACE International.

APPENDICES

Appendix A **: Conference Papers**

1. Adegbite, M. A., Robinson, M. J. and Impey, S. A (2014) "The Influence of Hydrodynamics on the Preferential Weld Corrosion of X65 Linepipe Steel in Flowing Brine Containing Carbon Dioxide", NACE CORROSION 2014, paper C2014-3796, San Antonio, USA 09-13 March 2014. [*Oral Presentation*]

2. Adegbite, M. A., Robinson, M. J. and Impey, S. A. (2013), "Electrochemical Evaluation of Flow Accelerated Preferential Weld Corrosion of X65 Pipeline Steel Using Jet Impingement", Corrosion Management, Journal of The Institution of Corrosion, UK, Nov./Dec 2013, No. 116, pp 10-13. [*Journal Publication*]

3. Adegbite, M. A., Robinson, M. J. and Impey, S. A. (2013), "Electrochemical Evaluation of Flow Accelerated Preferential Weld Corrosion of X65 Pipeline Steel Using Jet Impingement", Eurocorr 2013, Paper 1139, 1 – 5 September 2013, Estoril, Portugal. [*Oral Presentation*]

4. Adegbite, M. A., Robinson, M. J. and Impey, S. A. (2012), "Electrochemical Evaluation of Flow Accelerated Preferential Weld Corrosion of X65 Steel in Brine Saturated with Carbon Dioxide", School of Applied Sciences DTC Annual Conference, Cranfield University, 5 December 2012. [*Oral Presentation*]

5. Adegbite, M. A., Robinson, M. J. and Impey, S. A. (2012) "Electrochemical Evaluation of Flow Accelerated Preferential Weld Corrosion of X65 Steel in Brine Saturated with Carbon Dioxide", 53rd Corrosion Science Symposium, Institute of Corrosion, 6–7 September 2012, London, UK. [*Oral Presentation*]

6. Adegbite, M. A., Robinson, M. J. and Impey, S. A., "Flow Accelerated Preferential Weld Corrosion of X65 Steel in CO_2 Saturated Brine", School of Applied Sciences DTC Annual Conference, Cranfield University, 17 January 2012. [*Poster Presentation*]

Appendix B **Electrochemical Measurements in the Three Hydrodynamic Regions**

(a)

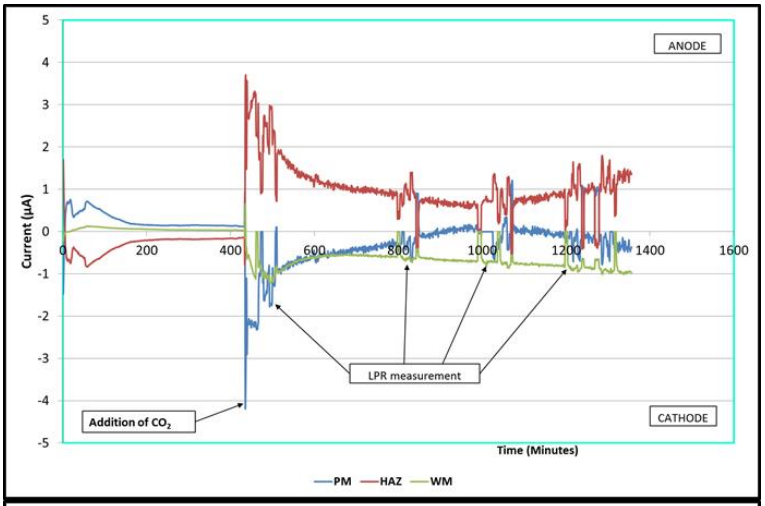

(b)

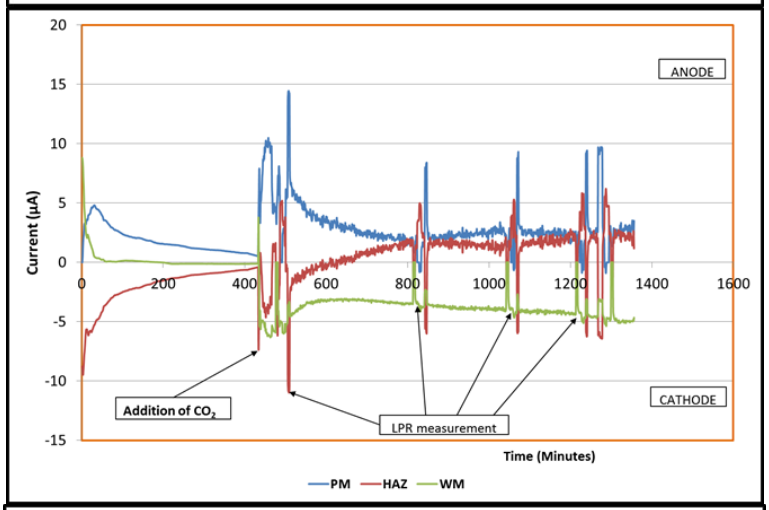

(c)

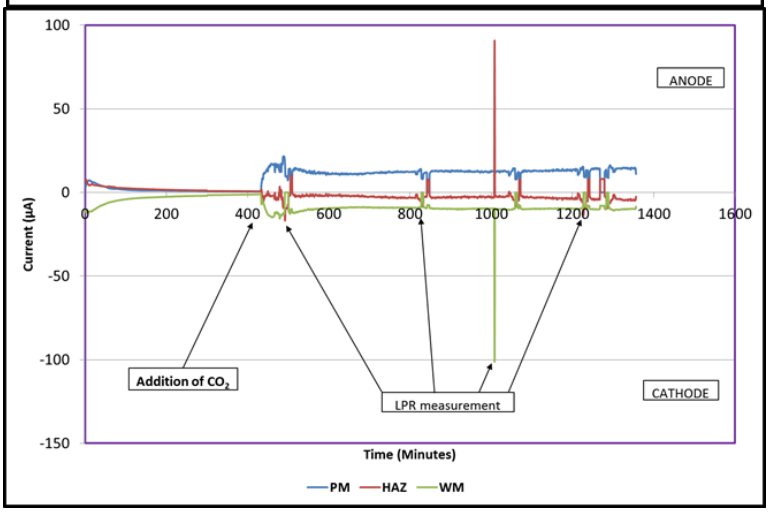

Figure B-1: Galvanic currents in the weld sections (placed at (a) centre, (b) the inner ring and (c) the outer ring of the target) in stagnant uninhibited brine saturated with CO_2.

(a)

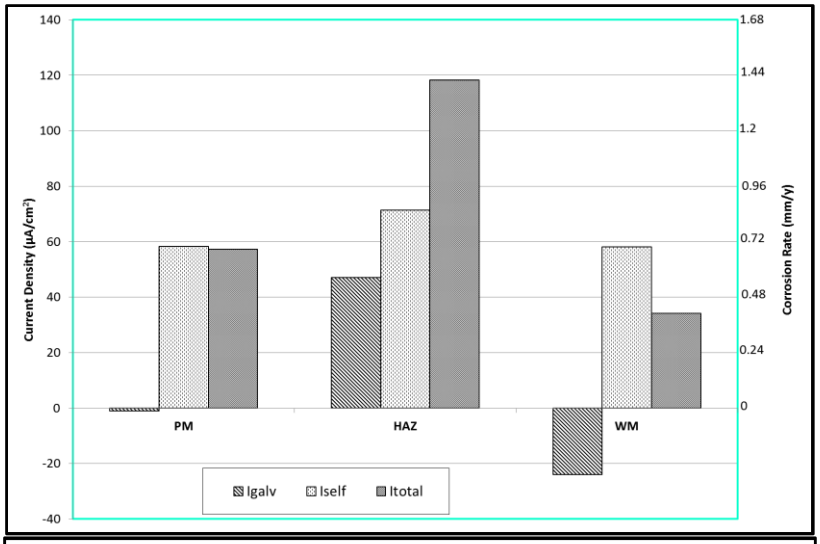

(b)

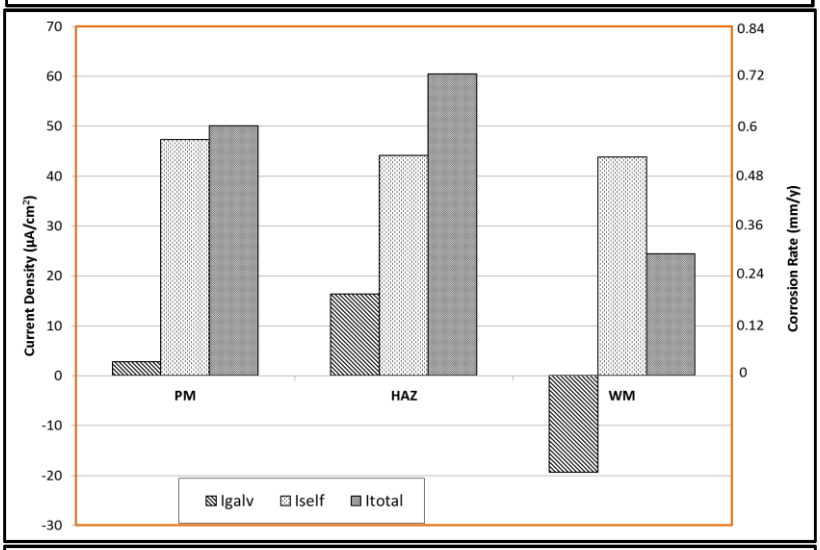

(c)

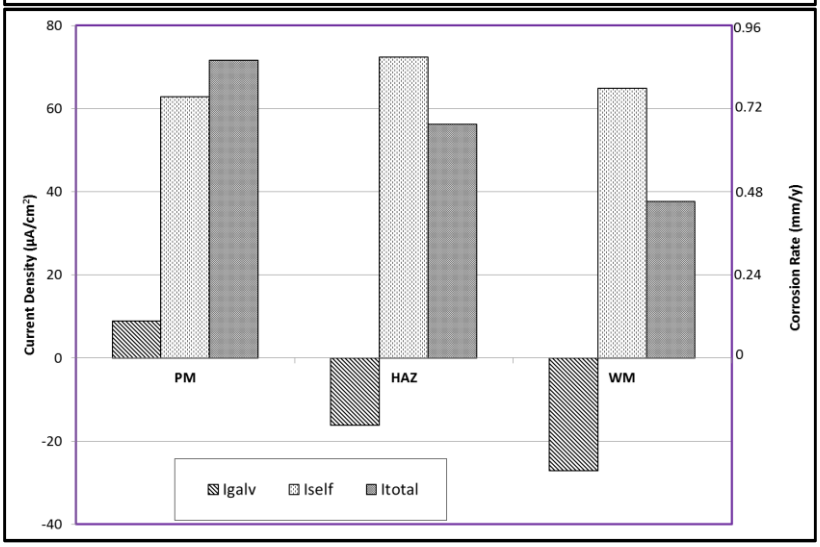

Figure B-2: Total corrosion rates in stagnant uninhibited brine saturated with CO_2, for each weld section in (a) the centre, (b) the inner ring and (c) the outer ring of the target.

(a)

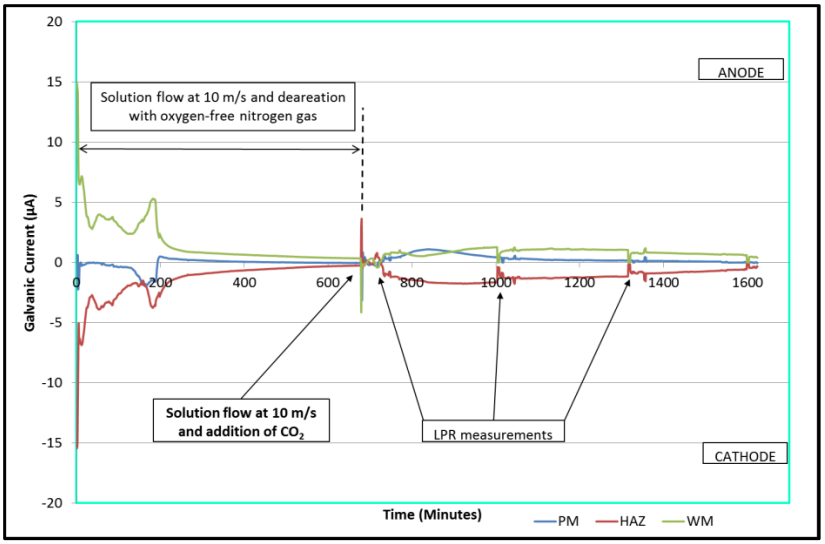

(b)

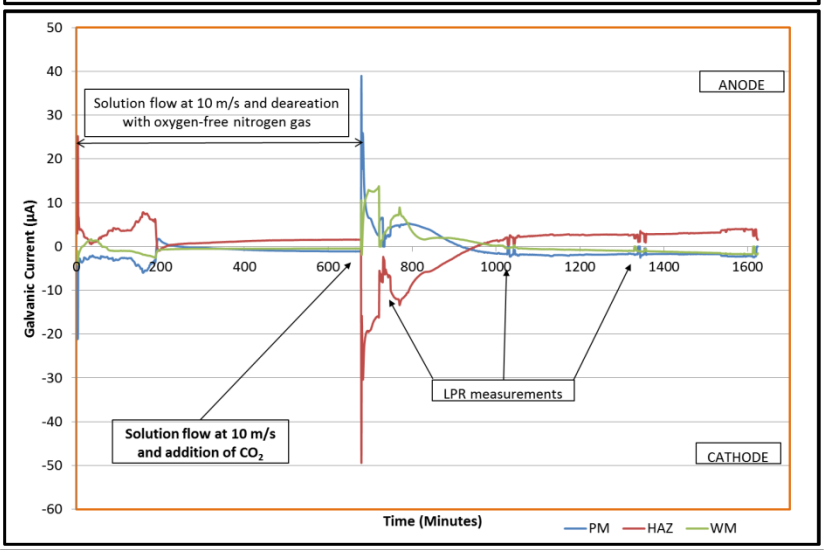

(c)

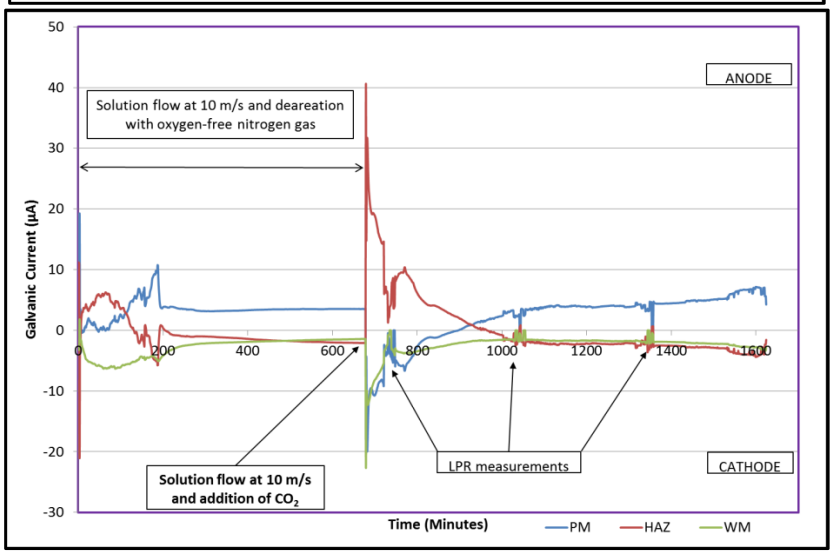

Figure B-3: Preliminary galvanic current measurements in brine saturated with CO_2 flowing at 10 m/s (a) the centre, (b) the inner ring and (c) the outer ring of the target.

(a)

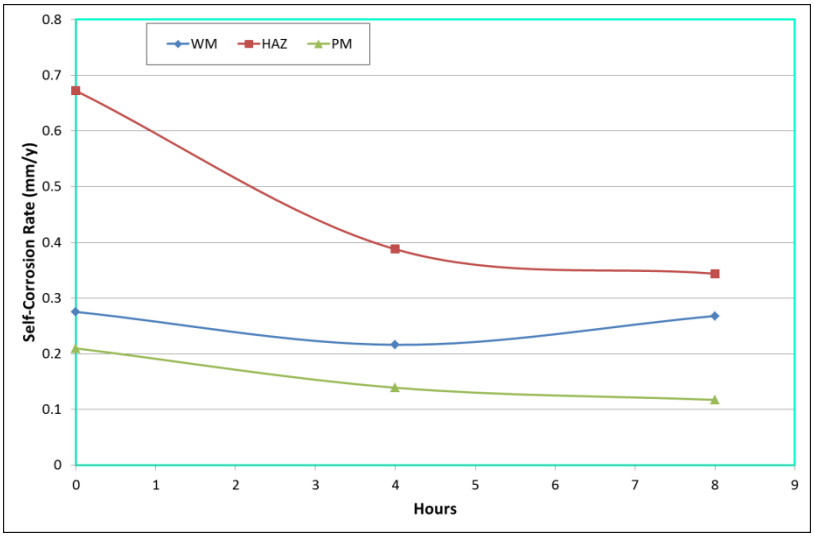

(b)

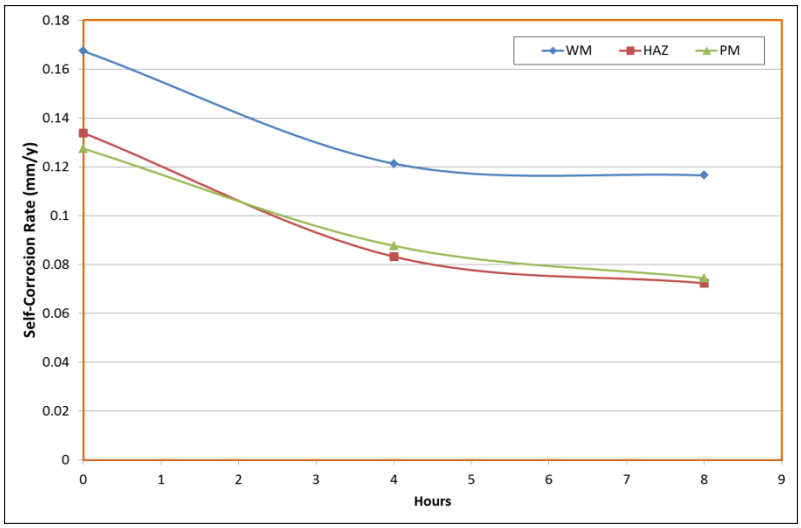

(c)

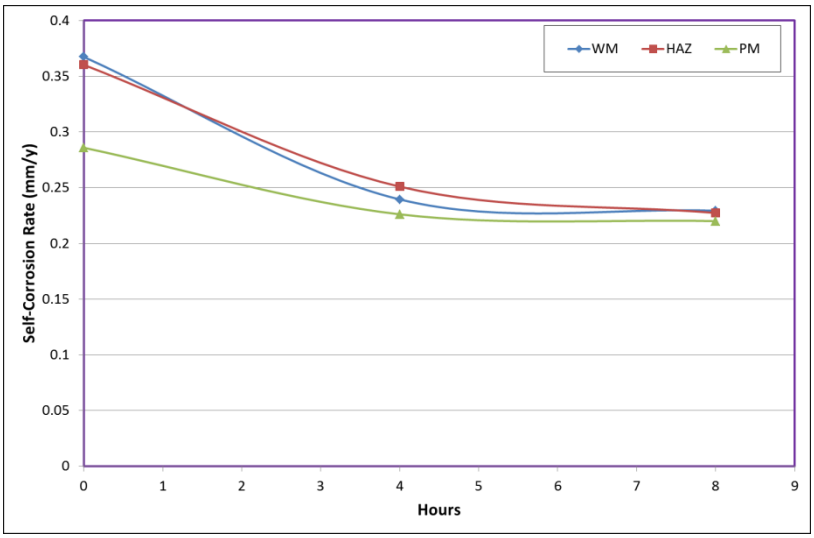

Figure B-4: Self-corrosion rates in uninhibited brine solution saturated with CO_2 flowing at 10 m/s (a) the centre, (b) the inner ring and (c) the outer ring of the target.

(a)

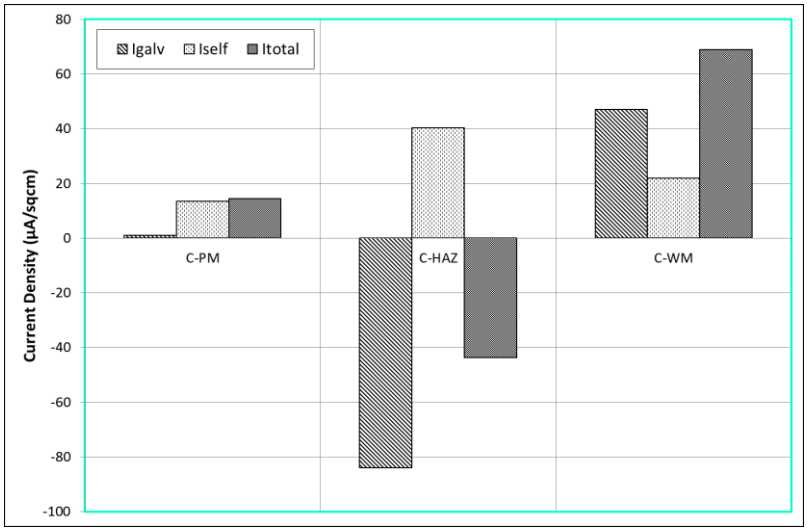

(b)

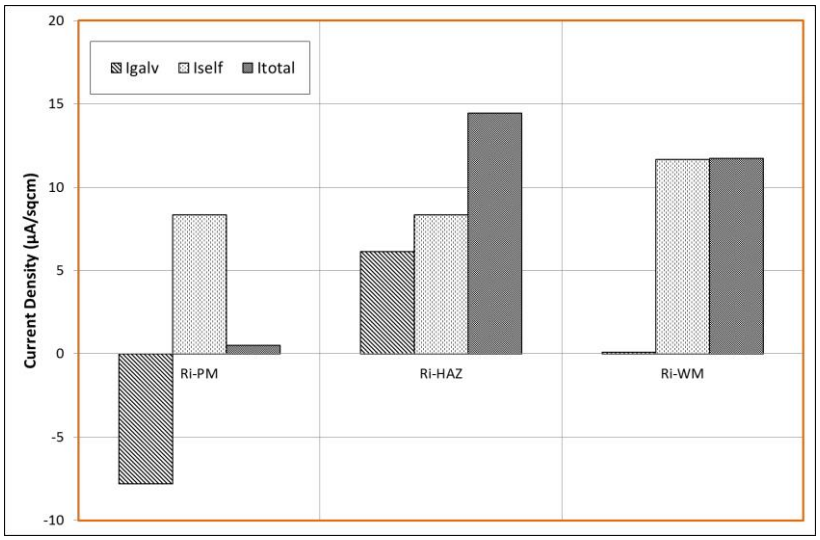

(c)

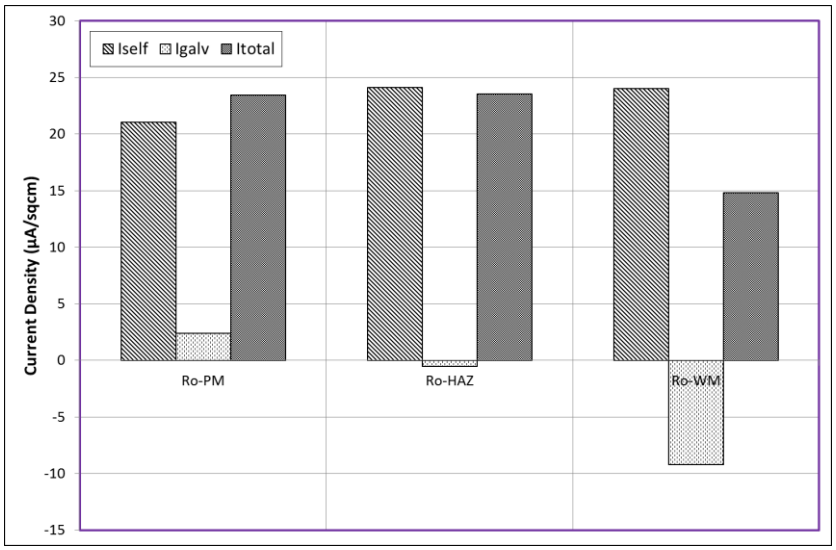

Figure B-5: Total corrosion rates in uninhibited brine solution saturated with CO_2 flowing at 10 m/s (a) the centre, (b) the inner ring and (c) the outer ring of the target.

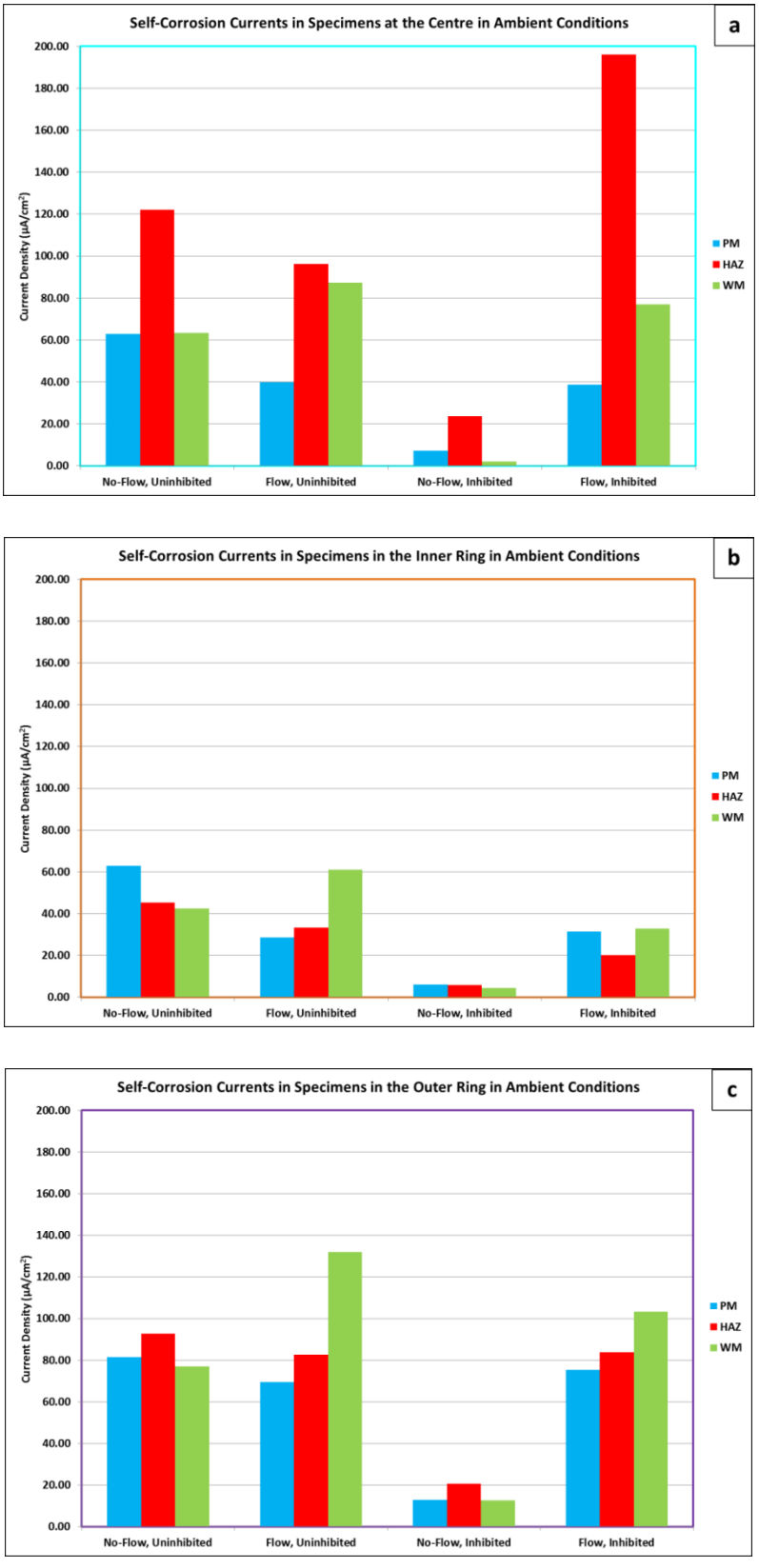

Figure B-6: Effect of flow (5 m/s) and inhibition on self-corrosion rates at (a) the centre, (b) the inner ring and (c) the outer ring.